MYELOID CELL FUNCTION IN HUNTINGTON'S DISEASE

A thesis submitted in partial fulfillment for the degree of Doctor of Philosophy to the University College London

by

Ulrike Träger Dipl. Biol.
Institute of Neurology, University College London

Declaration

I, Ulrike Träger, confirm that the work presented in this thesis is my original research work. Where contributions of others are involved, this has been clearly indicated in the thesis.

Acknowledgments

First and foremost, I would like to thank my supervisor, Prof Sarah Tabrizi, for all her support, advice and endless enthusiasm. Thanks also to Dr Mark Lowdell, my secondary supervisor and Dr Ralph Andre for constant, much appreciated help with my project. I would also like to acknowledge the members of the MRC Prion Unit/Department of Neurodegenerative Disease for their intellectual and practical help, as well as the humour to get over the drama that comes with a PhD. My special gratitude goes out to the members, past and present, of the Tabrizi lab: Dr Rob Goold, Dr Samira Rabbanian, Chris McKinnon, Anna Magnusson-Lind, Dr Nayana Lahiri and Lucianne Dobson, for their friendship, and intellectual and personal support. In addition I want to thank our collaborators: Dr Andreas Weiss, Dr Wanda Kwan, Dr Jill Bouchard, Prof Paul Muchowski, Prof Neil Aronin and Prof Gary Ostroff for their advice and support.

This project would not have been possible without the patients and control subjects who donated samples, and the staff of the HD clinic. A special thanks to Dr Ed Wild, Dr Salman Haider, Monica Lewis and Nicci Robertson. I would also like to thank Ralph, Wanda and Nicci for their support with writing-up and Ray Young for his capable and calm assistance with the preparation of figures.

Above all, I would like to thank my mum for being my role-model and her never ending support. I am also indebted to my husband Andreas for his constant encouragement, enormous patience and love - words are not enough.

Table of Contents

List of Figures

List of Tables

Abbreviations

AAV	adeno-assiciated virus
ADP	adenosine diphosphate
AMP	adenosine monophosphate
AP-1	activator protein 1
APC	allophycocyanin
APOE	apolipoprotein E
ARP2/3	actin-related protein 2/3
ASO	antisense oligonucleotide
ATP	adenosine triphosphate
ATTC	american type culture collection
BAC	bacterial artificial chromosome
BBB	blood brain barrier
BCA	bicinchoninic acid
BDNF	brain-derived neurotrophic factor
BSA	bovine serum albumin
C	celsius
cAMP	cyclic adenosine monophosphate
CB	cannabinoid receptor
CBP	CREB-binding protein
CD	cluster of differentiation
cDNA	complementary deoxyribonucleic acid

CLP	common lymphoid progenitor
CMP	common myeloid progenitor
CNS	central nervous system
CREB	cAMP response element-binding protein
CSE	control standard endotoxin
CSF	cerebrospinal fluid
DAPI	4',6-diamidino-2-phenylindole
DC	dendritic cell
DMSO	dimethyl sulfoxide
DNA	deoxyribonucleic acid
dNTP	deoxyribonucleotide
dsRNA	double stranded RNA
DTT	dithiothreitol
EDTA	ethylenediaminetetraacetic acid
e.g.	for example
ELISA	enzyme-linked immunosorbent assay
ELK	E twenty-six (ETS)-like transcription factor 1
FACS	fluorescence activated cell sorting
F-actin	filamentous actin
FCS	fetal bovine serum
FDA	food and drug administration
FITC	fluorescein
g	gravitational acceleration
G-actin	globular actin
GDP	guanosine-5'-diphosphate
GeRPs	beta1,3-D-glucan-encapsulated siRNA particles
GEF	guanine nucleotide exchange factors
GFP	green fluorescent protein

GM-CFU	granulocyte/macrophage colony-forming units
GM-CSF	granulocyte macrophage colony-stimulating factor
GRIK2	glutamate receptors ionotropic kainate 2 gene
GTP	guanosine-5'-triphosphate
h	hour
HAP1	huntingtin associated protein 1
HAT	histone acetyltransferase
HBSS	Hank's buffered salt solution
HD	Huntington's disease
HDACs	histone deacetylases
hESCs	human embryonic stem cells
HEPES	4-(2-hydroxyethyl)-1-piperazineethanesulfonic acid
HEAT	huntingtin, elongation factor 3, the PR65/A subunit of protein phosphatase 2A and the lipid kinase Tor
HSC	haematopoietic stem cells
Htt	murine huntingtin gene
HTT	huntingtin protein
HTT	human huntingtin gene
ID	immunodetection
i.e.	id est
IFNγ	interferon gamma
Ig	immunoglobulin
IGF	insulin-like growth factor
IgG-H	antibody heavy chain
IKK	IκB kinase
IκB	inhibitor of kappa B
IL	interleukin
IP	immunoprecipitation

iPSC	inducible pluripotent stem cell
IRAK	IL-1R associated kinase
IRFs	interferon response factors
JAK	janus kinase
JNK	c-Jun N-terminal kinases
kb	kilo base pair
kDa	kilo Dalton
KMO	kynurenine 3-monooxygenase
L	litre
LPS	lipopolysaccharides
M	molar
MACS	magnetic activated cell sorting
MAPK	mitogen-activated protein kinases
M-CFU	macrophage colony-forming unit
M-CSF	macrophage colony-stimulating factor
MCP-1	monocyte chemoattractant protein 1
MHC	major histocompatibility complex
min	minutes
miRNA	micro RNA
ml	millilitre
MPP	multipotent progenitor
MRI	magnetic resonance imaging
mRNA	messenger ribonucleic acid
MSNs	medium spiny neurons
mTOR	mammalian target of rapamycin
MyD88	myeloid differentiation primary response gene (88)
n	number
N	amino

NES	nuclear export sequence
NFκB	nuclear factor kappa-light-chain-enhancer of activated B cells
NLS	nuclear localisation signal
NMDAR	N-methyl-D-aspartate receptor
NRSF	neuron-restrictive silencer factor
P	proline
PAMPs	pathogen-associated molecular patterns
PB	polybrene
PBMC	peripheral blood mononuclear cell
PBS	phosphate buffered saline
PCR	polymerase chain reaction
PE	phycoerythrin
PET	positron emission tomography
PFA	paraformaldehyde
PGC-1α	peroxisome proliferator activated receptor gamma coactivator 1 alpha - protein name
PI3K	phosphatidylinositide 3-kinases
PIP_2	phosphatidylinositol (4,5)-bisphosphate
PKB	protein kinase B
PMA	phorbol 12-myristate 13-acetate
PMSF	phenylmethanesulfonylfluoride or phenylmethylsulfonyl fluoride
PPARGC1A	Peroxisome proliferator-activated receptor gamma, coactivator 1 alpha - gene name
PPC	positive PCR control
PRRs	pattern recognition receptors
PVDF	polyvinylidene fluoride

Q	glutamine
qPCR	quantitative polymerase chain reaction
RANTES	regulated and normal T cell expressed and secreted
REST	RE1-silencing transcription factor
RISK	RNA-induced silencing complex
RNA	ribonucleic acid
RNAi	RNA interferences
RTC	reverse-transcription control
s	seconds
SAHA	suberoylanilide hydroxamic acid
SDS	sodium dodecyl sulfate
SEM	standard error of the mean
shRNA	small hairpin RNA
siRNA	small interfering RNA
SNP	single nucleotide polymorphism
Sp-1	specificity protein 1
STAT	signal transducers and activators of transcription
T	tesla
TAK	transforming growth factor βactivated kinase
TBP	TATA-binding protein
TBS	tris-buffered saline
TCR	T cell receptor
TFC	total functional capacity
T_h	T helper cell
TLR	Toll like receptors
TNF	Tumour necrosis factor
TP53	tumour protein 53
TRAF	TNF receptor associated factors

TRAM	TRIF-related adaptor molecule
TRIF	TIR-domain-containing adapter-inducing interferon-beta
T_{reg}	regulatory T cells
UCL	University College London
UHDRS	unified Huntington's disease rating scale
UPS	ubiquitin-proteasome system
vs.	versus
YAC	yeast artificial chromosome
WASP	Wiskott-Aldrich syndrome proteins
WT	wild type

Abstract

Huntington's disease (HD) is an inherited neurodegenerative disorder caused by a CAG repeat expansion in the huntingtin (*HTT*) gene. The peripheral innate immune system contributes to HD pathogenesis and has been targeted successfully to modulate disease progression, but mechanistic understanding relating this to mutant (m)HTT expression in immune cells has been lacking.

This thesis demonstrates that human HD myeloid cells produce excessive inflammatory cytokines due to cell-intrinsic effects of mHTT expression on the NFκB pathway, whereby mHTT interacts with IKK, leading to increased degradation of IκB and subsequent nuclear translocation of RelA. Transcriptional alterations in intracellular immune signaling pathways were also observed. Using a novel method of siRNA delivery to lower HTT expression, this thesis shows a reversal of disease-associated alterations in cellular function - the first time this has been demonstrated in human cells. Glucan-encapsulated siRNA particles (GeRPs) were used to lower *HTT* levels in human HD monocytes/macrophages, resulting in reversal of HTT-induced elevated cytokine production and transcriptional changes. These findings improve our understanding of the role of innate immunity in neurodegeneration, introduce GeRPs as a tool for studying cellular pathogenesis *ex vivo* in human cells and raise the prospect of HTT lowering in immune cells as a therapeutic in HD.

Evaluating immune function in different mouse models of HD, blood and splenic monocytes replicated the hyper-reactive phenotype seen in HD patients demonstrating that HD mouse models can be of use to understanding HD immune pathology and to test immune modulatory therapies.

Furthermore, human HD myeloid cells demonstrated a striking defect in migration towards different chemokines. Looking at the cell's ability to form filopodia, it became apparent that actin-remodelling is reduced and causes decreased migration.

Work performed in collaboration with Novartis revealed that mHTT levels in immune cell subsets differ significantly between disease stages. Monocyte and T cell mHTT levels were significantly associated with disease burden scores and caudate atrophy rates in HD patients. mHTT fragments detected in HD immune cells may explain the progressive increase in mHTT levels. These findings indicate that quantification of mHTT holds significant promise as a non-invasive disease biomarker.

1 Introduction

1.1 Huntington's disease

Huntington's disease (HD) is a fatal, autosomal dominant inherited, progressive neurodegenerative disorder that results from the expansion of a trinucleotide CAG repeat within the *HTT* gene that encodes a protein called huntingtin (HTT). The mean age of onset for the disease is 40 years, with death typically occurring 15-20 years later (reviewed in (Ross and Tabrizi, 2011)). HD can be found worldwide, but there are significant geographic differences: in North America and Western Europe a minimum of 5 in 100,000 people are affected, whereas HD prevalence in China and Japan is 10-100 fold lower. The Maracaibo region in Venezuela has the highest prevalence (700 per 100,000) worldwide (Warby et al., 2011). In the UK the prevalence is thought to be around 6 per 100,000, although it could be as high as 12.4/100,000 due to unconfirmed, unspecific or mis-diagnosis (as schizophrenia and Alzheimer's disease) (Rawlins, 2010; Sackley et al., 2011).

1.1.1 Features of Huntington's disease

HD is a clinically heterogeneous disease, presenting with various combinations of cognitive, psychiatric and motor symptoms. The disease was described by and named after George Huntington in 1872 (Huntington, 1872) and whilst it was not

the first description of the disease, his paper comprehensively noted the genetic, movement, cognitive and neuropsychiatric characteristics of HD.

1.1.1.1 Clinical features

Clearly determining the onset of HD is difficult, as many patients have psychiatric or cognitive symptoms before motor problems present themselves. A definitive clinical diagnosis is only made when motor abnormalities are noted (Wild and Tabrizi, 2007).

In the early stages of the disease, minor motor features include restlessness, hyperreflexia, and fidgety movements of fingers, hands and toes during stress or when walking. Oculomotor abnormalities are a major feature in HD and are often one of the earliest features noticed. In later stages of the disease, 90 % of patients present with involuntary movements such as chorea, differing in the degrees of dystonia, Parkinsonism and bradykinesia. Moreover, impairments of voluntary movements leading to clumsiness, reduced motor speed and disturbance in fine motor control, are key features of HD (Wild and Tabrizi, 2007).

Cognitive changes are an early, near-universal feature in HD and include slowing of the thought process and executive functions. However, the severity of abnormalities varies between patients. Impaired functions include: poor planning and judgment, impulsive behaviour, disorganisation, lack of insight, distractibility and loss of initiative (Novak and Tabrizi, 2010).

Psychiatric symptoms, such as depression and anxiety are also common in HD patients. One study suggests that 40-50 % of HD patients suffer from depression (Paulsen et al., 2005). Suicide and suicide attempts are up to four times more common in HD patients compared with in the general population (Farrer, 1986). Aggressive behaviour or apathy can also be seen in some patients, and on rare

occasions patients suffer from hypersexuality or psychosis (Novak and Tabrizi, 2010).

1.1.1.2 Brain pathology

Most of the clinical features in HD can be attributed to degeneration within the central nervous system (CNS). Analysis of post-mortem, end-stage HD reveals that the total brain volume of HD patient is reduced by 19 % compared with matching controls (Halliday et al., 1998). The highest levels of atrophy are seen in the striatum, with around 50 % loss in the caudate and putamen, and to a lesser extent in the cortex (Halliday et al., 1998; Rosas et al., 2001; Vonsattel et al., 1985). Other regions, such as the cerebral cortex (Halliday et al., 1998), globus pallidus (Rosas et al., 2003), hypothalamus (Politis et al., 2008), subthalamic nucleus, substantia nigra and the subcortical white matter are also affected, but less notably so than the striatum (reviewed in (Ross and Tabrizi, 2011)).

The substantial striatal atrophy in HD patient brain is caused by neuronal death, with a loss of up to 95 % of GABAergic medium spiny neurons (MSNs) (Vonsattel and DiFiglia, 1998). As a hallmark of HD pathology, intranuclear inclusion bodies, containing large aggregates of mHTT, are found in neuronal nuclei of end-stage HD post-mortem brain tissue (Vonsattel, 2008), as well as in the otherwise normal brains of premanifest HD gene carriers (Gómez-Tortosa et al., 2001). Aggregates are not, however, restricted to the cellular nucleus, and can also be found in the cytoplasm, neuronal dendrites and axon terminals (Vonsattel, 2008). It has been reported that atrophy occurs before symptom onset, suggesting that the CNS is able to cope with some degree of neuronal damage before manifesting any behavioural changes (Rosas et al., 2005; Tabrizi et al., 2009).

Neuronal death may not, however, only be due to cell-autonomous processes occurring within neurons. Cellular interactions including inter-neuronal as well as

between glial cells and neurons may also play a role. Interestingly, both increased numbers of astrocytes (Vonsattel, 2008) and microglia have been detected in HD brains (Sapp et al., 2001; Tai et al., 2007). Furthermore, transgenic expression of *mHTT* in HD mouse astrocytes *in vivo* causes an age dependent neurological phenotype similar to HD, underlining the potential importance of non-neuronal cells in HD pathogenesis (Bradford et al., 2009).

1.1.1.3 Peripheral changes in HD

While primary pathology in HD arises from degeneration in the basal ganglia, HTT expression has been detected in every tissue tested (Hoogeveen et al., 1993; Li et al., 1993). Furthermore, HTT is known to interact with cellular processes and organelles important in both neuronal and non-neuronal cells, including mitochondrial function, protein degradation pathways and gene transcription (reviewed in (Ross and Tabrizi, 2011)). Indeed, widespread pathology can be found in peripheral organs, and is associated with weight-loss, skeletal muscle wasting, osteoporosis, diabetes, cardiac failure and testicular atrophy (van der Burg et al., 2009) (Figure 1.1).

Weight loss is a hallmark of HD (Sanberg et al., 1981). The progressive loss of weight starts in premanifest gene carriers and develops into cachexia in advanced patients (Djoussé et al., 2002; Trejo et al., 2004). The constant loss of weight is due to a high metabolic rate (Goodman et al., 2008; Mochel et al., 2007) rather than hyperactivity or malnutrition (Djoussé et al., 2002; Trejo et al., 2004). Studies in HD mice suggest that dysfunction of the gastrointestinal tract causes malabsorption of food, which could also contribute to weight loss in HD (van der Burg et al., 2011).

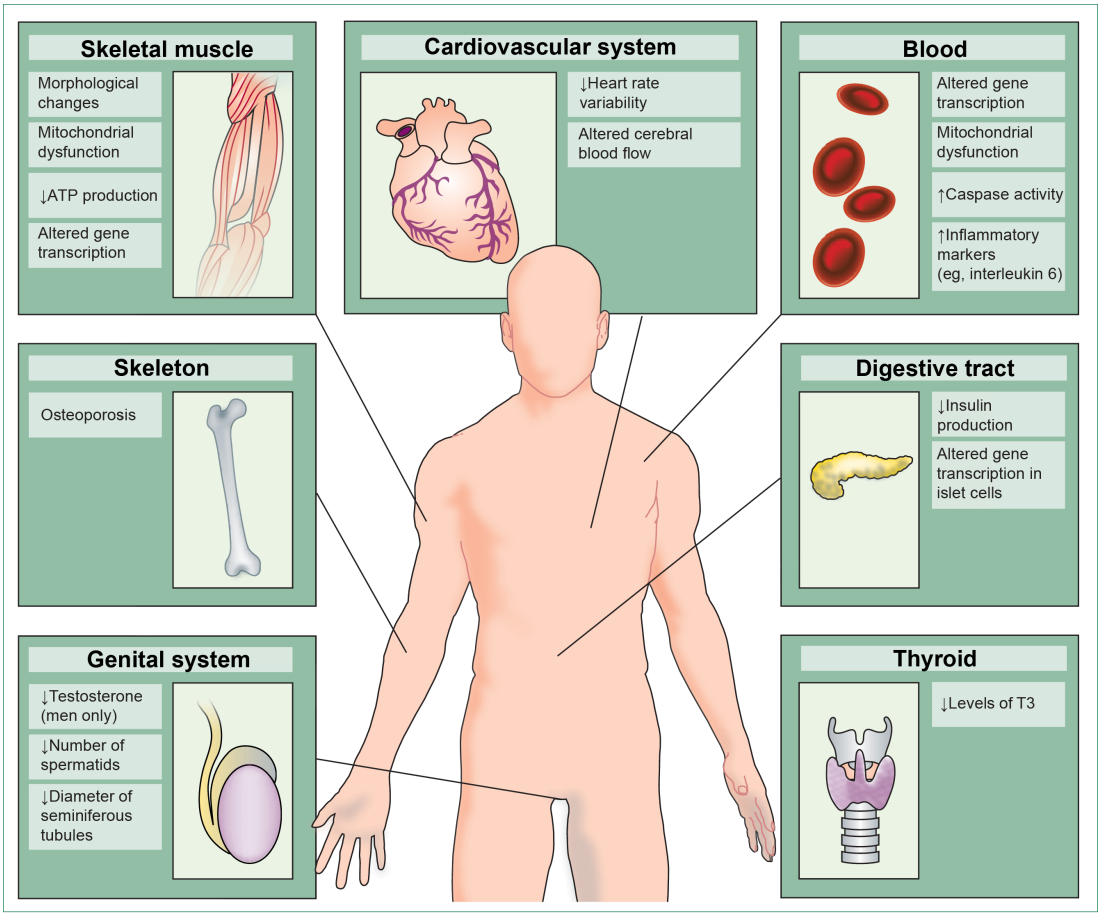

Figure 1.1: Peripheral phenotypes in HD patients. Besides neuronal loss, HD patients suffer from a wide range of peripheral symptoms caused by ubiquitous expression of mHTT in peripheral tissues. Re-printed from The Lancet, Vol.8, *Beyond the brain: widespread pathology in Huntington's disease*, 765-74, van der Burg et al., ©2009, with permission from Elsevier.

Skeletal muscle wasting is another feature of HD that is commonly found in patients (van der Burg et al., 2009). Interestingly, similar to the neuronal phenotype, myocytes from HD patients form mHTT inclusions, while a range of cellular abnormalities such as mitochondrial dysfunction, increased cell death and defective cell differentiation have been observed (Ciammola et al., 2006). Mutant HTT is known to repress peroxisome proliferator activated receptor γ co-activator 1 alpha (PGC-1α) transcription in neurons (Cui et al., 2006) and muscle cells (Chaturvedi et al., 2009). Inhibition of this transcriptional co-activator known to regulate genes playing a role in energy metabolism, mitochondrial respiration and number, disrupts mitochondrial function.

Second to the brain, testis are the organ with the highest HTT expression levels (Li et al., 1993). Testicular atrophy in HD patients does not affect fertility (Pridmore and Adams, 1991) but patients demonstrate lower testosterone levels than would be normally expected (Markianos et al., 2005). Interestingly, testosterone levels are negatively correlated to disease severity, not only in HD (Markianos et al., 2005), but also in other neurodegenerative diseases (Okun et al., 2004).

After pneumonia, heart disease is the second leading cause of death in HD and occurs in about 30 % of patients (Lanska et al., 1988). In HD mouse models, the myocardium has been found to be atrophic, and as mitochondria demonstrate altered ultrastructure and increased protein nitration is observed in myocytes, oxidative stress seems to be a likely reason for cardiac pathology in HD (Mihm et al., 2007).

Other organs affected in HD patients include bones, decreased density of which has been reported in premanifest HD gene carriers (Goodman and Barker, 2011), and the pancreas, where impaired insulin secretion by β-cells leads to diabetes (Smith et al., 2009). Widespread abnormalities in blood cells have also been detected; these are discussed separately in Section 1.3.2.

Peripheral changes could be secondary to dysfunction in the CNS. Pathology in the hypothalamus leads to differences in endocrine signalling such as altered production and release of growth hormones (Saleh et al., 2009) and cortisol (Aziz et al., 2009), leading to secondary changes in peripheral tissues. However, there is evidence that dysfunction is directly due to the expression of mHTT in peripheral cells. HTT is ubiquitously expressed in all cells of the body (Li et al., 1993) and loss of *Htt* (the mouse homologue to the human *HTT*) in mice is embryonic lethal (Nasir et al., 1995), underlining the importance of HTT expression in peripheral tissues. It would not, therefore, be surprising if a mutation in *HTT* leads to changes in peripheral cells as well. Moreover, peripheral cells demonstrate

dysfunction when cultured *in vitro*, indicating the direct effect of mHTT (Björkqvist et al., 2008).

While peripheral, non-neuronal symptoms in themselves greatly affect the quality of life for patients, they may also contribute to brain pathology. It is known that patients with higher body weight show slower rates of disease progression, suggesting that defects in peripheral metabolism may lead to insufficient nutritional support for the CNS contributing to brain dysfunction (van der Burg et al., 2009). In addition, several recent studies suggest that the peripheral immune system can be modulated to affect HD progression (see Section 1.3.3).

1.1.1.4 Juvenile HD

Around 7 % of all HD patients carry a *HTT* allele with more than 60 CAG repeats, which results in early-onset or juvenile (onset before the age of 20) HD. Five percent of these early onset patients carry CAG repeats of between 80 and 100, causing disease onset before the age of 10 (Squitieri et al., 2006). Large *HTT* CAG repeat expansions not only result in very early disease onset, but also lead to a fast and devastating rate of progression. While juvenile patients demonstrate some of the symptoms typical for HD, such as clumsiness, gait disturbance and depression they do not present with chorea. Furthermore, juvenile patients suffer from atypical symptoms such as seizures, epilepsy, psychosis, learning difficulties, rigidity and dystonia (Squitieri et al., 2000, 2006). Juvenile subjects suffer from more widespread brain atrophy, however, like in adult-onset HD the striatum is the worst affected region within the brain (Nance and Myers, 2001; Vonsattel et al., 2011). To date, it is unclear why the progression rate and symptoms differ between adult and juvenile onset HD, but it is likely that longer polyglutamine (polyQ) expansions in the HTT protein have different effects on its functions.

1.1.2 HD genetics and age of onset

The HD gene was mapped to human chromosome 4p16.3 in 1983 (Gusella et al., 1983). Ten years later, the associated *HTT* gene was isolated and a CAG repeat expansion was identified as the mutation underlying the disease. The repeat is located in exon 1, seventeen codons downstream of the ATG start codon (The Huntington's Disease Collaborative Research Group, 1993). The whole *HTT* locus is 180 kilo base pairs (kb) long and consists of 67 exons. The gene has a house-keeping like promoter, which allows wide-spread expression in all cell types (reviewed in (Ross and Tabrizi, 2011)).

In healthy individuals, the number of CAG repeats is fewer or equal to 35. Repeats of between 36 and 39 are reduced penetrance range repeats with which people are at risk of developing the disease in old age. CAG repeats of 40-55 result in an adult onset of HD, whilst longer repeats lead to young adult onset or juvenile forms of the disease (Bates et al., 2002). The CAG repeat expansion within the *HTT* gene is subject to meiotic instability and tends to increase over multiple generations. This effect is greater in paternal heredity, leading to strong inheritance via the paternal line (Trottier et al., 1994). There is a strong inverse correlation between the length of the CAG repeat in the mutant *HTT* (*mHTT*) allele and age of disease onset with longer CAG repeats causing an earlier age of onset (Figure 1.2).

However, only 50-70 % of variance in age of disease onset depends on the length of the CAG repeat. The remaining variation is influenced by modifying genes and the environment. A study on a large Venezuelan HD pedigree found that 59 % of the age of onset depends on genetic and environmental modifiers (Wexler et al., 2004), whilst a study looking at siblings found that the CAG repeat length accounted for 65-71 % of the variance (Rosenblatt et al., 2001).

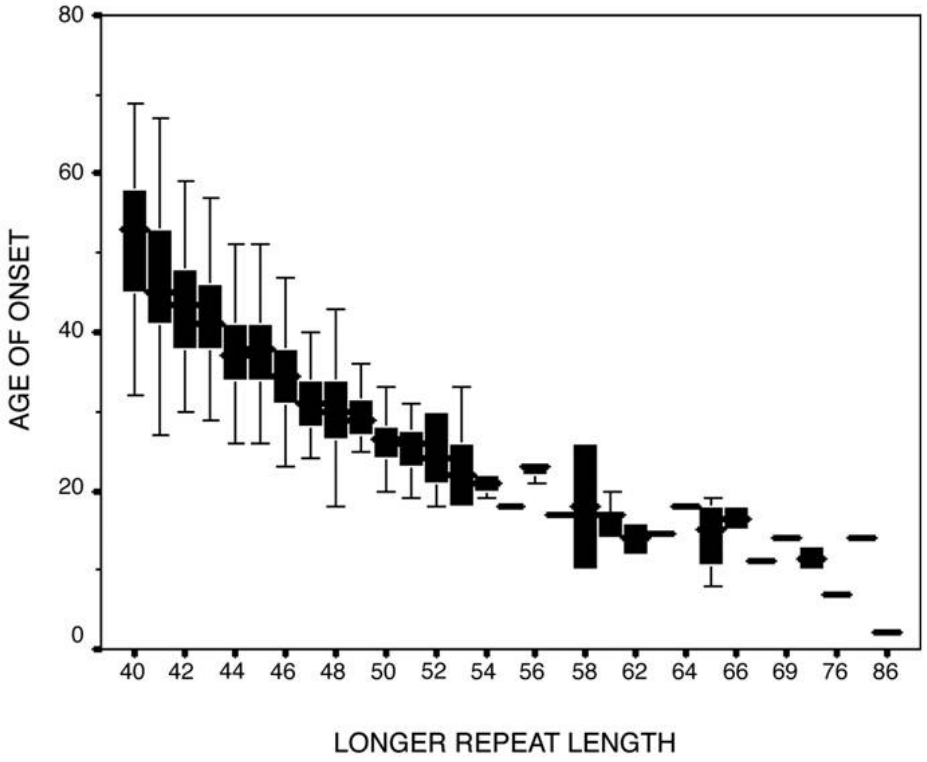

Figure 1.2: Correlation between age of onset and CAG repeat length. A clear curvilinear relationship can be observed, showing that longer CAG repeats result in earlier age of onset. Picture re-produced from Wexler et al., 2004. ©with authors of original article.

Several genes such as *GRIK2, TP53, HAP1, APOE* and *PPARG1A* have been suggested as modifiers of disease onset. Several studies have reported the glutamate receptors ionotropic kainate 2 gene (*GRIK2*) as a modifier of age of onset in HD (MacDonald et al., 1999; Rubinsztein et al., 1997; Zeng et al., 2006). The gene encodes for a subunit of the glutamate receptor, which mediates excitatory neurotransmission in the brain. Interestingly, excitotoxicity has been implicated in neurodegeneration. However, a recent study genotyping a much larger cohort did not replicate these findings (Lee et al., 2012). Another possible modifier of age of onset is Peroxisome proliferator-activated receptor gamma, co-activator 1 alpha (*PPARGC1A*) (Taherzadeh-Fard et al., 2009; Weydt et al., 2009), a transcriptional co-activator facilitating its function via the cyclic adenosine monophosphate (cAMP) response element-binding protein (CREB), a transcription factor thought to be affected by the presence of mHTT in a cell (Ross and Poirier, 2004).

Non-genetic modifiers of HD age of onset include lifestyle and physical activity. A questionnaire based study demonstrated that a more passive lifestyle (defined as passive activities lacking physical or intellectual challenges) leads to earlier disease onset (Trembath et al., 2010). Similarly, studies in a mouse model of HD showed that environmental enrichment by adding cardboard, paper and plastic objects into the cages delays disease onset in the R6/1 mouse model of HD (van Dellen et al., 2000). Furthermore, physical activity has been shown to be inversely associated with the risk of dementia (Hamer and Chida, 2009).

1.1.3 Huntingtin

1.1.3.1 Huntingtin protein structure

HTT is a 348 kDa protein encoded by the *HTT* gene, which is ubiquitously expressed throughout the CNS, peripheral tissues and during embryonic development (Li et al., 1993). The CAG repeat located in exon 1 of *HTT* is translated into a polyQ stretch located in the amino (N)-terminus of HTT starting at amino acid 18. The polyQ is followed directly by a poly-proline (P) region, thought to stabilise the polyQ tract and retain HTT's solubility (Southwell et al., 2008; Steffan et al., 2004). While the structure of the whole HTT protein has not yet been resolved, X-ray crystallography has shown that the wild-type protein N17 region (the first 17 amino acids of the HTT protein) is α-helical and that the proline rich region takes a polyP helix II formation. The polyQ (17Q) is more flexible forming an α helix, extended loop and random coil conformation (Kim et al., 2009). While the N17 headpieces can fold back to bind the polyP region in the wild-type protein, this interaction gets weaker once the polyQ domain expands, opening the N-terminus up for possible interactions with other proteins (Dlugosz and Trylska, 2011). Indeed, a yeast-two-hybrid screen found that the HTT polyP region is the

main domain mediating protein-protein interactions. For example, it binds WW domain protein, which contain two highly conserved tryptophan residues (Faber et al., 1998). Changes in HTT protein structure caused by the polyQ expansion, may change the interaction strength between HTT and its interaction partners, causing both loss and gain of function.

HTT also has multiple HEAT (huntingtin, elongation factor 3, the PR65/A subunit of protein phosphatase 2A and the lipid kinase Tor) repeat sequences. These sequences are around 50 amino acids long and comprise two anti-parallel α-helices with a helical hairpin in between (Li et al., 2006). Such HEAT sequences are thought to be involved in protein-protein interactions. The protein also contains a NES (nuclear export sequence) domain near the C-terminus (Xia et al., 2003), but a nuclear localisation signal has not yet been identified.

1.1.3.2 Post-translational modifications of huntingtin

HTT contains several sites for post-translational modifications, which can regulate half-life, localisation, aggregation and toxicity of the protein. Three lysine residues (K6, K9, K15) found immediately prior to the polyQ expansion at the N-terminus of the protein appear to compete for SUMOylation and ubiquitination. SUMOylation of the residues results in nuclear translocation of HTT and promotes its effects on transcription, while ubiquitination induces HTT degradation, reducing HTT toxicity and abrogating neurodegeneration in a *Drosophila* model of HD (Steffan et al., 2004). Furthermore, HTT can be phosphorylated at one threonine (T3) and several serine residues (S13, S16, S421, S434, S536, S1181, S1201, S2076, S2653 and S2657). The effect of phosphorylation varies depending on the residue modified. Phosphorylation of S421 and S434 protects HTT from proteolytic cleavage, while modification of S13 and S16 results in HTT clearance by the ubiquitin-proteasome system (UPS) and via lysosomes (Thompson

et al., 2009). S421 phosphorylation has been shown to modulate vesicle transport (Zala et al., 2008). Acetylation takes place at residues K9, K178, K236, K345 and K444 (Cong et al., 2011), while the pamitoylation side is cysteine 214 (Yanai et al., 2006) (all modification sites are shown in Figure 1.3).

Both wild-type and mutant HTT are cleaved by various proteases, including caspase 2, 3, 6 and 8, cathepsins and calpains, generating a range of fragments (Figure 1.3) (reviewed in (Ross and Tabrizi, 2011)). In addition to proteolysis, CAG repeat length dependent alternative splicing of HTT exon 1 has been shown to result in an short poly-adenylated mRNA that is translated into a HTT exon1 protein fragment (Sathasivam et al., 2013). Fragmentation of HTT may therefore occur on both RNA and protein level. While the physiological role of fragmentation by proteolysis or splicing is unclear, it has been shown that N-terminal mHTT fragments are necessary for pathology and can be more toxic than the full-length protein (Graham et al., 2006). Furthermore, expression of N-terminal mHTT fragments is sufficient to cause HD-like syndromes in animals (Mangiarini et al., 1996).

1.1.4 Wild-type huntingtin function

The function of wild-type HTT is poorly defined due to the large size of the protein and a lack of homology to other proteins. Genetic depletion of *Htt* has shown that HTT is essential in embryonic development and neurogenesis, as $Htt^{-/-}$ mice die during embryogenesis (Nasir et al., 1995; Zeitlin et al., 1995). HTT also plays a crucial role in neuronal function, as conditional knock-out of *Htt* in adult mice causes neural loss (Dragatsis et al., 2000). High levels of apoptosis in the *HTT* knock-out mice suggest an anti-apoptotic role of the protein (Zeitlin et al., 1995). Indeed, overexpression of wild-type *HTT* in an HD mouse model is as

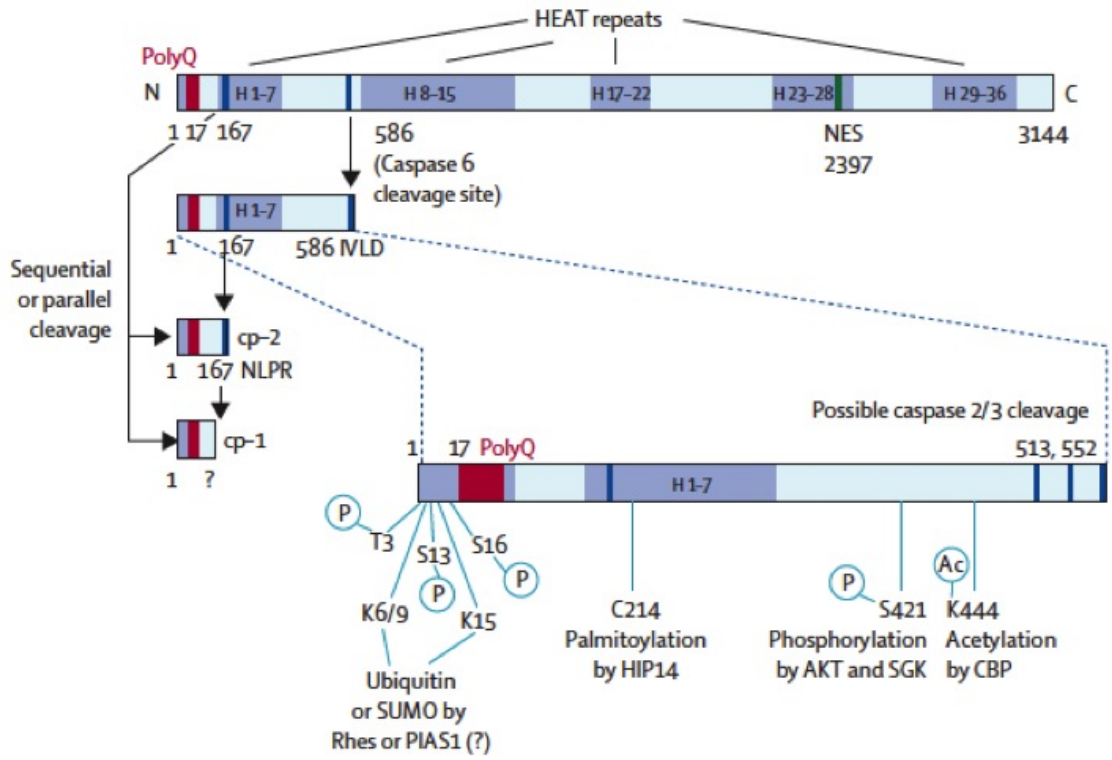

Figure 1.3: HTT protein structure and post-translational modifications. Human huntingtin structure showing protein domains as well as cleavage sides and other post-translational modification sides. Re-printed from The Lancet, Vol.10, *Huntington's disease: from molecular pathogenesis to clinical treatment.*, 83-98, Ross and Tabrizi, ©2011, with permission from Elsevier.

an anti-apoptotic factor and protects striatal neurons from N-methyl- D-aspartate receptor (NMDAR) mediated excitotoxicity (Leavitt et al., 2006).

Further evidence for possible functions of HTT is provided by examining its cellular localisation. Within the cell HTT can be found in the cytoplasm; often associated with microtubules, the Golgi, the endoplasmatic reticulum (ER) and mitochondria (Bhide et al., 1996; Hilditch-Maguire et al., 2000; Panov et al., 2002). HTT has also been detected on the membranes of synaptic and clathrin-coated vesicles of the endocytic or secretory pathway, suggesting HTT may be involved in long- and short-term transport along microtubules, endocytosis, and synaptic vesicle exocytosis and recycling (Velier et al., 1998). Indeed, wild-type HTT

has been shown to be crucial for the transport of brain-derived neurotrophic factor (BDNF) vesicles along microtubules in neurons by binding dynactin via huntingtin-associated protein 1 (HAP1) (Gauthier et al., 2004). Interestingly, BDNF transport is disrupted both in HD and when wild-type HTT levels are reduced, suggesting reduced BDNF levels as one pathogenic pathway for HD due to loss of wild-type protein function.

Additionally, HTT is involved in transcriptional regulation. The protein interacts with transcription factors, and is also proposed to be involved in mRNA and transcription factor shuttling into the nucleus (Imarisio et al., 2008). For example wild-type HTT stimulates transcription of the gene encoding BDNF by sequestering the repressor element-1 transcription factor/neuron restrictive silencer factor (REST/NRSF) in the cytoplasm and thereby inhibiting its repressing function at the BDNF promoter (Zuccato et al., 2003). When HTT is mutated, this interaction is lost and lower levels of BDNF are seen in the brain.

1.1.5 Mutant huntingtin and HD pathogenesis

While the loss of wild-type HTT function may be important for HD pathology, it is commonly thought that a toxic gain of function by mHTT, due to abnormal protein conformation and fragmentation, is the primary cause for HD. This hypothesis is supported by the fact that mHTT expression can substitute wild-type HTT function in mice. While knocking out *Htt* is lethal (Nasir et al., 1995; Zeitlin et al., 1995), mice homozygote for the mutant *Htt* allele such as the *Hdh*$^{150Q/150Q}$ are viable (Lin et al., 2001). Furthermore, heterozygote and homozygote HD patients show no difference in symptom severity (Wexler et al., 1987), demonstrating that a loss of wild-type HTT has a smaller effect than the gain of the mutant allele.

Due to the protein's size and range of interaction partners, mHTT has been shown to cause dysfunction in several cellular pathways, cascades and mechanisms.

The main effects of mHTT are discussed below, and include aggregation, protein degradation pathways, energy metabolism and transcriptional dysregulation. In addition, the reasons why neurons are especially vulnerable to the effects of mHTT expression will be discussed.

1.1.5.1 Aggregate formation

The formation of both intranuclear and cytoplasmic aggregates have been well described in HD patients (DiFiglia et al., 1997) and mouse models (Davies et al., 1997). Whilst wild-type HTT is mainly located in the cytosol, mutated protein relocates to the nucleus where it forms nuclear inclusions. Interestingly, antibody staining has shown that these inclusions are mainly made up from N-terminal fragments, underlining the important role of HTT fragmentation in HD (DiFiglia et al., 1997). However, in addition to inclusions, mHTT is also present diffusely in the nucleus and cytoplasm.

Structurally, toxic mHTT fragments as well as the N-terminus of the full-length mutant protein are composed of a compact hairpin comprised of two β-strands and a turn (reviewed in (Ross and Tabrizi, 2011)). The abnormally folded protein can aggregate and build fibrillar structures, a feature typical of disease-associated misfolded proteins in other neurodegenerative diseases such as Alzheimer's and Parkinson's diseases (Ross and Poirier, 2004; Scherzinger et al., 1999). The kinetics of and exact mechanisms causing the formation of mHTT aggregates are still unclear. However, studies of synthetic polyQ repeats have shown that they can form β-sheets held together by hydrogen bonds, termed polar zippers (Perutz et al., 1994). These polyQ interactions could function as aggregation nuclei by precipitating not only mHTT, but also other polyQ proteins. Kinetics of aggregation are influenced by the surrounding protein domains. Phosphorylation of mHTT at S13 and S16 for example, reduces the accumulation of aggregates

found in HD mouse models and decreases disease pathology (Gu et al., 2009).

The role mHTT aggregates play in disease pathology is still debated. Large intranuclear inclusions have been shown to sequester vital proteins such as transcription factors (Steffan et al., 2000), chaperones (Hay et al., 2004) and ubiquitin (Bennett et al., 2007); thereby interfering with various proteins' normal function. In addition, studies have shown that less mHTT aggregation correlates with improved disease progression (Gu et al., 2009; Mielcarek et al., 2011). Conditional expression of *mHTT* in MSNs demonstrated, however, that the formation of intranuclear mHTT inclusions alone is not sufficient to cause HD pathology (Gu et al., 2007, 2005). Moreover, studies have suggested that the formation of aggregates is a cellular coping mechanism in response to mHTT expression. Interestingly, levels of diffuse intracellular GFP-exon 1 *HTT* rather than the formation of inclusion bodies predict when neuronal death will occur (Arrasate et al., 2004; Miller et al., 2011), highlighting the particular role of monomers and oligomers.

1.1.5.2 Protein degradation pathways

Evidence of mHTT aggregates points towards a defect in protein degradation pathways that normally eliminate damaged or misfolded proteins such as mHTT. Indeed, another effect of mHTT is the inhibition of cellular protein-recycling and degradation pathways, such as the UPS (Bennett et al., 2007) and autophagy (Martinez-Vicente et al., 2010), which add to the accumulation of misfolded proteins.

Ubiquitin, a small regulatory molecule directing proteins to the proteasome to be recycled, has been found to be strongly associated with mHTT inclusions (Bennett et al., 2007; DiFiglia et al., 1997). Therefore, it may be that mHTT is targeted for degradation, but the UPS then fails to do so. Indeed, studies have shown decreased proteasome activity in HD patient's brain and fibroblast cultures (Seo

et al., 2004). Furthermore, it has been hypothesised that the proteasome may not be able to degrade polyQ repeats; and that mHTT could block the proteasome and hinder protein degradation (Holmberg et al., 2004).

Besides the UPS, the principal mechanism for bulk degradation of cytosolic proteins and organelles, autophagy, is also dysfunctional in HD. Large numbers of autophagosomes containing mHTT are found in post-mortem HD brain tissue (Sapp et al., 1997) and HD mouse models (Kegel et al., 2000), suggesting increased levels of autophagy to degrade toxic mHTT. The expansion of the autophagy pathway may however, not result in an increase in proteolysis, as cargo is not loaded effectively into autophagy vesicles in both HD mouse models and HD patient lymphoblasts (Martinez-Vicente et al., 2010).

So while cells have mechanisms to degrade both soluble HTT and mHTT aggregates, the processes are not completely effectual. This makes enhancing protein degradation pathways a promising target for possible therapeutic approaches.

1.1.5.3 Energy metabolism

Mitochondria are another target of mHTT's toxic function, resulting in compromised energy metabolism, altered calcium handling, apoptosis and oxidative damage (Browne, 2008). Mitochondria isolated from HD patient lymphoblasts and HD mouse brains demonstrate reduced membrane potential and depolarisation at lower calcium loads compared with control mitochondria (Milakovic et al., 2006; Panov et al., 2002). Choo et al. also found impairments in Ca^{2+} handling, showing that a lower Ca^{2+} threshold is needed to open mitochondrial permeability transition pores, this dysfunction is linked to mHTT binding the outer mitochondrial membrane (Choo et al., 2004). Depolarisation of the mitochondrial membrane can lead to programmed cell death by release of cytochrome c and increased caspase activity. Indeed, increased apoptosis, cytochrome c release and cas-

pase -3, -8 and -9 activity has been demonstrated in myoblast cell cultures from HD patients (Ciammola et al., 2006). Moreover, neuronal energy metabolism is hindered by mHTT aggregates which block mitochondria transport along processors (Chang et al., 2006).

1.1.5.4 Transcriptional dysregulation

Several studies provide substantial evidence for transcriptional dysregulation in HD. Altered gene expression levels have been observed in both HD patients (Hodges et al., 2006) and HD mouse models (Luthi-Carter et al., 2002, 2000). Interestingly, abnormalities are highly comparable between mouse models and HD patients (Kuhn et al., 2007). Mutant HTT expression in primary striatal neurons has proven the cell-intrinsic effect of mHTT on gene expression (Runne et al., 2008). Transcriptional changes are already apparent long before symptoms onset in the brains of premanifest gene carriers (Dunah et al., 2002), as well as in embryonic stem cells (Feyeux et al., 2012), indicating transcriptional dysregulation as a major contributor to HD pathogenesis.

The CREB binding protein (CBP), a transcriptional co-activator, which links CREB to the basal transcription machinery and plays a role in neuronal survival, is dysregulated in HD (Nucifora et al., 2001). CBP is depleted from its normal nuclear location and interacts with mHTT, both through its histone acetyltransferase (HAT) domain and polyQ tract, whereby it is recruited into HTT aggregates (Kazantsev et al., 1999; Nucifora et al., 2001; Steffan et al., 2000). Several other transcription factors such as Sp1 (specificity protein 1) (Dunah et al., 2002; Li et al., 2002), TBP (TATA-box binding protein) (Schaffar et al., 2004) and p53 (Steffan et al., 2000), have also been shown to selectively interact with the expanded polyQ of mHTT, causing dysregulation of the genes that they control. Interestingly, mHTT also represses components of the basal transcription apparatus such as transcription

factor II D and F (Zhai et al., 2005). Thus, mHTT mostly decreases gene expression by sequestering transcription factors away from the promoters at which they act (Chen-Plotkin et al., 2006). However, mHTT can also directly bind to deoxyribonucleic acid (DNA) and alter DNA conformation and transcription factor binding, also resulting in gene expression changes (Benn et al., 2008).

Besides abnormal transcription factor binding, changes in chromatin remodelling in the form of abnormal histone modification have been demonstrated in HD. Histone H3K9 hyper-methylation, which is known to cause gene repression, has been observed in HD post-mortem brains and mouse models (Ryu et al., 2006). Furthermore, chromatin silencing hypoacetylation of H3 and H4 has been shown at promoters of genes down-regulated in HD (Labbadia et al., 2011; Sadri-Vakili et al., 2007). In keeping with the observation that the majority of dysregulated genes in HD are down-regulated, this suggests a possible general shift towards a more repressive chromatin state in HD. Taken together these findings suggest a central role for transcriptional dysregulation in HD pathogenesis.

1.1.5.5 Specific vulnerability of neurons

While HTT is expressed in all cells of the body, the CNS and specifically MSNs are the most severely affected areas/cells in the body. The origin of this selective vulnerability remains unclear, but a number of theories have been postulated and some are discussed below.

One of the first mechanisms proposed for selective vulnerability is excitotoxicity. In contrast to relatively spared, interneurons, MSNs express high levels of the NMDAR, which can be activated by glutamate. Overactivation of the receptor causes abnormal Ca^{2+} influx, resulting in apoptosis (Nicholls, 2009). *In vivo* stimulation of NMDAR in rats using its agonist quinolinic acid causes striatal lesion and resembles HD closely (Beal et al., 1991; Schwarcz et al., 1983), sup-

porting the hypothesis of excitotoxicity as a major pathogenic pathway in HD. Indeed, metabolites of the kynurenine 3-monooxygenase (KMO) pathway such as 3-hydroxykynurenine and quinolinic acid are elevated in HD brain (Guidetti et al., 2006). Furthermore, glutamate removal from synapses by glial cells is reduced in HD leaving elevated levels of the neurotransmitter in the HD brain (Liévens et al., 2001). Thus, increased levels of these neurotransmitters may cause excitotoxicity in MSNs in HD leading to striatal atrophy.

Another possible reason for increased atrophy in the striatum over other regions is altered BDNF signalling. BNDF is a neurotrophin implicated in neurogenesis, neuronal differentiation, neuronal survival and synaptic plasticity. As described in Section 1.1.4, loss of wild-type HTT levels causes reduced BDNF levels in HD patient brains due to both transcriptional dysregulation and trafficking defects (Gauthier et al., 2004; Zuccato et al., 2001, 2003). Major sites of BDNF synthesis are the hippocampus and cortex, while the striatum, even though it contains similar levels of BDNF, has no means of BNDF production on its own and depends on delivery of the neurotrophin from the cortex (Altar et al., 1997). This may result in a greater effect of defective BDNF trafficking on the striatum then other parts of the brain.

Whether either of the mechanisms described above explain selective cellular vulnerabilities is still debated. It is clear however, that while they contribute to HD pathology, neither of them explains all the defects found in HD patients, such as wide spread transcriptional dysregulation and defects in metabolism. This suggests multiple pathogenic mechanisms in HD rather than just one cause.

1.1.6 Models of Huntington's disease

Representative experimental animal models allow the investigation of human disease to better understand the underlying biology in ways impossible in human patients. Moreover, animal models are crucial to test experimental therapeutics. Since the discovery of the HD gene, a variety of animal models have been established to help study the disease. While cell culture, fly (Kazemi-Esfarjani and Benzer, 2000) and worm (Parker et al., 2001) models are helpful in understanding the basics of HD pathology and high-throughput drug screens (Voisine et al., 2007), their similarities to the human disease is limited (*C. elegans* genome is only 40 % homologous to the human one). Investigating the effects of a CAG expansion in the *HTT* gene on the mammalian organism is crucial to understand complex disease pathology. Transgenic mice are the most commonly used model organism in the HD field, but rat (von Hörsten et al., 2003), pig (Yang et al., 2010), sheep (Jacobsen et al., 2010) and monkey (Yang et al., 2008) models are also used.

HD mouse models can be classified depending on how they were generated. Transgenic fragment models express an N-terminal part of *HTT* rather than the full-length gene, while full-length models express the entire *HTT* sequence. So called knock-in models also express the whole gene, but are generated by expanding the CAG repeat in the original mouse *Htt* gene allowing expression of the mHTT at normal allelic levels.

1.1.6.1 Fragment mouse models of HD

The R6/2 model was the first transgenic HD model to be developed and is currently the most commonly used in research. The mice ubiquitously express a transgene for the 5' end of the human *HTT* gene carrying only exon 1, including

150 CAG repeats (Mangiarini et al., 1996). As the mouse model does not express the full-length *HTT* gene, it is referred to as a fragment model. The age of disease onset in the R6/2 mice is around 8 weeks and death occurs between weeks 12 and 15 (Li et al., 2005). The mice display a progressive neurological phenotype including motor features such as resting tremor, movements resembling chorea and stereotypic involuntary movements. The underlying brain pathology shows a 20% reduction in brain volume in R6/2 mice when compared with wild-type (WT) mice, although no significant neuronal loss is detected (Mangiarini et al., 1996). Widespread HTT inclusions are found in the brains of R6/2 mice (Meade et al., 2002) and intranuclear inclusions, present before symptom onset are strikingly similar to the human phenotype (Davies et al., 1997). Detailed behavioural testing reveals motor deficits in form of reduced rotarod and balance beam performance, as well as learning difficulties in the T-maze and Morris water maze (Carter et al., 1999; Lione et al., 1999). R6/2 mice also demonstrate peripheral changes such as weight loss and muscle wasting (van der Burg et al., 2008), key features of the human disease. At the weaning age of 3 weeks, the R6/2 mice are no different to WT mice, but with the development of motor features, the weight of the mice starts to decrease. In addition, R6/2 females are sterile while males are not (Mangiarini et al., 1996). Further mimicking the peripheral phenotypes of HD patients, R6/2 mice develop diabetes (Björkqvist et al., 2005) and show changes in their hypothalamic-endocrine system (Björkqvist et al., 2006).

The mice display an aggressive and fast-progressing form of HD, although they only express the first of the 67 exons of *HTT*. This highlights the importance of the N-terminus and polyQ domain of the HTT protein. However, the potentially important process of HTT proteolytic cleavage cannot be modelled in a fragment model.

The HD-N171 mouse is another transgenic mouse model used less widely. The mice express the first 171 amino acids of HTT carrying 82Q under the control of the *PRNP* promoter. They display a similar phenotype to the R6/2 model, but with a less aggressive progression. Motor deficits start at 4 months of age and end-stage disease is reached after around 6 months (Schilling et al., 1999).

1.1.6.2 Full-length HD mouse models

The most commonly used full-length HD models are the bacterial artificial chromosome (BAC) and yeast artificial chromosome (YAC) HD mice, expressing the full-length human *HTT* gene under its own promoter.

While the YAC mice are available with 46 or 72 polyQ repeats (Hodgson et al., 1999), the most commonly used mice carries 128Q (Slow et al., 2003). A control line carrying a normal polyQ of 18Q is also available (Hodgson et al., 1999). The YAC128 mice initially exhibit hyperactivity and develop progressive motor deficits from the age of 6 months. At 12 months of age, the disease progresses to hypokinesis (Slow et al., 2003). Cognitive impairments, manifest as poor performance in a swimming T-maze test, are also apparent in YAC128 mice (Van Raamsdonk et al., 2005a). Within the brain YAC128 mice demonstrate selective degeneration similar to the pattern seen in HD patients. Significant atrophy is seen in the striatum, globus pallidus and cortex while the hippocampus and cerebellum are spared (Van Raamsdonk et al., 2005b). Appearance of nuclear mHTT inclusions coincides with onset of behavioural abnormalities and occur with greater prevalence in atrophy-prone brain regions (Van Raamsdonk et al., 2005b).

BACHD mice carry 97Q and, similar to the YAC128 mice, demonstrate slow disease progression with a normal life span. Motor deficits are first detected at 2 months and manifest robustly around 6 months of age, although no brain atrophy is detected at this age. After 12 months of age, selective neurodegeneration,

primarily in the striatum and cortex, is seen in BACHD mice (Gray et al., 2008).

Interestingly, both the YAC128 and BACHD mice are 20-30 % heavier than WT mice at all ages (Gray et al., 2008; Slow et al., 2003). Weight loss is a major feature of HD and is observed in other mouse models (see Section 1.1.6.1 and 1.1.6.3).

1.1.6.3 Knock-in HD mouse models

The most commonly used knock-in models for HD are the *Hdh*^{Q111} (Wheeler et al., 1999), CAG140 (Menalled et al., 2003) and *Hdh*$^{150Q/150Q}$ (Lin et al., 2001) mice, in which 111, 140 or 150 CAG repeats, respectively, were inserted via gene targeting into the endogenously expressed *Htt* gene. Overall the knock-in models have milder phenotypes and a later onset than other models. The CAG140 mice for example do not show motor symptoms before 1 year of age (Menalled et al., 2003). For *Hdh*$^{150Q/150Q}$, disease onset can be observed from 12 months when weight starts to drop, to 18 months of age when the motor task deficits are first noted (Woodman et al., 2007). A recent report found cognitive impairments as early as 6 months of age, showing deficits in a water maze test (Brooks et al., 2012). At 22 months, *Hdh*$^{150Q/150Q}$ mice demonstrate a phenotype similar to 12 week old R6/2 mice, including features such as transcriptional dysregulation in the striatum and cerebellum, and 20% weight loss (Woodman et al., 2007). Furthermore behavioural and motor deficits, including gait abnormalities, loss of grip strength and reduced performance at motor tasks, are also observed (Lin et al., 2001). Widespread Htt aggregates are also detected in the brain and peripheral organs of *Hdh*$^{150Q/150Q}$ mice (Moffitt et al., 2009).

In this study, one model of each of the three categories was used to evaluate immune function and an overview of all three can be found in Table 1.1.

Table 1.1: Overview of HD mouse models used in this thesis.

	R6/2 mice	*Hdh*$^{150Q/150Q}$	YAC128
gene	human *HTT* carrying only exon 1	expansion inserted in the endogenous gene - both alleles	entire human gene
CAG repeat length	150	150	128 (control line expressing 18)
age of onset	8 weeks	12-18 months	6-9 months
late stage	12-15 weeks	22 months	12 months
motor phenotype	resting tremor, movements resembling chorea and involuntary movements	gait abnormalities, loss of grip strength	Motor deficits as the other models, with hypokinesis late on
brain pathology	20 % reduction in brain volume, but no significant neuronal loss	Similar to R6/2, transcriptional dysregulation found	specific cortical and striatal atrophy, with striatal neuron loss
peripheral phenotypes	weight loss, muscle wasting, diabetes	20 % weight loss	no weight loss-mice are fat
usage	widely used	less widely used	widely used

1.1.7 Therapeutic intervention in HD

1.1.7.1 Treatment of symptoms

While no treatment to slow disease progression is available, a wide range of symptomatic drug treatments are available for HD (reviewed in (Novak and Tabrizi, 2010; Ross and Tabrizi, 2011)). Chorea, one of the most prominent motor phenotypes in HD, is commonly treated with neuroleptics such as olanzapine, risperidone and haloperidol. Tetrabenazine, the first HD specific symptomatic drug approved by the FDA (food and drug administration, USA), is a dopamine-depleting agent used to treat chorea. Selective serotonin reuptake inhibitors such as citalopram and fluoxetine are given to HD patients to treat depression, anxiety or aggression. In addition, non-pharmacological treatments such as physiotherapy to strengthen gait and balance, and nutritional advice to counteract weight loss are important to improve the quality of life for HD patients.

1.1.7.2 Strategies to slow disease progression

To date, no cure or treatments to slow the progression of the disease are available. However, a large amount of research is focused on finding an effective disease-modifying therapy and several putative approaches are discussed below.

Targeting transcriptional dysregulation

One possible therapeutic target is the transcriptional dysregulation caused by mHTT. The use of histone deacetylases (HDACs) inhibitors could prevent the chromatin silencing, hypoacetylation of H3 and H4 found in HD (Labbadia et al., 2011; Sadri-Vakili et al., 2007) and open chromatin up again. HDACs inhibitors are already used in cancer and several compounds are available for potential

clinical trials. In HD, the HDAC inhibitors sodium butyrate (Ferrante et al., 2003) and SAHA (suberoylanilide hydroxamic acid) (Hockly et al., 2003) have been shown to improve motor deficits in the R6/2 mouse model of HD by increasing histone acetylation both in the brain and periphery. Further studies revealed that SAHA decreases HDAC4 and HDAC2 protein levels in the cortex (Mielcarek et al., 2011). As SAHA treatment demonstrates toxic side effect (weight loss) in mice (Hockly et al., 2003), other HDAC4 inhibitors are now being investigated.

Improvement of neuronal function

One way to improve neuronal function and stop neuronal loss is to block excitotoxicity caused by overactivation of the NMDAR by glutamate or kynurenine metabolites. Glutamate receptor antagonists such as rituzole and memantine have shown promise in HD mouse models, but have shown little effect in clinical settings (Mestre et al., 2009; Milnerwood et al., 2010). Modulation of the KMO pathway to reduce the levels of the NMDAR agonists 3-hydroxykynurenine and quinolinic acid, while increasing the levels of the neuroprotective NMDAR antagonist kynurenic acid, has shown beneficial effects in yeast, fly and mouse models of HD (Campesan et al., 2011; Giorgini et al., 2005; Zwilling et al., 2011).

Another possible way to improve neuronal function in HD is to increase the levels of the neurotrophin BDNF, which is depleted in the HD brain (Gauthier et al., 2004; Zuccato et al., 2003). Indeed, overexpression of the *BDNF* gene in YAC128 prevented neuronal loss and motor abnormalities (Xie et al., 2010). Adenoviral administration of BDNF into the striatum of R6/2 mice delayed motor impairments and prolonged survival (Cho et al., 2007), demonstrating the promise of this strategy.

Cellular replacement therapy

Given the striking loss of striatal MSNs early on in the disease, cell replacement therapies may have great therapeutic potential in later stages of the disease. Several studies using allogenic striatal cell grafts in rodent (Hurelbrink et al., 2002; Pundt et al., 1996) and non-human primates (Palfi et al., 1998) demonstrate graft integration and recovery of motor and cognitive function. These findings promoted several clinical studies with mixed outcome (reviewed in (Benraiss and Goldman, 2011)). While some studies saw no clear clinical improvements (Furtado et al., 2005; Kopyov et al., 1998), other groups reported temporary functional integration of the graft and clinical stabilisation (Bachoud-Lévi et al., 2000). One major drawback for this approach is the limited access and ethical concerns surrounding fetal donor cells. Readily renewable sources for transplants have therefore been investigated. Human embryonic stem cells (hESCs) can be differentiated into MSNs *in vitro* and integrate *in vivo* following xenotransplantation in rats (Aubry et al., 2008). However, ESC-derived grafts have been reported to induce formation of teratomas (Roy et al., 2006). Another problem, using allogenic graft, is the immune response the host may mount towards the graft.

In a new approach, inducible pluripotent stem cells (iPSCs) isolated and engineered from the patient themselves, are being considered for use, avoiding activation of the immune system. This strategy involves genetically reprogramming fibroblasts to iPSCs (Park et al., 2008; Takahashi et al., 2007), before correcting the CAG repeat expansion via homologous recombination, differentiating the cells into MSNs and transplanting the cells into the brain of the patient. So far, several human HD iPSC lines have been established (The HD IPSC Consortium, 2012) and it has been shown that correction of the CAG repeat in iPSCs can reverse mHTT-driven transcription changes (An et al., 2012). Furthermore, iPSCs differentiate into DARPP-32 positive striatal neurons *in vitro* and *in vivo* (in mice)

after correction of the CAG repeat, demonstrating the potential of this approach for therapy (An et al., 2012).

HTT lowering therapies

A conditional *mHTT* exon 1 expressing mouse model, in which *mHTT* expressing can be turned off using doxocycline, showed that lowering the mHTT load in mice improves brain pathology and behavioural phenotypes (Yamamoto et al., 2000). For therapy, HTT load can be reduced by either lowering *mHTT* transcript expression levels using RNA interference (RNAi) or antisense oligonucleotides (ASOs), or by increasing the clearance of mHTT protein.

In order to enhance mHTT clearance, the autophagy pathway can be stimulated (Renna et al., 2010). The use of the autophagy activator rapamycin demonstrates a decrease in toxic effects in fly and mouse HD models (Ravikumar et al., 2004). However, the stimulation of cellular protein degradation processes is not specific to one protein and therefore leads to increased degradation of all proteins, increasing the likelihood of unwanted side-effects.

Small interfering RNAs (siRNA), short hairpin RNA (shRNA) or ASOs, on the other hand, can be designed to be highly selective for the *HTT* mRNA transcript. Both siRNA and shRNA use the cell's internal micro RNA (miRNA) pathway (Sah and Aronin, 2011). While miRNAs are naturally encoded in the genome, shRNAs are delivered and inserted into the genome via viral transduction. The sequences of both RNAs are then transcribed and cleaved by drosha into hairpin RNAs. Once exported into the cytoplasm via exportin-5, the hairpins are cut by dicer into double stranded RNA (dsRNA). siRNA is already a dsRNA molecule and is delivered into the cytoplasm, joining the miRNA pathway at this stage. All three types of short RNA can now be incorporated into the RNAi silencing complex (RISC), where the active guide strand can bind the corresponding target mRNA, activating

argonaut-2 mediated cleavage and RNA degradation (Rand et al., 2005). ASOs are single stranded 15-25 bp long oligonucleotides, which also bind their target mRNA and either cause RNase-H-mediated degradation of the target mRNA or physically hinder protein translation (Bennett and Swayze, 2010).

When discussing gene silencing approaches for HD, one main question is whether to lower gene expression of both the wild-type and mutant *HTT* alleles, or to take a *mHTT* specific approach. Since wild-type HTT has a range of functions (discussed in Section 1.1.4), lowering wild-type *HTT* levels in cells may have deleterious effects on the cells. Indeed, *HTT* knock-out mice die during embryogenesis at day E8.5 (Nasir et al., 1995; Zeitlin et al., 1995) and deletion of wild-type HTT in adult mice causes neuronal loss (especially in the striatum and cortex), motor deficits and behavioural changes (Dragatsis et al., 2000), underlining the crucial role wild-type HTT plays in brain development and function.

Initial proof-of-principle studies have knocked-down *mHTT* by targeting regions specific to the human *mHTT* transgene used to generate the mouse (Harper et al., 2005; Rodriguez-Lebron et al., 2005). These studies showed that partial lowering of mHTT load (around 70 %) can reduce neuropathology, improve motor behaviour and extend life in HD-N171(Harper et al., 2005) and R6/1 mouse models (Rodriguez-Lebron et al., 2005). Interestingly, suppressing wild-type HTT expression by 60 % in the striatum of mice was found to be tolerated for at least four months (McBride et al., 2008). Furthermore, non-allele-specific silencing, by injection of shRNA containing adeno-associated virus (AAV) into the striatum, has been shown to improve HD phenotypes, while being tolerated in the HD-N171 mice (Boudreau et al., 2009). These data suggest that non-allele-specific silencing may also be usable as therapy for HD, although more research is needed to determine the effects of lowering wild-type *HTT* levels in the cells. Nonetheless, the prospect of total HTT lowering as therapy is positive, seen that allele-specific

silencing is likely not to be available for all HD patients. While RNAi is not able to distinguish between HTT alleles carrying different length CAG repeats, several single nucleotide polymorphisms (SNPs) have been identified in the *HTT* gene, three of which are associated with 75 % of HD patients and can be targeted with five siRNAs (Lombardi et al., 2009; Pfister et al., 2009). This leaves 25 % of HD patient without targetable differences between their wild-type and mutant allele at this point in time. Additionally, all different SNP targeting siRNA are likely to need separate safety and toxicity evaluations and trials, demonstrating the practical advantages of one siRNA targeting total *HTT* (Sah and Aronin, 2011).

Consistent *in vivo* delivery of the siRNA or ASOs is crucial in CNS disorders. While peripheral administration is less invasive and capable of targeting peripheral tissues affected in the disease, crossing of the blood brain barrier (BBB) is challenging. Direct delivery into the brain via intraparenchymal or intracerreboventricular routes are a way around this and have been used successfully in different HD mouse models using both RNAi (Boudreau et al., 2009; DiFiglia et al., 2007) and ASOs (Carroll et al., 2011). Using *rhesus macaques*, it has been shown that RNAi delivery into the brain is also safe in larger mammals, although distribution within the brain and away from the injection site has been limited (McBride et al., 2011). Implantable infusion systems are used in trials for Parkinson's disease to deliver glia-cell derived neurotrophic factor (Lang et al., 2006; Patel et al., 2005) and could be used in HD. However, peripheral administration using subtypes of AAV (e.g. AAV9) known to pass the BBB should be investigated for the use in HD, as they are less invasive and also target peripheral organs, which are known to also be affected in HD (van der Burg et al., 2009).

Treatment in the premanifest phase of disease

In the search for a treatment, it is important to note that a significant amount of neuronal loss occurs before clinical onset of the disease. Treatment of premanifest gene carriers would be optimal to rescue this neuronal function. As HD is caused by a single, fully penetrant mutation in the *HTT* gene, HD gene carriers can be identified before onset of clinical symptoms. This allows the study of pathogenic events preceding clinical onset by many years and makes pre-symptomatic treatment a feasible possibility (reviewed in (Ross and Tabrizi, 2011)).

However, in order to treat HD gene carriers without symptoms, robust biomarkers are needed to track the success of any treatment. These biomarkers should track with disease progression and already be changed in premanifest gene carrier, while not being present in the control population. So far a range of clinical assessments in the form of motor and cognitive tasks, and neuroimaging measures have been validated as endpoints for clinical trials. A set of nineteen cognitive tasks assessing psychomotor, memory and facial recognition has proven sensitive to distinguish individuals according to the time to predicted onset (Stout et al., 2011). The TRACK-HD study further identified emotion recognition and speed tapping tasks as clinical endpoints for trials (Tabrizi et al., 2012). Using 3 tesla magnetic resonance imaging (3T MRI), striatum and white matter atrophy were found to be significantly increased in premanifest gene carriers compared with controls over 24 months (Tabrizi et al., 2012). Given the need to measure atrophy rates over 24 months to acquire robust data usable as biomarker, the need for new instantly measurable biomarkers remains high.

Biochemical biomarkers are molecules that can be measured in body fluids. The use of cerebrospinal fluid (CFS) is particularly appealing as it carries high concentrations of brain proteins, but due to the invasive nature of lumbar puncture

the method is less usable in a clinical setting for HD. Blood samples on the other hand, are easy to acquire and contain molecules from the periphery and CNS. In addition dysfunction of blood cells (Björkqvist et al., 2008) may also be quantifiable as biomarker. Discrepant and highly variable findings from many biochemical compounds tested so far limit their potential as biomarkers and no robust wet biomarker has been identified for HD yet. However, increased levels of 8-hydroxy-2-deoxyguanosine and pro-inflammatory cytokines interleukin (IL)-6 and tumour necrosis factor (TNF)α, and decreased levels of (insulin-like growth factor) IGF-1, BDNF, glutathione peroxidase and copperzinc superoxide dismutase all show promise as possible biomarkers (reviewed in (Weir et al., 2011)), but further work to validate each of these molecules is needed.

1.2 The immune system

The immune system is a collection of various haematopoietic cells and molecules, which work together to protect the body from infectious organisms and the damage these may cause. In order to protect individuals effectively against diseases, the immune system has to recognise and detect the infection to then eliminate it. The immune system is subdivided in two arms: the innate and the adaptive immune system (Walport et al., 2008).

1.2.1 The innate immune system

The innate immune system provides immediate defence against pathogens by a process called inflammation. Specialised chemical mediators, such as cytokines and chemokines, are produced at the site of infection, and innate immune cells such as monocytes, macrophages, dendritic cells (DCs) and granulocytes are thereby recruited. These cells have the ability to identify simple, regularly oc-

curring molecules on microbes, called pathogen-associated molecular patterns (PAMPs) with their germ line-encoded pattern recognition receptors (PRRs). Depending on the cell type, they can either kill the microbe by releasing toxic substances (granulocytes) or phagocytose them (macrophages and DCs). Engulfing the microorganism not only aids the clearance of the infection locally, but is also the first step to activate the adaptive immune system as it results in antigen presentation (Walport et al., 2008).

1.2.1.1 Haematopoiesis of myeloid cells

Haematopoietic stem cells (HSC) are located within the bone marrow and give rise to all blood cell types, including lymphocytes, myeloid cell, erythrocytes and megakaryocytes, the cells producing platelets. HSCs differentiate into multipotent progenitor (MPP) cells before committing to common lymphoid progenitors (CLPs) or common myeloid progenitors (CMPs). CMPs can then either become megakaryocyte/erythrocyte progenitors or granulocyte/monocyte progenitors (GM-CFUs) (Gereige and Mikkola, 2009).

During development, the first wave of haematopoietic progenitors appear in the extra-embryonic yolk sack leading to the production of primitive macrophages (Gordon and Taylor, 2005). Later during fetal development, progenitor cells start colonising in the fetal liver and produces large numbers of macrophages, which in turn migrate to all organs to establish tissue macrophages populations (Gordon and Taylor, 2005). In adults, monocytes differentiate within the bone marrow. GM-CFUs differentiate via different developmental stages such as macrophages colony-forming unit (M-CFU), monoblasts and pro-monocytes, into inflammatory monocytes and enter the blood stream (Figure 1.4). These circulating monocytes patrol the blood stream for danger signals and can migrate into tissues to give rise to different antigen presenting cells: tissue resident macrophages and DCs.

Recruitment into tissues is increased by pro-inflammatory and metabolic stimuli, contributing to host defense and tissue repair (Gordon and Taylor, 2005). Research into the origin of the brain macrophage population has shown that these cells, called microglia, originate from a erythromyeloid precursor during the initial wave of haematopoisis in the yolk sack and not from blood monocytes like the other tissue macrophage types (Chan et al., 2007; Ginhoux et al., 2010; Kierdorf et al., 2013).

It is to note that, while monocytes can differentiate into DCs, classical DCs and plasmacytoid DC differentiate directly from CMPs. Furthermore, the lymphoid DC subtype originated directly from CLPs (Geissmann et al., 2010).

1.2.1.2 Monocytes

Monocytes are a heterogenous population compromising 10 % of peripheral blood leukocytes in humans and 4% in mouse. The cells vary in size as well as nuclear morphology and degree of granularity (Auffray et al., 2009). In humans, monocytes are characterised by their high surface expression of Cluster of differentiation (CD)14. Depending on CD16 expression levels on the cell surface, two monocyte subtypes are functionally distinguishable: $CD14^{high}$ $CD16^{-}$ monocytes and $CD14^{+}$ $CD16^{+}$ monocytes (Passlick et al., 1989).

All monocytes circulating in the blood stream will migrate into different tissues sooner or later. Therefore, monocytes express different chemokine receptors. Chemokines are small molecules that establish a chemotactic gradient from their release point, which attracts cells carrying the corresponding receptor. The monocyte chemoattractant protein 1 (MCP-1, also called CCL2) is one of the key regulators of monocyte and macrophage migration during inflammation, and acts via its cell surface receptor (CCR2). Interestingly, monocytes and macrophages are also the main producer of MCP-1 (Deshmane et al., 2009). Classical $CD14^{high}$

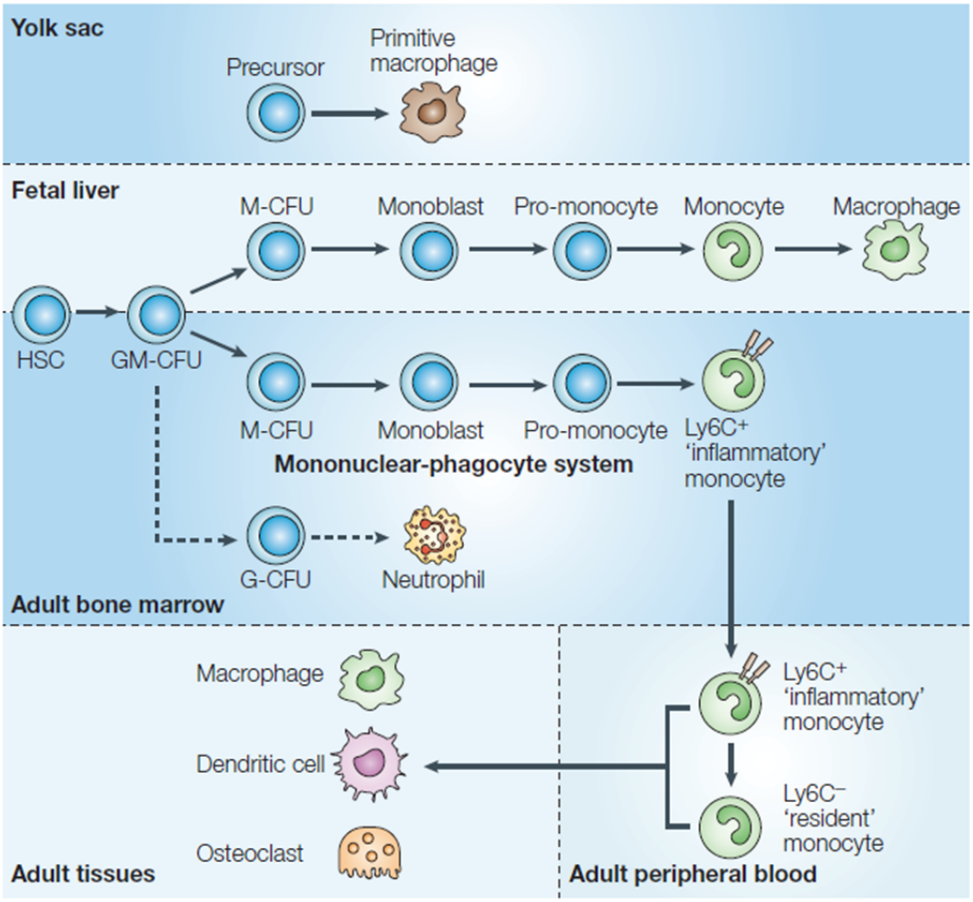

Figure 1.4: Development of monocytes, macrophages and DCs. Fetal and adult monocyte development shown from its origin in the bone marrow over blood to their final destination in different tissue. HSC: haematopoietic stem cell, GM-CFS: granulocyte/macrophage colony-forming units, M-CFU: macrophage colony-forming units, G-CFU: granulocyte colony-forming units. Reprinted by permission from Macmillan Publishers Ltd: Nature Reviews Immunology, Gordon and Taylor, 2005. ©2005.

$CD16^-$ monocytes express high levels of the CCR2 chemokine receptor, whilst $CD14^+CD16^+$ monocytes express CCR5 and not CCR2. It is therefore thought that $CD14^{high}$ $CD16^-$ monocytes circulate in the blood and respond to inflammatory activators such as MCP-1, while $CD14^+$ $CD16^+$ monocytes represent a more mature phenotype found in one place in the tissue producing high levels of pro-inflammatory cytokines (Ziegler-Heitbrock, 2007). In mouse, monocytes express CD11b and two subsets similar to humans are distinguishable: $CCR2^+CXCR1^-$ $Ly6C^+$ migratory monocytes and $CCR2^-$ $CXCR1^+$ $Ly6C^-$ resident, inflammatory monocytes (Gordon and Taylor, 2005).

1.2.1.3 Macrophages

Tissue-specific macrophages are the resident phagocytic cells and play an important role in homeostasis as well as inflammation. They are highly specialised after differentiation and demonstrate different phenotypes depending on their location (Gordon and Taylor, 2005). For example, osteoclasts are macrophages specialised in bone remodelling and Kupffer cells can be found in the liver clearing debris from the blood and regenerating liver tissue after damage (Mosser and Edwards, 2008; Pollard, 2009).

The CNS is populated by more than one type of macrophage. Microglia are distributed equally throughout the brain, while perivascular macrophages and meningeal macrophages can only be found in regions where they are exposed to circulating blood. Interestingly, while all three cell types are from mesenchymal/ myeloid origin, microglia demonstrate distinct differences from the other central and peripheral macrophage types. Firstly, while macrophages are typically round, microglia have numerous process extensions with which the cells constantly and actively survey the whole brain (Nimmerjahn et al., 2005). Secondly, microglia demonstrate an actively repressed phenotype compared with other tissue macrophage populations. Interactions between neurons and microglia, e.g. the interaction between surface molecule CD200 and its receptor CD200R, keeps microglia in their inactive state. Disturbance of this interaction, for example by neuronal loss leads to activation of microglia (Hoek et al., 2000). Thirdly, macrophages and microglia differ in the way they can be activated (Ransohoff and Perry, 2009). Peripheral macrophages respond to both stranger signals (e.g. lipopolysaccharide (LPS) or dsRNA) and danger signals (cytokines such as TNFα). Macrophages can be activated either classically with LPS and type-1 cytokines such as interferon (IFN)-γ or alternatively with IL-4 and IL-10. Classically activated macrophages usually produce pro-inflammatory

response triggering cytokines such as IL-6, IL-1, IL-12 and TNF-α as well as reactive nitrogen and oxygen species (NO, superoxide). Alternatively activated macrophages are more anti-inflammatory, producing low levels of IL-6 and IL-1, but high levels of IL-10 and transformation growth factor (TGF)-β (Martinez et al., 2006; Van Ginderachter et al., 2006). Triggers for microglia activation are distinctively different. Microglia are located behind the BBB and therefore normally protected from serum proteins. The presence of serum protein such as fibrinogen indicates a breach of BBB integrity and activates microglia (Adams et al., 2007). Given their close interaction with neurons in steady state, microglia are also activated by changes in neurotransmitter levels such as glutamate and adenosine triphosphate (ATP) (Haynes et al., 2006; Taylor et al., 2003), and by the loss of neuronal input (Hoek et al., 2000). But microglia also respond to chemokine and cytokine similar to peripheral macrophages (reviewed in (Ransohoff and Perry, 2009)). Thus, while microglia are from the same myeloid progenitor as other peripheral macrophages they differ distinctively, while sharing some signalling cascades such as NFκB.

Tissues are populated by macrophages and DCs during development, raising the question as to whether these populations are self-renewing or constantly replenished by infiltrating blood monocytes. Most tissue-specific macrophage populations are thought to be self-renewing under steady state conditions but can be replenished from blood monocytes under stress/inflammation (Merad et al., 2002). Microglia, however, seem to originate from erythromyeloid precursors during the first wave of haematopoiesis in the embryo (Kierdorf et al., 2013) and be sustained by self-renewal life long (Ajami et al., 2007). During inflammation microglia expand rapidly locally, causing microgliosis solely by expansion of the endogenous microglia population with little contribution and infiltration of peripheral cells (Ajami et al., 2007). While microglia are self-renewing, stem cells are capable of replenishing the microglia pool in the brain. This has been shown using trans-

plantation studies in which lethally irradiated mice were injected with green fluorescent stem cells (Simard and Rivest, 2004). The cells migrated into the CNS and differentiated into fully functional microglia. However, while this proves the haematopoetic origin of microglia, it does not model steady state conditions as γ-whole body irradiation induces temporary holes in the BBB allowing infiltration of peripheral cells (Diserbo et al., 2002).

1.2.1.4 Innate immune cell function

In response to inflammatory stimuli, peripheral as well as central innate immune cells migrate to the site of infection or injury. They produce increased levels of cytokines, chemokines and other inflammation markers in order to recruit and activate other immune cells. Furthermore, presentation of antigens to the adaptive immune system is a key function of macrophages and DCs. The cells acquire these antigens via phagocytosis. Protein fragments of the particles taking up can then be processed and presented to T cells via major histocompatibility complex (MHC) class II (Walport et al., 2008).

Migration

Blood monocytes and tissue macrophages can, once activated by a danger signal, migrate into tissues or secondary lymphoid tissues, respectively. Migration is driven by chemoattractants forming a gradient towards the site of infection, requires adhesive interactions between the leukocytes and endothelial cells, and remodeling of the actin cytoskeleton.

Actin is a 42 kDa protein, which in monomeric form is called globular (G)-actin. G-actin can be transformed into a polymeric filament (F-actin) by binding of ATP which stimulates the formation of G-actin dimers, which function as nucleation

sites for the formation of long filaments. F-actin fibres are polarised with a barbed-end which is elongated. Capping of the barbed-end stops filament growth (Stossel et al., 2006). This process is regulated and modulated by different intracellular molecules and signalling pathways.

On immune cells, chemokine receptors, which are typically guanosine-5'-diphosphate (GDP) heterotrimeric G-protein binding serpentine receptors, induce a signalling cascade modulating the actin cytoskeleton. Activation of the phosphatidylinositide 3-kinases (PI3K) leads to the phosphorylation of phosphatidylinositol (4,5)-bisphosphate (PIP_2) to PIP_3, which can in turn activate guanine nucleotide exchange factors (GEFs). GEFs switch Rho GTPases, the critical signal transducer between membrane receptors and the cytoskeleton, from an inactivated state binding GDP to an activated guanosine-5'-triphosphate (GTP)-bound state (Jones, 2000). Members of the Rho family include RhoA (formation of stress fibres), Rac1 (formation of lammelipodia) and CDC42 (formation of filopodia) (Nobes and Hall, 1995). Upon activation, Rho GTPases interact with various proteins to initiate actin polymerisation. One protein complex they interact with is the actin-related protein 2/3 (ARP2/3) complex. ARP2/3 binds, mediated by Wiskott-Aldrich syndrome proteins (WASP), pre-existing actin filaments and functions as a nucleation seed, mimicking dimeric G-actin, for polymerisation of new actin branches (Prehoda et al., 2000). Linear elongation of actin without branching is mediated by formins, which remain bound to the growing end of the actin fibre and mediate linear polymerisation (Chesarone et al., 2010). Profilin aids polymerisation, by binding G-actin, catalysing the exchange of adenosine diphosphate (ADP) to ATP on the actin monomers and recruiting the actin-ATP monomer to a barbed end of a actin filament (Kang et al., 1999). Other proteins such as cofilin severs existing actin filaments and contribute to actin dissociation. Cofilin is inhibited by phosphorylation, allowing F-actin growth. In the leading edge actin severing generates new actin filaments to which ARP2/3 can bind and stimulate

branching (Ridley, 2011).

Reorganisation of the actin network and polymerisation of actin filaments against cell membranes provides the force necessary for cellular movement, which occurs in three steps (Figure 1.5) (Mattila and Lappalainen, 2008). At first, protrusive structures, called lamellipodia and filopodia, form at the leading edge. Lamellipodia are thin (0.1-0.2 μm) sheet like structures containing a branched network of actin. Filopodia are 0.1-0.2 μm in diameter and up to 20 μm long finger-like structures developing on the edge of the lammelipodia. They are supported by a core of tightly bundled F-actin filaments. In both structures, the barbed-ends of the actin fibres are located towards the cell membrane, with elongation of the filaments leading to cell extension (Jones, 2000). The leading edge then connects to the surface, while the cell nucleus and plasma moves towards the new centre of the cell due to the actinmyosin contraction forces on the cells. Lastly, the actin myosin fibres retract at the tail of the cell, the cell detaches from the substrate and the whole cell retracts (Mattila and Lappalainen, 2008).

Cytokine production during inflammation

Innate immune cells are activated by PAMPs, these are molecules that different bacteria and virus have in common and present a danger signal. To recognise these molecules innate immune cells express PPRs such as Toll like receptors (TLRs) (Walport et al., 2008). The eleven TLRs described in humans so far comprise a major group of PPRs and play a key role in inflammation (reviewed in (Kumar et al., 2009; Takeda et al., 2003)). TLRs dimerise to achieve highly specific molecule recognition (reviewed in (Kumar et al., 2009; Okun et al., 2009)). While most TLRs build homodimers, TLR2 forms heterodimers with TLR6 (to recognise peptidoglycan, the main component of the gram-positive bacterial cell wall, and fungal zymosan) and TLR1 (to recognise lipopeptides). TLR4 is the

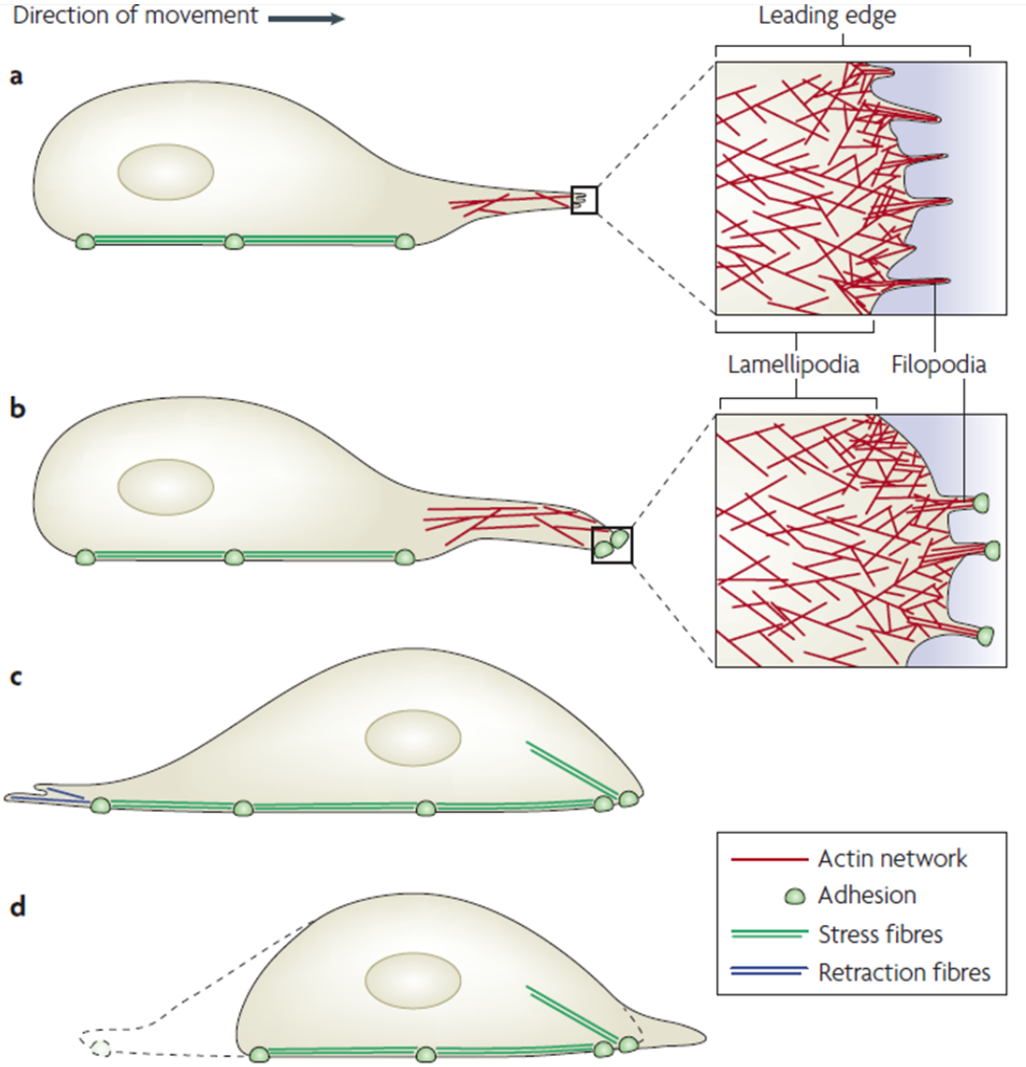

Figure 1.5: Cell migration occurs in three steps. **(a)** The actin driven protrusion of lammelipodia and filopodia at the leading edge, is followed by **(b)** adhesion of the leading edge to the substrate, initiated by filopodia. Finally, **(c+d)** contraction of the cytoplasmic actin fibre and disassembly of the cell adhesion points lead to retraction of the tail end. Reprinted by permission from Macmillan Publishers Ltd: Nature Reviews Molecular cell biology, Mattila and Lappalainen, 2008. ©2008.

main receptor for LPS, an endotoxin from gram-negative bacteria known to elicit strong immune responses in mammals and frequently used as an experimental stimulus *in vitro* (Kumar et al., 2009). Following TLR stimuli, several signalling cascades are activated (Figure 1.6).

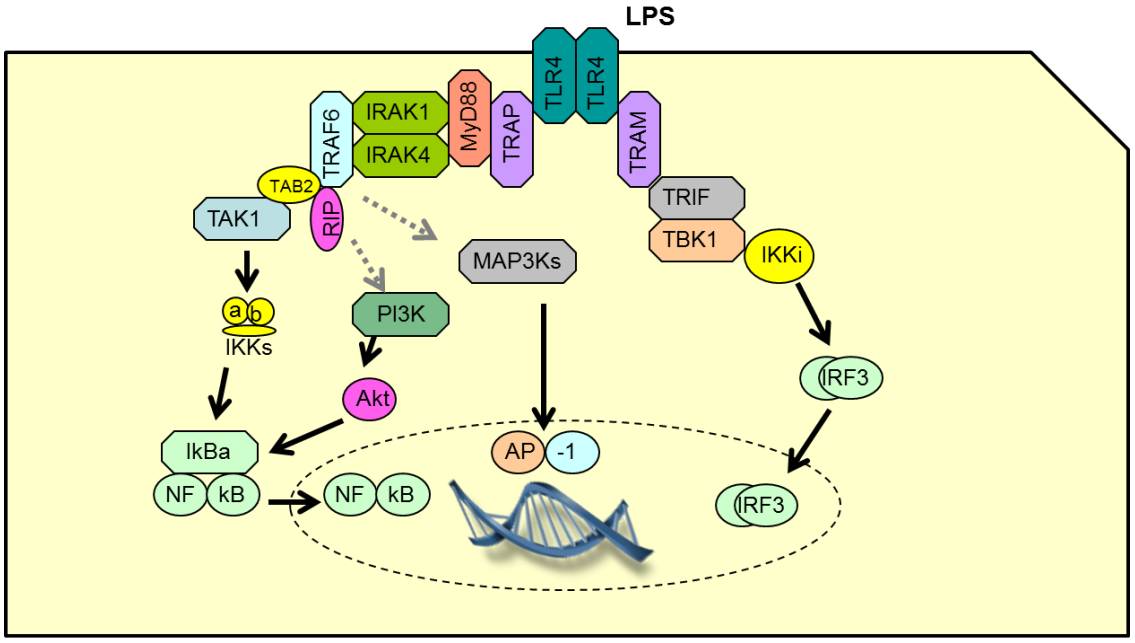

Figure 1.6: Signalling downstream of TLR4. Activation of TLR4 leads to activation of different signalling pathways including activation of the NFκB, MAPK and PI3K/AKT pathway via MyD88, IRAK1/4 and TRAF6. Independent from MyD88, interferon response factors (IRFs) are activated.

One of the signalling cascades activated downstream of TLR4 is the nuclear factor kappa-light-chain-enhancer of activated B cells (NFκB) pathway. Toll-interleukin 1 receptor domains of ligand-bound TLRs interact with adapter molecules such as myeloid differentiation primary response gene 88 (MyD88), TIR-domain-containing adapter-inducing interferon-β (TRIF) and TRIF- related adaptor molecule (TRAM) (Yamamoto et al., 2003). MyD88 carries a death domain with which it activates IL-IR-associated kinases (IRAK), leading to the phosphorylation and activation of IKK (IκB kinase). This kinase in turn phosphorylates IκB (inhibitor of kappa B), which is then ubiquitinated and degraded by the protea-

some, thereby dissociating from NFκB transcription factors it sequestered in the cytoplasm. The free NFκB molecules can then translocate to the nucleus and activate gene transcription (Figure 1.6) (Beinke and Ley, 2004). The NFκB family has five members- NFκB1 (or p50), NFκB2 (or p52), RelA (or p65), RelB and c-Rel. These molecules build homo- or heterodimers to activate transcription of over 150 target genes including pro-inflammatory cytokines (IL-6, TNF-α, IL-1β), cell adhesion molecules (ICAM-1, P-selectin), and acute phase proteins as well as growth factors (GM-CSF) (Pahl, 1999).

Other pathways activated downstream of TLR4 are the PI3K/ AKT/ mTOR (Phosphatidylinositide 3-kinases/ Protein Kinase B (PKB)/ mammalian target of rapamycin) and MAPK (mitogen-activated protein kinases) pathways. PI3K is activated downstream of TLR by the adapter proteins MyD88, which binds PI3K's catalytic p85 subunit and thereby activates the kinase (Laird et al., 2009). PI3K then produces phosphatidylinositol-3,4-bisphosphate, which AKT can bind via its pleckstrin homology domain (Franke et al., 1997). Once membrane bound, AKT phosphorylates itself and interacts with downstream effectors such as the NFκB pathway by inducing the activation of IKK via mTOR (Dan et al., 2008). The MAPK pathway is activated via the adapter protein TNF receptor associated factors 6 (TRAF6) downstream of MyD88, which activates the MAPK kinase kinase called transforming growth factor β activated kinase (TAK-1). TAK-1, in turn, phosphorylates the MAPK kinases, MKK3 and MKK6, upstream of p38 MAPK and c-Jun N-terminal kinases (JNK), and thereby leads to the activation of the transcription factors AP-1 (activator protein 1) and ELK (E twenty-six (ETS)-like transcription factor 1) (Barton and Medzhitov, 2003).

In addition to signalling downstream of TLR receptors, the JAK/STAT (janus kinase/ signal transducer and activator of transcription) signalling pathway is a key element in the communication between immune cells and is mainly activated

through cytokine receptors. Cytokines binding their receptors lead to the activation and cross-phosphorylation of JAK molecules. In turn the tyrosine kinases phosphorylate the intracellular domain of the receptor. STAT molecules then bind these phosphotyrosine residues with their SH2 domain and get phosphorylated by JAK allowing the STATs to dimerise via a phosphotyrosine-SH2 interaction and STAT dimers translocate into the nucleus to act as transcription factors and induce transcription of cytokine genes (Figure 1.7) (Shuai and Liu, 2003).

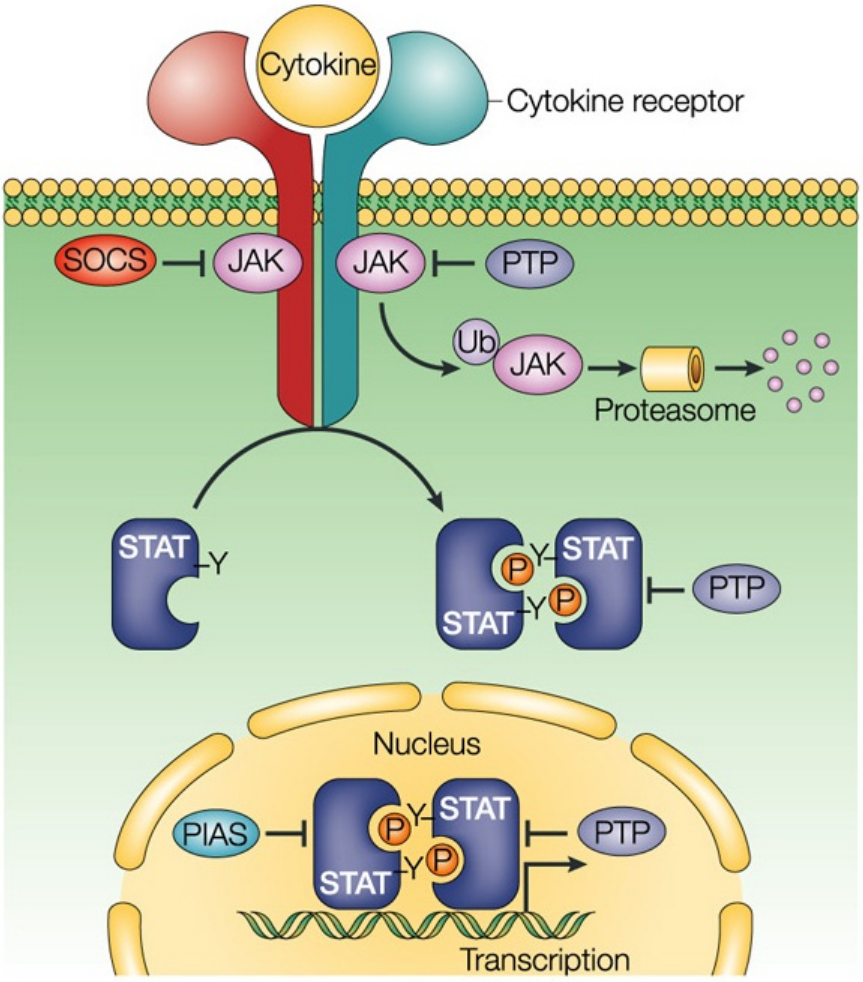

Figure 1.7: JAK/STAT signalling pathway. Cytokine receptor dimerisation leads first to phosphorylation of janus kinases (JAK) followed by STAT phosphorylation. Phospho-STATs dimerise and affect transcription in the nucleus. Reprinted by permission from Macmillan Publishers Ltd: Nature Reviews Immunology, Shuai and Lui, 2003. ©2003.

Transcription of the genes encoding for cytokines is followed by the translation into proteins and cytokine release from the cell. In the classical cytokine release pathway, cytokines are translated in the ER and Golgi before they are secreted via secretory granules or vesicles. This release can be constitutive or regulated by receptor binding of the vesicle before release (Lacy and Stow, 2011). Non-classical ways of cytokine release include membrane transporters, exosome release, microvesicle shedding and cell lysis (Lacy and Stow, 2011). TNFα and IL-6 are both secreted via the classical ER/ Golgi pathway. TNFα is membrane bound and cleaved extracellularly by metalloproteases (Shurety et al., 2000), while IL-6 is released in a soluble form (Manderson et al., 2007). IL-1β is released in a non-classical way; first a pro-form is produced and accumulates in the cytoplasm, before upon cell activation the proform is cleaved by caspase-1 and IL-1β is secreted. The exact way of IL-β secretion depends on the cell type, but mechanisms include cell lysis, exocytosis via the secretory lysosomes and microvesicle shedding (Eder, 2009).

Phagocytosis

Both macrophages and immature DCs can ingest particles in a process called phagocytosis. Special receptors on the phagocytic cells can bind either PAMPs on the intruder, complement factor C3b or antibodies bound to the intruder, triggering the cytoskeleton to change and the cell membrane to close around the particle forming a phagosome. The phagosome then fuses with the lysosome and internalised particles or microbes are degraded by proteases. The resulting peptides are loaded onto MHC II molecules and presented on the cell surface to activate the adaptive immune system (Walport et al., 2008).

1.2.2 The adaptive immune system

The adaptive immune response is mediated by two types of lymphocytes: T cells, which develop in the thymus and B cells, that develop in the bone marrow.

The T cell receptor (TCR) on the surface of T cells recognises peptide fragments presented on MHC molecules on the surface of other cells. In addition, T cells express a co-receptor, either CD4 or CD8. These molecules determine whether the TCR can bind MHC class II (only expressed on specialised antigen presenting cells like DCs, macrophages and B cells) or MHC class I molecules (expressed on all cells). There are different types of $CD4^+$ effector T cells, which differ in their cytokine production profile: $T_{helper}1$ (T_h1), which mainly activate macrophages; T_h2, which activate B cells; T_h17, which enhance the neutrophil response and regulatory T cells (T_{reg}), which dampen the immune response. $CD8^+$ effector T cells specific for the displayed peptide kill the presenting cell by releasing toxic substances (degranulation).

Naive B cells express a receptor called surface immunoglobulin (Ig). Immunoglobulins can bind soluble and membrane bound chemical structures. When B cells bind their antigen, they internalise it and present it on MHC class II to antigen-specific $CD4^+$ T_h2 cells. These in turn stimulate the B cells by providing co-stimulatory signals like CD40-CD40 ligand interaction and cytokine production. Effector B cells are called plasma cells as the cells enlarge their cytoplasm and ER to produce antibodies, soluble forms of the B cell receptor. Both T and B cells have the ability of establishing a long-lasting memory immune response (Walport et al., 2008).

1.3 Immune dysfunction in Huntington's disease

1.3.1 Central immune dysfunction

Neuroinflammation is becoming increasingly associated with neurodegenerative disorder such as Parkinson's, Alzheimer's and Huntington's disease. In all three diseases, microglia are found to be activated. It remains, however, unclear as to whether the cells act in an immunoprotective manner, or if they contribute to the disease pathology (reviewed in (Björkqvist et al., 2009)).

Increased complement production by microglia (e.g. C3 and C4), and complement activation of neurones, myelin and astrocytes, has been demonstrated in the striatum of HD patients (Singhrao et al., 1999). Furthermore, post-mortem studies of HD brains found an accumulation of activated microglia and reactive gliosis in regions affected by HD such as the striatum and cortex (Sapp et al., 2001; Vonsattel et al., 1985). Positron-emission tomography (PET) studies, using 11C-(R)-PK11195 binding peripheral benzodiazepine receptors as a surrogate marker of microglial activation, supported these finding by demonstrating early microglial activation in premanifest gene carriers in the striatum and cortex (Tai et al., 2007). Microglial activation further correlates to striatal neuronal dysfunction measured by 11C-raclopride PET (Tai et al., 2007). The same group showed that the level of microglial activation correlates with the neuronal loss, again measured by 11C-raclopride PET and disease severity, measured by the Unified Huntington's Disease Rating Scale (UHDRS) score (Pavese et al., 2006).

1.3.2 Peripheral immune dysfunction

Alongside dysfunction of CNS immune cells, peripheral immune cells such as monocytes are found to behave abnormally. Proteomic profiling of HD plasma

samples identified several abnormal proteins that correlate with disease progression and that are involved in the regulation of the innate immune system. Those include immune molecules IL-6 and complement proteins C7 and C9, as well as clusterin and β-actin, each of which were identified as significantly up-regulated in HD patient plasma compared with controls (Dalrymple et al., 2007).

Widespread activation of the innate immune system is detectable in HD plasma throughout the course of disease. Abnormal IL-6 levels in plasma are detectable on average sixteen years before the predicted onset of clinical signs. Additionally, serum levels of other pro-inflammatory cytokines such as IL-8 and TNFα are increased significantly in HD versus control samples (Björkqvist et al., 2008). Similarly chemokine levels are elevated in HD patients plasma compared with control (Wild et al., 2011). Furthermore, cytokines levels are also up-regulated in post-mortem striatal tissue and IL-6 and IL-8 levels in human CSF correlate strongly with peripheral cytokine levels (Björkqvist et al., 2008). It has been shown that peripheral human monocytes express mHTT and are hyper-reactive in terms of IL-6 production upon LPS stimulation *in vitro*. The same was found after stimulation of macrophages and microglia from different HD mouse models, suggesting that mHTT triggers cell-autonomous innate immune activation in the CNS and periphery in parallel (Björkqvist et al., 2008) (Figure 1.8).

The NFκB pathway has previously been implicated in HD. Khoshnan et al. have shown that overexpression of *mHTT* exon 1 can activate the NFκB pathway by directly interacting with IKK in inducible rat PC12 cells and striatal extracts from R6/2 mice (Khoshnan et al., 2004). This pathway is therefore a possible mechanistic candidate for the increased production of IL-6 in peripheral and central immune cells in HD. However it remains to be seen that this interaction also occurs in a human system with expression of full-length HTT at normal allelic expression levels. Another candidate pathway for alteration in HD is JAK/STAT signalling

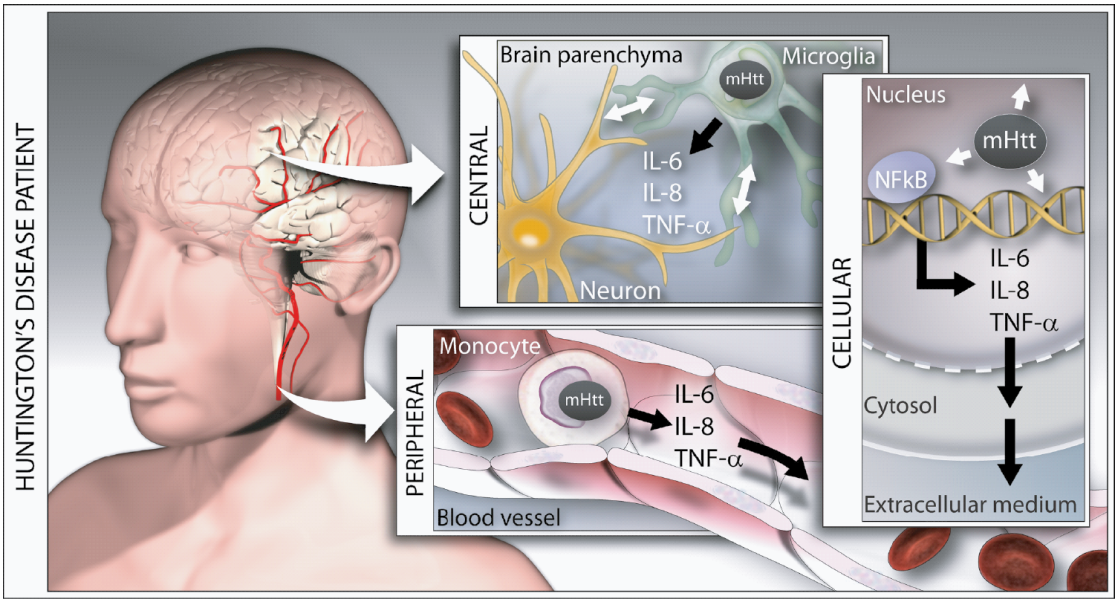

Figure 1.8: Immune activation, induced by mutant HTT, in both peripheral and central immune cells in HD. Innate immune cell dysfunction is caused by mHTT independently in microglia and blood monocytes leading to increased cytokine production and thereby interaction with surrounding cells. On a cellular bases these changes might be caused by altered cellular signalling. ©Björkqvist et al., 2008. Originally published in J Exp Med 205: 1869-1877. DOI jem.20080178.

pathway, which takes part in the regulation of cellular responses to cytokines.

1.3.3 The immune system as modifier of disease progression

Alongside immune cell dysfunction, several recent studies have suggested that the peripheral immune system can act as a modifier of HD neuropathology. Bone marrow transplantation of wild-type cells into two lethally irradiated HD mouse models normalises abnormal peripheral levels of cytokines and chemokines, and partially suppresses motor and neuropathological defects (Kwan et al., 2012a).

In HD, excitotoxicity has been linked to metabolites of the KMO pathway. While quinolinic acid is an agonist for NMDA causing excitotoxicity, kynurenic acid is a neuroprotective antagonist. Oral administration of a small-molecule prodrug inhibitor of KMO increases kynurenic acid levels, while extending the life span, preventing synaptic loss, and decreasing microglial activation in a mouse model

of HD. As the drug cannot cross the blood brain barrier, the neuroprotective effect via increased brain kynurenic acid levels is secondary to inhibition of KMO in peripheral immune cells (Zwilling et al., 2011). Studies in an HD fly model have shown similar results, as inhibition of KMO leads to the accumulation of neuroprotective metabolites and ameliorates neurodegeneration in the fly (Campesan et al., 2011).

Furthermore, modulation of the cannabinoid receptor 2 (CB2) has proven to modulate HD progression (Bouchard et al., 2012). CB2 is expressed on central and peripheral immune cells and is critical in decreasing the production of pro-inflammatory cytokines during inflammation by dampening the NFκB signalling cascade. Genetically deleting CB2 accelerated the disease onset and behavioural deficits (Bouchard et al., 2012; Palazuelos et al., 2009), while treatment with a CB2 agonist suppresses motor deficits and CNS inflammation while extending life span in an HD mouse model. Strikingly, this positive effect can be blocked with an antagonist that is restricted to the periphery, demonstrating the importance of peripheral immune cells in modulating the pathogenesis of HD (Bouchard et al., 2012).

Together, these studies provide strong evidence that the immune system plays a disease-modifying role in HD neuropathogenesis, but the mechanism by which mHTT expression in human immune cells causes this effect has not yet been established.

1.4 Aims of my thesis

1. Characterisation of monocytes and macrophage cell functions such as cytokine production, phagocytosis and migration in HD patients versus control samples.

2. Identification of the mechanism(s) by which mHTT expression causes human immune cell dysfunction.

3. Modulation of HTT levels by overexpression and siRNA-mediated knockdown techniques to investigate the role cell-intrinsic HTT plays in human HD monocyte and macrophage function and test the feasibility of reversing peripheral immune dysregulation by cell-targeted HTT-lowering.

4. Measurement of total and mHTT levels in primary human immune cell subsets, as a potential biomarker for HD progression.

5. Evaluation of HD mouse models as to the models' ability to mimic the immunological changes found in HD patients.

2 Material and Methods

2.1 Materials

Standard tissue culture plates and flasks were bought from Corning. Primary human and murine monocytes were grown in BD Primaria plates (BD Biosciences). Other tissue culture materials such as phosphate buffered saline (PBS), Hank's buffered salt solution (HBSS), RPMI1640 media, OptiMEM media, trypsin, fetal calf serum (FCS), L-glutamine and penicillin/streptomycin were bought from Invitrogen. If not stated otherwise lab chemicals were bought from Sigma Aldrich. Recombinant cytokines and chemokines such as human and murine MCP-1, human RANTES, human granulocyte-macrophage colony-stimulating factor (GM-CSF), human IL-6, human and murine IFNγ and murine macrophage colony-stimulating factor (M-CSF) were bought from R&D Systems. ATP and LPS were bought from Sigma Aldrich and C5a from Calbiochem. Magnets, magnetic beads and columns for magnetic cells sorting (MACS) were bought from Miltenyi.

2.2 Human subjects

All human experiments were performed in accordance with the Declaration of Helsinki and approved by the University College London (UCL)/UCL Hospitals Joint Research Ethics Committee (LREC 03/N008). All subjects provided in-

formed written consent. Blood samples were obtained from control subjects and genetically-diagnosed HD patients, recruited from the Huntington's disease clinic at the National Hospital for Neurology and Neurosurgery, London. Premanifest HD mutation carriers were identified according to the absence of diagnostic motor abnormalities on the UHSRS (Huntington Study Group, 1996), whilst patients with motor abnormalities were classed as having early or moderate-stage disease using the total functional capacity (TFC) scale (13-7, early; 6-3, moderate) (Shoulson, 1981). Subjects with inflammatory or infective conditions were excluded.

2.3 Animals

R6/2 (Mangiarini et al., 1996) and *Hdh*$^{150Q/150Q}$ (Lin et al., 2001) mice were kindly provided by Prof Gillian Bates and bred in facilities at King's College London. The R6/2 mice were bred by backcrossing R6/2 males to (CBA$\times$C57BL/6)-F1 females. *Hdh*$^{150Q/150Q}$ mice were on a mixed C57BL/6/CBA background, crossing CBA *Hdh*$^{150Q/150Q}$ males with C57BL/6 *Hdh*$^{150Q/150Q}$ females. All animals had unlimited access to water and breeding chow (Special Diet Services) in open-top cages. R6/2 mice were also given mashed food consisting of powdered chow mixed with water from 12 weeks of age. Mice were housed with WT mice and were subject to a 12 h light dark cycle.

2.4 Magnetic resonance imaging (MRI)

Volumetric 3T MRI sequences were obtained as part of the TRACK-HD study London cohort. Details of the imaging protocols and rigorous quality control procedures used in the study are published (Tabrizi et al., 2009, 2012, 2011). Follow-

up scans were positionally matched to the baseline images and change over 36 months was calculated using the robust boundary shift integral technique (Leung et al., 2010). Rates of atrophy were expressed as a percentage of baseline volume and annualised. All image analysis was carried out blinded to subject identity and group.

2.5 Tissue culture

Work with cell lines and primary cells was carried out in a designated tissue culture facility using strict aseptic technique. All media and solutions were bought pre-sterilised and sterile plastic-ware was used. All procedures, including preparation of media, were performed in a tissue culture hood with a laminar flow unit. All solutions and media were pre-warmed to 37 °C prior to use. All cells were cultured in an incubator at 37 °C with 5% CO_2.

2.5.1 Maintenance of cell lines

Vials containing frozen cells were removed from liquid nitrogen and were thawed rapidly in a 37 °C water bath. The cell suspension was added to 10 ml of appropriate pre-warmed media and centrifuged at 300×g for 5 min. The supernatant was then decanted, the cells resuspended in 5 ml fresh standard growth medium and seeded into 25 mm^2 filter-capped tissue culture flasks.

For freezing, cells were counted using a Neubauer counting chamber and 2×10^6 cells were centrifuged for 5 min at 300×g. Pellets were resuspended in 1.5 ml freezing media (90 % FCS and 10 % DMSO), dispensed into sterile cryovials and put in an isopropanol-regulated cryopreservation box at -80 °C overnight before long term storage in liquid nitrogen.

U937 cells

U937 cells are a human histiocytic lymphoma cell line, established in 1974 (Sundström and Nilsson, 1976) and were obtained from the American Type Culture Collection (ATCC). They were cultured in suspension in RPMI1640 media (Invitrogen #31870074, formulation in Appendix A.1) containing 10 % FCS, 2 mM L-glutamine, 50 Units/ml penicillin and 50 μg/ml streptomycin using 175 mm^2 filter topped tissue culture (T175) flasks. Cells were maintained at a density between 1×10^5 and 2×10^6 cells per ml by replacing or adding fresh media every 3-4 days. In order to differentiate the cells into mature monocytes 10 nM 12-O-tetradecanoylphorbol-13-acetate (PMA) was added to the culture media for 3 days (Alciato et al., 2010). U937 cells were lentivirally transduced to express *(m)HTT* exon 1 as described in Section 2.5.2.

HEK293T cells

HEK293T is a human embryonic kidney cell line, purchased from ATCC. These adherent cells were cultured in T175 flasks using complete OptiMEM media (Invitrogen #31985047, formulation is confidential as it contains components to allow the use serum-free media during transfections without loss of cell viability, see protocol in Section 2.5.2) containing 10 % FCS, 50 Units/ml penicillin and 50 μg/ml streptomycin. They were split every 2-4 days at a 1:3 to 1:10 ratio. Culture media was removed, cells were washed with PBS before 3 ml of 0.25 % trypsin solution were added to the flask. After 5-10 min incubation at 37 °C, when the cell layer was dispersed, 10 ml of complete OptiMEM media were added and cells were aspirated by pipetting. Cell suspensions was divided into new culture flasks.

2.5.2 Establishing a mHTT-expressing myeloid cell line

Lentiviral vectors

The A2UCOE HD exon 1 vectors used in this study were (see Appendix A.2 for plasmid maps):

- p'HRsincpptUCOEeGFP+linker+WPRE (vector backbone without *HTT*)
- p'HRsincpptUCOE+htt exon1 IRES eGFP 29CAG
- p'HRsincpptUCOE+htt exon1 IRES eGFP 71CAG
- p'HRsincpptUCOE+htt exon1 IRES eGFP 129CAG

All four vectors were generous gifts from Prof Gillian Bates, King's College London. The A2UCOE vector backbone was modified from (Zhang et al., 2007) as follows: a polylinker containing PmeI-SnaBI-BstBI sites was ligated into the NdeI site, at the same time destroying the NdeI site at the 3 end of the polylinker; a woodchuck post-translational regulatory element was ligated into the BstBI site; exon 1 human HTT-IRES-eGFP was ligated into the SalI-NdeI sites.

Plasmid DNA preparation

Plasmid DNA was multiplied by transformation of chemically competent OneShot TOP10 *E. coli* (Invitrogen). Chilled *E.coli* cells were mixed with 100 ng A2UCOE plasmid DNA and incubated for 30 min on ice. Cells were heat shocked for 30 s in a 42 °C water bath before being placed back onto ice for 2 min. Next, 250 μl S.O.C media (Invitrogen) were added and the vials were incubated in a 37 °C shaker for one hour. The bacteria was then streaked out onto sterile agar plates, containing 100 μg/ml ampicillin (Sigma Aldrich) to select for clones containing the plasmid DNA, which encodes for an ampicillin resistance gene. Single colonies were

picked and grown in LB broth containing 50 μg/ml ampicillin overnight. Standard QIAGEN Maxiprep kits were used to isolate plasmid DNA from 400 ml bacterial culture the next day. Bacteria was centrifuged for 15 min at 6000$\times$g and pellets were resuspended in 10 ml lysis buffer (P1- provided with the kit). After adding 10 ml of buffer P2 (provided with the kit) and an incubation for 5 min at room temperature, 10 ml of ice-cold buffer P3 (provided with the kit) was added. Suspensions were mixed by inversion and incubated for 20 min on ice. Following a 60 min spin at 8000$\times$g, supernatants were filtered through a QIAfilter (provided with the kit) and loaded onto Qiagen-tip 500 columns (provided with the kit), previously equilibrated with 10 ml QBT buffer (provided with the kit). After the supernatant had dripped through by gravity, columns were washed twice with 30 ml QC buffer (provided with the kit) and DNA was eluted with 15 ml QF buffer (provided with the kit). Plasmid DNA was then precipitated with 10.5 ml 100 % isopropanol, followed by a 60 min spin at 6000$\times$g. After washing the DNA pellet with 5 ml 70 % ethanol (diluted in ddH_2O) and a 30 min 6000$\times$g centrifugation step, pellets were air-dried, resuspended in water and concentration was measured using a Nano Drop Spectrophotometer.

DNA sequencing

To ensure stability of the CAG repeat length and integrity of the inserted *HTT* exon 1, all constructs were sequenced. Sequencing reactions were carried out in non-skirted 96-well plates (Thermo Scientific), mixing 1 μl BigDye (Applied Biosystems), 5 μl BetterBuffer (Microzone), 0.75 μl 5 μM primer (CCG TGC GGA GGT GCT CCT CG), 7.25 μl ddH_2O and 1 μl (=150ng) cleaned DNA. After a short spin down, plates were run on a Tetrad thermal cycler (Bio-rad) (program: 96 °C for 1 min followed by 25 cycles of 96 °C for 10 secs and 65 °C for 2 mins). PCR products were extracted, adding 3.75 μl 0.125 M ethylenediaminetetraacetic acid

(EDTA) and 45 μl 100 % ethanol to each well before leaving the plate at room temperature for 15 min. After spinning the plate at 3000$\times$g for 30 min at 4 °C, the plates was inverted onto tissue and centrifuged again at 185$\times$g. Next, 60 μl 70 % ethanol was added to each well and the plate was centrifuged at 1650$\times$g for 15 min at 4 °C, followed by an inverted spin at 185$\times$g for 1 min. Plates were then placed uncovered on a PCR block and held at 37 °C for 5 min to remove final traces of ethanol. Finally samples were analysed via electrophoresis using a 3730XL DNA Analyzer (Applied Biosystems) and data was viewed using the Applied Biosystems Sequence Analysis Software V5.2.

All vectors showed no mutations from the reference *HTT* sequence from national center for biotechnology information (alignments in Appendix A.3). However, the CAG length in the A2UCOE HD 29Q vector had expanded to 31 repeats, but as this is still within the non-pathological CAG repeat range the vector was used as control.

Virus production and titration

For virus production, 50 μg A2UCOE HD vector DNA, 17.5 μg pMD.G2 envelope and 32.5 μg pCMVdR8.74 packaging plasmids (both produced by PlasmidFactory, patent with Michael Antoniou) were added to 6 ml serum free OptiMEM media and sterilised by filtration through a 0.22 μm filter. This DNA solution was mixed with 6 ml sterile filtered serum-free OptiMEM media containing 1.6 μM polyethylenimine (PEI) (Sigma Aldrich) and incubated for 20 min at room temperature. Twelve ml of the PEI/DNA mix were then added to one 70 % confluent T175 flask of HEK293T cells and incubated for 4 h before fresh complete OptiMEM media was added. Viral supernatants were collected and concentrated by filtration through a 0.22 μm syringe filter and centrifugation (4000$\times$g for 24 h at 4 °C) after 48 h.

For virus titration, U937 cells were seeded at 1×10^5 into 24-well plates before adding either 1, 0.1 or 0.01 μl of concentrated virus and 8 μg/ml polybrene (PB) per well. After two days the percentage of virally transduced cells was assessed according to green fluorescent protein (GFP) expression, which is co-transduced with all A2UCOE plasmids, using flow cytometry (Section 2.9). The number of infectious units was then calculated from the percentage of transduced cells (Figure 2.1), assuming 10^8 virus particles per ml and dividing the percentage of transduced cells by the percentage virus used (1μl virus is 100 %, 0.1μl virus is 10 %, 0.01μl virus is 1 %). For the example in Figure 2.1, a concentration of 2×10^6 virus particles per ml was calculated. To achieve 15 % final transduction rate for 1×10^6 cells, 1.5×10^5 viral particles were needed, equating to 50 μl viral supernatant.

Lentiviral transduction

In order to limit the number of viral DNA integration events in the transduced cell to a minimum, a transduction rate of 10-20 % was choosen for these experiments. This level of efficiency is though to result in a single DNA insertion per cell reducing the likelyhood of unwanted gene disruptions during the transduction protocol.

One$\times10^6$ U937 cells were incubated with an appropriate amount of titrated virus and 8 μg/ml PB in serum free OptiMEM media. After 4 h of incubation, media was changed into complete OptiMEM media. Three days later transduced cells were sorted using fluorescence-activated cell sorting (FACS) with a MoFlo cell sorter (Beckman Coulter). Using the 488 laser, successfully transduced GFP expressing cells were sorted from non-transduced cells in order to isolate a 100 % pure population of U937 cells expressing the A2UCOE vectors. GFP expression in the cells did not change over a period of 4 weeks in culture. For a mature monocyte phenotype, transduced and sorted cells were differentiated using 10 nM PMA added to the media for 3 days.

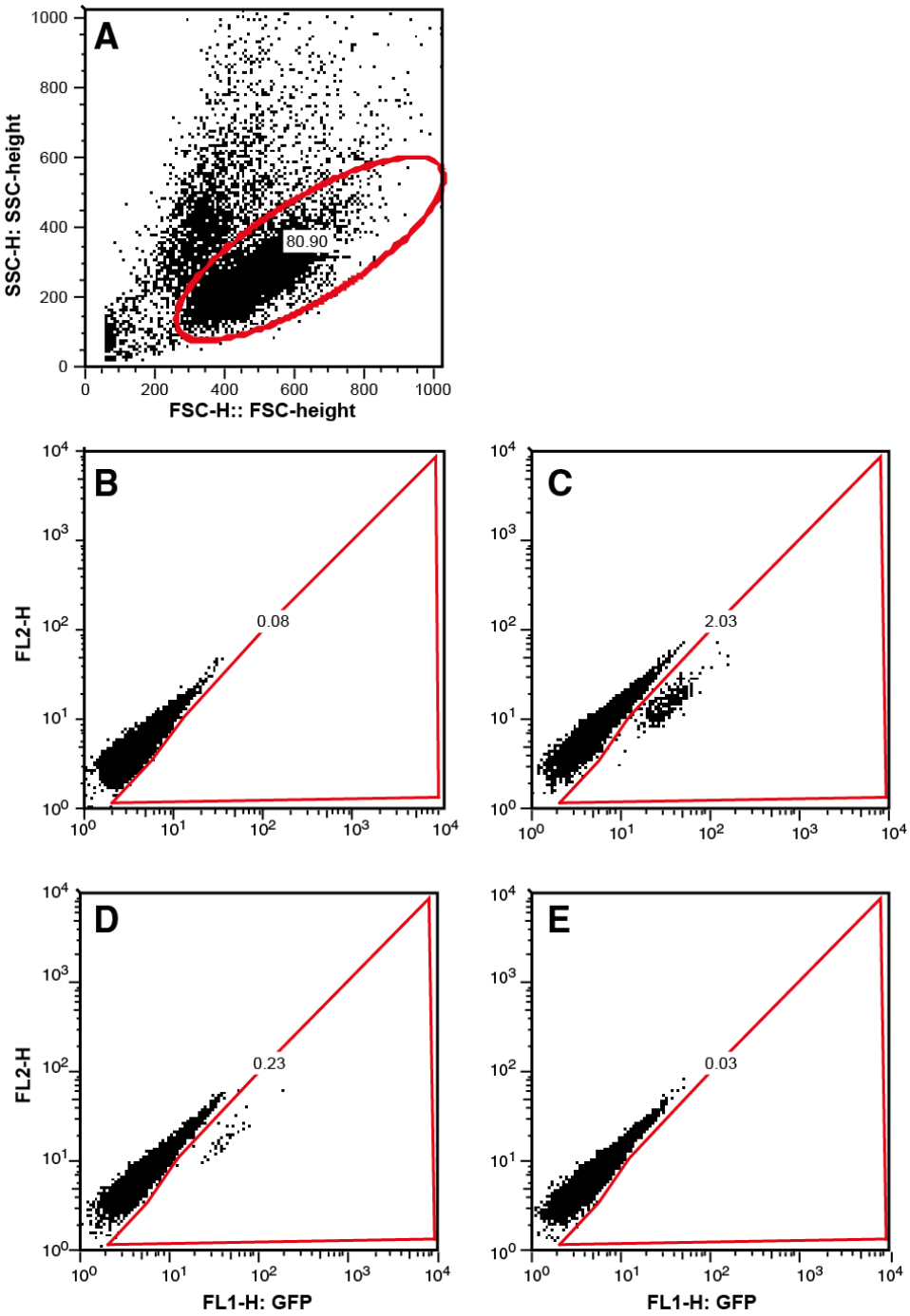

Figure 2.1: Titration of lentivirus expressing *HTT* exon 1. U937 cells were incubated with different amounts of lentivirus containing *HTT* exon 1 and GFP; and the percentage of transduced cells was measured by assessing GFP expression by flow cytometry. After **(A)** gating on living, single cells, gates for positive GFP expression were drawn using **(B)** untransduced U937 cells. Using virus at **(C)** 1:100, **(D)** 1:1 000 or **(E)** 1:10 000 fold dilution resulted in a titration curve from which virus concentration was calculated.

2.5.3 Collection of buccal epithelial cells

Buccal swabs were collected in Catch-ALL sample collection swabs (Epicenter Biotechnologies). Each subject rinsed their mouth twice before rolling the swab firmly on the inside of their cheek, approximately twenty times on each side. Swabs were then snap frozen and stored at -80 °C before shipping to Novartis, where cells on the swab were lysed and used for HTT quantifications (Section 2.8.6).

2.5.4 Preparation of primary human immune cells

Isolation of primary human blood monocytes

Peripheral blood mononuclear cells (PBMCs) were isolated from blood samples using density centrifugation, by layering the samples on top of sterile, 100 % Histopaque-1077 solution (Sigma Aldrich). After spinning for 30 min at 400×g the layer of PBMCs was carefully transferred into a fresh, sterile 50 ml centrifuge tube and washed with PBS (centrifuged for 5 min at 300×g). Cells were then resuspended and counted using a Neubauer counting chamber. Following centrifugation (300×g for 5 min), the supernatant was carefully decanted and the cells were resuspended in 10 μl anti-human CD14 beads (Miltenyi Biotec) and 90 μl MACS buffer (PBS including 1 % bovine serum albumin (BSA) and 2 mM EDTA) per 10^7 cells. After incubating for 15 min in the fridge, the samples were washed with 2 ml MACS buffer (300×g for 5 min) and resuspended in 500 μl MACS buffer. Magnetic cell sorting was prepared by rinsing MACS columns placed in the magnet with 500 μl MACS buffer before loading the samples onto the columns. After allowing the cell suspension to drop through by gravity, the columns were washed three times with 1 ml MACS buffer. Labelled $CD14^+$ monocytes were

eluted by taking the columns out of the magnetic field and pushing 2 ml MACS buffer through the column using a plunger. Isolated monocytes were counted and used for experiments. Following each cell sorting a proportion of cells was used to check sorting efficiency by flow cytometry. On average, the sorted cell population contained 85-95% $CD14^+$ cells (Figure 2.2).

Isolation of primary human blood T and B cells

Isolation of T cells and B cells was carried out by dividing the flow-through of the monocyte isolation, described above, in two equal parts. After spinning the sample for 5 min at 300×g at 4 °C, cell pellets were resuspended in 540 μl MACS buffer and 60 μl anti-CD3 (for T cells) or anti-CD19 (for B cells) MACS microbeads were added. Following a 15 min incubation in the fridge and centrifugation (300×g for 5 min), cells were purified using a MACS column as described above for monocytes. After eluting the purified cells, they were counted using a Neubauer counting chamber, centrifuged (300×g for 5 min), snap-frozen in 20 μl protease inhibitor solution (PBS with complete protease inhibitor cocktail (Roche)) and shipped to Novartis for TR-FRET measurements (Section 2.8.6). Sorting of T cells resulted in around 90 % purity, while B cells were around 80-85 % pure (Figure 2.2).

Differentiation of human macrophages

Monocytes were isolated as described above and cells were seeded in R10 media (RPMI1640 media containing 10 % FCS, 2 mM L-glutamine, 50 Units/ml penicillin and 50 μg/ml streptomycin) supplemented with 20 ng/ml recombinant human GM-CSF to induce macrophage differentiation. The medium was changed three days after seeding, providing the cells with fresh media and growth factors. Cells demonstrated a macrophage phenotype after 6 days in culture.

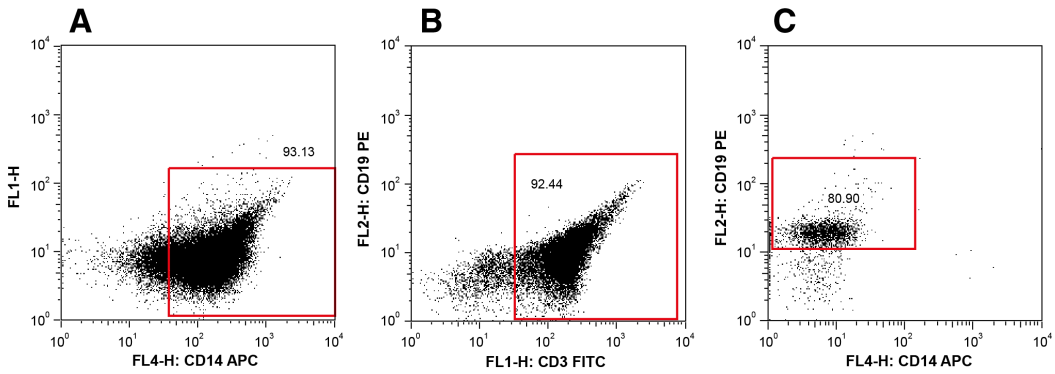

Figure 2.2: Purity of CD14$^+$ monocytes, CD3$^+$ T cells and CD19$^+$ B cell post magnetic cell sorting. Mononuclear blood cells were isolated from whole blood by density centrifugation. **(A)** CD14$^+$ monocytes were further purified using magnetic activated cell sorting, providing a 85-95 % pure monocyte suspension. Flow-through from the magnetic sorting of monocytes was used to isolate **(B)** CD3$^+$ T and **(C)** CD19$^+$ B cells. T cells were around 90 % pure following the sort, B cells around 80-85 % .

2.5.5 Knock-down of *HTT* in primary human monocytes and macrophages

Production of glucan encapsulated siRNA containing particles (GeRPs)

Glucan particles were prepared as described previously (Soto et al., 2012). *Saccharomyces cerevisiae* (100 g of SAF-Mannan; SAF Agri) was suspended in 1 L 0.5 M NaOH and heated to 80 °C for 1 h. The insoluble material containing the yeast cell walls was collected by centrifugation at 5000×g for 20 min. This insoluble material was then resuspended in 1 L 0.5 M NaOH, and incubated at 80 °C for 1 h. The insoluble residue was again collected by centrifugation (5000×g for 20 min) and washed three times with 1 L of water, three times with 200 ml propan-2-ol and three times with 200 ml acetone. The resulting slurry was placed in a glass tray and dried at room temperature (20 °C) to produce 12.7 g of a fine, slightly off-white powder.

Fluorescent glucan particles were prepared as described previously (Aouadi et al., 2009). Briefly, glucan particles (1 g) were washed with sodium carbonate buffer

(0.1 M sodium carbonate, pH 9.2) and resuspended in 100 ml sodium carbonate buffer. 5-(4,6-Dichlorotriazinyl) aminofluorescein (Invitrogen; 1 mg/ml in ethanol) was added to the buffered glucan particle suspension (10 % v/v) and mixed at room temperature in the dark overnight. Tris buffer (2 mM Tris/HCl, pH 6.8) was added, incubated for 15 min and glucan particles were washed with 100 ml sterile pyrogen-free water until the supernatant was clear (repeat centrifugation at 3,000$\times$g for 10 min). The glucan particles were then flash-frozen, freeze-dried in the dark and stored at room temperature in the dark.

To load siRNA into 10^7 glucan particles, siRNA (10 μl 7 mM siRNA, from Dharmacon, Table 2.1) was mixed with sterile, pyrogen-free saline (Sigma Aldrich, 40 μl), HEPES buffer (Invitrogen, 30 μl 0.1 M, pH 7.5 in saline) and glucan particles (10 μl 10^9 particles/ml in saline), and incubated for 2 h at room temperature in the dark. The siRNA was trapped by complex formation inside the glucan particles by adding 10 μl EndoPorter (GeneTools, diluted 1:1 with saline) and incubated for 15 minutes at room temperature as previously described (Tesz et al., 2011). Loaded GeRPs were snap-frozen on dry ice in single use aliquots and stored at -80 °C. Loading reactions were scaled up or down proportionately to produce the desired number of GeRPs.

Table 2.1: siRNA sequences used in *HTT* knock-down experiments

Primer		Sequence
anti-HTT siRNA	Guide strand	5'- pUUCAUCAGCUUUUCCAGGGUC-3'
	Passenger strand	5' -CCCUGGAAAAGCUGAUGACGG -3'
scrambled siRNA	Guide strand	5'-pUUUCGAAGUACUCAGCGUGAG-3'
	Passenger strand	5'-CACGCUGAGUACUUCGAACUU-3'

Transduction of primary cell cultures

Monocytes were isolated from whole blood (Section 2.5.4), seeded onto poly-L-lysine coated coverslips and treated with fluorescent GeRPs, which contained no siRNA for 12 h to assess GeRP uptake using microscopy (Section 2.11.2).

Macrophages, which were transfected on day three of the differentiation protocol, were transfected with green fluorescent GeRPs containing no siRNA at various ratios (1:1; 1:3; 1:10) for 4 h, after which fresh culture medium was added to the cultures. Uptake rates were measured 24 h later by flow cytometry (Section 2.9).

Macrophages were treated with either scrambled or anti-*HTT* siRNA containing GeRPs at a 1:10 cell to particle ratio on day 3 of the differentiation protocol. Four hours after adding GeRPs, fresh media was added to the cells. Analysis of *HTT* RNA and protein levels via qPCR (Section 2.10) and TR-FRET (Section 2.8.6), respectively and cytokine profiling (Section 2.6.1) took place three days later.

Monocytes were rested for 16 h post isolation before treatment with either scrambled or anti-*HTT* siRNA containing GeRPs at a 1:10 cell to particle ratio for 4 h. Three days later, transcriptional changes were analysed using qPCR (Section 2.10).

2.5.6 Preparation of primary murine cells

Blood

Blood was obtained by cardiac puncture in mice culled by a rising concentration of CO_2. In order to prevent clotting, blood was collected into EDTA coated tubes (BD Vacutainer collection tubes). To analyse white blood cells, 1 ml red blood cell lysis buffer (ammonium chloride buffer from eBioscience) was added per 1 ml of blood and the samples were incubated for 5 min at room temperature.

After spinning at 300×g for 5 min, the lysis step was repeated twice. Cells were then resuspended in 270 µl MACS buffer and 30 µl anti-mouse CD11b magnetic beads. After 15 min incubation in the fridge, the samples were isolated using MACS columns as described in Section 2.5.4.

Spleen

Spleens were dissected from the mice and stored in RPMI1640 media until the preparation started. To obtain a single cell suspension, spleens were cut into pieces and digested using 2 ml digest buffer (RPMI media including 10 % FCS, 15 mM HEPES, 0.5 % Collagenase type 4 (Sigma Aldrich C1889)). After 30 min incubation at room temperature the remaining spleen pieces were filtered through a 70 µm nylon cell strainer (BD Falcon). Afterwards the splenocytes were centrifuged (300×g for 5 min) and the pellet was incubated with 1 ml red blood cell lysis buffer (ammonium chloride buffer from eBioscience) for 5 min at room temperature. After another spin, the cells were resuspended in 20 ml PBS and counted using a Neubauer counting chamber. An appropriate number of cells was used either for flow cytometry (see Section 2.9) or MACS using 10 µl anti-mouse CD11b magnetic beads and 90 µl MACS buffer per 10^7 cells as described in Section 2.5.4.

Bone marrow

Mice were sacrificed by neck dislocation or by rising concentration of CO_2. Femur and tibia were dissected out at the hip joint and any remaining muscle tissue was carefully removed. The bones were placed in a petri dish filled with cold RPMI1640 media and cut at the joints. Bone marrow was flushed out into a sterile 50 ml tube by rinsing the shaft with media using a 5 ml syringe and 26 gauge needle, while holding the bone shaft with forceps. Cell lumps were disaggregated

by pipetting up and down several times before the cells were passed through a 70 μm nylon cell strainer. After washing with RPMI1640 media (centrifuge for 5 min at 300$\times$g) cells were counted using a Neubauer counting chamber. The cell suspension was labelled with 10 μl anti-mouse CD11b magnetic beads and and 90 μl MACS buffer per 10^7 cells and sorted as described in Section 2.5.4.

The isolated CD11b positive cell population resembled an early monocyte population, but was also used as a source for bone marrow-derived macrophages. For the differentiation sorted bone marrow cells were seeded at 3×10^6 million cells in 2 ml R10 media supplemented with 20 ng/ml recombinant murine M-CSF onto 6-well plates. After 3 days cells were provided with fresh media and growth factor. The cells resembled a macrophage phenotype from day 6.

Peritoneal macrophages

In order to prevent bleeding into the abdominal cavity mice were killed using rising concentration of CO_2, not neck dislocation. Fur covering the peritoneum was carefully removed and 5 ml of ice-cold, serum free RPMI1640 media were injected into the abdominal cavity using a 26 gauge needle. After massaging the mouse abdomen for 1-2 min, cells were recovered through a small incision using sterile plastic pasteur pipettes and put on ice as quick as possible. To remove contamination with red blood cells, the centrifuged (5 min at 300$\times$g) cell suspension was incubated with 1 ml red blood cell lysis buffer (ammonium chloride buffer from eBioscience) for 5 min at room temperature. Afterwards, cells were washed with 5 ml PBS (centrifuged at 300$\times$g for 5 min). The obtained cell suspension contained macrophages as well as neutrophils. Cultures were enriched for macrophages by removing non-adherent neutrophils by media changing and washing the cells after 2 h in culture.

2.6 Functional analysis of myeloid cells

2.6.1 Cytokine profiling

Primary human monocytes and macrophages, (m)HTT expressing U937 cells and GeRP treated macrophages were isolated and differentiated as described in Sections 2.5.4, 2.5.2 and 2.5.5, respectively. Five hundred thousand cells, seeded in 24-well plates, were primed with 10 ng/ml human IFNγ and stimulated with 2 μg/ml LPS. After 24 h, supernatants were collected for analysis of cytokine levels (Section 2.7.2) and cells were lysed for protein measurement (Section 2.8). For experiments using primary human cells, n numbers represent samples from different individuals (biological repeats). For the cytokine profiling of mHTT expressing U937 cells, several wells of the same cell line were stimulated and analysed separately (technical repeats).

To evaluate the cytokine profiles of murine cell cultures, blood monocytes isolated from individual *Hdh*$^{150Q/150Q}$ mice were seeded at 100,000 cells into 96-well plates in 100 μl R10 media. Due to the low cell numbers of blood monocytes recovered from R6/2 mice, cells were pooled according to genotype and multiple wells were seeded at 100,000 cells into 96-well plates in 100 μl R10 media. Splenic and bone marrow monocytes, and peritoneal macrophages were seeded in 24-well plates at a density of 500,000 cells per well. Bone marrow derived macrophages were used for stimulation experiments after differentiation in 6-well plates at 3×10^6 million cells per well (see Section 2.5.6). All murine culture were primed with 10 ng/ml murine IFNγ and stimulated with 2 μg/ml LPS. After 24 h, supernatants were collected for analysis of cytokine levels (Section 2.7.2) and cells were lysed for protein measurement (Section 2.8).

2.6.2 Migration assay

To assay migration abilities of the myeloid cells a Boyden chamber/ transwell system (Corning) was used.

Migration assay for blood monocytes

The lower chamber of the 5μm transwell was filled with RPMI media containing 1 % FCS, 2 mM L-glutamine, 50 Units/ml penicillin and 50 μg/ml streptomycin supplemented with either 50 ng/ml CCL2 (MCP-1), 100 μM ATP, 10 nM C5a or 100 ng/ml RANTES (concentrations established in dose-response curve shown in Figure 2.3). Half a million monocytes were added on top of the 5 μm transwell inserts and incubated at 37 °C for 1.5 h to allow migration. Afterwards the transwells were removed and the contents of the lower chamber was centrifuged at 300$\times$g for 5 min. Cell pellets were resuspended in 50 μl PBS and counted using a Neubauer counting chamber.

Migration assay for macrophages

One hundred thousand macrophages were seeded into 8 μm transwell inserts, which were placed into wells filled with RPMI media containing 1 % FCS, 2 mM L-glutamine, 50 Units/ml penicillin and 50 μg/ml streptomycin supplemented with either 50 ng/ml CCL2 (MCP-1), 100 μM ATP, 10 nM C5a or 100 ng RANTES (same stimuli as used for monocytes above). The cells were incubated for 16 h, after which the inserts were removed from the wells. Cells on the upper side of the insert membrane were gently removed using cotton buds, while the cells on the lower side were fixed in ethanol and stained with 1 mg/ml crystal violet. The fixed, stained cells were counted in multiple fields of view using ImageJ software. Pictures were taken on a light microscope (Nikon Eclipse TS100, Objective 20$\times$) with

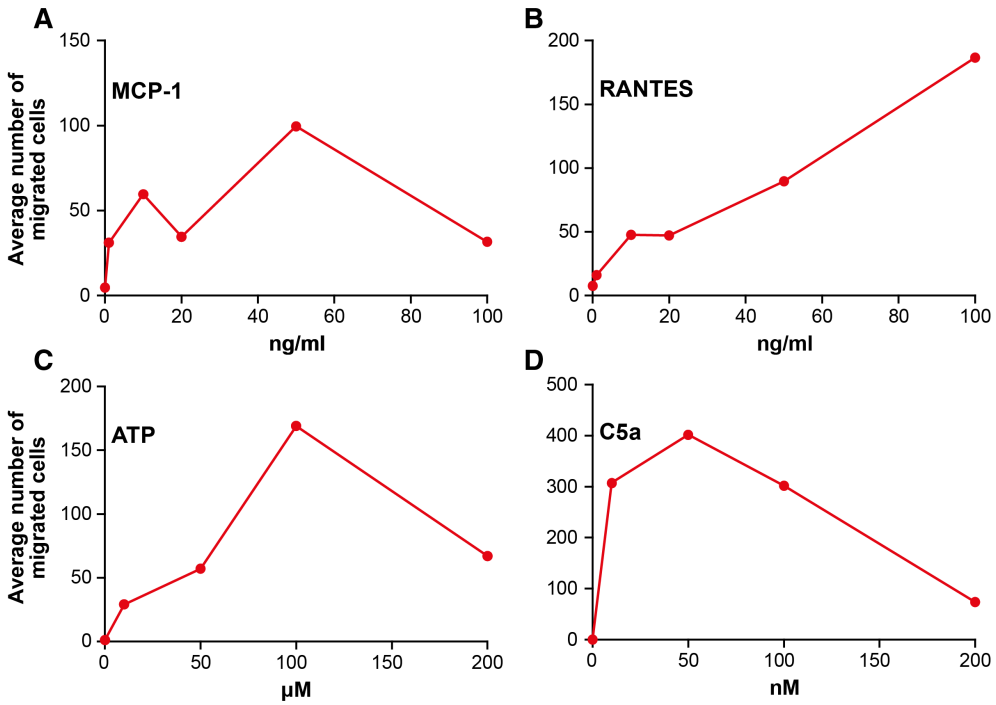

Figure 2.3: Dose-response for different chemokines used in migration assay. (A+B) Monocyte migration towards 1, 10, 20, 50 and 100 ng/ml MCP-1 and RANTES was tested in one control sample establishing a peak for migration towards **(A)** MCP-1 at 50 ng/ml, while migration towards **(B)** RANTES increased further using 100 ng/ml. Validating finding in murine HD microglia (Kwan et al., 2012b), monocyte migration towards **(C)** ATP and **(D)** C5a was tested and found to peak at 100 μM and 50 nM, respectively. In order to replicate the findings in murine microglia, 100 μM ATP and 10 nM C5a were used in all experiments.

attached digital camera (Nikon DS-Fi1) with the NIS-Elements F 3.00 software.

2.6.3 Phagocytosis assay

Murine peritoneal (Section 2.5.6) and human (Section 2.5.4) macrophages were stimulated with 2 μg/ml LPS in R10 media overnight. One hour before the assay, macrophages were washed three times with PBS and serum-free RPMI1640 was added to the cells. Carboxylate-modified fluorescent yellow-green latex beads (Sigma Aldrich) were added to the cells at a 10:1 ratio and were incubated at 37 °C for 1 h. Cells were then washed with cold PBS twice and incubated with PBS containing 10 nM EDTA for 10 min on ice before the cells were detached from

the culture wells by trituration. The cells were then fixed using 3.7 % paraformaldehyde (PFA). After 20 min at room temperature, the PFA was washed off the cells and they were stained with surface markers specific for the macrophage lineage for analysis by flow cytometry (as described in Section 2.9).

2.6.4 Adhesion assay

In order to assess cell adhesion, murine peritoneal macrophages were harvested as described in Section 2.5.6. Macrophages were seeded in 24-well plates and left to adhere to the plastic for 2 h. Afterwards adhered cells were removed and counted using a Neubauer counting chamber.

2.7 Immunoassays

2.7.1 Enzyme-linked immunosorbent assay - ELISA

To analyse the IL-6 production by stimulated myeloid cells isolated from mice, the R&D Systems mouse IL-6 Quantikine immunoassay kit was used. Culture supernatants were diluted 1:50 and loaded onto the pre-coated IL-6 ELISA plate. After adding 50 μl assay diluent RD1-14 to the 50 μl cell culture supernatant the plate was mixed by tapping for 1 min and incubated at room temperature for 2 h. Next, the plate was washed with wash buffer five times using a squirt bottle. In order to remove the liquid the plate was inverted and blotted against a clean paper towel. Then 100 μl IL-6 conjugate were added into each well and incubated for 2 h at room temperature. Following another five washes 100 μl substrate solution were added to each well and incubated in the dark for 30 min at room temperature. Finally 100 μl of stop solution were added to each well and the optical density of each well was measured using a microplate reader (Tecan Sunrise) set to 450

nm (wavelength correction set to 540 nm) using the Xfluor software. Each sample was run in duplicate and IL-6 concentrations were calculated using a standard curve.

The human CCL2/MCP-1 Quantikine ELISA kit (R&D) was used to assess *in vitro* MCP-1 production by primary human macrophages treated with IFNγ and LPS (Section 2.6.1). Culture supernatants were diluted 1:20 before 200 μl sample or standard were added to each well. After incubation for 2 h, plates were washed three times with wash buffer (included in kit). After inverting the plate to dry out the wells, 200 μl MCP-1 conjugate were added to each well and incubated for 1 h at room temperature. Following another three wash steps, 200 μl substrate solution were added and incubated for 30 min at room temperature. Finally, 50 μl stop solution were added into each well and optical density was determined using a microplate reader (Tecan Sunrise) set to 450 nm (wavelength correction set to 540 nm) using the Xfluor software. Each sample was run in duplicate and MCP-1 concentrations were calculated using a standard curve.

2.7.2 Mesoscale assay

The MSD 96-well 4-spot assay for IL-1β, IL-6, IL-8 and TNFα was used to analyse cytokine production by primary human macrophages, (m)HTT expressing U937 cells and GeRP-treated macrophages. For primary human monocytes a MSD 96-well 7-spot plate analysing IL-1β, IL-12p70, IFNγ, IL-6, IL-8, IL-10, TNFα was used. Cytokine production from murine cells was measured using the MSD mouse pro-inflammatory 7-Plex tissue culture kit analysing IL-1β, IL-12p70, IFNγ, IL-6, KC, IL-10, TNFα levels.

Depending on the type of stimulation, 25 μl of undiluted, 1:10 or 1:20 diluted culture supernatants were added onto the MSD plate and incubated with vigorous shaking for 2 h at room temperature. Then, the plate was washed three times

with PBS containing 0.05 % Tween before 25 μl detection antibody were added and incubated with vigorous shaking for 1.5 h at room temperature. Following a second wash step, 150 μl read buffer were added and the plate was analysed using the SECTOR machine and analysis software. An eight point calibration curve was run on every plate to calculate the concentrations of cytokine in each sample. Unless stated otherwise cytokine levels were normalised to the amount of protein measured in the corresponding well.

2.8 Protein chemistry

2.8.1 Protein isolation

Protein was isolated by lysing cells in RIPA buffer (25 mM Tris HCl pH7.6, 150 mM NaCl, 1% NP-40, 1% sodium deoxycholate, 0.1% sodium dodecyl sulfate (SDS)) containing one complete protease inhibitor cocktail (mini) tablets (Roche) per 10 ml buffer. The appropriate amount of RIPA buffer was added directly into the culture well and the plates shaken in the fridge for 5 min. Protein solutions were frozen at -80 °C before analysis.

2.8.2 Bicinchoninic acid (BCA) protein assay

Cell lysates were diluted appropriately (between 2-10 fold depending on the cell type analysed) and 20 μl of the protein solution were analysed by adding 200 μl working solution (1:50 ratio of BCA reagent A to B)(Thermo Scientific) in a 96-well format. The plate was incubated for 2 h at 37 °C before reading at 562 nm in a microplate absorbance reader (Tecan Sunrise) using the XFluor software. Each assay was performed in duplicate and the BSA standards provided by the kit were run on each plate.

2.8.3 Immunoprecipitation

HTT immunoprecipitations were performed as described (Landles et al., 2010), with the following adaptations. PBMCs, collected by density centrifugation of 50 ml whole blood, were lysed in 500 μl ice-cold lysis buffer (50 mM HEPES (pH 7.0), 150 mM NaCl, 10 mM EDTA, 1 % NP-40, 0.5 % sodium deoxycholate, 0.1 % SDS, 0.1 % BSA, 10 mM dithiothreitol (DTT), 1 mM phenylmethanesulfonylfluoride (PMSF), one complete protease inhibitor cocktail (Roche)). Lysates were pre-cleared prior to immunoprecipitation by incubation with 50 μl (1:1 slurry) prewashed G-Sepharose-agarose beads (Invitrogen) for 6 h at 4 °C. Immunoprecipitations were carried out overnight, mixing 1.5 mg pre-cleared protein supernatant, 30 μl protein G-Sepharose-agarose beads (1:1 slurry) and 2 μg antibody (Table 2.2) in a 1 ml final volume. Beads were pelleted by centrifugation at 13,000$\times$g for 30 s, washed four times with lysis buffer, resuspended in 16 μl 2$\times$ Laemmli buffer and denaturated at 75 °C for 5 min. Immunoprecipitates were then used for immunodetection of HTT, and in some case immunodetection of co-precipitated IKK via western blot (Section 2.8.5).

Table 2.2: Antibodies used for immunoprecipitation of HTT.

Antibody	Epitop	Company
anti-human IgG	-	Alpha Diagnostic (#20008-250)
2166	HTT aa443-457	Millipore (MAB2166)
2B7	HTT aa7-13	obtained from Novartis (Weiss et al., 2011)
3B5H10	N171 (65Q)	Sigma Aldrich
4C9	HTT aa51-71	obtained from Novartis

2.8.4 Immunoblot analysis of IκB degradation

Monocytes were isolated from whole blood (Section 2.5.4) and seeded at a density of 1x10^6 cells/well into 24-well plates and rested for 16 h. Cells were stimulated with 2 μg/ml LPS over a 2 h time-course before western blotting (Section 2.8.5).

2.8.5 Western blotting

Cell pellets were lysed in RIPA buffer (Section 2.8.1) and protein content was measured using a BCA protein assay (Section 2.8.2). Ten μg of protein were mixed with 5x Laemmli buffer, before denaturation at 95 °C for 10 min. Lysates were run on Novex(R) Tris-Glycine gels (depth 1.5 mm) (Invitrogen), using 8 % gels to dissolve large proteins such as HTT and 4-20 % gradient gels for smaller proteins ($\leq$100kDa). The kaleidoscope precision plus protein standard (Bio-rad) was loaded on every gel to mark protein size. Gels were run for 2-4 h at 130 V in the XCell II Blot Module CE Mark tank (Invitrogen) filled with 1$\times$ Tris-Glycine SDS page buffer (SLS). Gels were transferred onto polyvinylidene fluoride (PVDF) membranes (pre-wetted in 100 % methanol for 1 min) using the same XCell II Blot Module at 30 V for 2 h for smaller proteins and 14 V for 20 h for HTT. Membranes were then blocked with 5 % skimmed milk in Tris-buffered saline (TBS), pH 7.0, containing 0.1 % Tween20 (TBS-T) for 2 h. Blocked membranes were incubated with primary antibody (Table 2.3) in 5 % milk in TBS-T overnight. After washing several times with TBS-T, membranes were incubated for 1 h with the matching anti-mouse or anti-rabbit secondary alkaline phosphatase (AP) antibody (Sigma Aldrich; both used 1:10,000 diluted). Signals were visualised using CDP-Star substrate (Applied Biosystems) on Kodak BioMax MR-1 film, after washing vigorously with TBS-T. Membranes were stripped using ReBlot Plus strong solution

(Millipore) for 10min, before reprobing with anti-GAPDH antibody and secondary anti-rabbit-AP antibody as a loading control. Developed films were scanned using an Epson scanner and densitometry of digital images was achieved by using the TotalLab TL100 software.

Table 2.3: Primary antibodies used for western blot

Antibody	Dilution	Company
anti-human HTT, 1H6	1:1000	Abnova (Lunkes et al., 2002)
anti-human HTT, 2166	1:1000	Millipore
anti-human HTT, 4C9	1:500	obtained from Novartis
anti-human HTT, MW1	1:500	obtained from the Developmental Studies Hybridoma Bank developed under the auspices of the NICHD and maintained by The University of Iowa (Ko et al., 2001)
anti-human GAPDH	1:2000	Sigma Aldrich
anti-human IκB	1:500	Santa Cruz
anti-human IKKγ	1:2000	Santa Cruz
anti-human phospho-Cofilin	1:500	Cell Signaling

2.8.6 Time-resolved Förster resonance energy transfer - TR-FRET

Cells were lysed in 100 μl PBS containing 1 % TritonX-100 and a protease inhibitor cocktail (Roche) per 1x10^6 cells and 5 μl cell lysate were transferred into low-volume wells of white 384-microtiter plates (Greiner). A total of 1 μl detection buffer (50 mM NaH_2PO_4, 400 mM NaF, 0.1 % BSA, and 0.05 % Tween, plus antibody mix) was added, with the final antibody amount per well for soluble mHTT and total HTT detection being 0.25 ng 2B7-Tb plus 20 ng MW1-D2, or 1 ng 2B7-Tb plus 10 ng 2166- Alexa Fluor 488, respectively. Plates were rotated at 1000$\times$g for 30 s and incubated for 1 h. TR-FRET readout was performed with an EnVision

Reader (PerkinElmer). After the excitation of the donor fluorophore Tb (CisBio) at 320 nm and a time delay of 100 ms, the resulting Tb and acceptor D2 (CisBio) or Alexa Fluor 488 (Invitrogen) emission signals were read at 620 nm and 665 or 520 nm, respectively (Figure 2.4A/B). Ratios of 665/620 nm and 520/620 nm signals corresponded to mutant and total HTT levels, respectively. TR-FRET detection of insoluble, aggregated mHTT was performed by using MW8 antibodies labelled with either Tb (donor) or D2 (acceptor) fluorophores (Figure 2.4C). The TR-FRET protocol was the same as the one used for soluble mutant HTT. Total protein levels of cell lysates were quantified using a BCA protein assay (Section 2.8.2). HTT protein levels are shown as a percentage of the signal intensity over lysis buffer background signal after normalisation to total protein levels ($\triangle$F). All assays were carried out blinded to subject group.

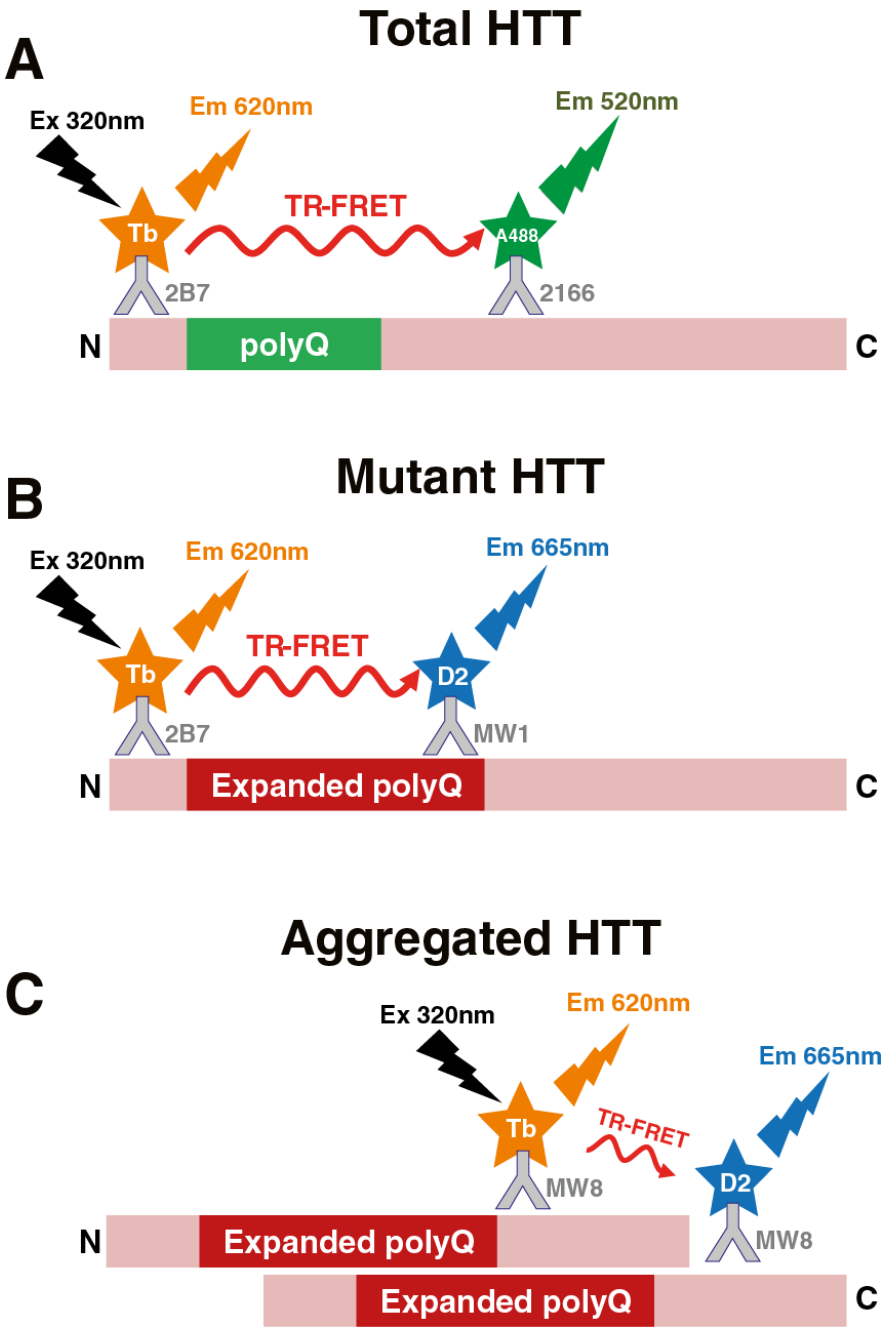

Figure 2.4: Antibody combinations used in the TR-FRET immunoassay. **(A)** Measuring total HTT, cell lysates were incubated with the 2B7-Tb and the 2166-AlexaFluor 488(A488) antibodies detecting both wild-type and mutant HTT. **(B)** For mHTT-specific detection, cell lysates were stained with N-terminal 2B7-Tb and the polyglutamine specific MW1 antibody. **(C)** MW8-Tb and MW8-D2 antibodies were used to detect insoluble mHTT aggregates.

2.9 Flow cytometry

2.9.1 Cell surface marker staining

A maximum of 1x10^6 cells were transferred into a round bottom 96-well plate. The plate was centrifuged at 300×g for 5 min and supernatants were removed by flicking the plate. Fifty μl of the relevant, diluted antibody (Table 2.4), prepared in FACS buffer (PBS with 1 % FCS and 0.02 % sodium azide) were added to each well and mixed by trituration. Cells were stained, in the dark, for at least 20 min on a shaker at 4 °C. Afterwards the cells were washed once in 200 μl FACS buffer (centrifuged at 300×g, 5 min) and either resuspended in 200 μl FACS buffer, transferred to FACS tubes and analysed directly or fixed in 200 μl FACS buffer containing 0.5 % PFA and kept at 4 °C, in the dark until analysis.

Table 2.4: Directly conjugated antibodies used for FACS.

Antibody	Used concentration	Company
anti-human CCR2 PE	0.25 μg/ml	R&D Systems
anti-human CD14 APC	0.25 μg/ml	eBioscience
anti-human CD206 PE	0.5 μg/ml	BioLegend
anti-human CD64 FITC	5 μl per test	BD Pharmingen
anti-mouse CD3e PE	2 μg/ml	eBioscience
anti-mouse CD3e APC	2 μg/ml	eBioscience
anti-mouse CD4 APC	2 μg/ml	eBioscience
anti-mouse CD8a FITC	5 μg/ml	eBioscience
anti-mouse CD11b PE	2 μg/ml	eBioscience
anti-mouse CD11c FITC	2 μg/ml	eBioscience
anti-mouse CD19 FITC	5 μg/ml	eBioscience
anti-mouse CD45R(B220) APC	2 μg/ml	eBioscience
anti-mouse F4/80 APC Cy7	2 μg/ml	BioLegend
anti-mouse MHC II APC	2 μg/ml	eBioscience

Non-stained and single-colour stained cell controls were always performed. Samples were run on a FACScalibur (BD Bioscience) with CellQuest software Pro (BD Bioscience). Data analysis was performed using FlowJo7.2.5 (Tree Star).

2.9.2 Phosphoflow analysis of STAT phosphorylation

PBMCs were isolated from blood using density centrifugation. In order to remove platelets, cells were washed with 25 ml HBSS (centrifuged at 200×g for 10 min). Cell pellets were resuspended in 5 ml HBSS and counted using a Neubauer counting chamber. 1×10^6 cells were distributed in six FACS tube (BD Biosciences) each per subject and each tube was filled up to 1 ml with HBSS before resting the cells for 30 min at 37 °C; followed by trituation and resting for additional 10 min at 37 °C. After centrifugation at 300×g for 5 min, the pellet were vortexed before 5 μl of CD64 antibody (Table 2.4), diluted 1 in 3 in HBSS, were added and incubated for 15 min in the dark at room temperature. Samples were washed with 1 ml HBSS (centrifuged 300×g for 5 min) before stimulation. For each subject, three tubes remained unstimulated with the addition of 1 ml fresh HBSS and one tube was stimulated with either 20 ng/ml IFNγ, IL-6 or GM-CSF in 1 ml HBSS. Samples were incubated for 20 min at 37 °C before adding 1 ml 37 °C pre-heated BD Phosflow Cytofix buffer and incubating at 37 °C for an additional 10 min. After centrifugation at 300×g for 5 min, the supernatants were poured off and 1 ml -20 °C cold BD Phosflow Perm Buffer III was added and the samples were incubated for 30 min in the dark on ice. Afterwards, the samples were washed twice with 1 ml BD Phosphoflow stain buffer (centrifuged at 300×g for 5 min). Finally, samples were stained intracellularly with pSTAT antibodies (Table 2.5) for 30 min in the dark at room temperature. After washing with 2 ml BD Phosphoflow stain buffer (centrifuged at 300×g for 5 min) samples were analysed on a FACScalibur with CellQuest software Pro. Data analysis was performed using FlowJo7.2.5.

Table 2.5: Intracellular antibodies used for FACS

Antibody	Used concentration	Company
Alexa Flour 647 anti-human pSTAT1	10 μl per test	BD Biosciences
Alexa Flour 647 anti-human pSTAT3	5 μl per test	BD Biosciences
Alexa Flour 647 anti-human pSTAT5	5 μl per test	BD Biosciences

2.9.3 Imaging flow cytometry

Primary human CD14$^+$ monocytes were seeded at 2×10^6 into 6-well plates and left to rest for 16 h. The cells were stimulated with 2 μg/ml LPS over a 90 min period before being scraped off the plates. Pelleted cells (300$\times$g for 5 min) were fixed for 15 min and permeabilised for 10 min using the eBioscience Fix/Perm solutions, before NFκB p65 XP antibody (1:200; Cell Signaling) diluted in permeabilisation buffer was added. After 30 min incubation shaking at 4 °C, cells were washed twice with FACS buffer and centrifuged for 5 min at 400$\times$g. Secondary anti-rabbit IgG PE antibody (eBioscience) was added at 1:100 in FACS buffer and incubated for 30 min before washing the cells twice with FACS buffer. Cells were resuspended in 80 μl FACS buffer and stained with 1 μg/ml 4',6-diamidino-2-phenylindole (DAPI) just before analysis. Samples were run on the ImageStreamX analyser (Amnis) and analysed using the IDEAS software. Gating on in focus, single cells, the similarity feature (Similarity_Erode(Object(M04,BF,Tight)2)_Dapi_p65) was used to establish the rate of p65 translocation by measuring the overlap of DAPI and p65 staining. Translocation rate was normalised to baseline levels.

2.10 Transcriptome analysis

2.10.1 RNA isolation

RNA was isolated using the QIAGEN RNAeasy Mini kit. Cells were lysed in 600 μl lysis buffer, before RNA was precipitated by adding an equal amount of 70 % ethanol (diluted in ddH_2O). Samples were then transferred onto spin columns (provided with the kit) and washed once with 350 μl RW1 buffer(provided with the kit) (centrifuged 15 s at 8,000$\times$g), before adding 80 μl DNase solution (QIAGEN). After 15 min incubation at room temperature, columns were washed again with 350 μl RW1 buffer (centrifuged 15 s at 8000$\times$g), followed by two washes with 500 μl RPE buffer (provided with the kit) (15 s and 2 min spins at 8,000$\times$g). The columns were then dried at 8000$\times$g for 1 min and RNA was eluted using 20-40 μl RNase-free water (provided with the kit). Finally, the RNA concentration was measured using a Nano Drop Spectrophotometer. RNA was stored at -80 °C.

2.10.2 Reverse transcription of RNA to cDNA

For the reverse transcription reaction, SuperScript II reverse transcriptase (Invitrogen) was used, mixing 500 ng RNA diluted in 10 μl RNase-free water with 1 μl random primers (500 μl/ml) and 1 μl dNTPs (10 mM each) (both Invitrogen). The mix was heated to 65 °C for 5 min, then quickly chilled on ice before 4 μl 5$\times$ First-Strand buffer, 1 μl 0.1M DTT and 1 μl RNaseOUT (40 units/ μl) (all Invitrogen) were added. After incubating for 2 min at room temperature, 1 μl (200 Units) SuperScript II reverse transcriptase was added. To start transcription the mix is incubated at 25 °C for 10 min followed by 42 °C for 50 min. To stop the enzyme, the mix was incubated for 5 min at 95 °C and put on ice immediately afterwards. cDNA was then stored at -20 °C.

2.10.3 Quantitative PCR

For quantitative PCR (qPCR) analysis, SYBR Green master mix from Applied Biosystems was used. For the reaction 12.5 μl SYBR Green, 10.75 μl H_2O, 1 μl cDNA (equating to 5 ng cDNA per reaction) and 0.75 μl of primer (300 pM, Table 2.6) were mixed. The PCR reactions were prepared in MicroAmp fast optical 96-well reaction plates and subsequently covered with MicroAmp optical adhesive film (Applied Biosystems). After centrifuging the plates for 10 s at 300$\times$g, they were run on a 7500 fast real-time PCR system (Applied Biosystems) using 7500 software. The PCR cycling conditions were as followed: 95 °C for 10min followed by 40 cycles of 95 °C for 15 s and 60 °C for 1min. All reactions were run in triplicate. In addition to the genes of interest, endogenous control genes (GAPDH, B2M and BACTIN) were always run as well for each sample. In order to analyse the data, the Ct value of each sample was determined by the 7500 software (example shown in Figure 2.5).

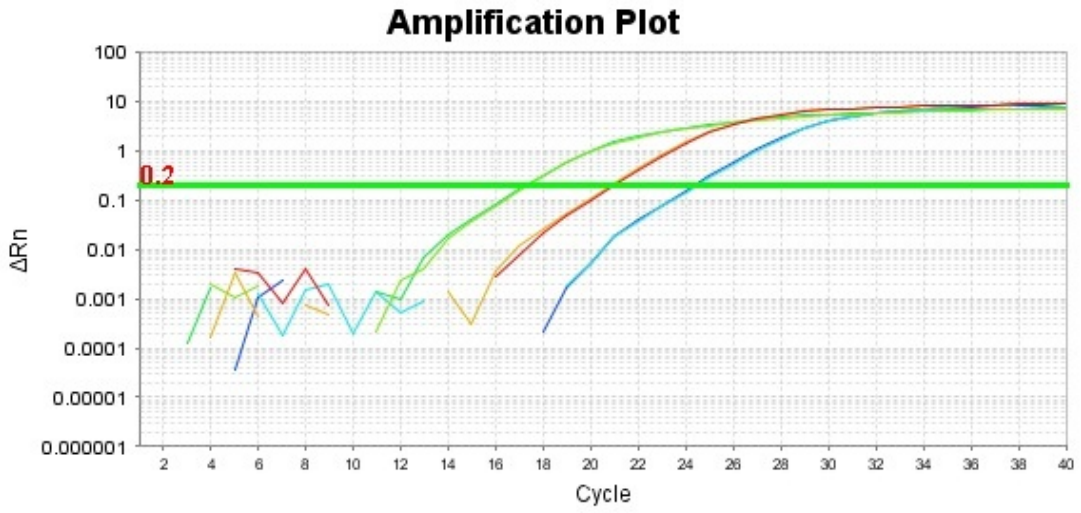

Figure 2.5: Example of Ct values for qPCR. Example graph showing Ct value determination for three genes, run in duplicate from the same sample (green- B2M, red and yellow - GAPDH, blue- HTT). X-axis shows number of PCR cycles run and y-axis shows the corresponding level of SYBR Green fluorescences (Rn) over the background. The green horizontal line shows the threshold determining the Ct value (point where threshold cuts amplification curve) for each gene.

Table 2.6: Primers used for qPCR

Primer		Sequence
human BACTIN	forward	AAG GCC AAC CGT GAA AAG AT
	reverse	GTG GTA CGA CCA GAG GCA TAC
human AKT1	forward	CAT CAC ACC ACC TGA CCA AG
	reverse	CTC AAA TGC ACC CGA GAA AT
human B2M	forward	GAA TTC ACC CCC ACT GAA AA
	reverse	CCT CCA TGA TGC TGC TTA CA
human CD40	forward	CAC CTC GCT ATG GTT CGT CT
	reverse	CTG GTG GTG GCA GTG TGT CTC TC
human CCR1	forward	CCC TTG GAA CCA GAF AGA AG
	reverse	CCA GGC CAA TGA CAA ATA CC
human CCR2	forward	GAC AAG CCA CAA GCT GAA CA
	reverse	CAC CGC TCT CGT TGG TAT TT
human CCR5	forward	CTG AGA CAT CCG TTC CCC TA
	reverse	GCT CTT CAG CCT TTT GCA GT
human GAPDH	forward	AAC AGC GAC ACC CAT CCT C
	reverse	CAT ACC AGG AAA TGA GCT TGA CAA
human HTT	forward	AGT GAT TGT TGC TAT GGA GCG G
	reverse	GCT GCT GGT TGG ACA GAA ACT C
human IL6	forward	TAC CCC CAG GAG AAG ATT CC
	reverse	AGT GCC TCT TTG CTG CTT TC
human IL10	forward	TGC CTT CAG CAG AG GAA GA
	reverse	GGT CTT GGT TCT CAG CTT GG
human IRAK1	forward	CTA CCT GCC CGA GGA GTA CA
	reverse	GTG CTT CTC AAA GCC ACT CC
human JUN	forward	TTT CGG GAG TGT CCA GAG AG
	reverse	GAG AAG CCT AAG ACG CAG GA
human TLR4	forward	CTC CTG CGT GAG ACC AGA AA
	reverse	GGT TGA GAA GGG GAG GTT GT

In order to normalise the samples, the Ct value for each gene was subtracted by the mean Ct value of the three house-keeping genes for the same condition. The relative gene expression was then calculated, setting one condition as standard, using the following formula :

relative gene expression = $2^{-(\text{Ct from gene of interest}/\text{Ct from standard gene})}$

2.10.4 SABioscience Human NFκB Signaling Pathway RT Profiler PCR Arrays

RNA quality control

For the PCR arrays, RNA was isolated from 2x10^6 unstimulated monocytes using the QIAGEN RNeasy Mini Kit (Section 2.10.1). RNA integrity was evaluated using 2100 RNA bioanalyser chips (Agilent). The eukaryote total RNA 6000 nano chip is a miniature electrophoresis system analysing the integrity of the S18 and S28 ribosomal RNA molecules. High quality RNA samples demonstrate clear 18S and 28S RNA bands (Figure 2.6) and only samples demonstrating non-degraded RNA were used.

To run the chip, 550μl Agilent RNA 6000 nano gel matrix was transferred into a spin filter tubes and centrifuged for 10 min at 1500$\times$g. Then, 65 μl of the filtered gel was mixed with 1μl RNA 6000 nano dye, vortexed thoroughly and centrifuged for 10 min at 13,000$\times$g. With the chip in the loading station, 9 μl gel-dye mix was pipetted into the bottom of the well marker G before pressurising the system using the syringe in the loading station. After 30 s the pressure was released and 9 μl gel-dye mix was transferred in the two wells above the well labelled G. Next, 5 μl of the RNA 6000 nano DNA marker were dispensed into all sample and the ladder well. This twenty five nucleotide marker allows aligning of all electrophoresis reactions, as each well was read separately. Following this, 1 μl

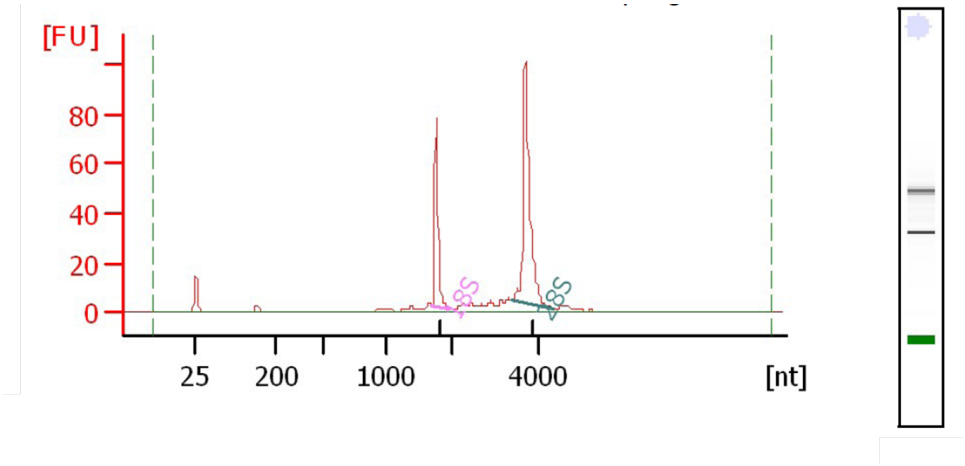

Figure 2.6: Example of high quality RNA sample analysed on the bioanalyser. RNA samples were run on RNA 6000 chips in miniature electrophoresis reactions. Non-degraded RNA demonstrates two clear bands on the gel and two clear peaks for 18S and 28S ribosomal RNA.

ladder and 1 μl of each sample were added into the corresponding wells and the chip was vortexed for 60 s. Chips were run on a Agilent 2100 bioanalyser using the Agilent 2100 expert software.

Reverse transcription

RNA was reverse transcribed using the RT2 First Strand kit for cDNA transcription, adding 1 μg RNA resuspended in 8 μl water to 2 μl GE buffer before incubating the mix for 5 min at 42 °C. After chilling the mix on ice, 10 μl of RT cocktail (4 μl 5$\times$RT buffer 3, 1 μl P2 (primer control mix), 2 μl RT enzyme and 3 μl water) were added to each RNA sample and incubated at 42 °C for 15 min before the reaction was stopped by heating to 95 °C for 5 min. Ninety one μl non-DEPC treated nuclease-free water were added to each 20 μl reaction and the cDNA was stored at -20 °C until use.

PCR reactions

For the PCR reaction, 1350 μl 2$\times$ RT2 SYBR Green qPCR Mastermix and 1248 μl water were added to the cDNA synthesis reactions, before adding 25 μl of this experimental cocktail into each well of the primer coated array plates using a multichannel pipette. Plates were centrifuged for 10 s at 300$\times$g and run on a 7500 fast real-time PCR system (Applied Biosystems) using the 7500 software. PCR cycling conditions were as followed: 95 °C for 10 min followed by 40 cycles of 95 °C for 15 s and 60 °C for 1 min. A melting curve, ranging from 60-95 °C was run on each plate to exclude the occurrence of primer dimers.

Each PCR array plate included primers for 84 genes of interest, five housekeeping genes (*B2M, BACTIN, GAPDH, RPL13A* and *HPRT1*) and seven wells for quality controls. One control well was the genomic DNA control, which includes primers specific for genomic DNA. If the Ct value for this well was below 35, the results for the whole plate were discarded. Three wells for the reverse-transcription control (RTC) tested the efficiency of the reverse-transcription reaction performed with the RT2 First strand kit by detecting template synthesised from the kits built-in external RNA control. The three wells for the positive PCR control (PPC) consists of a predispensed artificial DNA sequence, testing the efficiency of the PCR itself. Plates with an average (Ct^{RTC}-average Ct^{PPC}) $\geq$ 5 were discarded, as values higher than 5 indicate an inhibitor of reverse transcription in the sample. To guarantee the same PCR efficiency between plates, the average Ct of the PPC controls had to range within two cycles for all plates analysed.

Analysing the data, the Ct value of each sample was determined by the 7500 software (Figure 2.5). In order to normalise the samples, the Ct value for each of the 84 genes of interest was subtracted by the mean Ct value of the five housekeeping genes for the same sample. The relative gene expression was then calculated, setting one condition as standard, using the following formula :

relative gene expression = $2^{-(\text{Ct from gene of interest}/\text{Ct from standard gene})}$

Fold changes were calculated by dividing the relative gene expression of one condition by the relative gene expression of the control.

Network analysis

A gene network was constructed using STRING, a database and web resource composed of known and predicted protein-protein interactions of both physical, functional and bibliometrical nature collected from a large number of biological resources (Jensen et al., 2009). Cytoscape, an open source software for integrating interaction networks with high-throughput expression data (Shannon et al., 2003) was utilised to highlight and analyse differential gene expression in monocytes isolated from HD and control subjects. This produced a network with 9366 interactions (edges) between the 84 genes (nodes), with only five genes connected solely by 'textmining interactions'.

Promoter analysis

Genomatix Gene2Promoter software was used to compare the transcription factor binding sites in the promoters of different genes. After entering the gene names, the program lists all known transcription factor binding sites in the gene's promoter (set to look at 1000 bp upstream the first transcription start site and 500 bp downstream of the last transcription start site). Grouping the genes into changed and unchanged allowed comparisons between transcription factor binding site prevalence in the genes changed in HD samples. Multiple binding sites of a certain transcription factor in one gene promoter were not valued higher than a single binding site.

2.11 Microscopy

2.11.1 Imaging differentiated macrophages

Monocytes were seeded at a density of 2×10^6 cells per well in 6-well plates and differentiated into macrophages. After six days macrophage morphology was assessed under the microscope (Nikon Eclipse TS100, Objective $40\times$) and representative pictures were taken using the attached camera (Nikon DS-Fi1) and NIS-Elements F 3.00 software. The number of macrophages was counted in three or four fields of view, including 20-30 cells each, using the ImageJ software.

2.11.2 Analysis of GeRP uptake

For immunofluorescence experiments on primary monocytes, autoclaved 13 mm glass coverslips (VWR) were coated with 1 mg/ml poly-L-lysine for 10 minutes at room temperature. Coverslips were subsequently washed three times with sterile double-distilled water and air dried. Monocytes were seeded onto the coverslips at a density of 1×10^5 per coverslip and left to attach overnight. Monocytes were then incubated with empty green fluorescent GeRPs (1:10 ratio) for 12 h, washed three times with PBS and fixed with 4 % PFA, for 20 min at room temperature. After fixation, coverslips were washed three times with PBS and mounted in anti-fade medium (DAKO) with 1 μg/ml DAPI. Images were acquired using a Zeiss 510 meta microscope (Objective 63x/1.4 Oil DIC, 1024x1024, zoom 4) with Zeiss LSM software, overlaying the bright-field image of the cells with the 405 nm and 488 nm fluorescence channels for DAPI and green fluorescence, respectively.

2.11.3 Phalloidin staining to assess actin remodeling

To analyse actin remodeling in primary monocyte-derived macrophages, 1×10^5 monocytes were seeded on non-coated autoclaved 13 mm glass coverslips and differentiated into macrophages as described in Section 2.5.4. Macrophages were stimulated with 100 μM ATP or 50 ng/ml MCP-1 for either 5 or 10 min before being fixed with 4 % PFA, for 20 min at room temperature. After fixation, coverslips were washed three times with PBS and treated with 0.1 % Triton X-100 in PBS for 5 min. After washing the coverslips three times again with PBS, cells were stained with one Unit of Alexa Fluor 568 phalloidin (Invitrogen) for 20 min at room temperature. After washing again with PBS, cells were mounting in anti-fade medium (DAKO) with 1 μg/ml DAPI. Images were acquired using a Zeiss 510 meta microscope (Objective 63$\times$/1.4 Oil DIC, 512$\times$512) with Zeiss LSM Image browser software. The number of filopodia forming cells as well as the number of total cells were counted in at least 10 fields of view, including 20-30 cells each, using the ImageJ software.

2.12 Statistical analysis

Chapter 3

To allow for repeated measures for some subject and potential heteroskedasticity, generalised estimating equations with robust standard errors were used to estimate the associations between HTT protein levels and disease stage, and with disease burden. For models relating atrophy to mHTT levels, ordinary least squares regression was used with mean mHTT levels used for multiple measures. Statistical analyses were adjusted for age and gender. Analysis was performed in STATAv12.

Chapter 4

For cytokine profiling data, inter-group differences were identified by one-way ANOVA with post-hoc Tukey HSD testing to allow for multiple comparisons. Data were corrected for age and gender before analysis. Cytokine profiling data from U937 cells and *HTT* knock-down cells were analysed by two-way ANOVA with Bonferroni post-tests. Changes in phagocytosis ability and gene expression changes measured by qPCR were analysed using unpaired two-tailed student t tests. Paired two-tailed student t tests were used to analyse the effects of anti-*HTT* siRNA compare to scrambled siRNA in cells from the same individual.

Chapter 5

Inter-group differences in migration ability were identified by two-way ANOVA with Bonferroni post tests. Chemokine receptor expression differences were analysed using one-way ANOVAs with Dunnett's multiple comparison for multiple groups, while unpaired two-tailed student t tests were used for comparisons between two groups only. MCP-1 production by macrophages as well as p-cofilin levels in monocytes were statistically evaluated using an unpaired two-tailed student t tests. Lastly filopodia formation after different treatment conditions was analysed using two-way ANOVAs with Bonferroni post-tests.

Chapter 6

Cytokine production by transgenic HD mice was compared with WT mice using unpaired two-tailed student t tests. The abundance of different immune cell subtypes in the spleen of HD mice as well as all functional comparisons between HD and wild-type mice were analysed using unpaired two-tailed student t tests.

3 mHTT protein accumulates in immune cells of HD patients

3.1 Background

Mutant HTT expression in the CNS is the primary pathogenic factor for the development of HD and increasing expression levels are associated with disease severity and toxicity in various models (de Almeida et al., 2002). However, HTT is expressed ubiquitously (Li et al., 1993) and HD patients exhibit multiple systemic changes (van der Burg et al., 2009). One of the peripheral tissues affected is the immune system, where increases in innate immune proteins found in patient plasma track with disease progression (Dalrymple et al., 2007). Inflammatory cytokines and chemokines are elevated in the plasma of HD patients, the origin of which appears to be hyper-reactive monocytes (Björkqvist et al., 2008; Wild et al., 2011). Work presented in Chapter 4, demonstrates that this phenotype is caused by cell-intrinsic effects of mHTT expression, likely by interaction with the NFκB pathway. Furthermore, recent studies using peripherally-administered KMO inhibitors (Zwilling et al., 2011) and bone marrow transplantation (Kwan et al., 2012a) show that both can improve the HD phenotype in mice, suggesting the immune system as a modifier of HD. Hyper-reactivity, as observed in monocytes, is also found in murine HD microglia (Björkqvist et al., 2008), and microglial

activation is seen before symptom onset in HD mutation carriers (Tai et al., 2007). Peripheral immune dysfunction, therefore, may be pathogenically important in itself, but may also offer a window onto relevant CNS dysfunction.

While many putative therapeutic approaches for HD attempt to lower mHTT levels in the CNS or systemically (Sah and Aronin, 2011), non-invasive means of quantifying mHTT in the CNS and thereby measuring the success of any HTT lowering attempts, do not exist. Peripheral readouts using easily available tissues such as blood, may be of value in assessing the effects of systemically-delivered HTT-lowering therapies and detecting peripheral effects of centrally-delivered therapies. Furthermore, given the cell-intrinsic nature of the immune defects in HD patient immune cells (see Chapter 4), mHTT levels may track with disease progression and be of value as biomarker. The HD field has the unique opportunity of predictive genetic testing, which allows identification of individuals who carry the gene defect before the onset of symptoms. This provides the opportunity for early intervention, ideally preventing or delaying disease onset. However, in order to track the success of any therapeutic approach in premanifest HD gene carriers, robust and practical measures of disease progression (i.e. biomarkers) are needed. While TRACK-HD has provided evidence that imaging measures such as brain atrophy and cognitive tests such as an emotion recognition task could be useful biomarkers for HD (Tabrizi et al., 2012), robust wet biomarkers are still to be found.

The aim of this project was to utilise a recently described TR-FRET immunoassay (Weiss et al., 2011) to quantify total HTT and mHTT levels in different peripheral cells obtained from HD patients, including different immune cells subsets and epithelial cells. To evaluate whether total HTT and/or mHTT levels may be useful as biomarker, measures were correlated with known markers of disease progression such as brain atrophy and disease burden score.

3.2 Contributions

The study was a collaboration between UCL, London and Novartis, Basel. Ulrike Träger collected all samples, sorted the immune cell types, performed quality control, and shipped them to Dr Andreas Weiss and Stephan Grueninger for HTT quantification. Dr Weiss also performed all assay quality control experiments. Data was then unblinded by the statisticians Ruth Farmer and Prof Chris Frost for analysis. Brain scan data was provided from the TRACK-HD study. Dr Christian Landles has quantified HTT fragmentation in the human PBMC samples collected by Dr Ralph Andre and Ulrike Träger. Findings presented in this chapter were published in the Journal of Clinical Investigation:

Weiss A, Träger U, Wild EJ, Grueninger S, Farmer R, Landles C, Scahill RI, Lahiri N, Haider S, Macdonald D, Frost C, Bates GP, Bilbe G, Kuhn R, Andre R, Tabrizi SJ (2012) Mutant huntingtin fragmentation in immune cells tracks Huntington's disease progression. *J Clin Invest* 122: 3731-3736

3.3 Methods

Different immune cell subsets were isolated from whole blood using magnetic cell sorting (Section 2.5.4), while epithelial cells were harvested using buccal smears (Section 2.5.3). TR-FRET immunoassays were used to quantify total and mutant HTT levels (Section 2.8.6). Brain atrophy measures were obtained as part of the TRACK-HD study (Section 2.4) and disease burden scores were calculated as [CAG repeat length - 35.5] $\times$ age. HTT fragments were visualised by immunoprecipitation and western blot (Section 2.8.3 and 2.8.5). Statistical methods used are detailed in Section 2.12.

3.4 Results

3.4.1 Mutant but not total HTT accumulates in immune cells from HD patients

In order to measure mutant and total HTT protein levels in different immune cell subsets, monocytes, T cells and B cells were isolated from blood samples collected from eight premanifest HD mutation carriers, ten early-stage and eight moderate-stage HD patients, and twelve control subjects. Cheek swabs to harvest buccal epithelial cells were collected from 84 subjects including all blood donors. For some participants multiple swabs and/or blood samples were taken over a period of one year.

Most HD patients carry 40-50 CAG repeats in their *mHTT* allele (Myers, 2004). The patient cohort used in this study was broadly within this range with the exception of one early HD patient expressing mHTT with 59 polyQ repeats (Table A.2). In order to validate that the 2B7-MW1 antibody pair used in the TR-FRET immunoassay selectively detects mutant ($\geq$40Q) over wild-type HTT ($\leq$40Q, but with an average of 18 repeats), an allelic series of purified HTT with increasing polyQ repeat lengths was analysed by TR-FRET. This showed a ten fold higher sensitivity for mHTT containing 40Q compared with the wild-type protein with 18Q (Figure 3.1). Furthermore, while there is a steep increase in TR-FRET signal between 20-40 polyQ repeats, the signal reaches a plateau at 40 repeats being the same between 40 and 60 polyQ repeats. This shows that an increase in mHTT signal in this range correlates with an increase in mHTT concentration, unrelated to polyQ repeat length.

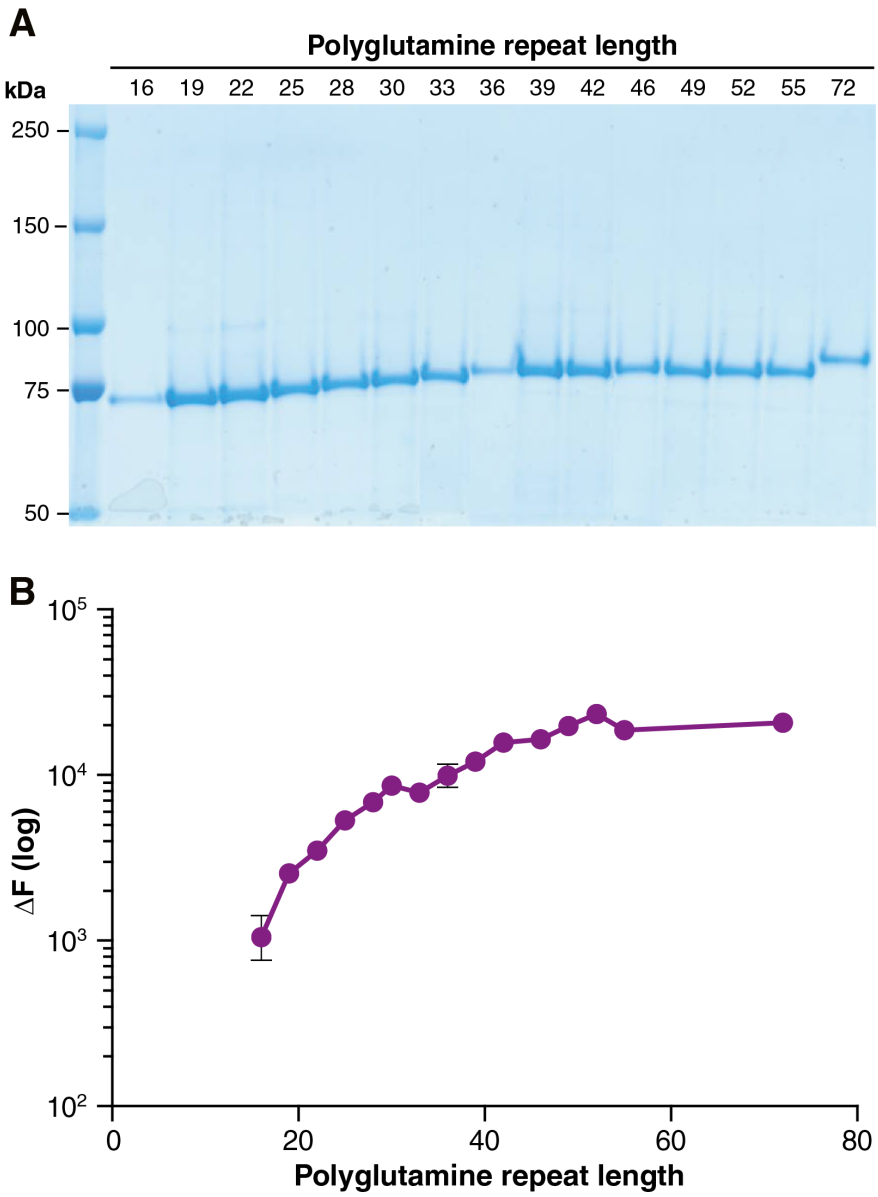

Figure 3.1: TR-FRET detects mHTT protein with a ten fold higher sensitivity than wild-type HTT protein. **(A)** Coomassie-stained gel verified lengths and purity of N-terminal HTT protein fragments (548aa) with increasing polyglutamine repeat lengths. GST-tagged HTT proteins were expressed in *E. coli* and isolated via PreScission column purification followed by GST-cleavage. **(B)** 2B7-MW1 TR-FRET signal intensities for detection of 11 fmol purified HTT protein with increasing polyglutamine repeat lengths. Figure by Dr Andreas Weiss.

Measuring total HTT levels by TR-FRET using the 2B7-2166 antibody pair, showed no significant difference ($p>0.05$) between HD patients and controls in any of the cell types analysed (Figure 3.2).

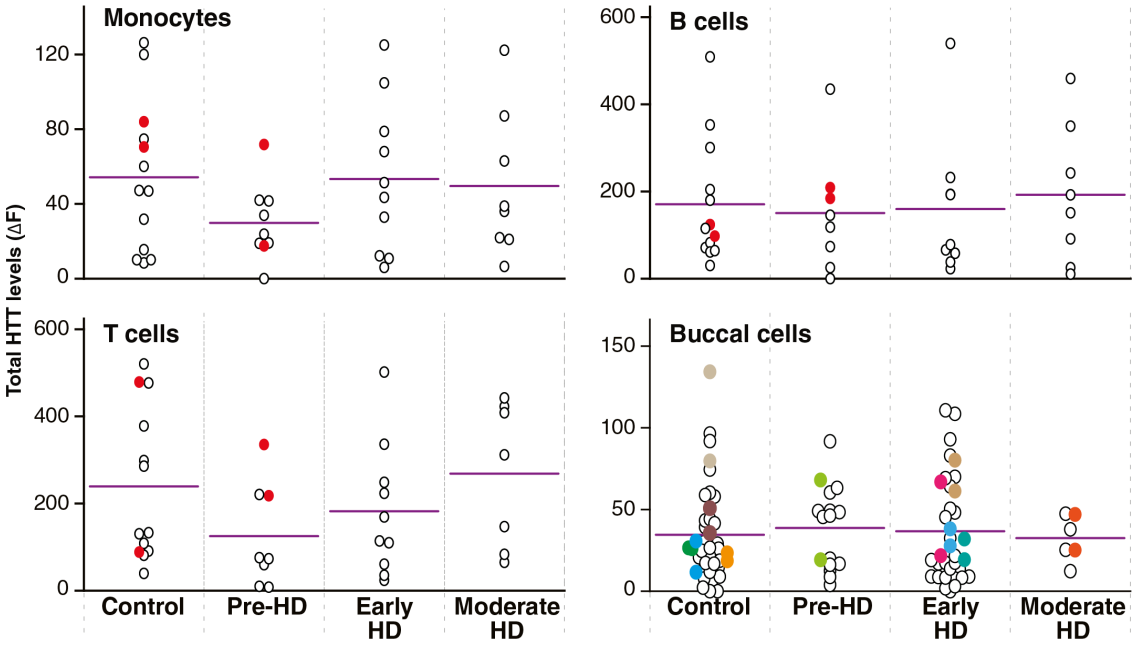

Figure 3.2: Relationship between total HTT levels and disease stage. Total HTT protein levels in monocytes, T cells, B cells and buccal cells were quantified by TR-FRET using 2B7 and 2166 anti-HTT antibodies. Total HTT levels in all four cell types showed no significant differences between HD patients and control subjects, or between HD gene carriers at different disease stages. Coloured circles indicate multiple samples from a single subject. Experiment performed in collaboration with Dr Andreas Weiss and Stephan Grueninger.

Mutant HTT levels, analysed using the 2B7-MW1 antibody pair in an TR-FRET immunoassay, were statistically significantly higher ($p\leq0.001$) in all cell types isolated from HD patients compared with controls. Furthermore, mean mHTT levels increased with successive disease stage in each leukocyte cell type, with differences ($p\leq0.01$) between premanifest and manifest HD patients, and between premanifest and early HD ($0.021\leq p\leq0.051$), but not between early and moderate HD (Figure 3.3, Table 3.1). Mutant HTT levels in buccal epithelial cells were significantly elevated in HD compared with control cells, but not different between disease stages (Figure 3.3).

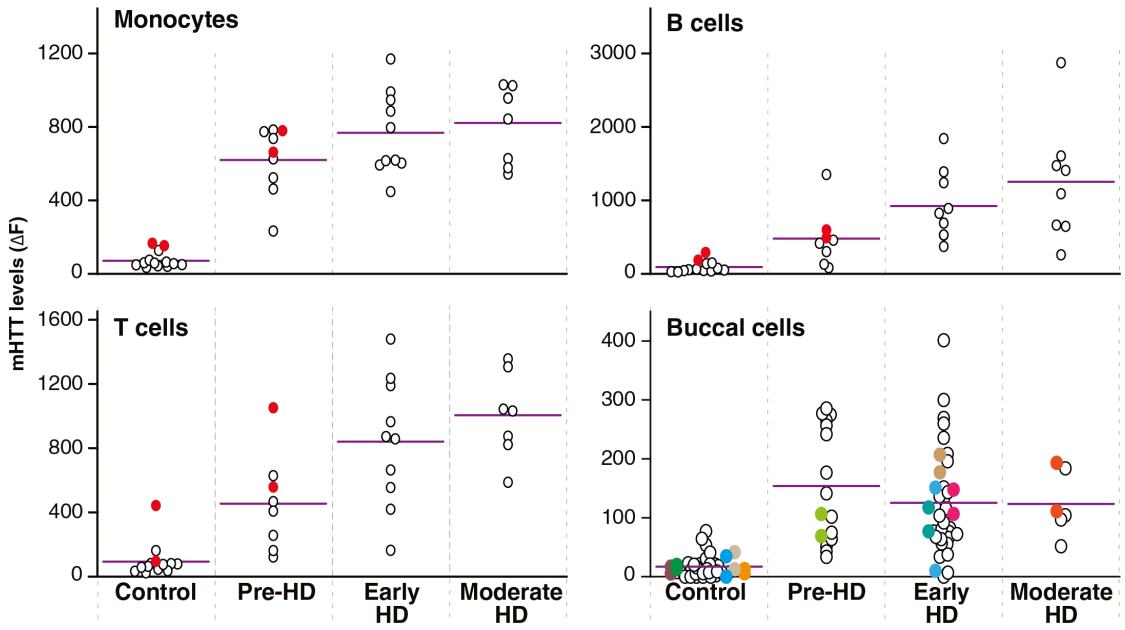

Figure 3.3: Relationship between mHTT levels and disease stage. Mutant HTT protein levels in monocytes, T cells, B cells and buccal cells were quantified by TR-FRET using the 2B7 antibody and a polyQ-specific antibody, MW1. Mutant HTT protein was detected in all samples from HD patients and premanifest HD mutation carriers, as compared with controls. Differences in mean mHTT levels in leukocytes were observed between premanifest and manifest HD patients ($p \leq 0.01$), and between premanifest and early-stage HD subjects ($p=0.051$ and $p \leq 0.05$ for monocytes and T cells/B cells, respectively). No differences were detected between HD disease stages in buccal cells. Coloured circles indicate multiple samples from a single subject. Experiment performed in collaboration with Dr Andreas Weiss and Stephan Grueninger.

Table 3.1: P-values for associations between cellular mHTT levels and disease stage adjusted for age and gender.
^{A} estimated using linear contrasts

	Number of observations/ subjects	p-value			
		HD vs. control^A	pre-HD vs. manifest^A	early HD vs. pre-HD	moderate vs. early HD
Monocytes	40/38	<0.001	0.007	0.051	0.404
T cells	38/36	<0.001	0.001	0.021	0.217
B cells	38/36	<0.001	<0.001	0.024	0.260
Buccal cells	98/84	<0.001	0.406	0.439	0.923

3.4.2 Levels of mHTT in HD immune cells correlate to disease burden score

Disease burden scores (Penney et al., 1997) are based on an individual's age and *HTT* CAG repeat length. The score correlates with clinically relevant endpoints (Tabrizi et al., 2012), and is therefore an important and easily accessible marker for disease progression in HD. To correlate the HTT levels measured in primary human cells with this marker, disease burden scores were calculated for each HD patient. After adjustment for age and gender, there was a strong ($p<0.001$) positive association between disease burden and mHTT levels in monocytes and T cells (Figure 3.4). A significant ($p<0.05$) association was also observed for B cells, but no evidence of an association was found in buccal epithelial cells (Figure 3.4).

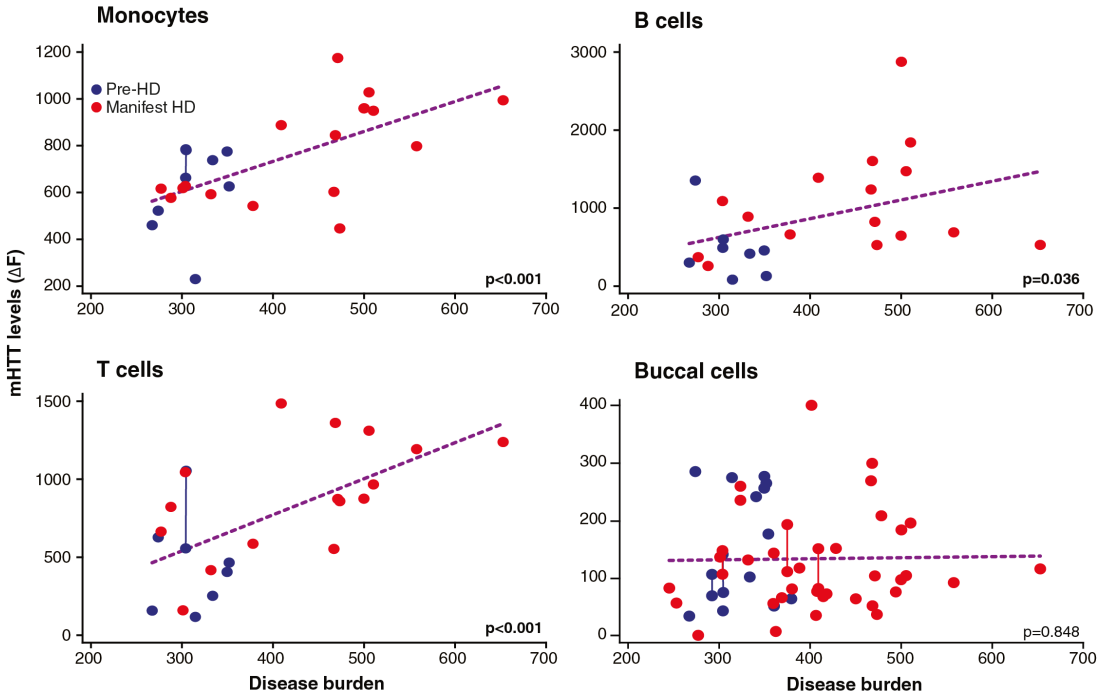

Figure 3.4: Associations between mHTT levels and disease burden score. Mutant HTT protein levels in leukocytes showed a statistically significant positive association with HD disease burden score, while levels in buccal epithelial cells do not show an association with HD disease burden score. Repeated measurements for a single subject are joined by a line.

Given that disease burden score is a function of CAG repeat length, and to investigate whether mHTT accumulates more in immune cells with longer CAG repeats, mHTT levels were correlated with the CAG expansion length of the patient. A significant association between the two factors was observed in monocytes and T cells (Figure 3.5). Interestingly, however, B cells did not show a significant association between CAG and mHTT, while the association between disease burden score and mHTT levels was significant in these cells. Buccal epithelial cells also did not demonstrate any association between CAG repeat and mHTT levels.

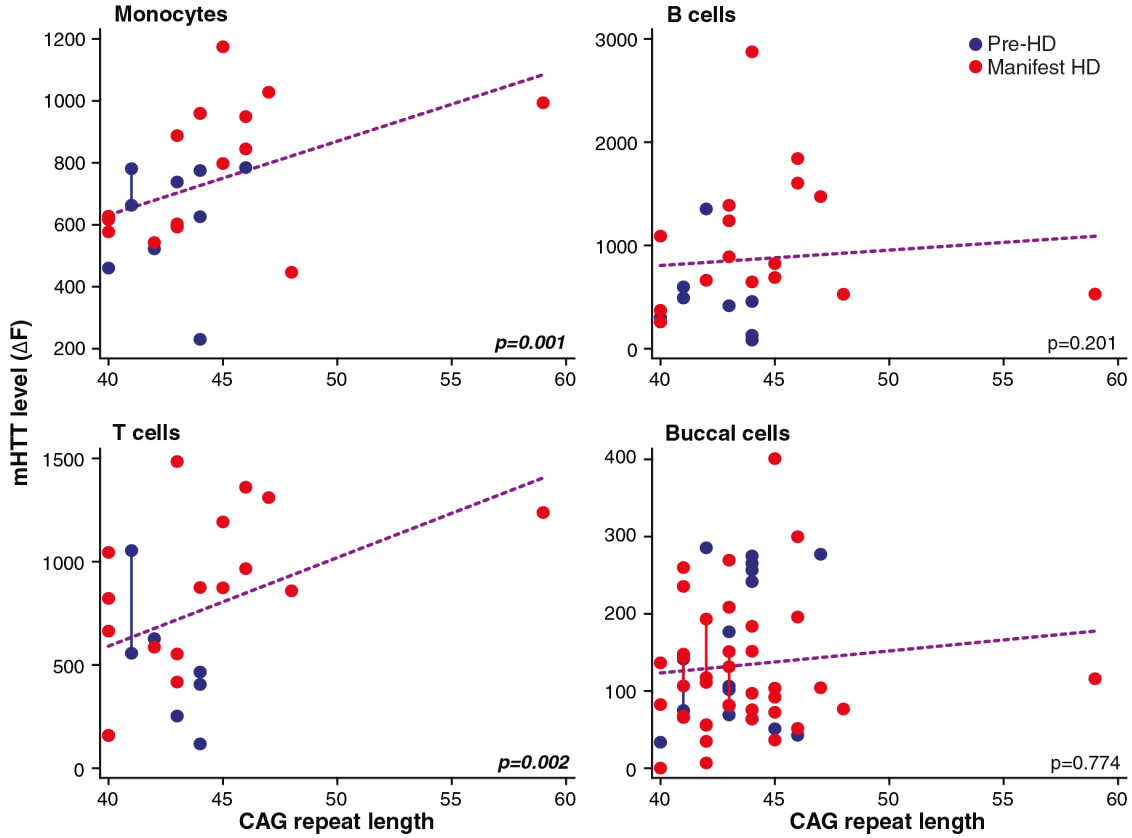

Figure 3.5: Associations between mHTT levels and CAG repeat length. Mutant HTT protein levels in monocytes and T cells, but not B cells and buccal epithelial cells, show a statistically significant association with CAG repeat length. Repeated measurements for a single subject are joined by a line.

3.4.3 Levels of mHTT in HD immune cells correlate to brain atrophy

Brain changes, in particular caudate atrophy, provide a quantifiable measure of disease-associated changes in brain volume and have proven to be valuable markers of disease progression that could be used as biomarker for future clinical trials, tracking disease progression even in premanifest HD carriers (Tabrizi et al., 2012). Investigating whether mHTT levels, which were shown to associate with disease burden score, may be useful as a biomarker, the relationship between mHTT levels in peripheral cells and rates of caudate atrophy, whole brain atrophy and ventricular expansion was examined, in a subset of HD subjects. These subjects had undergone 3T MRI as part of the TRACK-HD study (Tabrizi et al., 2009, 2012, 2011). Mutant HTT levels in monocytes were significantly ($p<0.05$) associated with rates of caudate atrophy, while the association between caudate atrophy and mHTT levels in T cells was borderline significant ($p=0.086$) (Figure 3.6).

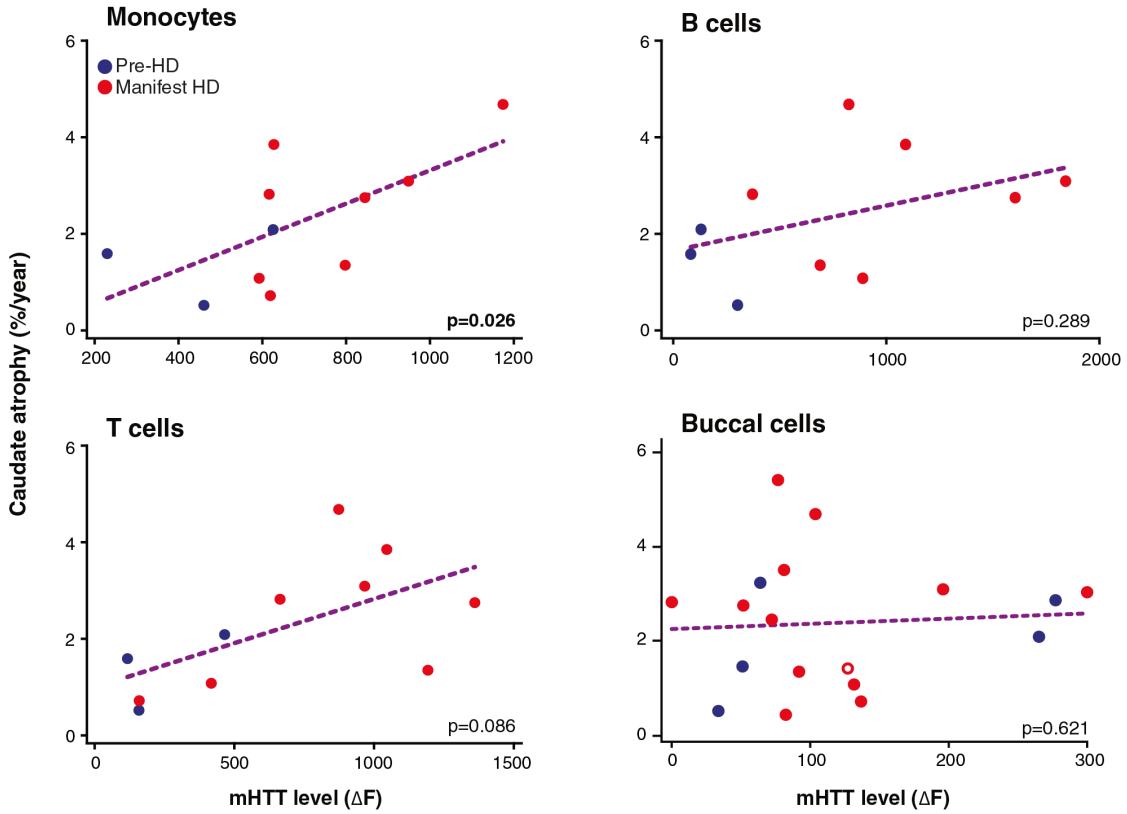

Figure 3.6: Relationship between mutant HTT levels and caudate atrophy. Mutant HTT levels in monocytes are significantly associated with caudate atrophy rates measured by serial volumetric MRI. Hollow points indicate an average of two mHTT readings for a single subject.

Furthermore, mHTT levels in monocytes also significantly associated with whole brain atrophy and ventricular expansion. The association with whole brain atrophy was also significant in T cells (Figure 3.7). No association between mHTT levels and caudate, whole brain atrophy or ventricular expansion was detected in B cells and buccal epithelial cells (Figure 3.6 and 3.7)

Figure 3.7 *(following page)*: Relationship between mutant HTT levels and whole brain atrophy and ventricular expansion. Mutant HTT levels in monocytes are significantly associated with whole brain atrophy rates as well as ventricular volume gain measured by serial volumetric MRI. A weak association was also observed between mHTT levels in T cells and whole brain atrophy, while B cells and buccal cells are not associated with brain changes. Hollow points indicate an average of two mHTT readings for a single subject.

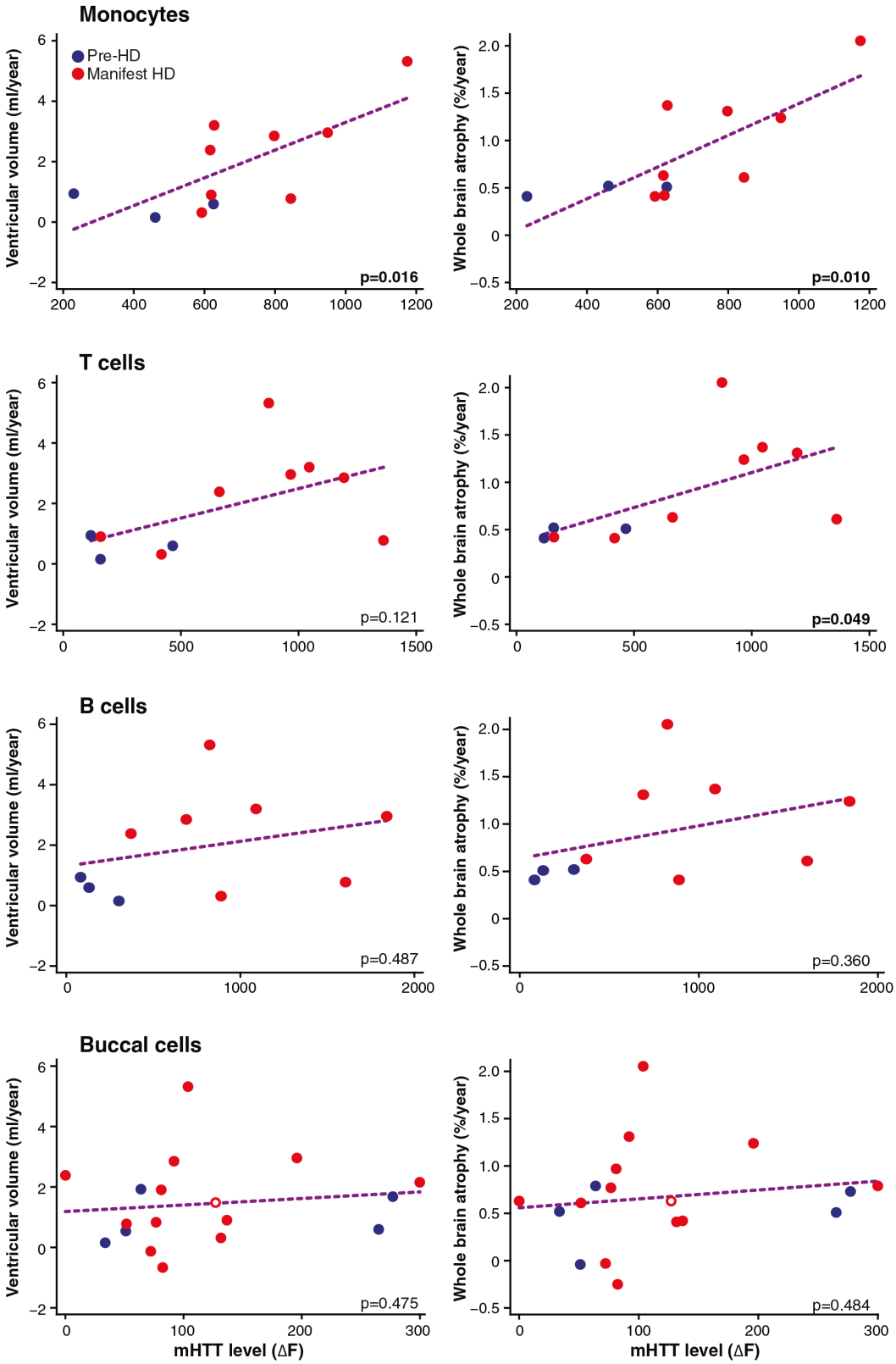
Monocytes
Pre-HD
Manifest HD
Ventricular volume (ml/year)
Whole brain atrophy (%/year)
p=0.016
p=0.010
T cells
p=0.121
p=0.049
B cells
p=0.487
p=0.360
Buccal cells
p=0.475
p=0.484
mHTT level (ΔF)
mHTT level (ΔF)

To investigate whether the association between brain atrophy and mHTT levels merely reflects their mutual associations with disease burden, this factor was adjusted for in a secondary analysis by adjusting the formula used in the statistical regression model. The association between mHTT and brain atrophy remained significant or close to significance for caudate atrophy and ventricular expansion in monocytes (p=0.007, p=0.093, respectively), and for caudate atrophy in T cells (p=0.099) (Table 3.2). However, these results must be interpreted cautiously due to the small sample size. Nonetheless, this is the first report of a biochemical measure known to cause pathology in peripheral cells, that is significantly associated with measures of structural brain changes in a neurodegenerative disease.

Table 3.2: P-values to assess the level of association between mHTT levels in peripheral immune cells and brain changes.
[A] One mHTT observation (two for buccal epithelial cells) is based on the mean of two measurements taken for that subject
[B] Adjusted for age and gender
[C] Additionally adjusted for disease burden

		Caudate atrophy (%/year)			Ventricular expansion (%/year)			Whole brain atrophy (%/year)		
	n[A]	Crude	Adjusted[B]	Burden adjusted [C]	Crude	Adjusted[B]	Burden adjusted [C]	Crude	Adjusted[B]	Burden adjusted [C]
Monocytes	11	0.031	0.026	0.007	0.013	0.016	0.093	0.005	0.010	0.138
T cells	11	0.047	0.086	0.099	0.090	0.121	0.685	0.052	0.049	0.518
B cells	10	0.215	0.289	0.474	0.410	0.487	0.864	0.289	0.360	0.883
Buccal cells	18	0.786	0.621	0.392	0.560	0.475	0.475	0.545	0.484	0.806

3.4.4 HTT proteolysis occurs in human peripheral tissues

Mutant HTT fragments accumulate in HD rodent brain (Landles et al., 2010) and have been detected in HD patient brain post-mortem (DiFiglia et al., 1997; Vonsattel et al., 2011). One possible explanation for the progressive increase in mHTT levels in leukocytes, while total HTT levels are unchanged, is a progressive accumulation of mHTT N-terminal fragments that are not detected in the TR-FRET total HTT signal. While HTT fragments can be detected directly by western blot, cross-reactivity of some anti-HTT antibodies targeting the polyQ region of other polyQ domain proteins makes interpretation of the blots difficult. To avoid this problem, an unbiased strategy combining immunoprecipitation and immunodetection was employed to identify HTT fragments (Landles et al., 2010). HTT was immunoprecipitated from PBMCs from early-stage HD and control subjects, using three different anti-HTT antibodies (the N-terminal aa7-13 binding 2B7 antibody, the aa443-457 binding 2166 antibody and the polyproline domain binding aa51-71 binding 4C9). Immunodetection by western blot was done using the 4C9 and 2166 antibodies. Several sizes of HTT fragments were immunoprecipitated and detected by each of the anti-HTT antibodies in both the control and HD samples (Figure 3.8). Genuine HTT fragments are seen in precipitates from all three anti-HTT antibodies but not in the IgG control.

There are no antibodies specific for either wild-type or mutant HTT available. Detection of mHTT relies on the use of a HTT-specific antibody (such as 2B7, 2166, 4C9, 1H6), in combination with antibody recognising the polyQ domain such as MW1 and 3B5H10. PolyQ-specific antibodies, however, work better the longer the repeat in the protein is, making it difficult to specifically detect N-terminal mHTT fragments using samples with the typical adult onset CAG repeat length between 40-50 CAG repeats. Neither the MW1 or 3B5H10 antibodies will detect mHTT by western blot analysis of such samples. Therefore, samples were taken

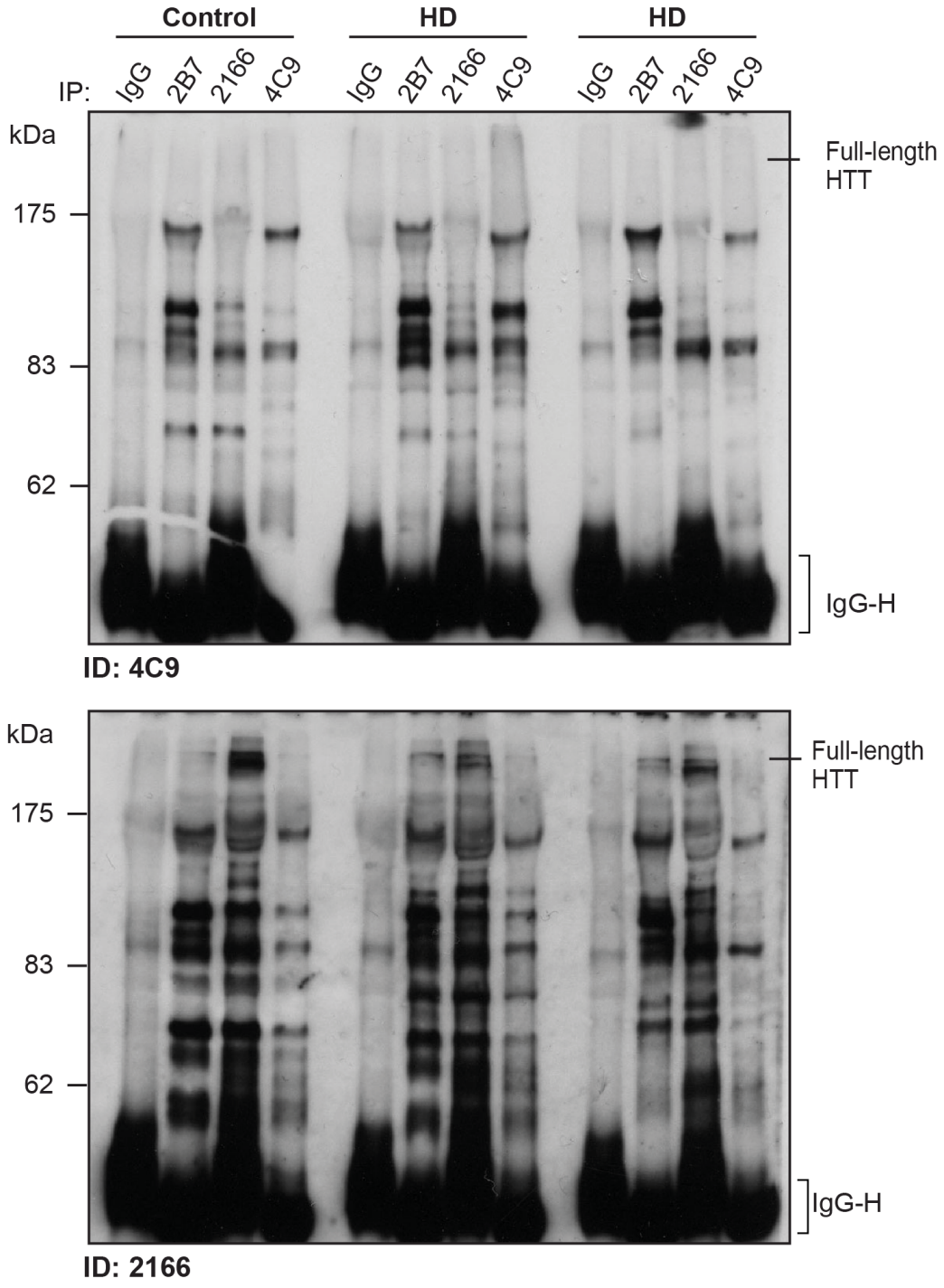

Figure 3.8: HTT protein fragments are present in PBMCs. HTT in PBMCs from two HD subjects and an age-matched control was immunoprecipitated with 2B7, 2166 or 4C9 anti-HTT antibodies, as compared with an IgG control. Immunoprecipitates were blotted with 4C9 (top panel) and 2166 (bottom panel) anti-HTT antibodies. Several HTT-specific bands were found in HD patient and control subject PBMC samples. IP = immunoprecipitation; ID = immunodetection; IgG-H = antibody heavy chain. Experiment performed in collaboration with Dr Christian Landles.

from two young onset HD patients with 73 and 59 repeats and an age-matched control. HTT was immunoprecipitated using the HTT-specific 2B7 and 2166 antibodies as well as the polyQ domain-specific 3B5H10 antibody, which does not immunoprecipitate any wild-type HTT. HTT fragments were immunodetected with the 2166 (Figure 3.9, top panel) and 1H6 (Figure 3.9, middle panel) anti-HTT antibodies. Furthermore, mHTT fragments were detected with the MW1 antibody (Figure 3.9, bottom panel), which only specifically recognises expanded polyQ tracts. Using this approach, mHTT-specific fragments were readily identified in young onset HD patient PBMCs, as compared with those from a control subject. As expected 3B5H10 does not precipitate any proteins detectable with anti-HTT antibodies in controls, while both 2B7 and 2166 precipitates from control samples demonstrated HTT fragments when immunodetected with 2166 or 1H6. In addition to HTT fragments, young onset HD patients also demonstrate specific mHTT fragments. Mutant HTT fragments were not present in controls cells and precipitated by all three antibodies (see red boxes in Figure 3.9). Moreover, some small mHTT fragments (see yellow boxes in Figure 3.9) were only precipitated using the N-terminal 2B7 anti-HTT antibody and the polyQ MW1, and not the more C-terminal 2166 antibody. These findings indicate that some of the fragments were derived from the N-terminus of the mHTT protein and suggest that full-length mHTT is continuously cleaved to produce N-terminal fragments in patients' peripheral immune cells.

Figure 3.9 *(following page)*: Mutant HTT protein fragments are present in HD PBMCs. HTT protein in PBMCs from two young-onset HD patients (HTT CAG repeat lengths of 76 and 59) and an age-matched control was immunoprecipitated with 2B7, 3B5H10 or 2166 anti-HTT antibodies as compared with an IgG control. Immunoprecipitates were blotted with either the 2166 anti-HTT (top panel); the 1H6 anti-HTT antibody (middle panel) or the polyQ-specific MW1 antibody (bottom panel). Several mHTT-specific bands were found in the lysates from the young-onset HD patient PBMCs (coloured boxes), including N-terminal HTT fragments (yellow boxes) immunoprecipitated with the 2B7 and 3B5H10 antibodies, but not with the more C-terminal epitope-binding 2166. IP = immunoprecipitation; ID = immunodetection; IgG-H = antibody heavy chain. Experiment performed in collaboration with Dr Christian Landles.

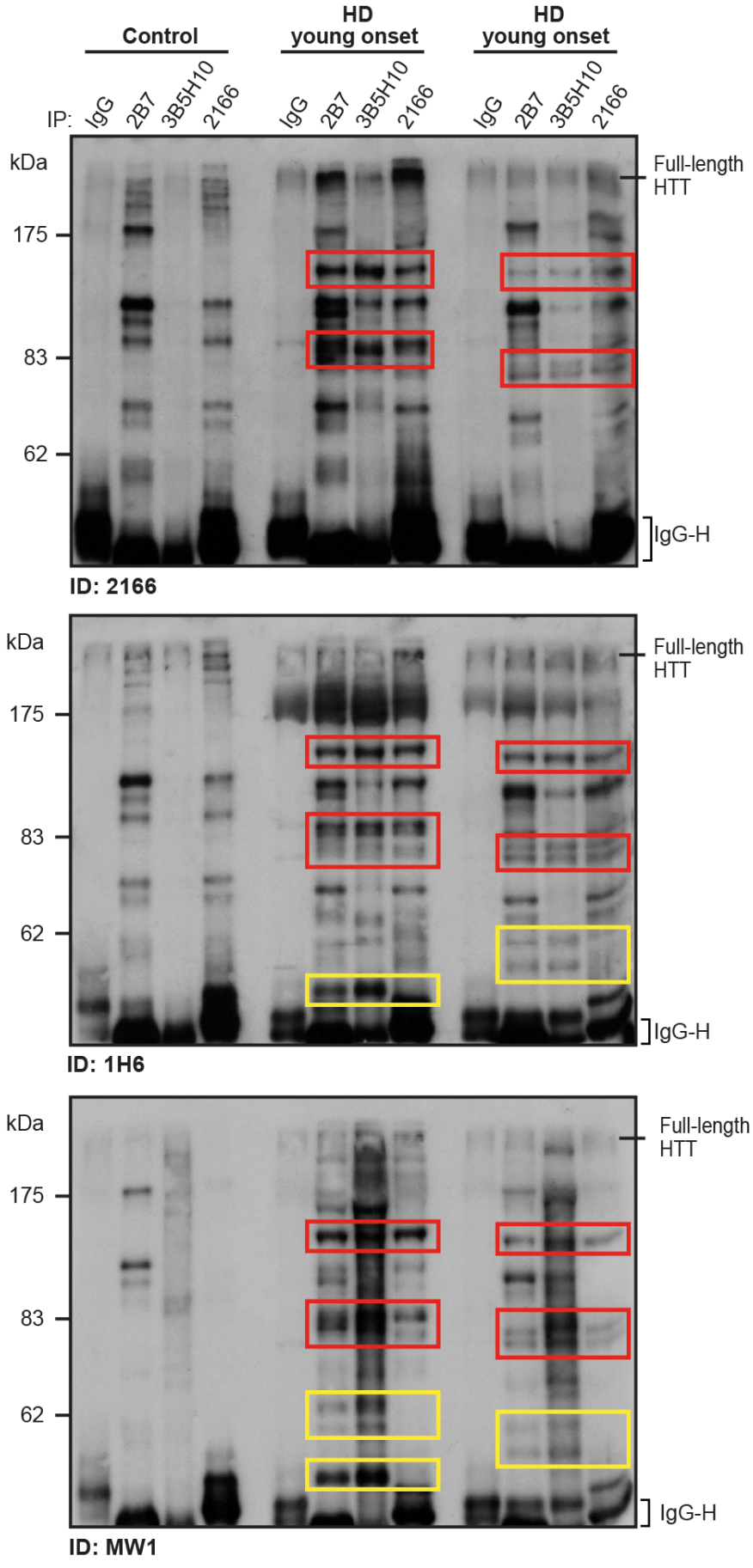
Control
HD young onset
HD young onset
IP:
IgG
2B7
3B5H10
2166
kDa
175
83
62
Full-length HTT
IgG-H
ID: 2166
ID: 1H6
ID: MW1

3.5 Discussion

The search for robust biomarkers is vital in order to commence therapeutic intervention before disease onset in HD gene carriers. The TRACK-HD study has proven that brain imaging measures and selected cognitive tests can be used as endpoints in such studies (Tabrizi et al., 2009, 2012, 2011). Changes in the immune system have been identified long before the appearance of the first symptoms, with plasma cytokine being present on average sixteen years before disease onset (Björkqvist et al., 2008). In this study, a significant increase of mHTT over disease progression has been detected in peripheral immune cells, but not other peripheral cells. These findings suggest that mHTT levels but not total HTT levels, measured in peripheral immune cells could be a possible biomarker for HD. Furthermore, mHTT levels in monocytes and T cells were significantly associated with disease burden and brain atrophy indicating the potential relevance of these cell types to pathogenic and clinical events in HD, given that other peripheral cells tested in this study did not demonstrate any association with markers of disease progression.

mHTT levels were also found to be associated with CAG repeat length in monocytes and T cells. As disease burden score is, at least in part, a function of CAG and also correlates with mHTT levels in these cells, this result is unsurprising. Interestingly, however, mHTT levels correlated with disease burden score but not CAG repeat length in B cells, indicating that CAG is not the only factor contributing to the accumulation of mHTT in these cells.

In order for mHTT measures to be used as a part of a biomarker battery for trials, the assay needs to be validated using a larger cohort. Given the overlap between the different disease stages and the fact that no significant difference between early and moderate patients could be detected (Figure 3.3), longitudinal

data will help understand how mHTT levels change over disease progression and how robust changes will relate to other disease progression measures such as brain atrophy. In addition to this, the protocol used in this study would not be suitable for a clinical trial with several endpoint measures. Here, three immune cell subtypes were isolated in a time consuming protocol before mHTT levels were assayed. However, given that all three cell types show an increase in mHTT that correlates with disease burden score, the use of unsorted PBMC pellets for mHTT measurements should be considered in taking this strategy forward.

There are several possible explanations for the progressive increase in mHTT levels in leukocytes, while no differences were apparent in total HTT levels. Accumulation of mHTT over the lifespan of the cells is unlikely as, although some leukocytes are long-lived, monocytes typically persist for only 2-8 days in the bloodstream (Whitelaw, 1966). Another possible explanation is the accumulation of extended CAG repeat expansions in the *HTT* gene due to somatic DNA instability. However, this is not seen in peripheral immune cells (MacDonald et al., 1993). A selective increase in mHTT expression as the disease develops and progresses cannot be excluded, but seems improbable as total HTT levels did not change. The most likely explanation is a progressive accumulation of mHTT N-terminal fragments that are not detected in the TR-FRET total HTT signal. Indeed, using a immunoprecipitation and immunodetection strategy both HTT and mHTT fragments could be detected in primary human immune cells. Comparing the fragment profile in PBMCs from young onset HD patients precipitated with an N-terminal (2B7) antibody and with a more C-terminal (2166) antibody, small mHTT fragments were only detected with 2B7 suggesting proteolysis at the N-terminus. Given a recent publication demonstrating that CAG repeat dependent aberrant splicing of HTT causes translation of HTT exon 1 protein fragments (Sathasivam et al., 2013), one of the small HTT fragments detected in this study may be due to splicing events. However, testing splicing events in primary human

PBMCs, Sathasivam et al. only detected a splicing product in one out of eight PBMC samples suggesting alternative splicing events may be rare in this cell type (Sathasivam et al., 2013). While, mHTT fragments are known to accumulate in HD rodent brain (Landles et al., 2010) and HD patient brain (DiFiglia et al., 1997; Vonsattel et al., 2011), and HTT protein proteolysis has been demonstrated in lymphoblast cell lines from HD patients (Toneff et al., 2002), this is the first time fragmentation has been shown in primary human peripheral cells.

Lastly, the findings in this study may be of use in future HTT lowering studies (Sah and Aronin, 2011), as non-invasive quantification of mHTT in CNS tissue or CSF in human subjects is not currently possible. The success of any forthcoming trials to lower mHTT levels will rely on indirect pharmacodynamic outcome measures. While it is not know how lowering of HTT levels specifically in the brain, for example by injection of a viral vector containing siRNA or ASOs would effect peripheral cells, it would be of interest to investigate the effect on blood cells in upcoming animal studies. Furthermore, studies looking into lowering HTT systemically, for example using small molecules aimed at enhancing HTT clearance, may be enhanced by the application of such quantification to investigate levels of HTT lowering. *Ex vivo* testing of peripheral immune cells before the trial may also prove to be useful in identifying subjects in whom such therapies are most likely to succeed.

Overall this study identified mHTT levels as potential wet, easily assessable biomarker for HD progression. N-terminal HTT proteolysis is the likely cause for the increase of mHTT over total HTT in peripheral immune cells.

4 Myeloid cell function in HD patients

4.1 Background

Whilst primary pathology in HD is believed to arise from basal ganglia degeneration, HTT expression has been detected in all tissues studied (Li et al., 1993), and expression in non-neuronal cells both within the brain and in the periphery may contribute to HD pathology. Indeed, numerous studies of HD patients and mouse models have described abnormalities in peripheral tissues, including weight loss and muscle wasting despite high caloric intake, diabetes and changes in the neuro-endocrine system (van der Burg et al., 2009).

HTT is also expressed in immune cells (Weiss et al., 2012), and both central and peripheral immune system abnormalities have been shown in HD patients (Soulet and Cicchetti, 2011). Microglia, the resident immune cells of the brain and peripheral myeloid cells share the same haematopoietic origin, although it remains controversial as to whether circulating blood monocytes can replenish the microglial population within the brain during an individual's lifetime (Ransohoff and Perry, 2009). Whilst microglia seem to be sustained largely by self-renewal (Ajami et al., 2007), disruption of the blood brain barrier by irradiation has shown that blood monocytes are able to populate the brain and differentiate into microglia

(Simard and Rivest, 2004). Microglial activation is observed in post-mortem HD brain tissue (Sapp et al., 2001) and by PET imaging, showing that this activation is already present in HD gene carriers before symptom onset (Tai et al., 2007). Peripheral immune system dysfunction has previously been demonstrated in HD, including changes in innate immune proteins such as complement components and cytokines in HD patient plasma (Dalrymple et al., 2007). Moreover, elevated plasma cytokine (Björkqvist et al., 2008) and chemokine (Wild et al., 2011) levels in HD patients correlate with disease progression and can be detected years before disease onset. It has been shown that primary human monocytes are hyperreactive in response to LPS, producing increased levels of IL-6. This phenotype is replicated in murine mHTT expressing macrophages and microglia, demonstrating that peripheral cells may be able to mirror pathology in the CNS in HD (Björkqvist et al., 2008).

Several recent studies have suggested that the peripheral immune system can act as a modifier of HD neuropathology. Bone marrow transplantation (Kwan et al., 2012a), administration of a KMO inhibitor (Zwilling et al., 2011) and reduction of the immune response by modulating of the CB2 pathway (Bouchard et al., 2012) have proven to suppress or delay the HD phenotype in mice. These studies provide strong evidence that the immune system plays a disease-modifying role in HD neuropathogenesis, but the mechanism by which mHTT expression in immune cells causes this dysfunction has not yet been established.

Activation of immune cells by pathogens binding TLRs leads to the activation of several signalling cascades including the NFκB and MAPK pathways. Intracellular signalling pathways leading to the activation of the transcription factor NFκB are important regulators of cytokine production and play a key role in inflammation. Activation of TLRs leads to signal transduction via adapter proteins such as MyD88 and IRAK1, leading to the phosphorylation and activation of IKK. This

kinase phosphorylates IκB, which is then ubiquitinated and degraded by the proteasome. This results in its dissociation from the NFκB transcription factor subunits (RelA, RelB, cRel, NFκB1, NFκB2), which are sequestered in an inactive state in the cytoplasm when bound to IκB. The free NFκB molecules can then translocate into the nucleus and activate gene transcription (Hayden and Ghosh, 2012). The NFκB pathway has previously been implicated in HD, with Khoshnan et al. having shown in inducible PC12 cells and striatal extracts from R6/2 mice that overexpression of *mHTT* exon 1 can activate the NFκB pathway by directly interacting with IKKγ (Khoshnan et al., 2004). It remains to be shown that this interaction also occurs in a human system with expression of full-length HTT at normal allelic expression levels.

The aim for this part of my PhD project was to identify the mechanism of dysfunction in primary human HD *ex vivo* monocytes and macrophages. This involved, characterising the immune cell dysfunction in HD and the study of upstream intracellular signalling pathways, identifying NFκB pathway dysregulation as the cause of HD immune dysfunction. Furthermore, overexpression and knock-down techniques were used to investigate the role cell-intrinsic HTT plays in human HD monocyte and macrophage function, while testing the feasibility of reversing peripheral immune dysregulation by cell-targeted HTT-lowering.

4.2 Contributions

Dr Peter Klöhn helped with the fluorescent activated cell sorting, Gary Adamson helped with the DNA sequencing and Dr Holger Hummerich helped with the bioinformatic analysis (all part of the MRC Prion Unit, UCL). All measurements of HTT levels were done by Stephan Grueninger and Dr Andreas Weiss at Novartis, Basal. The initial cytokine profiling of adult onset HD monocytes was done

by Anna Magnusson-Lind (Lund University, Sweden) and Dr. Nayana Lahiri (Institue of Neurology, UCL). Glucan encapsulated siRNA particles were packaged by Professor Gary Ostroff (University of Massachusetts, USA).

4.3 Methods

Cytokine production by primary human monocytes and macrophages isolated from human HD and control samples (Section 2.5.4) and treated with IFNγ and LPS (Section 2.6.1) was measured using multiplex ELISA assays (Section 2.7.2). To further access the functionality of HD immune cells, uptake of latex beads was measured using flow cytometry (Section 2.6.3). The human histiocytic lymphoma cell line (U937) was lentivirally transduced to overexpress wild-type or mutant HTT (Section 2.5.2), before their cytokine production was analysed (Section 2.6.1) to establish whether cell-intrinsic mHTT expression is sufficient to induce immune dysfunction. Immunoprecipitation was used to detect interactions between HTT and IKK (Section 2.8.3). Further investigating the NFκB pathway, western blot analysis (Section 2.8.5) was used to assess IκB degradation and imaging flow cytometry (Section 2.9.3) to assess nuclear translocation of NFκB transcription factors. STAT signalling was assessed using intracellular flow cytometry (Section 2.9.2). Transcription changes in HD monocytes were detected using qPCR (Section 2.10) and visualised using bioinformatics (Section 2.10.4). Transcript lowering (Sections 2.5.5) was used to see whether HTT knock-down can reverse the immune dysfunction in primary human monocytes and macrophages.

4.4 Results

4.4.1 Establishing macrophages cultures from HD patients

Human blood monocytes are post-mitotic cells and were not cultured for longer than 48 hours. Macrophages were differentiated from monocytes by adding GM-CSF to the culture media. During differentiation, the cells flattened out and formed projections. Macrophages from HD patients and controls showed no obvious differences in cell morphology (Figure 4.1A). Counting the number of macrophages post differentiation suggested no difference in proliferation and differentiation rate between control and premanifest HD gene carriers, early- and moderate-stage HD patients (Figure 4.1B). CD206 is a specific marker for macrophages and up-regulated to the same extent during differentiation of either control or HD patient cells (examples shown in Figure 4.1C).

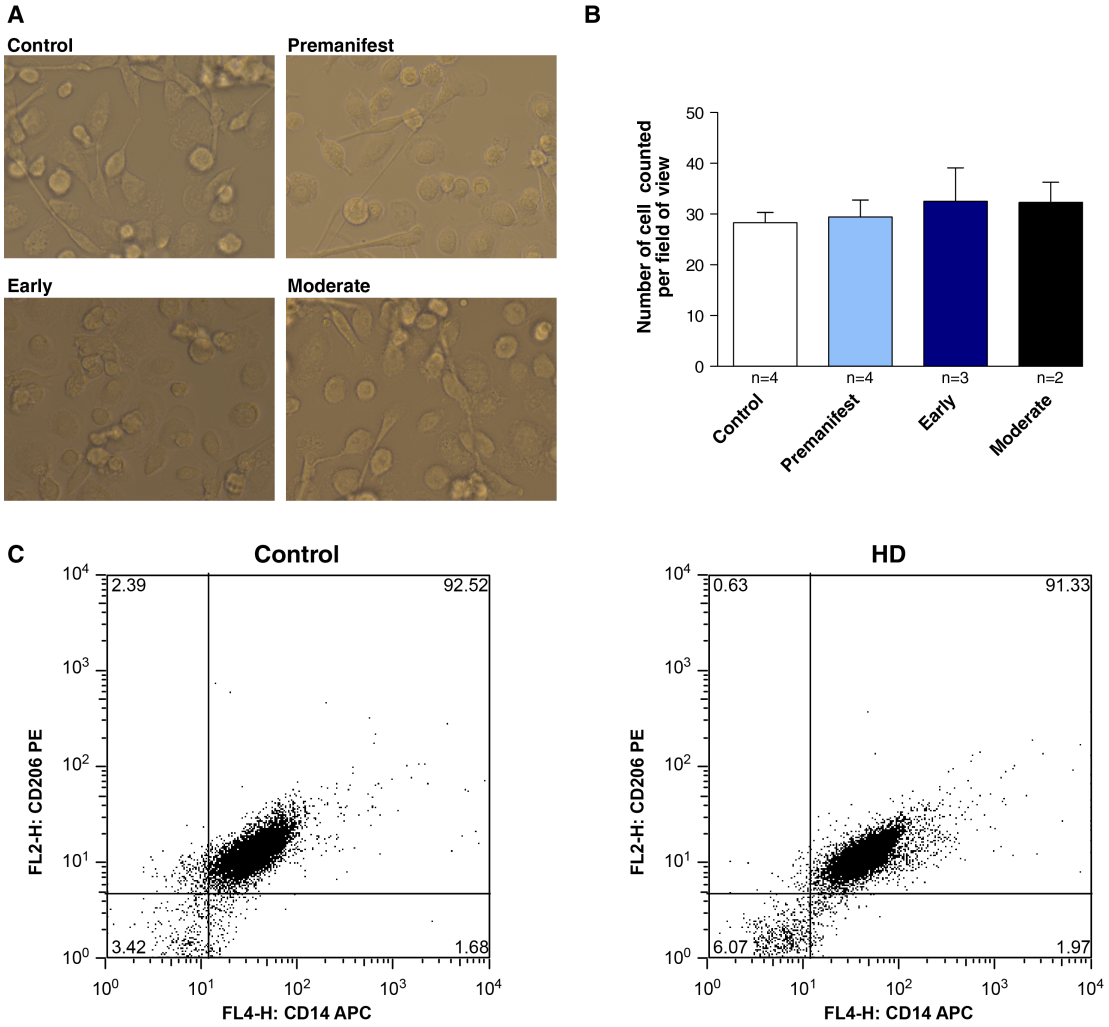

Figure 4.1: Characterisation of HD patient macrophages. Macrophages were differentiated with 20 ng/ml GM-CSF for six days. **(A)** Light microscope images of macrophage from control, premanifest HD gene carriers, early- and moderate-stage HD patients showed no morphological differences. **(B)** Number of macrophages do not differ between control and premanifest HD gene carriers, early- and moderate-stage HD patients (one-way ANOVA used as statistical test). Macrophages were counted on three or four representative fields of view pre coverslip. n= biological repeats. **(C+D)** Example of up-regulated CD206 expression on differentiated macrophages. CD206 was similarly up-regulated on macrophages from **(C)** control and **(D)** HD patients.

4.4.2 HD monocytes and macrophages are hyper-reactive after LPS stimulation

HD patient monocytes are hyper-reactive, producing increased levels of IL-6 upon stimulation with LPS *in vitro* (Björkqvist et al., 2008). To extend these findings to other cytokines, blood samples from a large cohort (n=53) of HD gene carriers ranging from premanifest to moderate-stage disease and control subjects (n=27) were collected (Table A.3). $CD14^+$ monocytes were isolated and seeded *in vitro*, before being primed with IFNγ and stimulated with LPS. In multiplex ELISA assays, stimulated monocytes from HD-mutation-positive subjects at each disease stage, including those who were premanifest, were found to produce more of the pro-inflammatory cytokines IL-6 and TNFα than control cells (Figure 4.2). Furthermore, production of the pro-inflammatory IL-1β was significantly increased in LPS-stimulated premanifest HD monocytes. Levels of the chemokine IL-8, anti-inflammatory IL-10 and pro-inflammatory IL-12 did not differ between stimulated HD and control cells (Figure 4.2).

Cytokine production by LPS-stimulated monocytes was normalised to the cytokine production of non-stimulated cells from the same subject. Cytokine production by non-stimulated monocytes was very low with 10 pg/ml for all cytokines besides IL-8, for which levels were around 1 ng/ml in supernatants from non-stimulated cells. Cytokine production by non-stimulated cells did not differ between control and HD-mutation-positive subjects at each disease stage.

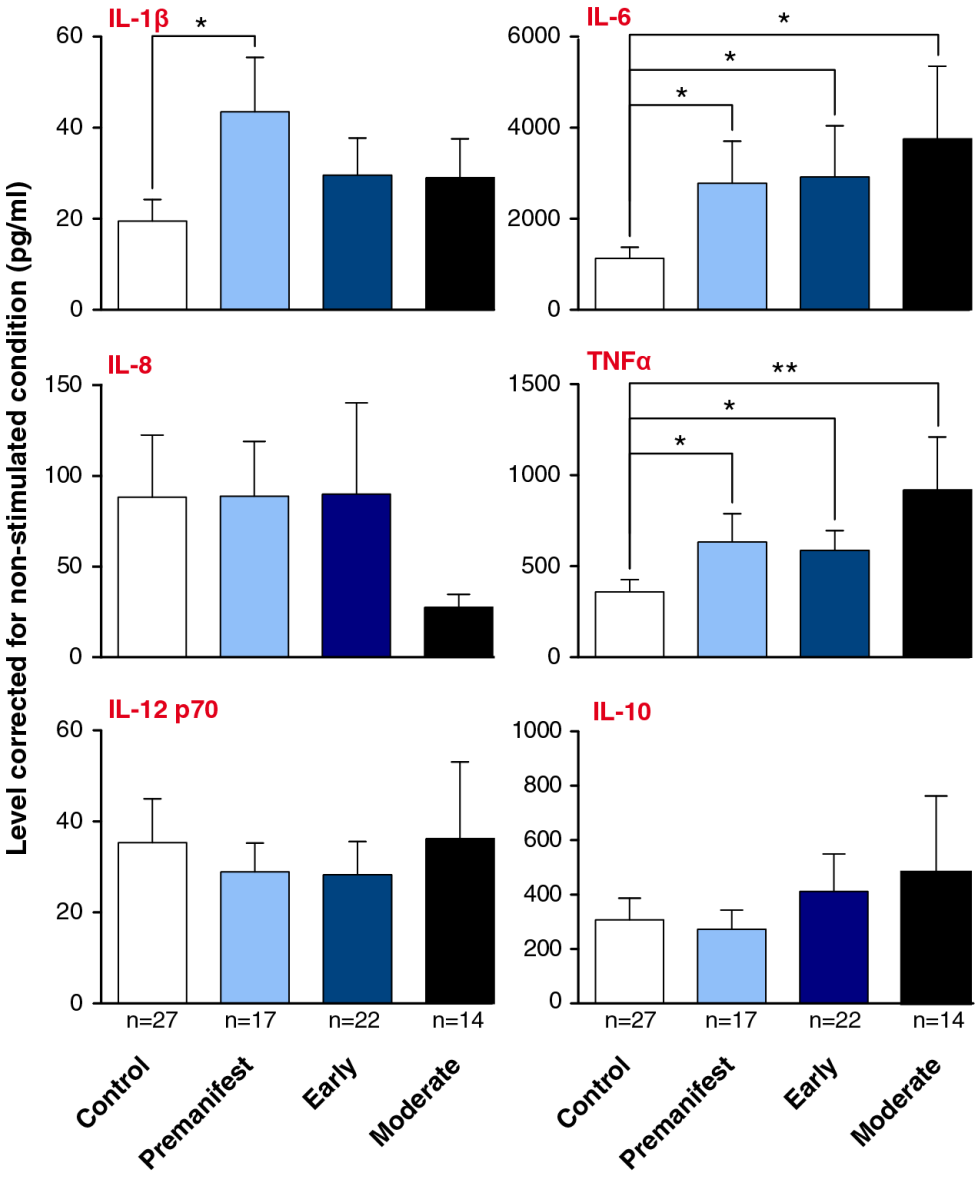

Figure 4.2: Pro-inflammatory cytokine production by monocytes is elevated in HD patients. Monocytes were isolated from control and HD patient blood samples using magnetic cell sorting. After stimulation with 10 ng/ml IFNγ and 2 μg/ml LPS for 24 h, multiplex ELISA demonstrated that innate immune regulators IL-1β, IL-6 and TNFα are elevated in culture media of HD patient blood monocytes. Data show mean concentrations corrected to basal condition $\pm$ SEM, n= individual biological repeats, ANOVA with post-hoc Tukey HSD test. *p$<$0.05; **p$<$0.01, ***p$<$0.001. Experiment performed by Anna Magnusson-Lind and Dr Nayana Lahiri.

Next, these findings were validated and expanded to juvenile HD patients carrying on average 57 CAG repeats (14 more than the adult patient cohort in Figure 4.2). Due to the higher number of CAG repeats juvenile HD patients not only suffer from an early disease onset but also a more progressive course of the disease and atypical symptoms such as seizures (Squitieri et al., 2006). Immune changes may therefore also be different in juvenile compared with adult onset patients. The cytokine profile of monocytes, isolated from juvenile HD patients and stimulated with IFNγ and LPS, showed a similar increase in the production of pro-inflammatory cytokines as seen in cells isolated from adult onset patients (Figure 4.3). However, due to the low sample size (n=4 for juvenile HD and n=6 for age matched control subjects) in this experiment, only IL-1β production was found to be significantly increased.

Cytokine production was normalised to the protein content of the corresponding well rather than non-stimulated samples for this experiment. Non-stimulated monocytes isolated from juvenile HD patients did not differ from control cells, producing less than 1 pg/μg IL-1β, IL-6 and TNFα and less than 10 pg/μg IL-8.

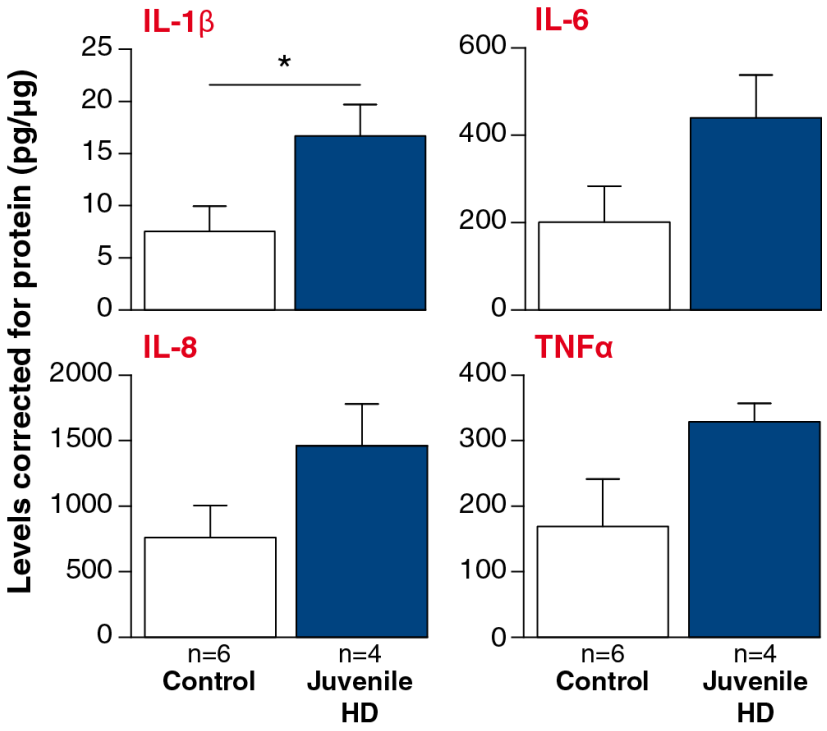

Figure 4.3: Cytokine profile of juvenile HD patient monocytes. Blood monocytes isolated from juvenile HD patients were primed with 10 ng/ml IFNγ and stimulated with 2 μg/ml LPS. After 24 h cytokine concentrations in the supernatants were measured using multiplex ELISA, showing significantly increased IL-1β levels compared with control samples. Graphs show mean concentrations corrected to protein content $\pm$ SEM, n= individual biological repeats, unpaired two-tailed student two-tailed t tests. *p$<$0.05.

When monocytes migrate into tissues, they differentiate into macrophages capable of eliciting effective immune responses to localised inflammatory signals (Gordon and Taylor, 2005). To test whether HD macrophages are also abnormal, blood monocytes were differentiated into macrophages using GM-CSF before being stimulated with IFNγ and LPS to assess their cytokine profile. Stimulated HD macrophages from all disease stages produced significantly higher levels of IL-8 and TNFα compared with control cells (Figure 4.4).

Similar to the monocyte cytokine profile of juvenile HD patients, macrophage cytokine production was normalised to protein content and non-stimulated cells did not differ in cytokine production comparing control with HD. Non-stimulated macrophages produced cytokine levels close to the lower detection range of the MSD assay, producing less than 1 pg/μg IL-1β, IL-6 and TNFα and less than 20 pg/μg IL-8.

Taken together, these data show that immune cells isolated from HD patients are hyper-reactive following stimulation.

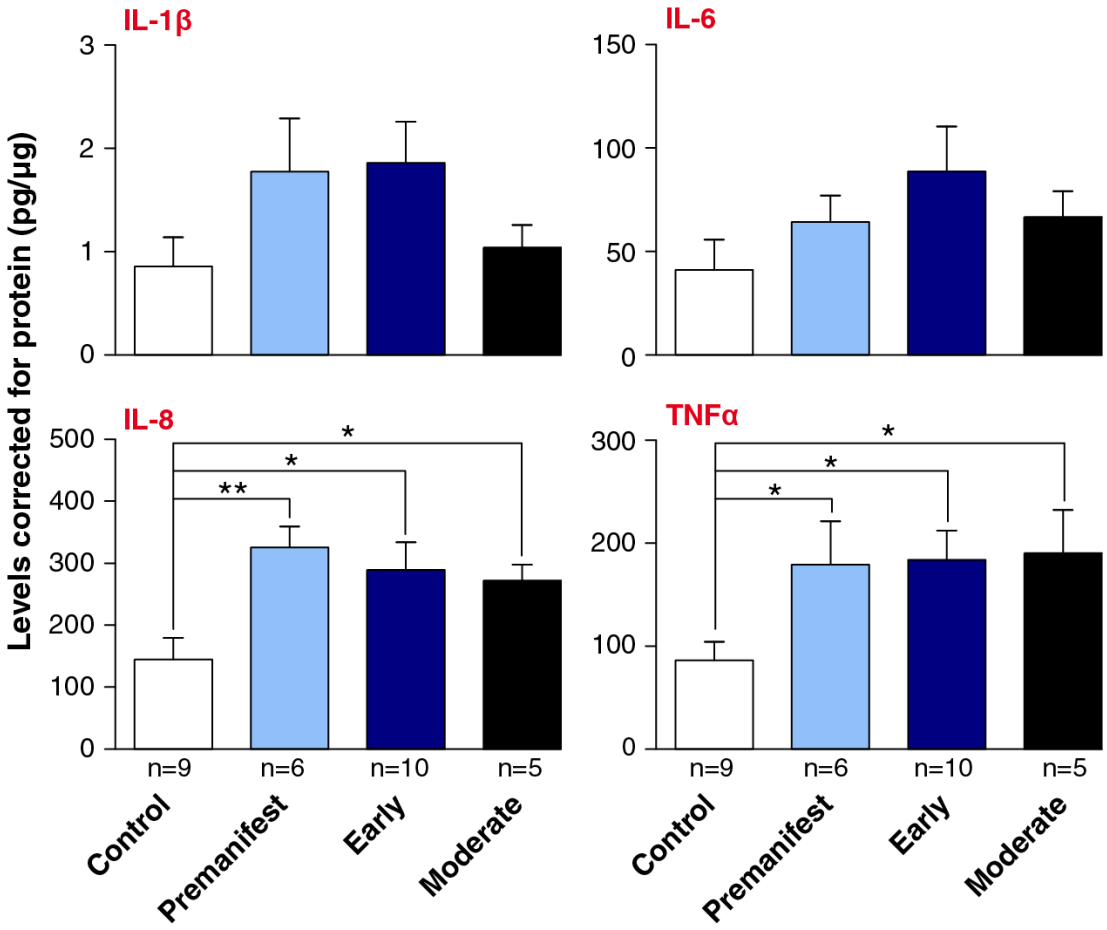

Figure 4.4: Pro-inflammatory cytokine production by macrophages is elevated in HD patients. Macrophages, derived from blood monocytes using 20 ng/ml GM-CSF for 6 days, were primed with 10 ng/ml IFNγ and stimulated with 2 μg/ml LPS for 24 h before cytokine concentrations in the supernatants were measured using MSD multiplex ELISA. Compared with control cells, HD patient macrophages produced higher levels of IL-8 and TNFα. Graphs show mean concentrations corrected to protein content $\pm$ SEM, one-way ANOVA with post-hoc t-tests. *p$<$0.05; **p$<$0.01.

4.4.3 The hyper-reactive immune phenotype is caused directly by mHTT expression

Mutant HTT levels in immune cells have been shown to track measures of HD progression, such as disease burden score and caudate atrophy (Chapter 3). To test whether immune cell dysfunction is caused by cell-intrinsic *mHTT* expression, or instead by external disease-associated factors, the histiocytic lymphoma U937 cell lines, a commonly used model of monocytes, was transduced with lentiviral vectors expressing human *HTT* exon 1. The constructs contained either wild-type *HTT* exon 1 with 29 CAG repeats or mutant *HTT* exon 1 with 71 or 129 CAG repeats, with all constructs also encoding for GFP. A vector expressing only GFP and no *HTT* was used as control. Sorting the transduced cells using the co-expressed GFP resulted in 99 % pure cultures (Figure 4.5).

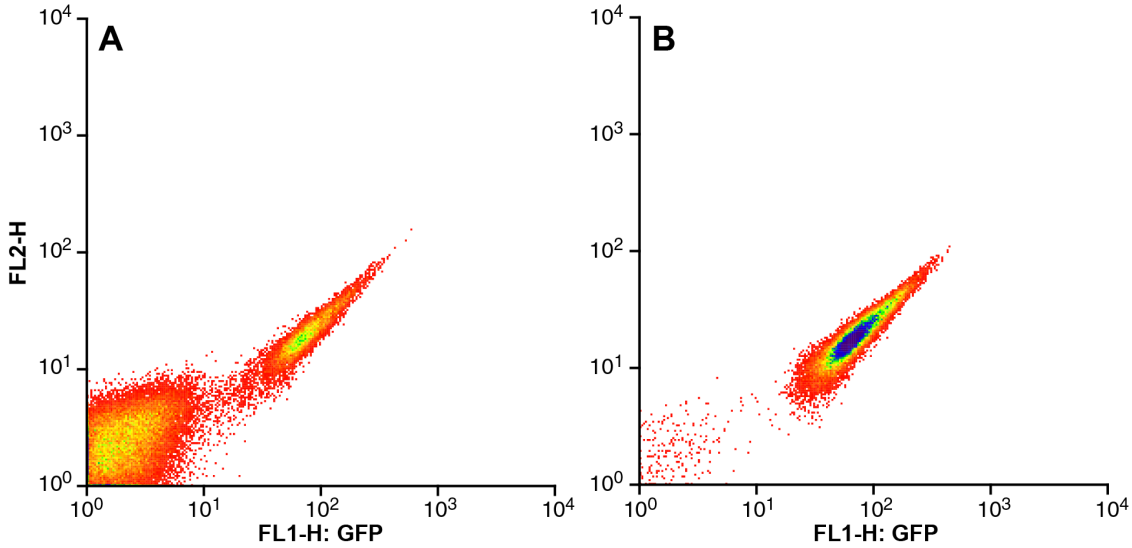

Figure 4.5: Sorting efficiency of U937 cells transduced with *HTT* exon 1. U937 cells were lentivirally transduced with *HTT* exon 1 carrying 29, 71 or 129 CAG repeats. All viral vectors also encoded GFP, which was used to fluorescence-activated cell sort transduced cells. FACS sorting was highly efficient, **(A)** showing cell population prior to sorting and **(B)** showing 99 % pure HTT expressing U937 cells. FACS was assisted by Dr Klöhn.

U937 cells represent an immature monocyte-like phenotype, but can be differentiated using PMA and are known to produce pro-inflammatory cytokines following stimulation (Alciato et al., 2010). Testing two different concentrations of PMA, U937 cells at both doses were found to up-regulate the macrophage marker CD206 indicating differentiation (Figure 4.6). As 10 ng/ml PMA already induced differentiation of U937 cells, this concentration was used in all future experiments.

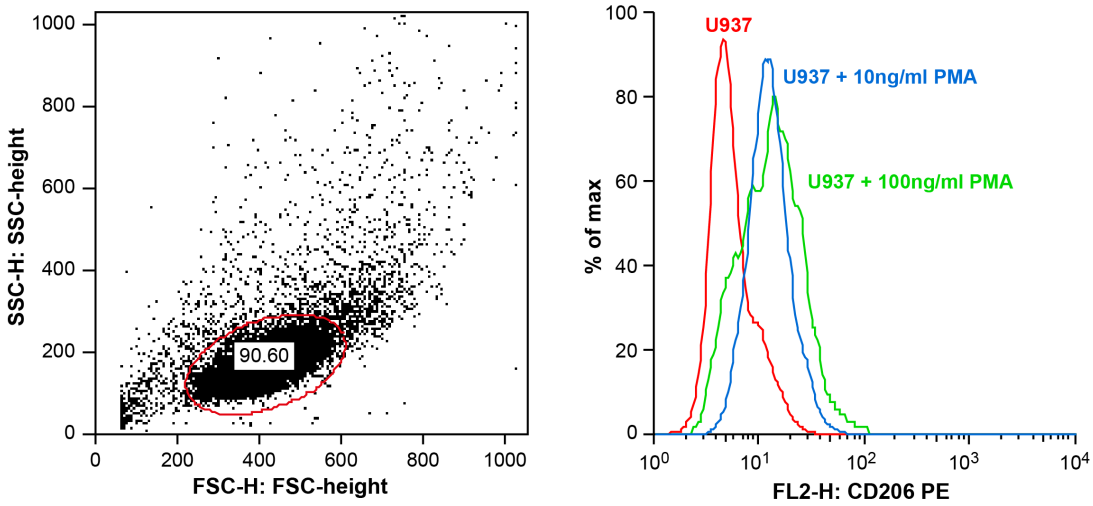

Figure 4.6: U937 cells differentiate into macrophage-like cells. U937 cells were treated with 10 or 100 ng/ml PMA for 3 days. During this time cells settled down to form a monolayer and expressed the macrophage marker CD206 as measured by flow cytometry.

HTT expression in the transduced cells was demonstrated using the TR-FRET immunoassay. In contrast to control lines (non-transduced U937 cells and empty vector transduced U937 cells), which showed no detectable HTT signal, CAG repeat length dependent expression of soluble mHTT is detectable in the two cell lines expressing HTT exon 1 carrying 71 or 129Q (Figure 4.7A). Previous studies have shown that the 2B7-MW1 antibody combination used to detect soluble mHTT can detect HTT with polyQ lengths starting at 17Q (Baldo et al., 2012), explaining why a small signal was observed in cells transduced with the 29Q construct. Interestingly, both of the mHTT expressing cell lines also contained aggregated mHTT, measured using the MW8-MW8 antibody combination, with the

cells expressing 129 CAG repeats containing 30 times more aggregates than the cells expressing 71 CAG repeats (Figure 4.7B). Interestingly, while this model of HD myeloid cells shows HTT aggregates, this has never been detected in primary human HD immune cells using the same assay (Weiss, personal communication).

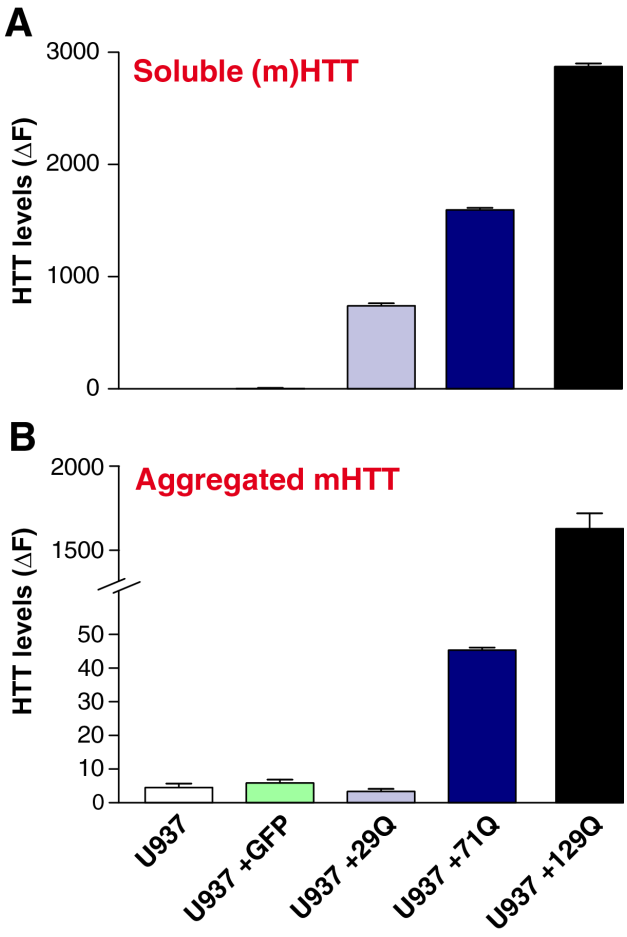

Figure 4.7: Transduced U937 cells express both soluble and aggregated HTT. U937 cells were lentivirally-transduced with (m)HTT exon 1 containing either 29, 71 or 129Q repeats. Expression of both soluble and aggregated (m)HTT protein post-transduction was confirmed using 2B7-2166 or MW8-MW8 TR-FRET, respectively, showing increased levels of soluble HTT in all three cell lines expressing exogenous HTT and aggregated mHTT in both mHTT expressing cell lines. TR-FRET measurements were performed in collaboration with Dr Andreas Weiss.

To assess whether intrinsic HTT expression causes the increase in cytokine production found in HD patient cells, the *HTT* exon 1 expressing U937 cell lines were differentiated with PMA for 3 days before stimulation with IFNγ and LPS and analysis of their cytokine profile. Stimulated U937 cells expressing either 71 or 129Q mHTT produced significantly increased levels of IL-6 and TNFα compared with those expressing the 29Q wild-type HTT construct (Figure 4.8). Cells expressing 129Q produced significantly higher IL-1β levels compared with control, whereas IL-8 levels did not differ. Therefore, cell-intrinsic expression of mHTT exon 1 seems to be sufficient to recapitulate the hyper-reactive immune phenotype observed in monocytes and macrophages from HD patients.

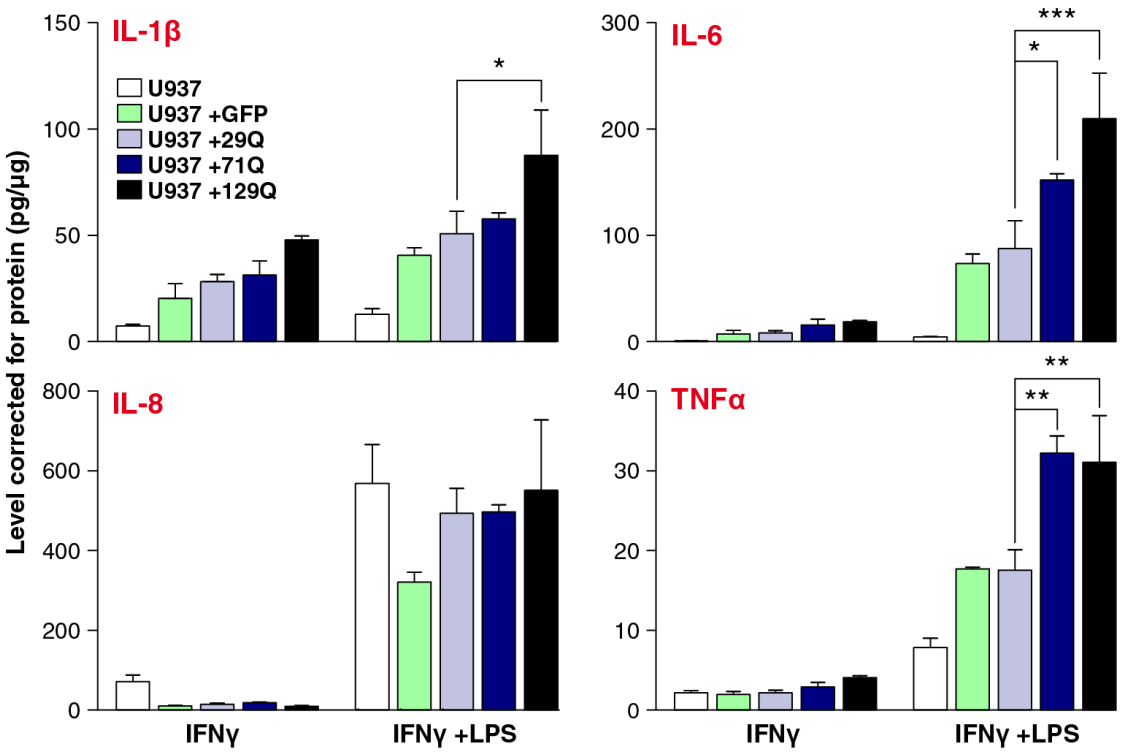

Figure 4.8: Expression of mHTT induces elevated cytokine production. U937 cells were lentivirally transduced with either wild-type HTT exon 1 containing 29Q or mHTT exon 1 containing 71 or 129Q repeats. Innate immune regulators were elevated in PMA-differentiated mHTT expressing U937 cells stimulated for 24 h with 10 ng/ml IFNγ and 2 μg/ml LPS. Data shown as mean corrected for protein content $\pm$ SEM, n=4 technical repeats for all conditions, two-way ANOVA with Bonferroni post-tests, *p$<$0.05; **p$<$0.01, ***p$<$0.001.

4.4.4 LPS stimulation of HD macrophages results in increased phagocytosis

In addition to cytokine production, the ability to ingest pathogens by a cellular process called phagocytosis is a key function of monocytes and macrophages. Phagocytosis not only clears pathogens and debris at sites of inflammation, but also forms the first step in the activation of the adaptive immune system (Walport et al., 2008). Phagocytosis by monocyte-derived macrophages was assessed by incubating cells with green fluorescent latex beads and measuring the percentage of cells having taken up beads via flow cytometry (gating shown in Figure 4.9A). Interestingly, basal phagocytosis (Figure 4.9B) was unchanged, but LPS stimulation for 24 h revealed a significant difference between HD and control macrophages (Figure 4.9C). A significantly higher percentage of HD patient macrophages phagocytosed beads compared with controls after LPS stimulation. The percentage of HD macrophages taking up only one bead was significantly increased, while the percentage of cells taking up two or three beads was not statistically different.

Figure 4.9 *(following page)*: Increased phagocytosis by HD patient macrophages. Monocyte-derived macrophages were incubated with green fluorescent latex beads for 1 h at 37 °C before the percentage of cells taking up green fluorescent beads was analysed using flow cytometry. **(A)** Macrophage were gated in the FCS and SSC channels according to their size before the FL-1 channel was used to determine what percentage of cells phagocytosed which number of beads. **(B)** Basal phagocytosis levels of unstimulated HD patient macrophages were unchanged compared with control cells, whilst **(C)** HD patient macrophages stimulated with 2 μg/ml LPS for 24 h showed a significant increase in the percentage of phagocytosing cells. Grey points represent control, red points represent HD macrophages. Unpaired two-tailed student t tests, *$p<0.05$. n= 5 for control and HD, representing biological repeats.

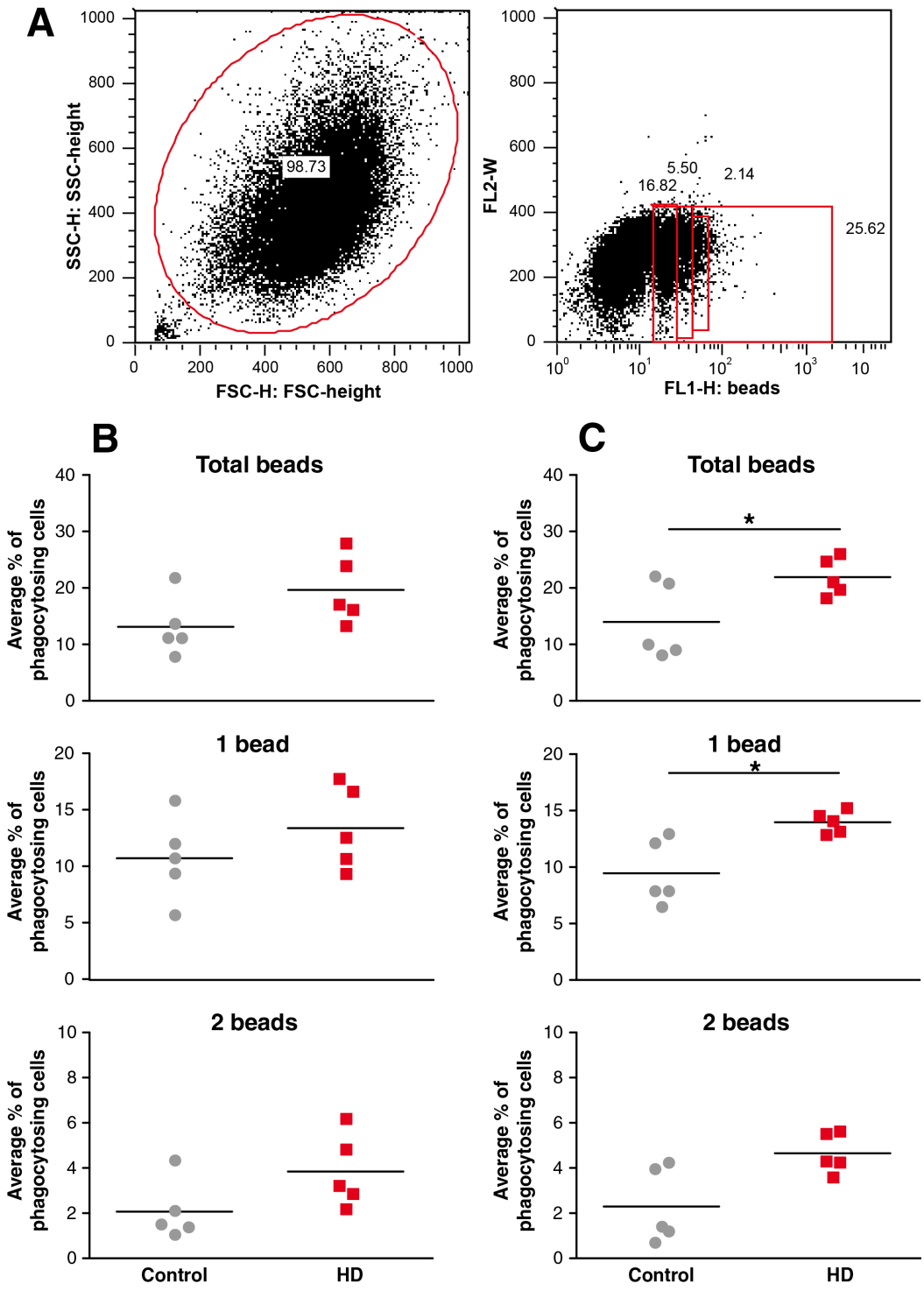
A
SSC-H: SSC-height
FSC-H: FSC-height
98.73
FL2-W
FL1-H: beads
5.50
16.82
2.14
25.62
B
C
Total beads
1 bead
2 beads
Average % of phagocytosing cells
*
Control
HD

Doublet discrimination was used to prove that the increase in green fluorescence intensity detected in the phagocytosis assay corresponded with an increase in the number of beads taken up by a cell. Therefore, the green fluorescent latex beads, used for the assay, were run on the FACS machine comparing the FL-1 height measure, used to measure fluorescence intensity, to FL-1 width, a measure of the time the beads need to pass the laser. Single beads will need a shorter amount of time to pass the laser than doublets or triplets allowing a comparison of the fluorescence emitted by singlet, doublet or triplet beads. Looking at the forward scatter (FSC-correlating to particle size) and side scatter (SSC-correlating to particle granularity) already showed different sized particles, which looking into the FL-1 width channel were confirmed as singlet, doublet of triplet beads (Figure 4.10). Comparing the fluorescence intensity, FL1-H, between the different beads revealed an increase similar to that seen in the phagocytosis assay between singlet, doublet and triplet beads, thus validating the assay.

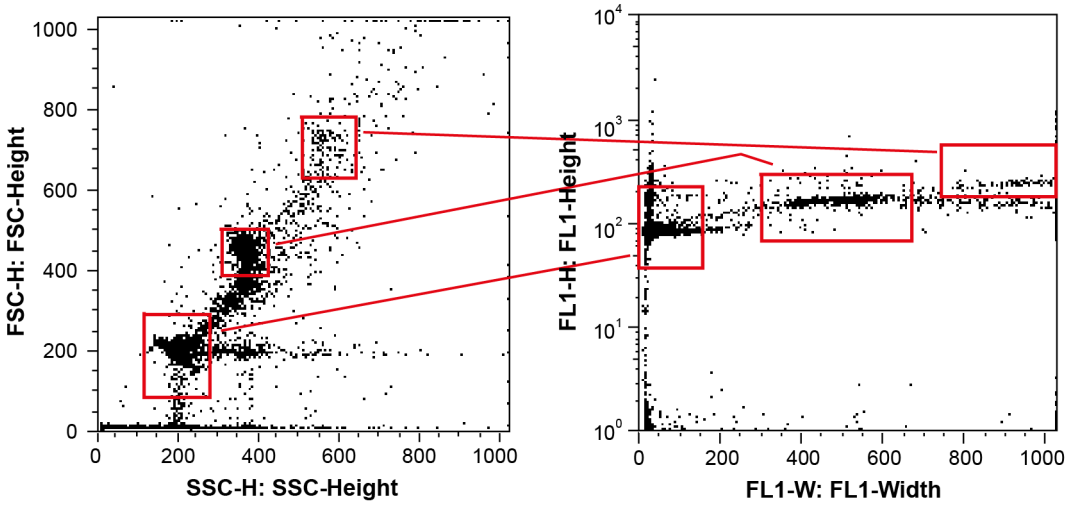

Figure 4.10: Doublet discrimination validates phagocytosis assay. Green fluorescent latex beads were run on the flow cytometer without adding cells. In the left graph comparing particle size (FSC on the y-axis) and particle granularity (SSC on the x-axis), three populations representing singlet, doublet and triplet beads are shown. In the right graph, comparing the fluorescence intensity (y-axis) with the time it takes the particle to cross the laser (x-axis) demonstrated an increase in fluorescence when detecting multiple beads compared with singlets.

4.4.5 Dissection of signalling pathways in HD monocytes

HD monocytes and macrophages resemble normal monocytes and macrophages when unstimulated, but are hyper-reactive in response to LPS showing increased cytokine production and abnormal phagocytosis. This suggests that mHTT affects the signalling cascade induced by LPS. Testing whether expression changes in the main LPS receptor, TLR4, were responsible for the HD phenotype, TLR4 transcript levels were analysed in native HD and control monocytes using qPCR. TLR4 levels were unaltered in HD monocytes isolated from patients across all disease stages (Figure 4.11), suggesting downstream effects.

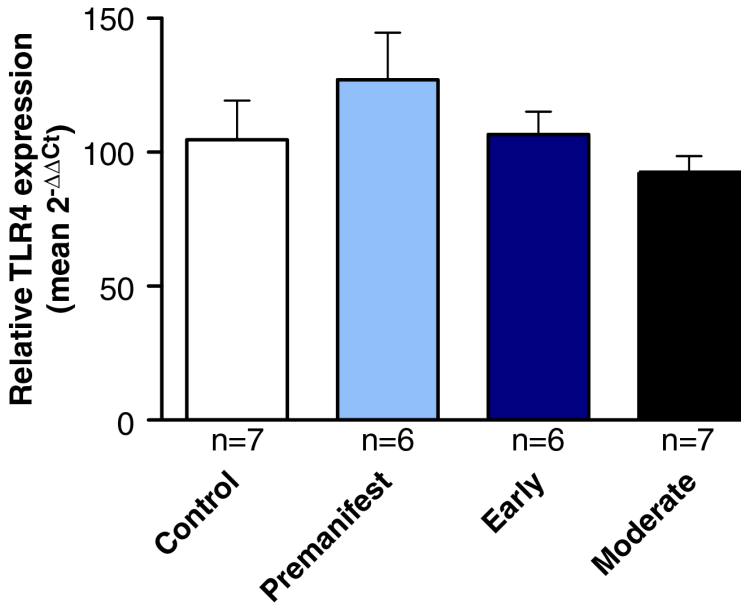

Figure 4.11: TLR4 expression does not differ between HD and control cells. $CD14^+$ monocytes from both HD patients and controls were isolated from whole blood using magnetic cell sorting. RNA was extracted from these unstimulated cells and used for gene expression analysis via qPCR, which showed no differences in TLR4 expression levels. Data shown as relative gene expression $\pm$ SEM, normalised against expression of B2M, GAPDH, BACTIN, one-way ANOVA.

4.4.5.1 mHTT interacts with the NFκB pathway

The NFκB pathway, one of the main signalling cascades downstream of TLR4, has previously been implicated in HD. Khoshnan et al. have shown that m*HTT* exon 1 expression activates the NFκB pathway by directly interacting with the γ subunit of the IKK trimer, both in inducible rat PC12 cells and striatal extracts from R6/2 mice (Khoshnan et al., 2004). To test whether this interaction occurs in human primary HD immune cells, PBMCs from early-stage HD patients and control subjects were isolated for co-immunoprecipitation experiments. Full-length HTT was detectable in both the control and HD samples with two anti-HTT antibodies (2B7 and 2166), whereas co-precipitation of IKKγ was observed only in the HD sample (Figure 4.12). This demonstrates a direct interaction between mHTT and IKKγ in primary human HD cells.

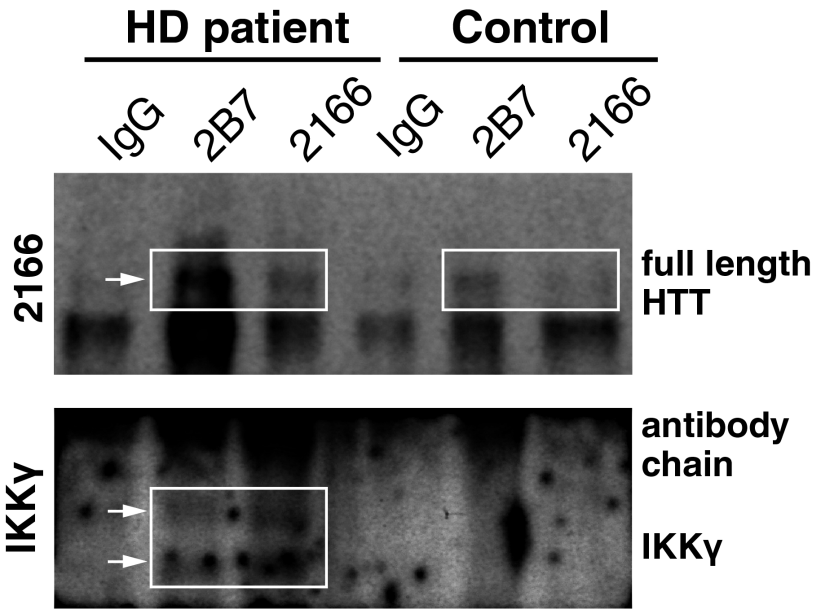

Figure 4.12: mHTT interacted directly with the NFκB pathway. HTT was co-immunoprecipitated from PBMC whole cell lysates using either 2166 or 2B7 anti-HTT antibodies, before immunoblotting for HTT and IKK. Shown is an example blot of samples from one control and one HD subject, with relevant bands marked. Experiment has been repeated six times with same result and similar (or stronger) background levels.

Activation of the IKK complex leads to the phosphorylation and degradation of IκB, the endogenous inhibitor of NFκB (Hayden and Ghosh, 2012). To evaluate whether the interaction of mHTT with IKKγ leads to increased IKK complex activation and subsequent changes in IκB degradation, HD and control monocytes were stimulated with LPS over a time-course of 2 hours to analyse IκB levels by western blot. Control monocytes demonstrated a drop in IκB levels over the first 15 minutes, followed by a recovery of IκB levels over the next two hours, representing a normal pattern of NFκB activation upon stimulation (Figure 4.13) (Gross and Piwnica-Worms, 2005). Following stimulation of HD monocytes, a different pattern was observed: IκB levels dropped within 5 minutes and did not recover to baseline levels within the two hour time-course (Figure 4.13). This demonstrates that IκB is degraded more rapidly and over a prolonged period of time in primary human HD cells due to IKK activation.

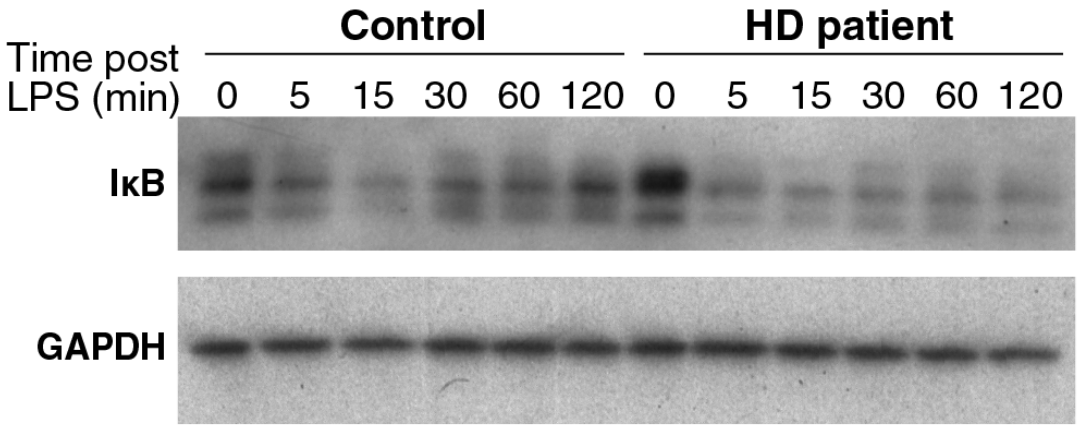

Figure 4.13: IκB degradation is faster in HD patients. Control and HD monocytes, isolated from whole blood using magnetic cell sorting, were stimulated with LPS over a two hour time-course after which cells were lysed for western blot analysis. While in control cells LPS-induced degradation of IκB occurred within 15 min of stimulation and recovered within 2 hours, HD monocytes demonstrated a rapid loss of IκB and no recovery of the protein. Shown are two example blot of samples from one control and one HD subject each. Repeated twice with similar results.

Under steady-state conditions, IκB binds NFκB and blocks its translocation to the nucleus. Degradation of IκB allows the NFκB transcription factors (RelA, RelB, cRel, NFκB1, NFκB2) to enter the nucleus and affect transcription (Beinke and Ley, 2004). In order to test whether increased IκB degradation in HD monocytes leads to more rapid nuclear translocation of NFκB, levels of RelA translocation in HD and control monocytes were analysed using imaging flow cytometry. Cells were stained with DAPI to mark the nucleus and with anti-RelA antibodies (Figure 4.14A). Analysis of the levels of RelA and DAPI co-localisation showed higher levels of RelA translocation in HD cells at every time point over a 90 minute period post-LPS stimulation, with significantly increased translocation at 5, 10 and 60 minutes (Figure 4.14B).

Thus, mHTT binds IKKγ and is likely to cause increased NFκB activity by increased IκB degradation and subsequent NFκB translocation. This would be expected to lead to increased transcription of NFκB target genes, as represented by increased cytokine production by the cells.

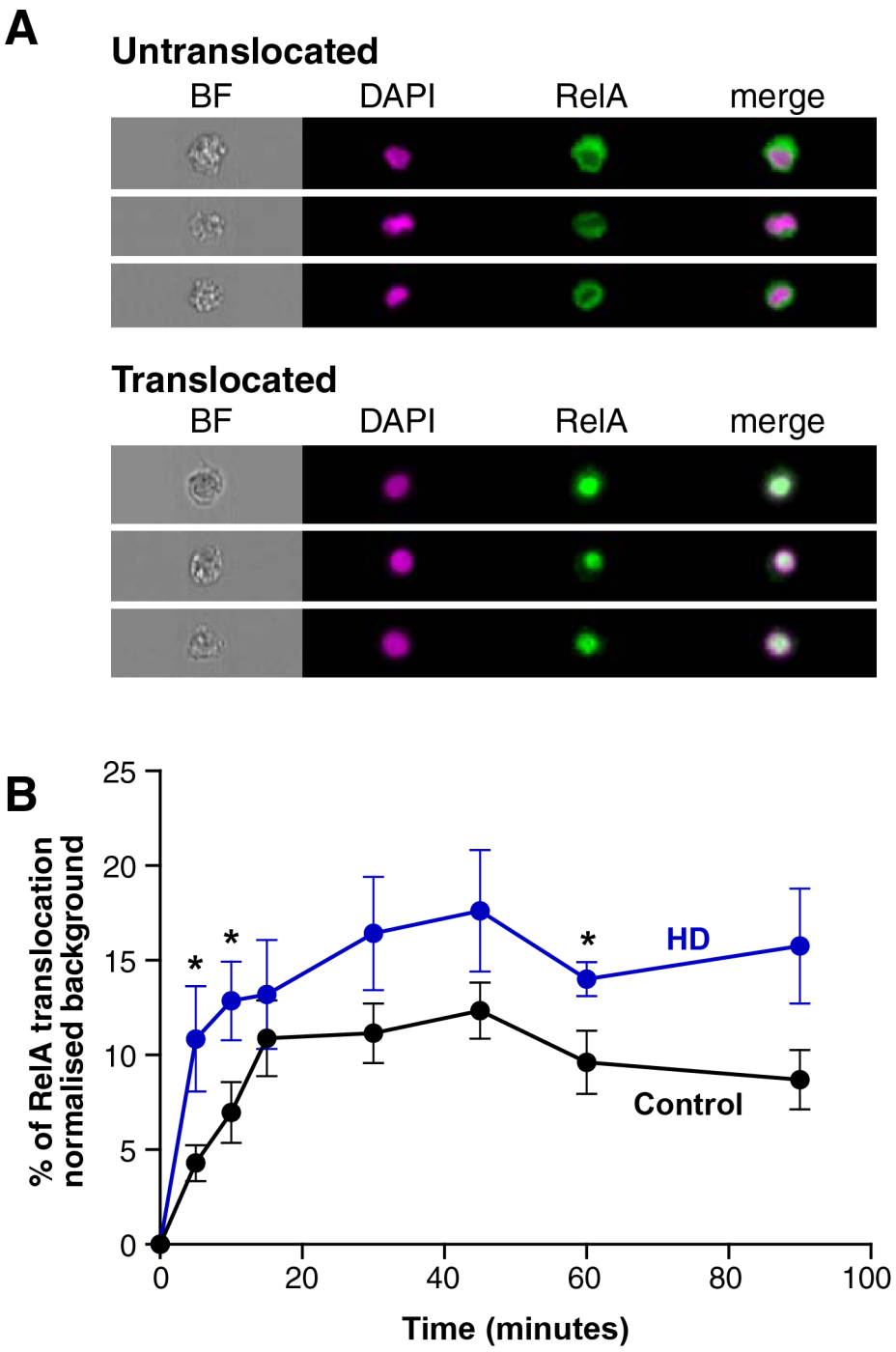

Figure 4.14: NFκB translocation into the nucleus is faster in HD monocytes. Translocation of the NFκB transcription factor RelA to the nucleus in LPS stimulated blood monocytes was measured using imaging flow cytometry; **(A)** example images are shown here. In untranslocated cells the green RelA staining surrounded the nuclear DAPI staining, whilst in cells demonstrating translocation of RelA the colours merge. **(B)** Increased RelA translocation into the nucleus following LPS stimulation was observed in HD monocytes (n=7) compared with controls (n=7). n= individual biological repeats.

4.4.5.2 Transcriptional changes affect signalling pathways in HD myeloid cells

Transcriptional dysregulation is a central pathogenic mechanism in HD (Hodges et al., 2006). Therefore, it was tested whether basal differences in transcription play a role in the mHTT induced immune hyper-reactivity by analysing differences in the expression of genes related to the NFκB pathway. The mRNA expression levels of 84 genes were tested in untreated human monocytes using the SABioscience NFκB signalling pathway PCR array, identifying seven genes that were significantly up-regulated (*TLR2*, *LTBR*, *CD40*, *TMED4*, *AKT1*, *IL10*, *FR2*) and one gene that was significantly down-regulated (*CHUK*) in HD compared with control cells (Table 4.1 for top 20 hits, full list in Appendix Table A.5). Four of the up-regulated genes showed a fold change (FC) equal or higher than 1.5: CD40 (FC=1.5); AKT1 (FC=1.5); IL10 (FC=1.85) and F2R (FC=2.23). Furthermore, the adaptor molecules *IRAK1*, *TICAM2*, *MYD88*, and *TRADD*, were also up-regulated (Table 4.1). Interestingly, *CHUK*, which encodes for IKK , was found to be down-regulated, whilst all other parts of the IKK complex, IκB and the NFκB transcription factors were unchanged. The array also screened intracellular signalling pathways closely linked to the NFκB pathway, such as the MAPK and PI3K/AKT pathways. Increased AKT protein levels have been found in HD patient lymphoblasts (Colin et al., 2005) and *AKT1* is one of the genes up-regulated in HD monocytes (FC=1.5, p= 0.031). Moreover, the genes composing the transcription factor AP-1, *CJUN* and *FOS*, are also up-regulated in HD monocytes (Table 4.1). Therefore, both of these pathways may also contribute to the increased immune response observed after stimulation of HD monocytes.

Table 4.1: The top twenty gene changes within the NFκB pathway observed in HD monocytes. Data presented as fold change calculated from $\Delta\Delta$CT values, unpaired two-tailed student t test was used as statistical method. n= 10 for HD and control.

Gene name	Fold change	p value
TLR2	1.48	0.01
LTBR	1.35	0.01
CHUK	0.77	0.02
CD40	1.51	0.02
TMED4	1.23	0.02
AKT1	1.54	0.03
IL10	1.85	0.04
F2R	2.23	0.04
IRAK1	2.00	0.05
CJUN	2.22	0.05
TICAM2	1.32	0.05
MYD88	1.26	0.05
FOS	1.87	0.06
TRADD	1.25	0.06
RAF1	1.12	0.07
SLC44A2	1.29	0.07
ATF1	1.16	0.07
IL6	2.49	0.08

To validate these findings, six candidate genes, chosen on the basis of array FC (*CD40*, *AKT1*, *IRAK1*, *CJUN*, *IL6* and *IL10*), were quantified by qPCR using different primer sets and cells from a different patient cohort (10 control and 10 HD subjects). The relative changes in gene expression when comparing HD and control human monocytes matched the previous findings for all six genes (Figure 4.15). Expression levels for *CD40*, *IRAK1* and *IL10* were significantly increased in HD compared with control monocytes, whilst expression changes in *AKT1*, *CJUN* and *IL6* demonstrated an upwards trend, not reaching significance due large inter-individual differences.

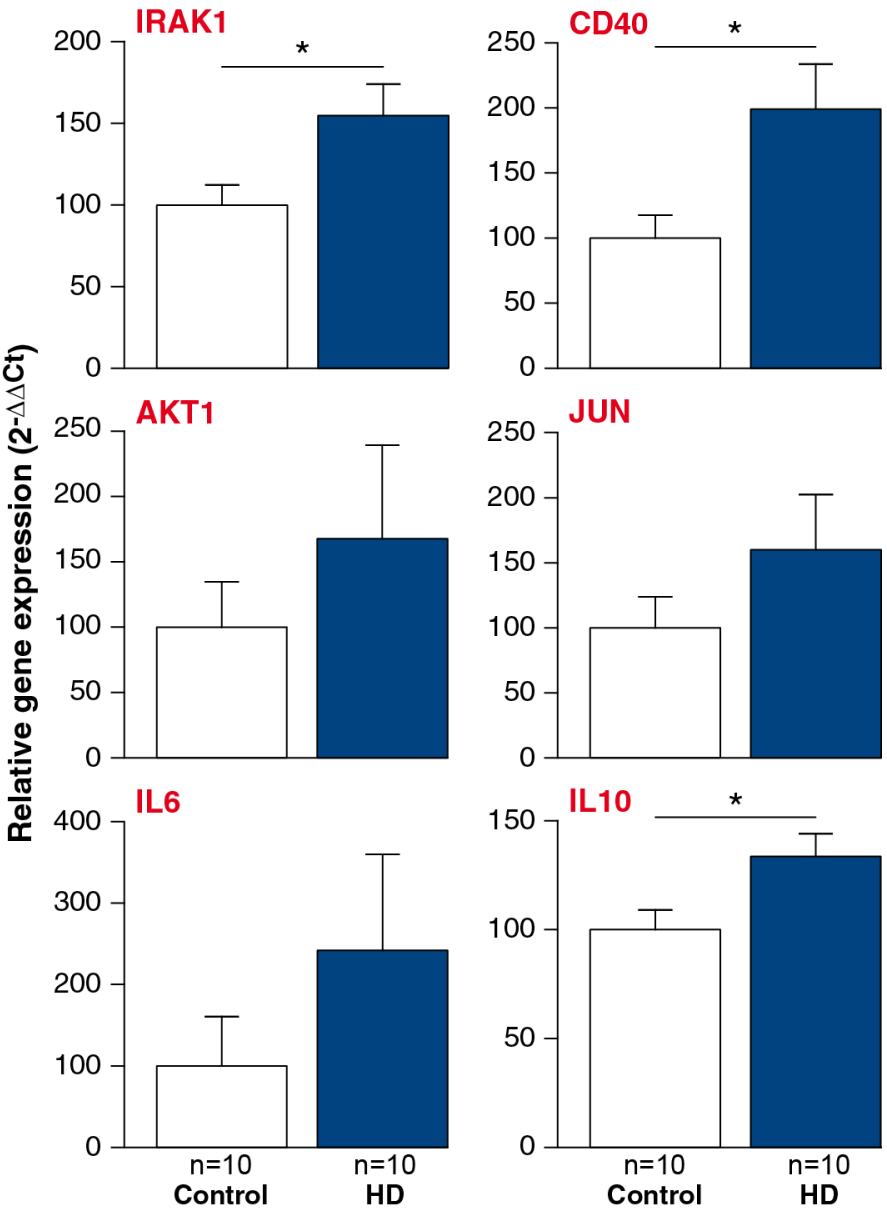

Figure 4.15: Validation of gene expression changes identified using PCR signalling arrays. After 3 days in culture, RNA was isolated from unstimulated monocytes and used for gene expression analysis via qPCR. This showed the same up-regulation in HD versus control cells as the original array. Data shown as relative gene expression ± SEM, unpaired two-tailed student t tests, *$p<0.05$; **$p<0.01$.

Using Cytoscape software (Shannon et al., 2003), the gene expression changes within the TLR4 signalling pathway were visualised (Figure 4.16) showing changes in several key molecules within the pathways activated by TLRs, including *AKT1*, *CJUN*, *FOS* and a range of adapter molecules such as *IRAK1* and *TICAM2*. These changes may lead to increased signalling along the NFκB sig-

nalling cascade upon stimulation. Known NFκB target genes such as *IL6*, *IL8* and *IL1B* also exhibited trends towards differential expression, although they did not reach statistical significance due to large inter-individual variability.

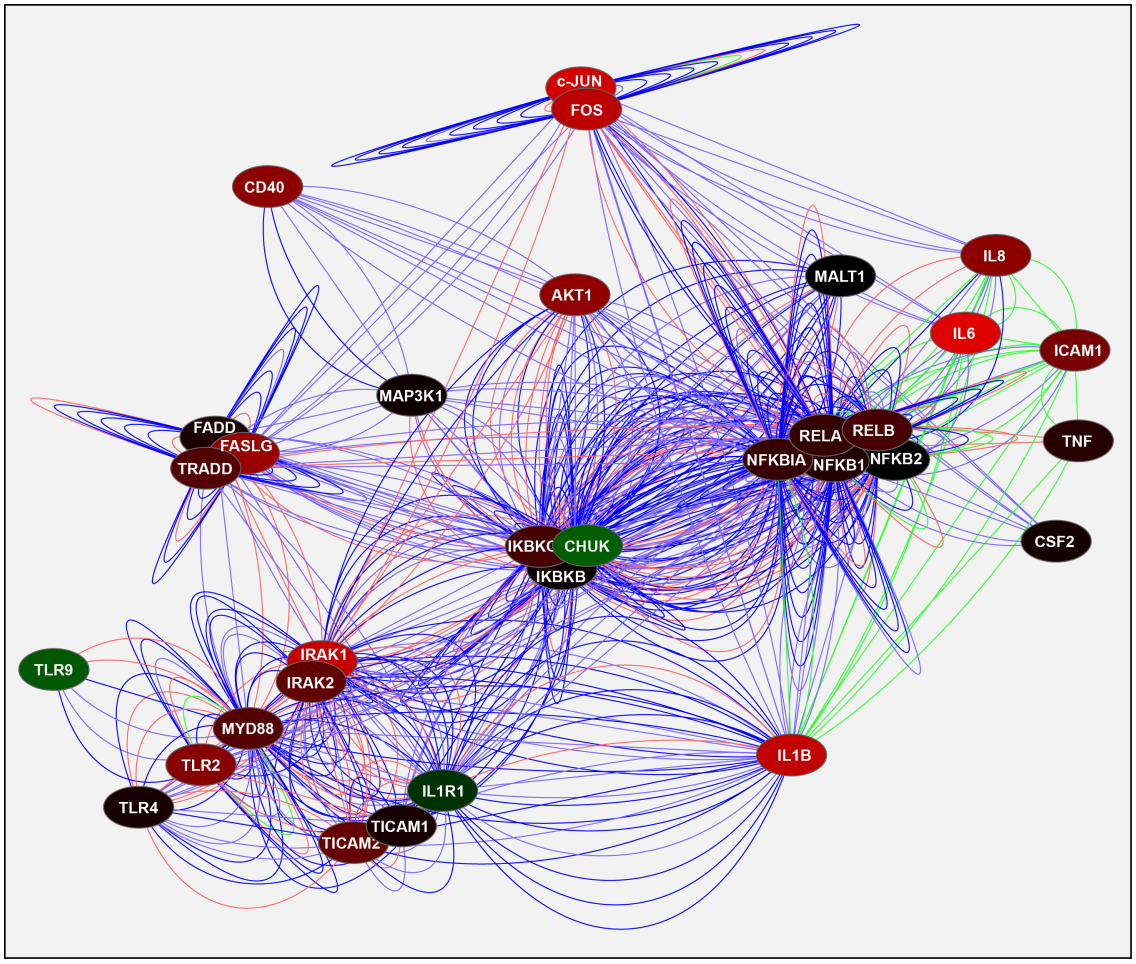

Figure 4.16: Expression of several key molecules within the NFκB pathway is altered in HD. Monocytes under basal unstimulated conditions were analysed by qPCR using pre-validated primers from SABioscience (n= 10 biological repeats, for control and early-stage HD patients). Changes in mRNA expression levels were analysed using Cytoscape, allowing construction of a pathway map to visualise gene expression changes within the TLR4/LPS signalling cascade. Nodes stand for the different genes, red and green colour indicating up- or down-regulation in HD compared with control cells, respectively. Connecting lines visualise connections between genes (red: experimental data; green: array data; lilac: STRING data; blue: combined data). Network analysis was performed in collaboration with Dr Holger Hummerich.

Next, bioinformatic approaches were utilised in an attempt to identify transcription factors involved in the transcriptional changes found in mHTT expressing monocytes. Using Genomatix gene2promoter software, promoter regions featured in the seven genes that were significantly up-regulated in HD monocytes were compared with the promoter regions of the 70 genes that were unchanged. Genes with near significance (*IRAK1*, *JUN*, *TICAM2*, *MyD88*, *FOS*, *TRADD* and *IL6*) were excluded from this analysis, as the sample size of 10 human subjects per group may be the reason for these changes not reaching statistical significance. Interestingly, the promoter regions of the excluded genes were more similar to the promoter regions found in genes with altered expression than in those that were unchanged.

Analysing whether genes found to be up-regulated in unstimulated HD monocytes are regulated by NFκB, the pathway identified to be hyper-activated in these cells after LPS stimulation, indicated that this may not to be the case as genes found up-regulated in baseline HD monocytes do not show higher abundance of NFκB binding sites in their promoters (Table 4.2). Interestingly, the promoter site for AP-1 is more than twice as prevalent in up-regulated genes compared with those that were unchanged. Additionally, five out of the seven promoter regions found to be more than two-fold more prevalent in up-regulated compared with unchanged genes were binding sites for different zinc finger transcription factors.

Table 4.2: Promoter analysis of genes found to be expressed differently in HD monocytes. Using the Genomatix software gene2promoter abundance of transcription factor binding sites was compared between genes found up-regulated and genes found unchanged in HD monocytes.

Promoter region	Transcription factor	Fold change	Abundance in unchanged genes	Abundance in changed genes
NFKB	p65/50	0.8	72(51/70)	57(4/7)
ZF05	C2H2 zinc finger transcription factor 5	3.3	13(9/70)	43(3/7)
CSEN	Calsenilin, presenilin binding protein, EF hand transcription factor	2.7	16(36/70)	43(2/7)
RP58	PRP58 (ZFP238) zinc finger protein	2.5	3(9/70)	29(2/7)
AP1F	JUN/FOS-activating protein a	2.5	23(16/70)	47(4/7)
BTBF	BTB/POZ (broad complex, Trantrach, Bric brac/pox viruses and zinc fingers) transcription factor	2	22(15/70)	43(3/7)
INSM	zinc finger protein insulinoma-associated 1 (IA-1)	1.9	51(36/70)	100(7/7)
SPZ1	Testis-specific bHLH-Zip transcription factors	1.9	38(27/70)	71(5/7)

4.4.5.3 JAK-STAT signalling is unchanged

In addition to signalling pathways downstream of TLR4, pathways activated by cytokine receptors may also play a role in HD immune dysfunction. Plasma cytokine levels are elevated in HD patients (Björkqvist et al., 2008), which could lead to chronic activation of the pathways downstream of cytokine receptors in HD monocytes and macrophages. The STAT signalling pathway is activated mainly via cytokine receptors and not TLRs, whilst also being involved in cytokine production (Levy and Darnell, 2002). To assess the level of phosphorylated STAT (pSTAT) molecules in HD cells, PBMCs were isolated from whole blood by density centrifugation and stained with the monocyte marker $CD64^{+}$. Cells were then either left unstimulated or treated with specific JAK/STAT activators such as IFNγ, IL-6 and GM-CSF for STAT1, 3 and 5, respectively. After staining the cells with intracellular antibodies for pSTAT1, 3 or 5, levels of the molecules were assessed using flow cytometry. For analysis, monocytes were identified by CD64 staining before pSTAT levels were quantified (gating shown in Figure 4.17).

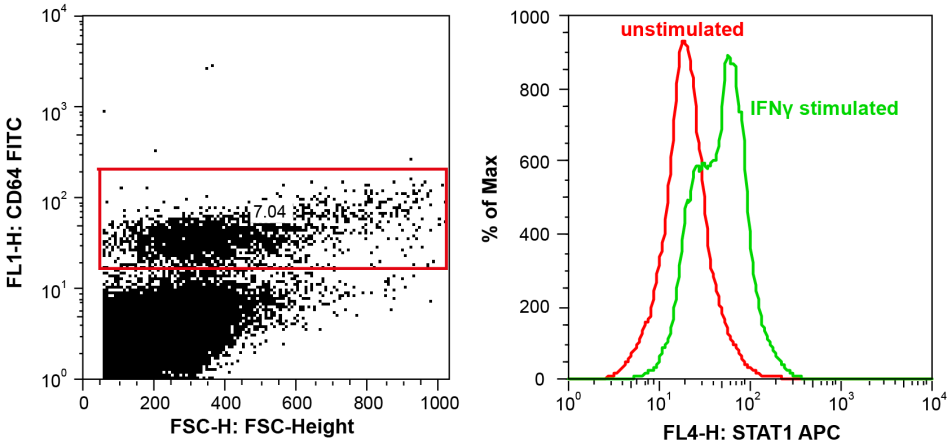

Figure 4.17: Example for gating for STAT phosphoflow analysis. PBMCs were isolated using density centrifugation, stimulated with for example IFNγ to initiated STAT1 phosphorylation. For flow cytometry analysis monocytes were identified by gating on CD64 positive cells (left panel) before pSTAT1 levels were blotted as histogram. Overlay of unstimulated and IFNγ-stimulated cells showed a shift in pSTAT1 expression levels in monocytes upon stimulation. pSTAT1 levels were quantified as geometric mean. The same gating was used for pSTAT3 and 5 stimulated by IL-6 or GM-CSF, respectively.

Comparing pSTAT levels between control and HD patients showed no difference in STAT phosphorylation in untreated monocytes, or after any of the treatments (Figure 4.18).

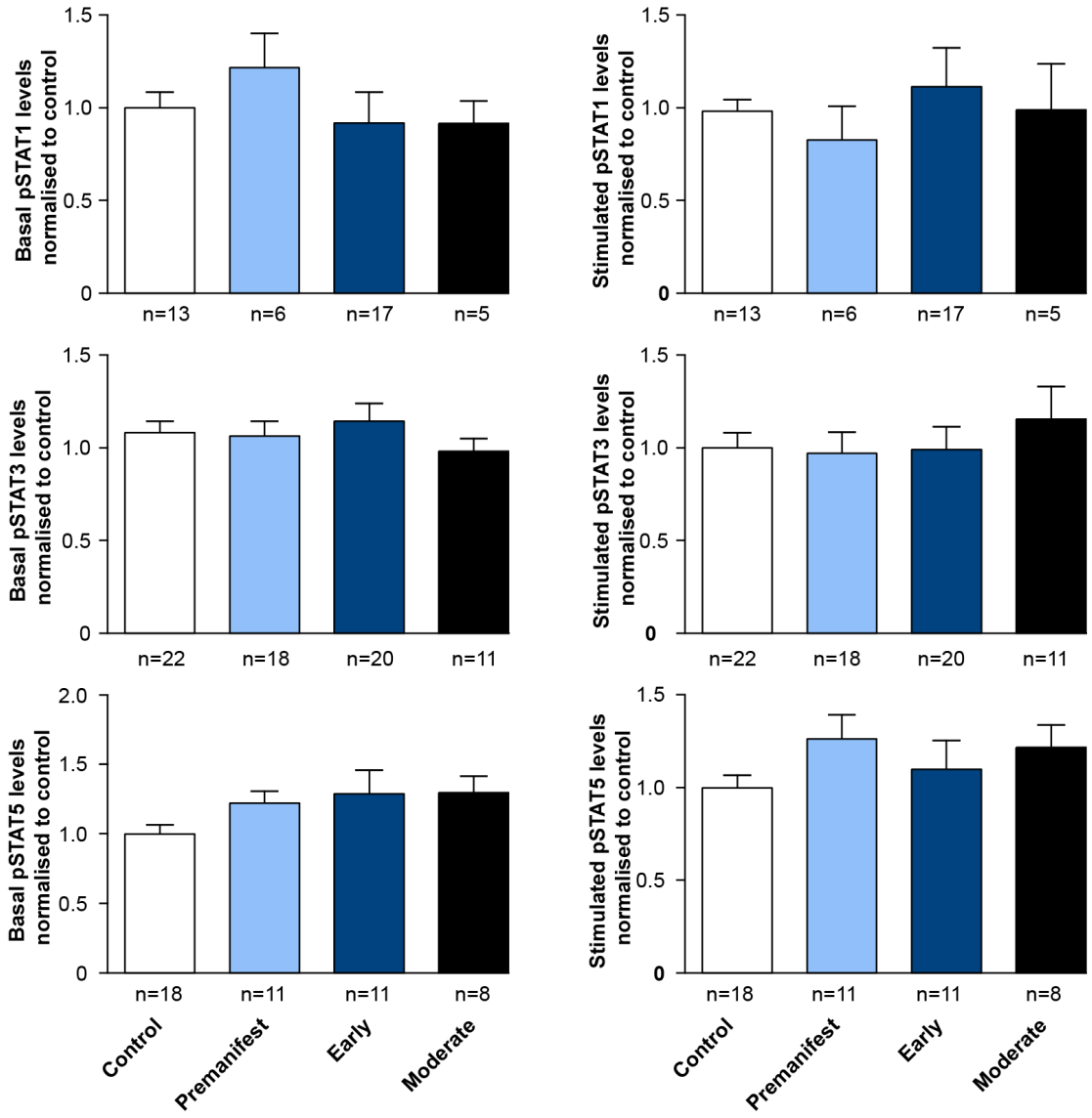

Figure 4.18: STAT signalling appears normal in HD patient monocytes. PBMCs were isolated using density centrifugation, stimulated with either IFNγ (causing STAT1 phosphorylation), IL-6 (causing STAT3 phosphorylation) or GM-CSF (causing STAT5 phosphorylation) and stained for $CD64^{+}$ and pSTAT1, 3 and 5, respectively. Flow cytometry was used to assess the amount of pSTAT molecules in untreated and treated cells. Data shown as mean pSTAT levels normalised to control levels $\pm$ SEM. One-way ANOVA showed no statical significance.

In addition, the fold change of activation, calculated by dividing the level of pSTAT after stimulation by pre-treatment levels, was also unchanged in HD compared with control cells (Figure 4.19). This suggests that STAT signalling is not abnormal in HD immune cells.

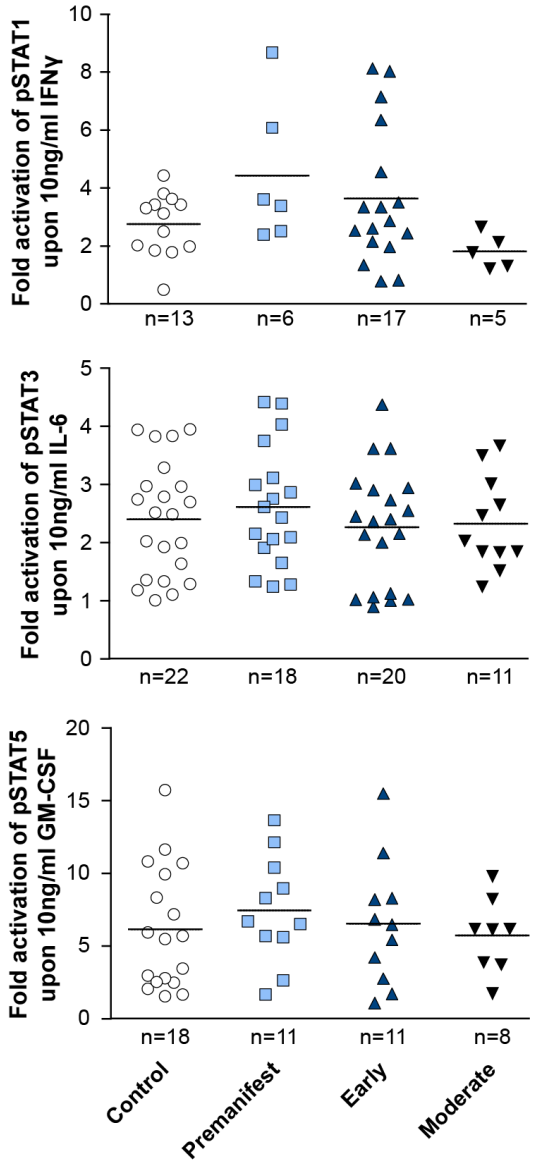

Figure 4.19: Fold change activation of STAT signalling appears normal in HD patient monocytes. PBMCs were isolated using density centrifugation, stimulated with either IFNγ (causing STAT1 phosphorylation), IL-6 (causing STAT3 phosphorylation) or GM-CSF (causing STAT5 phosphorylation) and stained for CD64$^+$ and pSTAT1, 3 and 5, respectively. Flow cytometry was used to assess the amount of pSTAT molecules before calculating the fold-activation by dividing post-treatment pSTAT levels by pre-treatment levels. Data shown as mean fold change $\pm$ SEM. One way ANOVA.

4.4.6 Lowering HTT levels reverses the HD immune phenotype

Lowering *HTT* expression using siRNA is a promising therapeutic approach for HD (Sah and Aronin, 2011). This PhD investigated whether lowering total *HTT* levels can reverse the hyper-reactive phenotype in primary human HD monocytes and macrophages. In a novel approach taking advantage of the cells ability to phagocytose, anti-*HTT* siRNA was packaged into 1,3-D-glucan-encapsulated siRNA particles (GeRPs) for delivery into primary human monocytes or macrophages (Aouadi et al., 2009). Cells seeded on coverslips and co-cultured with the GeRPs readily took them up via phagocytosis as shown by fluorescence microscopy (Figure 4.20A). Testing different macrophage to GeRP ratios, up to 90 % of macrophages took up green fluorescent GeRPs when they were added at a ten fold particle to cell ratio, demonstrating high transfection efficiency at this concentration (Figure 4.20B).

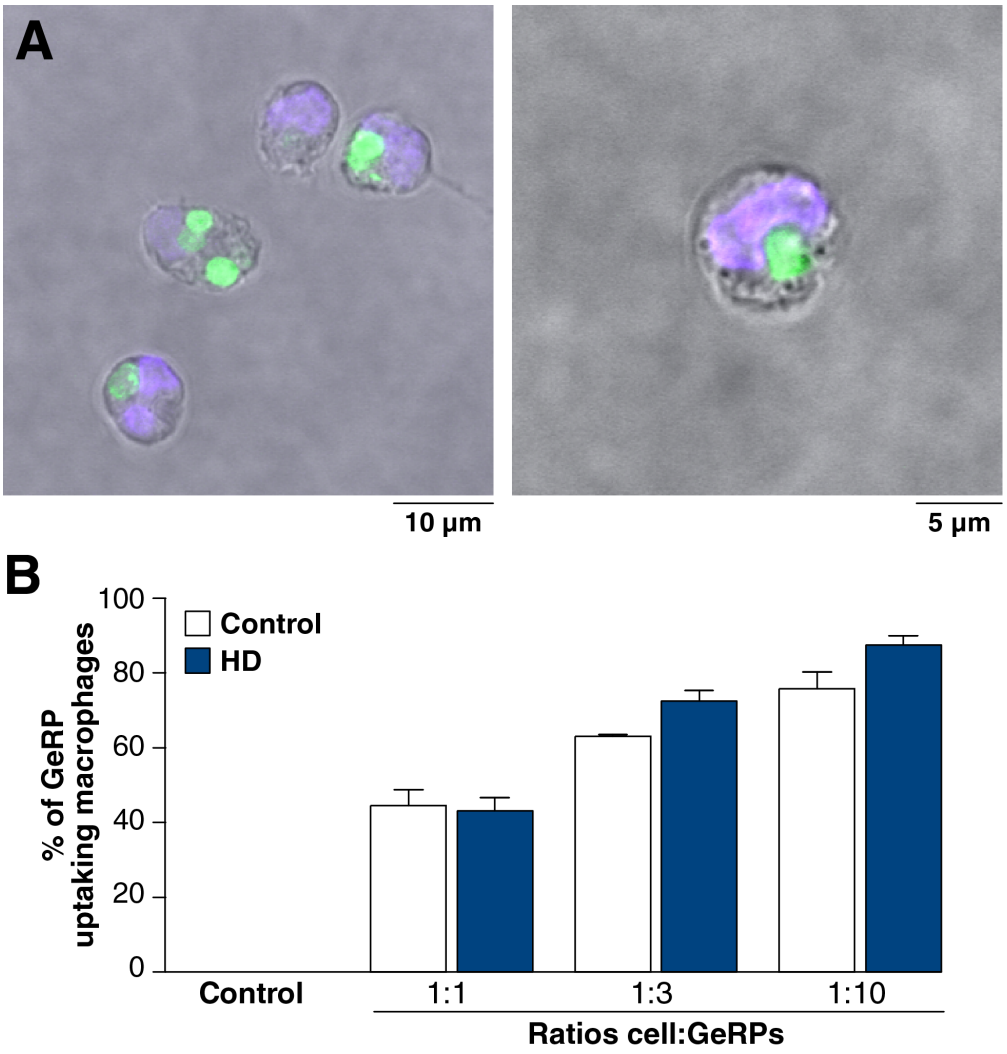

Figure 4.20: Primary human phagocytic cell can efficiently take up GeRPs. (A) Primary human control monocytes were seeded on poly-L-lysine coated coverslips and treated with empty GeRPs for 12 h. Uptake via phagocytosis was visualised via microscopy (GeRPs = green; DAPI = blue). **(B)** Monocyte-derived macrophages were incubated with empty GeRPs at different cell to particle ratio for 12 h. After fixing the cells with 3.7 % PFA, uptake was quantified by flow cytometry. Data shown as mean ±SEM (n=2 for controls and n=3 for HD). Experiment performed in collaboration with Prof Gary Ostroff, who produced all GeRPs.

Next, the efficacy of the anti-*HTT* siRNA GeRPs was tested three days after siRNA delivery in macrophages, using both qPCR for *HTT* RNA levels and TR-FRET for HTT protein levels. Macrophages treated with anti-*HTT* siRNA containing GeRPs had 60-70 % less *HTT* mRNA and 50 % less HTT protein, compared with macrophages treated with scrambled siRNA-containing GeRPs (Figure 4.21).

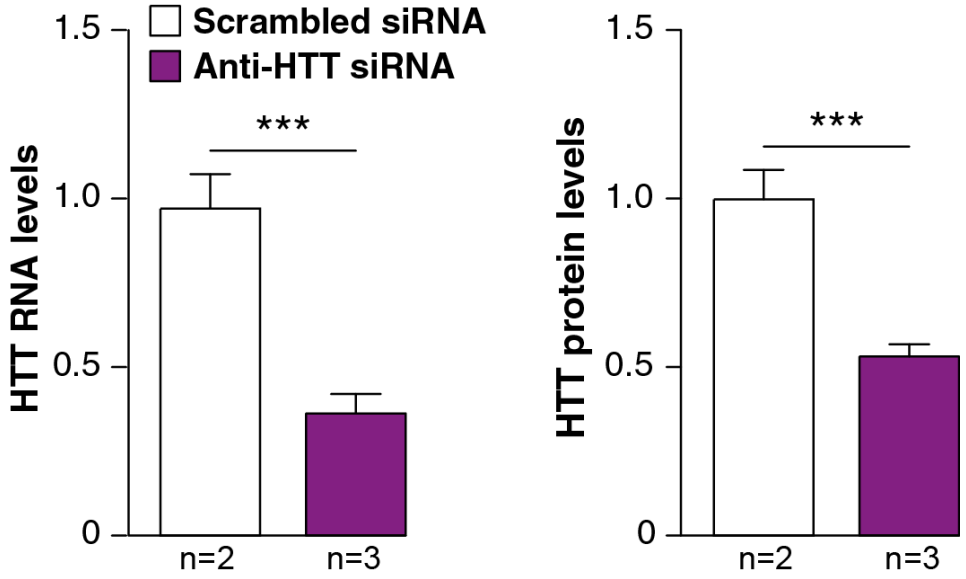

Figure 4.21: GeRPs effectively knock-down total *HTT* in primary human immune cells. Monocyte-derived macrophages were treated with either scrambled or anti-*HTT* siRNA containing GeRPs for 3 days, before cells were lysed for either RNA or protein extraction. Total *HTT* RNA measured by qPCR and protein levels measured by TR-FRET were reduced by 70 % and 50 %, respectively, in cells treated with anti-*HTT* siRNA compared with cells treated with scrambled siRNA. Data shown as mean HTT levels $\pm$SEM (n=10 for controls and HD for qPCR; n=2 for controls and n=3 for HD for TR-FRET, each combining 2 independent experiments, n stands for individual biological repeats). Paired t test ***$p<0.001$. Experiment performed in collaboration with Prof Gary Ostroff, who produced all GeRPs and Dr Andreas Weiss, who performed TR-FRET measurements.

As expected, the decrease in HTT levels was the same in both control and HD macrophages, and there was no preference of expression-lowering between the mutant and wild-type *HTT* alleles (Table 4.3).

Table 4.3: anti-*HTT* siRNA efficiently lowers both wild-type and mutant HTT alleles. Levels of total and mutant HTT were measured in monocyte-derived macrophages from HD patients using TR-FRET with antibody combinations, 2B7-2166 and 2B7-MW1, respectively. Experiment performed in collaboration with Prof Gary Ostroff, who produced all GeRPs and Dr Andreas Weiss, who performed TR-FRET measurements.

Subject	knock-down of protein level	
	mHTT levels	total HTT levels
control	-	45.89 %
HD	46.60 %	47.20 %
HD	28.10 %	23.25 %
control	-	48.90 %
HD	48.70 %	50.80 %

Next, the effect of lowering total HTT levels on cytokine production was analysed. After treating primary human monocyte-derived macrophages with GeRPs containing anti-*HTT* or scrambled siRNA for three days, IFNγ-primed cells were stimulated with LPS and cytokine production was measured using multiplex ELISA assays. In agreement with the previous findings, IL-8 and TNFα levels were significantly higher in HD as compared with control cells, when both had been treated with scrambled siRNA (Figure 4.22). However, lowering HTT levels in HD macrophages using anti-*HTT* GeRPs reversed this increase, by significantly reducing the production of IL-6, IL-8 and TNFα (Figure 4.22). IL-1β production showed a similar trend, but the difference was not statistically significant. Interestingly, lowering HTT levels in control cells also significantly reduced IL-6, IL-8 and TNFα levels, suggesting a role for wild-type HTT in cytokine production, in addition to the derangement of the NFκB pathway caused by mHTT binding IKK. It is possible that both a loss of wild-type function and a toxic gain of mutant function contribute to the phenotype. Thus, lowering HTT levels by 50 % can partially

reverse the hyper-reactivity in HD patient macrophages using a novel method of siRNA delivery. The use of GeRPs to achieve cell-targeted gene knockdown has to date shown significant promise in mice, but this is the first report showing efficient siRNA delivery, pathogenic gene knock-down and rescue of a deleterious phenotype using this method in primary human immune cells.

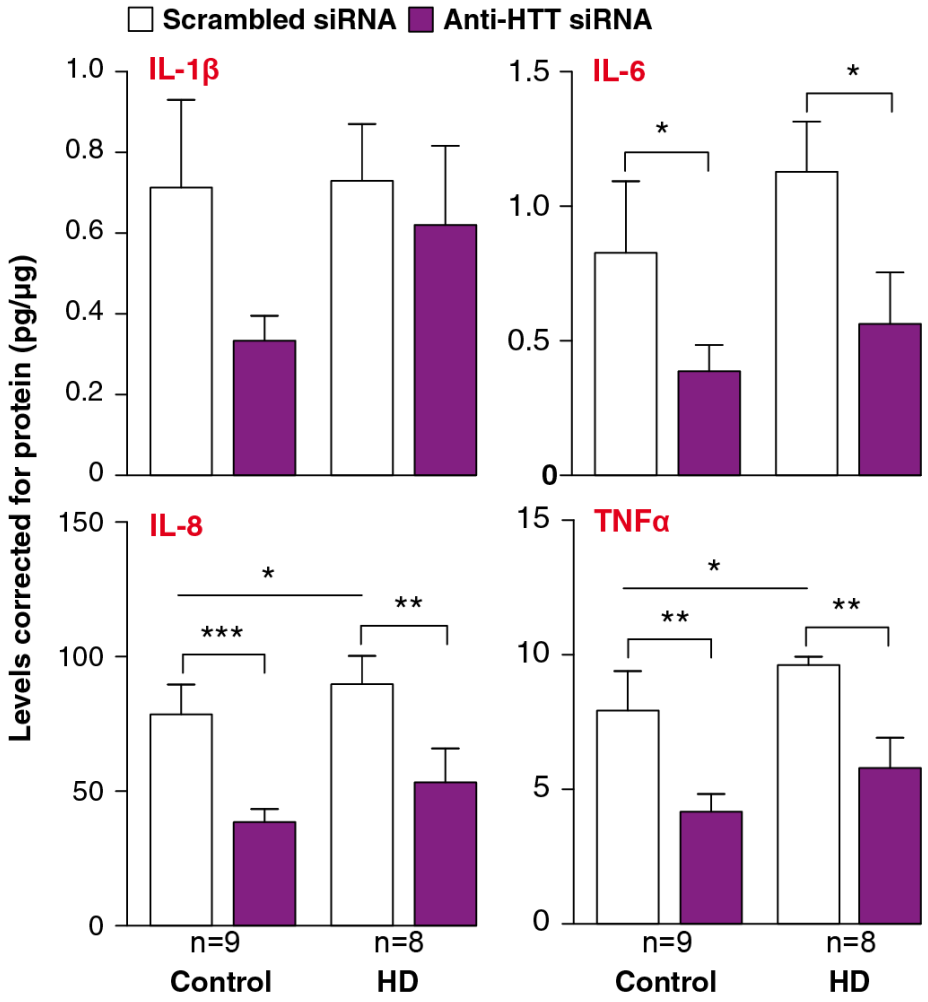

Figure 4.22: Anti-*HTT* siRNA containing GeRPs decreases elevated cytokine production in HD patient cells. HD and control macrophages were treated with either anti-*HTT* or scrambled siRNA for three days, before the cells were stimulated with 10 ng/ml IFNγ and 2 μg/ml LPS for 24 h. Measuring cytokine production with multiplex ELISA assays showed that lowering HTT levels reduces IL-6, IL-8 and TNFα levels following stimulation. Data shown as mean concentrations normalised to protein content $\pm$SEM (n= 9 for controls and n=8 for HD, combined from 3 independent experiments, n stands for individual biological repeats), two-way ANOVA with Bonferroni post-tests. *$p<0.05$; **$p<0.01$, ***$p<0.001$. Experiment performed in collaboration with Prof Gary Ostroff, who produced all GeRPs.

Subsequently, siRNA was used to test whether HTT lowering can reverse the transcriptional changes observed in baseline HD patient monocytes. *IRAK1* (main adapter molecule between TLR4 and NFκB), *CD40* (immunomodulatory molecule giving co-stimulatory signals to both innate and adaptive immune cells) and *CJUN* (part of the AP-1 transcription factor) expression was increased in HD monocytes (Table 4.1). Following three days of treatment with GeRPs containing either scrambled or anti-*HTT* siRNA, expression of these candidate genes analysed by qPCR. *HTT* levels were assessed to validate the levels of knock-down. Treatment with anti-*HTT* siRNA resulted in a 50 % reduction in *HTT* mRNA levels in both HD and control macrophages (Figure 4.23A/B). However, only the HD monocytes demonstrated a significant 20-30 % reduction in the expression of *IRAK1*, *CD40* and *CJUN* when treated with anti-*HTT* compared with scrambled siRNA (Figure 4.23A). Lowering HTT in control cells did not affect levels of *IRAK1*, *CD40* and *CJUN* transcript expression (Figure 4.23B), suggesting that the transcriptional dysregulation of these genes in HD myeloid cells is caused specifically by a gain of mHTT function, rather than loss of wild-type protein function.

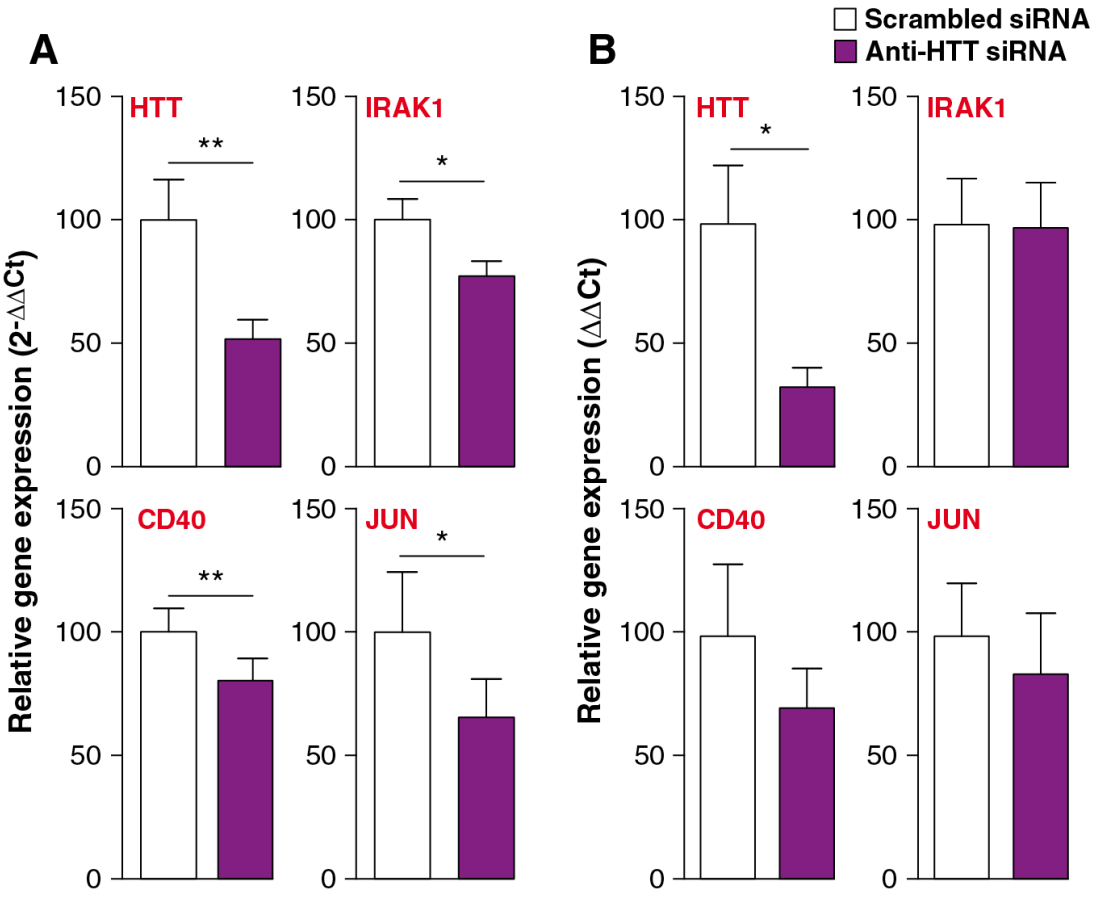

Figure 4.23: Lowering total *HTT* levels reverses transcriptional changes found in HD monocytes. HD and control monocytes were incubated with either scrambled or anti-*HTT* siRNA containing GeRPs for 3 days before RNA isolation. Using qPCR, efficient HTT knock-down was demonstrated as well, as lowering of key NFκB pathway molecules IRAK1, CD40 and JUN in **(A)** HD patient cells but not **(B)** controls. Data shown as relative gene expression (n= 10 biological repeats for controls and HD) with standard error bars, paired t test *$p<0.05$; **$p<0.01$. Experiment performed in collaboration with Prof Gary Ostroff, who produced all GeRPs.

4.5 Discussion

Plasma pro-inflammatory cytokine levels are elevated in HD patients, even in the premanifest stages of the disease (Björkqvist et al., 2008). Here, HD PBMCs are demonstrated to be a source of the increased pro-inflammatory cytokines, as both monocytes and macrophages isolated directly from HD patients and stimulated with LPS, produced significantly more IL-6, IL-8 and TNFα compared with controls. Supporting the finding that plasma cytokine levels are already elevated in premanifest subjects with a mean of 16 years to clinical onset (Björkqvist et al., 2008), myeloid cells isolated from premanifest HD patients were hyper-reactive to the same degree as cells isolated from late-stage disease patients. This suggests an early deficit that is already present many years before disease onset. This may offer an early marker as to when to intervene with potential modulatory therapies.

Expression of m*HTT* exon 1 in a monocyte-like cell line demonstrated that the hyper-reactive phenotype is due to a cell-intrinsic effect of mHTT expression and not to non-cell autonomous secondary factors. However, caveats of this experiment should be noted. Firstly, it was necessary to utilise a cell line, as transducing primary human myeloid cells is inefficient and technically challenging and secondly, *HTT* exon 1 constructs were used, due to the size of the full-length *HTT* gene. The cell model created therefore overexpressed a N-terminal HTT fragment, which cannot recapitulate all functions of the full-length HTT protein and carries a CAG repeat length significantly greater than adult-onset HD patients (who normally range between 40-50 CAGs (Myers, 2004)). In addition, the mHTT expressing U937 lines formed HTT aggregates, which are not observed in primary human immune cells. These may be caused either by the very long CAG expansion or the fragment nature of the overexpressed mHTT. HTT fragments

have been found in human PBMCs (Weiss et al., 2012), but these ranged in size and were lower in concentration than the fragments in overexpressing U937 cells. This may explain the lack of aggregate detection in primary human immune cells. Interestingly, U937 cells expressing HTT exon 1 with 129Q show 30 times more aggregates than U937 cell expressing 79Q while both cell lines express similar levels in cytokines, suggesting that aggregated mHTT is not the driver behind immune dysfunction.

Given the increased cytokine production and phagocytosis in LPS stimulated HD macrophages, as well as the fact that expression levels of the LPS receptor TLR4 did not differ between HD patients and control subjects, mHTT may interfere with signalling pathway(s) downstream of TLR4. One of the main pathways activated by TLR4 is the NFκB pathway, which had been previously implicated in HD in murine studies (Khoshnan et al., 2004; Steffan, 2010). Investigating the NFκB pathway, mHTT was shown to bind the regulatory γ subunit of IKK. Furthermore, enhanced activity of the NFκB pathway was identified in HD cells, with increased IκB degradation and concurrent RelA translocation into the nucleus. IKKγ is the regulatory subunit of the IKK trimer, consisting of one regulatory (γ) and two kinase subunits (α and β), and is a critical component without which cells are unresponsive to all upstream stimuli of this pathway (Israël, 2000). During signal transduction, polyubiquitin chains form the scaffold on which TAK1/TAB2/3 and IKK complexes are formed to induce TAK1-dependent activation of IKKγ (Miyamoto, 2011). In agreement with a model previously described (Khoshnan and Patterson, 2011), our data suggests that mHTT can function as an alternative scaffold in the NFκB pathway, binding IKKγ to initiate IKK complex formation, increase transduction down the signalling cascade and cause increased cytokine production (Figure 4.24). Interestingly, a recent study showed that activating the immune modulator CB2, which dampens NFκB signalling (Rajesh et al., 2007), reduces increased serum IL-6 levels in HD mouse models (Bouchard et al., 2012).

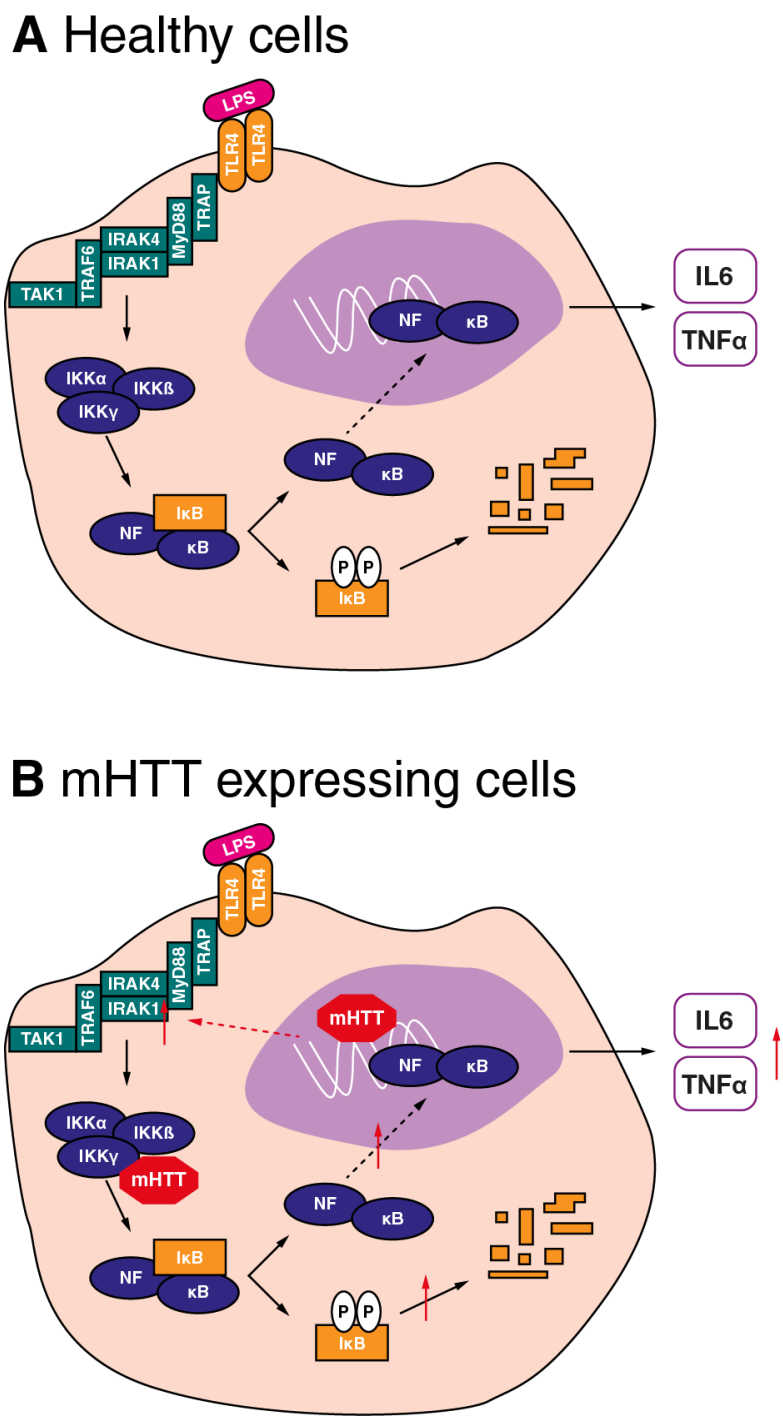

Figure 4.24: Proposed mechanism of immune dysfunction in HD. **(A)** In wild-type HTT expressing myeloid cells, LPS binds TLR4 and activates the NFκB pathway triggering production of pro-inflammatory cytokines such as IL-6 and TNFα. **(B)** mHTT interferes with the NFκB pathway by two distinct mechanisms. The mutant protein binds IKKγ directly causing increased IκB degradation and NFκB transcription factor translocation, allowing increased transcription of target genes such as IL-6 and TNFα. Moreover, mHTT causes transcriptional changes leading to increased expression of key molecules within the signalling cascade likely to increase signalling transduction rate.

Khoshnan et al. have described the same interaction of mHTT and IKKγ in both murine striatal neurons and rat PC12 cells (Khoshnan et al., 2004), with cells expressing exon 1- *mHTT* only and not the full-length mutant protein. This agrees with our findings that a N-terminal human exon 1 mutant *mHTT* fragment is sufficient to induce elevated cytokine production in a histiocytic cell line. This is also in keeping with a recent report demonstrating increasing N-terminal fragmentation of mHTT in human myeloid cells as the disease progresses (Weiss et al., 2012) (Chapter 3). Thus, the ability of mHTT to act as a scaffold for IKKγ must be mediated by either its N17, polyQ or polyP domains, or by a specific conformation of the mHTT N-terminus. It may be a combination of these factors, as the N17 region folds back onto the polyP region to form a hinge-like structure. When the polyQ region, linking the two protein domains expands, the N-terminal headpiece and the polyP region are unable to interact, leaving the polyP region open for other protein-protein interactions (Dlugosz and Trylska, 2011). Indeed, exon 1-encoded mHTT fragments lacking the polyP region do not bind IKK and intrabodies binding the polyP region inhibit NFκB activation (Khoshnan et al., 2004). This indicates the polyP region as a possible binding site. However, deletion of a protein domain will also change protein conformation so the possibility that mHTT displays conformation-specific binding sites cannot be excluded.

The finding that mHTT alters the NFκB pathway in human HD monocytes may be relevant to other cell types and tissues, including the CNS. The NFκB pathway is present and active in both neurons and glial cells (O'Neill and Kaltschmidt, 1997). Pharmacological inhibition of NFκB impairs memory and learning (Mattson and Meffert, 2006), and NFκB pathway activation is critical for neuronal survival and neurite outgrowth (Teng and Tang, 2010). Increased levels of NFκB activity have been shown in both Alzheimer's disease (Kaltschmidt et al., 1997) and Parkinson's disease (Hunot et al., 1997). In HD, blocking NFκB function in rat PC-12 cells leads to reduced mHTT toxicity, implying that the NFκB pathway contributes

to neurotoxicity in HD (Khoshnan et al., 2004). Glial cells have been shown to promote neuronal death by producing high levels of inflammatory cytokines, reactive oxygen species and excitotoxins, mediated by the NFκB pathway (Mattson and Meffert, 2006). In HD, microglia have been found to be activated using PET imaging (Tai et al., 2007) and were shown to be hyper-reactive as seen in *ex vivo* murine cell culture (Björkqvist et al., 2008), but the potential role of NFκB in these phenotypes remains to be examined.

This work further identified gene expression changes in key molecules involved in immune signalling in native HD patients' monocytes. Several adapter proteins downstream of TLR4, such as *IRAK1*, *TICAM2* and *MyD88* were found to be slightly elevated in native HD patient's monocytes. A cumulative baseline increase in expression of several of these adapter proteins may lead to increased signal transduction from TLR4 to NFκB, further increasing NFκB pathway dysregulation. Another gene found to be up-regulated in HD monocytes was *CD40*, which is expressed in peripheral and central cells such as monocytes, microglia and neurons. Interactions between CD40 and its ligand CD154, mainly expressed on T cells, regulate the immune response on several levels. Monocytes are activated leading to up-regulation of genes for cytokine production and antigen presentation, and priming of the adaptive immune system (Grewal and Flavell, 1998). This points to further functional abnormalities in the immune system of HD patients, suggesting a possible deficit in the communication between antigen presenting cells and the adaptive immune system. Furthermore, CD40 mediates cell adhesion needed for leukocyte trafficking (Alderson et al., 1993). Given recent studies showing defective migration in HD due to defective actin remodeling (Kwan et al., 2012b) (Chapter 5), the increase in CD40 expression could also be a compensatory response for immune cells to counteract their decreased motility. *FOS* and *CJUN*, subunits of the AP-1 transcription factor, were also up-regulated in primary human myeloid HD cells. Interestingly, FOS and JUN levels have been

found to be increased in AD patient brains (Anderson et al., 1994), and the MAP kinase needed for JUN activation, JNK, is elevated and involved in neurotoxicity in HD mouse (Fan et al., 2012) and rat models (Perrin et al., 2009). Thus, it can not be excluded that dysregulation in these signalling pathways may contribute to the HD immune phenotype.

Promoter regions of the altered genes in baseline monocytes did not contain more NFκB binding sites than the unaltered genes. This indicates that NFκB, while playing a role in the increased cytokine production after LPS stimulation, may not be involved in transcriptional changes in baseline monocytes. Binding sites for AP-1, however, were two-fold more prevalent in the promoter regions of the genes found to be up-regulated in unstimulated HD monocytes. It is known that the AP-1 subunits, FOS and CJUN, regulate their own expression in a feed-back loop (Angel et al., 1988), and transcript levels of these two transcription factors were found to be up-regulated in primary human myeloid HD cells. Thus, the JNK/MAPK pathway may, in addition to the NFκB pathway, be either affected by or play a role in the immune dysfunction observed in HD. Furthermore, mutant HTT binding directly to DNA to influence gene expression cannot be excluded. Benn et al. have proposed that mHTT might alter DNA conformation upon direct binding, affecting transcription factors binding to their promoter regions (Benn et al., 2008). Chromatin immunoprecipitation experiments are required to find which transcription factors bind the up-regulated genes in unstimulated HD monocytes.

Importantly, this study shows that lowering total HTT levels by only 50 % partially rescued the hyper-reactive HD phenotype, with a reversal of both elevated cytokine production and transcriptional changes observed in human HD myeloid cells *ex vivo*. This is the first report showing that lowering HTT in cells freshly isolated from HD patients can reverse cellular dysfunction caused by mHTT expres-

sion - an important first demonstration of the reversibility of cellular dysfunction after HTT lowering in human tissue. HTT lowering was achieved using a novel phagocytosis-dependent approach, in which siRNAs are packaged into glucan particles isolated from yeast (Aouadi et al., 2009). This study is the first to use this technique in primary human macrophages and demonstrated that a 90 % transfection rate can be achieved (Figure 4.20), much higher than the 10-20 % transfection rate achieved by traditional methods such as lentiviral transduction. These findings validate the potential of HTT lowering therapy as well as the possibility of using these peripheral cells to test siRNA efficiency and safety.

Interestingly, cytokine release was also decreased in control cells treated with anti-*HTT* siRNA, indicating a second mechanism by which wild-type HTT influences cytokine production beyond the effect of mHTT on IKKγ. Wild-type HTT has been shown to play a role in both to actin remodeling (Kwan et al., 2012b; Munsie et al., 2011) and microtubule-mediated transport (Gauthier et al., 2004). As both processes are needed for the trafficking of cytokines to the cell surface membrane for release (Lacy and Stow, 2011), a reduction of wild-type HTT levels might exert a loss of function by hindering normal actin and microtubule remodeling causing changes in cytokine release. A future study using allele specific silencing of mutant but not wild-type HTT will help determine the exact contributions loss of wild-type HTT and gain of mHTT function has on the myeloid cell dysfunction in HD.

This study demonstrates hyper-reactive immune cells in HD and represents the first demonstration of phenotypic reversibility on HTT lowering in primary human cells in HD. It also identifies the underlying intracellular mechanisms of immune dysfunction in human cells in HD. This is important as the immune system has clearly been shown to be a modifier of HD pathogenesis in various mouse models (Bouchard et al., 2012; Kwan et al., 2012a; Zwilling et al., 2011). There is

currently a search for genetic and environmental modifiers of HD as the CAG repeat expansion only explains 50-70% of variance in age of onset, and its role in modulating disease progression is variable (Andrew et al., 1993; Brinkman et al., 1997). The remainder of the variance is likely due to environmental and other genetic factors (Wexler et al., 2004). The immune system may be a powerful modifier of HD age of onset and progression, with an interaction of both genetic and environmental factors. This has already been shown to the case in large genome wide association studies in Alzheimer's disease where several key genes involved in the innate immune system were shown to increase susceptibility to developing AD (Harold et al., 2009; Lambert et al., 2009).

Finally, the work presented here, also suggests a potential new therapeutic target for HD through modulating NFκB activation and downstream targets. The muscle wasting, weight loss and depression that occurs in HD (van der Burg et al., 2009) may be related to increased peripheral cytokine levels. Therefore, modulating the immune system may have beneficial effects in both the CNS and the periphery. Indeed, an anti-inflammatory, anti-IL-6 antibody treatment in R6/2 HD mice has already been show to improve both weight loss and disease progression (Bouchard et al., 2012). This work therefore has implications for both understanding the role of the innate immune system as a modifier of neurodegeneration and modulation of the immune system as a possible therapeutic in HD.

5 Mutant huntingtin impairs migration of immune cells

5.1 Background

As shown in the previous chapters, mHTT levels in immune cells track with markers of disease progression such as disease burden score and brain atrophy (Chapter 3). Furthermore, mHTT expression in primary human monocytes and macrophages causes increased cytokine production by directly interfering with the NFκB pathway (Chapter 4). These findings, in addition to recent studies showing that the immune system can modify HD progression (Bouchard et al., 2012; Kwan et al., 2012a; Zwilling et al., 2011), provide strong evidence that the peripheral immune system is abnormal in HD and might contribute to neurodegeneration. Additionally, microglia, the resident immune cells in the brain, are also abnormal in HD and may contribute to pathogenesis. Microglia activation and reactive gliosis were found in the brains of HD patients (Sapp et al., 2001). Furthermore, PET of HD patients also demonstrated increased microglial activation in the striatum and cortex, correlating with clinical severity of the disease (Tai et al., 2007).

The migration of immune cells to sites of infection or injury is an early and essential step in the immune responses. Activated immune cells migrate into affected tissues and communicate through chemokines, small molecules that establish a chemotactic gradient from their release point, which attracts cells carrying the corresponding receptor. Monocytes, macrophages, and microglia express chemokine receptors and adhesion molecules that control and direct migration in response to inflammatory signals (Imhof and Aurrand-Lions, 2004; Moser et al., 2004). MCP-1 is one of the key regulators of monocyte and macrophage migration during inflammation, and acts via CCR2 expressed on the cell surface (Deshmane et al., 2009). For microglia, both ATP and C5a can effectively induce migration, interestingly through different and additive molecular pathways (Miller and Stella, 2009).

Efficient migration relies on the remodelling of the actin cytoskeleton, a key mediator of cell polarisation and chemotaxis (Jones, 2000). In the brain, microglia quickly rearrange their actin networks, form membrane ruffles and leading edges to extend their processes once activated by stimuli such as ATP (Inoue, 2002; Koizumi et al., 2007). Even in the healthy brain, microglia continuously survey their microenvironment by extending and retracting their processes, while their cell bodies remain motionless (Nimmerjahn et al., 2005). In the periphery, monocytes circulate the bloodstream before migrating into perivascular tissue and differentiating into tissue macrophages or DCs. Upon activation by inflammatory stimuli, peripheral immune cells migrate and accumulate at the site of infection, contribute to the local resolution of the infection or migrate further into lymph nodes (Imhof and Aurrand-Lions, 2004; Moser et al., 2004). Overall, migration of immune cells is a critical step during the initial response to injury or inflammation, and defects in cell migration prevent appropriate responses to infections (Kurihara et al., 1997).

Work by Kwan et al. studied the effect mHTT expression has on the migration abilities of microglia and peripheral myeloid cells in HD mouse models (Kwan et al., 2012b). Primary microglia from both the YAC128 and BACHD models display significantly decreased migration towards chemotactic stimuli such as ATP and C5a compared with microglia isolated from WT litter-mates (Figure 5.1).

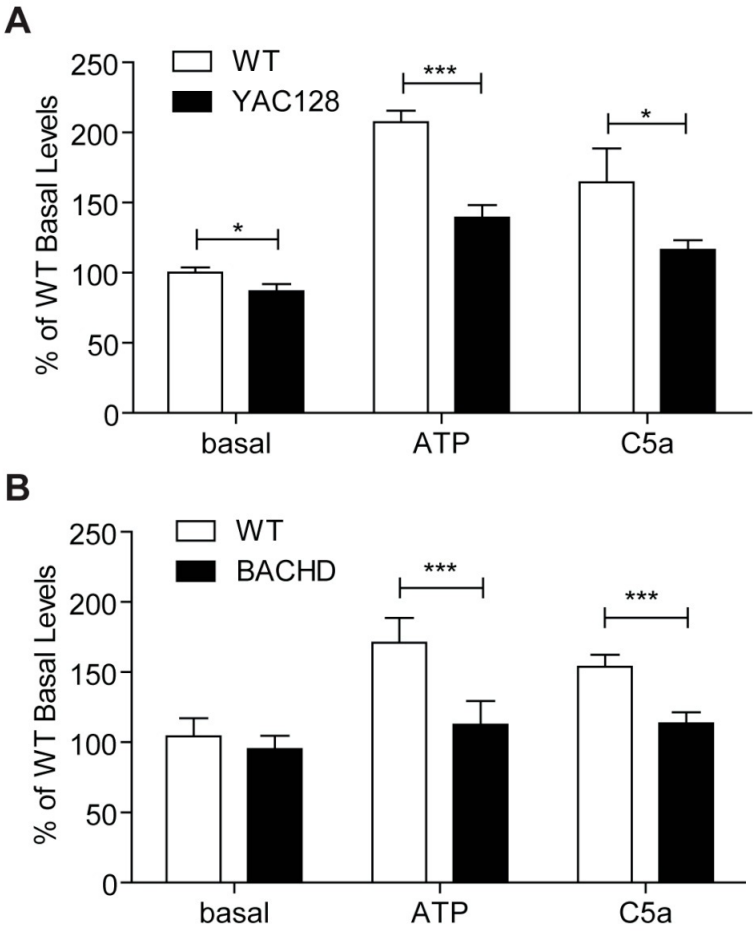

Figure 5.1: Microglia isolated from HD mice demonstrate impaired chemotactic responses to ATP and C5a. Primary microglia from **(A)** YAC128 and **(B)** BACHD mice show significantly less migration towards both 100 μM ATP and 100 nM C5a compared with WT litter-mates. Cells were allowed to migrate for 3 hours through the transwell system. Data shown as mean $\pm$ SEM. n is 6 experimental replicates. * $p<0.05$; ** $p<0.01$, *** $p<0.001$ (unpaired two-tailed student t test). Data by Dr Wanda Kwan, re-produced from Kwan et al. 2012b.

Microglia isolated from HD mice further demonstrate reduced extension and movement of their processes in an ATP gradient (Kwan et al., 2012b). Validating this *in vitro* data, Kwan et al. also showed impaired HD microglial function *in vivo* using time-lapse *in vivo* two-photon microscopy. Under basal conditions, process extension is less frequent in BACHD mice, and while WT microglia demonstrate rapid extension of processes and engulfment of an injury site caused by focal laser ablation, microglia from HD mice respond with a delay (Kwan et al., 2012b). Furthermore, murine peripheral HD macrophages show a similar migration defect, demonstrated by reduced macrophage recruitment into the peritoneum after thioglycollate challenge (Kwan et al., 2012b). Reduced membrane ruffling in microglia isolated from both the YAC128 and the BACHD mice, and reduced p-cofilin levels in microglia and peripheral immune cells indicate impaired actin remodelling in HD immune cells as possible reason for the reduced migration ability (Figure 5.2) (Kwan et al., 2012b).

The aim of this study was to test the hypothesis of impaired migration in HD immune cells caused by defective actin remodelling in primary human monocytes and macrophages, which will allow us to evaluate the importance of these findings for the human disease.

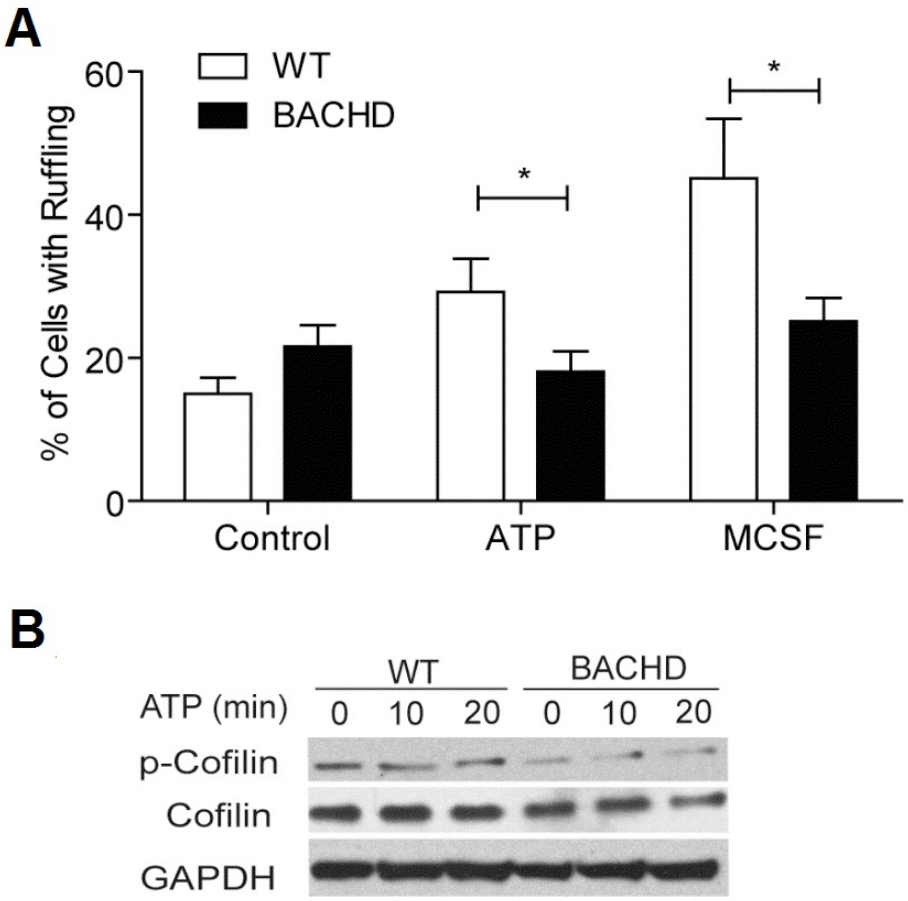

Figure 5.2: Murine HD microglia show decreases membrane ruffling and cofilin levels. (A) Primary microglia from BACHD mice have less membrane ruffling upon stimulation with 100 μM ATP and 100 ng/ml M-CSF compared with WT microglia. Cells were stained with rhodamine-phalloidin, and the percentage of cells with membrane ruffling was quantified within 10 min. Values are mean $\pm$ SEM of three independent experiments. * $p<0.05$; ** $p<0.01$ (unpaired two-tailed student t test). **(B)** Reduced cofilin and p-cofilin levels in HD versus WT microglia were revealed by western blot on primary BACHD and WT microglia stimulated with 100 μM ATP over 20 min. Data by Dr Wanda Kwan, re-produced from Kwan et al. 2012b.

5.2 Contributions

Initial migration assays looking at monocyte migration towards MCP-1 and RANTES were done in collaboration with Dr Ralph Andre (UCL, Institute of Neurology). Part of the work presented in this chapter has been published in the Journal of Clinical Investigation in Collaboration with Paul Muchowski's lab and the data described in the introduction.

Kwan, W., Träger, U., Davalos, D., Chou, A., Bouchard, J., Andre, R., Miller, A., Weiss, A., Giorgini, F., Cheah, C., Möller, T., Stella, N., Akassoglou, K., Tabrizi, S. J. and Muchowski, P. J. (2012b), Mutant huntingtin impairs immune cell migration in Huntington disease, J Clin Invest 122(12), 473747.

5.3 Methods

Primary human monocytes and macrophages were isolated and differentiated as described in Section 2.5.4. Migration abilities were analysed using a transwell migration assay, in which cells were separated by a membrane from a well containing a chemoattractant (Section 2.6.2). Chemokine receptor levels in unstimulated monocytes were measured on RNA and protein level using qPCR (Section 2.10) and flow cytometry (Section 2.9.1), respectively. In order to assess the actin cytoskeleton response, macrophages were stimulated with a chemoattractant and membrane ruffling was assessed using microscopy (Section 2.11.3). Phosphocofilin (p-cofilin) levels were assessed by western blot (Section 2.8.5) and MCP-1 production was measured by ELISA (Section 2.7.1).

5.4 Results

5.4.1 Monocytes and macrophages from HD patients show altered migration abilities

A transwell system was used to analyse the migration ability of monocytes isolated from HD patients. Primary monocytes were seeded in the upper chamber of the transwell, and the number of cells migrating into the lower, chemokine filled well was counted. In the absence of a chemoattractant, only very few cells migrated through the transwell and no difference was detected between HD and control cells. MCP-1 and RANTES are important pro-inflammatory chemokines mediating monocytes and macrophages migration *in vivo* (Moser et al., 2004). In addition to these two stimuli, migration towards ATP and C5a was tested since primary microglia isolated from HD mice show defective migration towards those two chemoattractants (Figure 5.1 from (Kwan et al., 2012b)). Upon stimulation, HD patient monocytes demonstrated a significant defect in migration towards MCP-1 and ATP (Figure 5.3A/B), independent of the donors disease stage, with cells isolated from premanifest HD gene carriers already demonstrating a striking defect. Furthermore, premanifest HD gene carrier cells also demonstrated decreased migration towards C5a (Figure 5.3C). Interestingly, migration towards RANTES was unchanged in HD compared with control monocytes (Figure 5.3D).

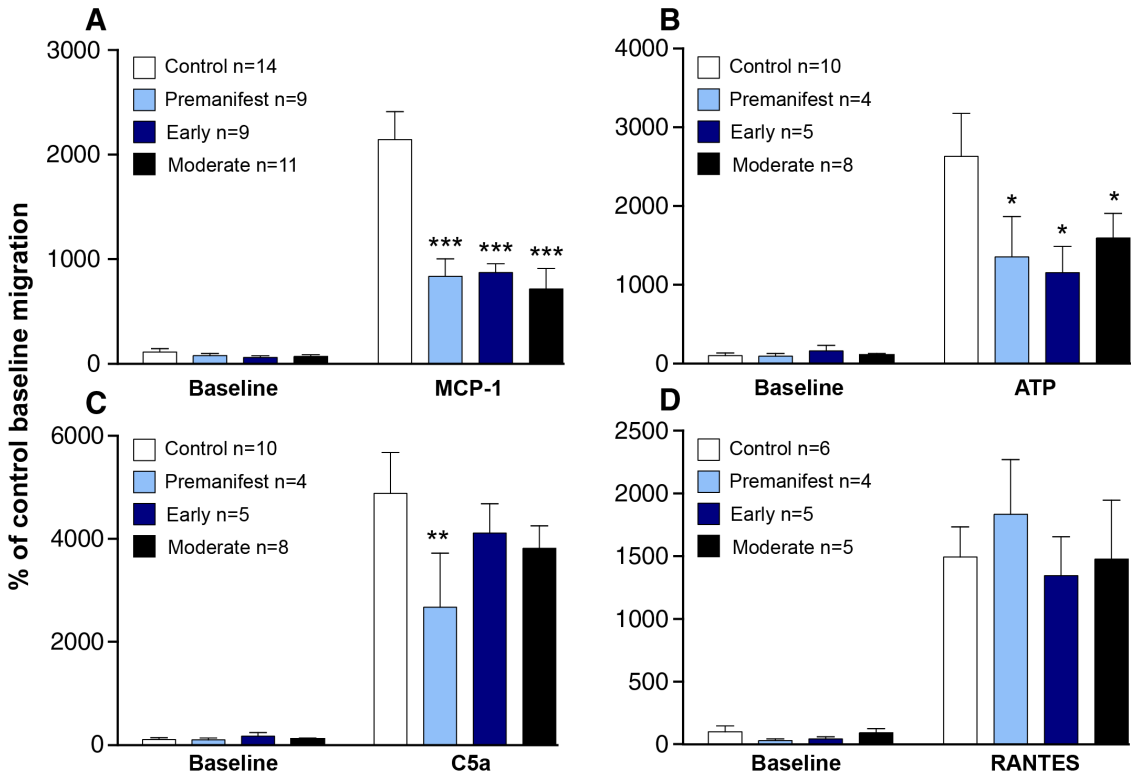

Figure 5.3: HD patient monocytes demonstrate a striking migration defect. Using a 5μm transwell system, blood monocytes isolated from HD patients showed a significant defect in migrating towards **(A)** 50 ng/ml MCP-1, **(B)** 100 μM ATP and **(C)** 10 nM C5a whilst migration towards **(D)** 100 ng/ml RANTES was normal compared with control cells. Monocytes were left to migrate for 1.5 h at 37 °C . Cells migrated into the lower chamber were counted using a Neubauer counting chamber. Data shown as mean ± SEM. n= individual biological repeats. Two-way Anova with Bonferroni post tests. * $p<0.05$; ** $p<0.01$, *** $p<0.001$. Experiment performed in collaboration with Dr Ralph Andre.

In addition to monocytes, tissue macrophages also migrate towards inflammatory stimuli within a tissue as well as into lymph nodes, after the cells have been activated to elicit an adaptive immune response (Imhof and Aurrand-Lions, 2004). To test the migration capability of HD patient macrophages, a similar set up as the one used for monocytes was utilised. Monocyte-derived macrophages were seeded in the upper chamber of the transwell and the number of cells that migrated through the membrane towards the chemoattractant stimulus was counted. While monocyte migration was assessed after 1.5 h by counting the number of cells in the lower chamber, the bigger and adherent macrophages were left to migrate for 16 h using transwells with larger pore-sizes. Macrophages adhere to the transwell membrane and cells stuck to the lower side of the membrane were counted.

HD patient macrophages showed the same defect in migration towards MCP-1, ATP and C5a as seen in HD monocytes, when compared with control cells (Figure 5.4A/B/C). However, HD macrophage migration towards RANTES also demonstrated a trend for impairment compared with control macrophages (Figure 5.4D). Thus, both primary human monocytes and macrophages demonstrated decreased migration to a wide range of different chemokines, similar to findings in primary murine HD microglia (Figure 5.1 from (Kwan et al., 2012b)).

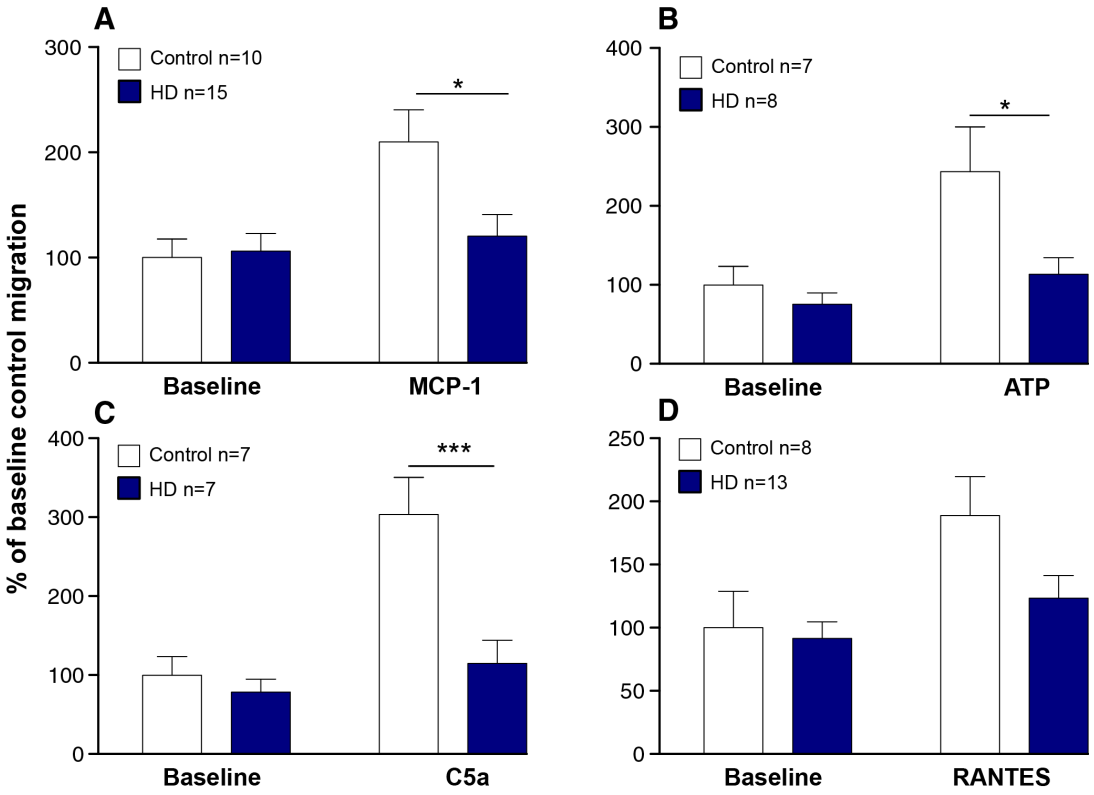

Figure 5.4: HD patient macrophages show decreased migration towards different stimuli. Using a 8μm transwell system, monocyte-derived macrophages from HD patients (premanifest and manifest subjects) showed a significant defect in migrating towards **(A)** 50 ng/ml MCP-1, **(B)** 100 μM ATP and **(C)** 10 nM C5a. Migration towards **(D)** 100 ng/ml RANTES was also decreased compared with control. Cells were left to migrate for 16 h after which the cells attached to the transwell membrane were stained with crystal violet and counted via light microscopy. Data shown as mean $\pm$ SEM. n= individual biological repeats. Two-way Anova with Bonferroni post tests.* $p<0.05$; ** $p<0.01$, *** $p<0.001$.

5.4.2 Chemokine receptor levels on HD monocytes

For chemoattractants to induce the necessary cellular change needed for cell movement, they must bind their receptors on the surface of the target cells. A decrease in chemokine receptors expression is, therefore, a possible explanation for lower migration of HD immune cells. To investigate this possibility, the levels of the MCP-1 receptor CCR2 and the two RANTES receptors CCR1 and CCR5 were assessed on both RNA and protein levels. CCR2 transcript levels (Figure 5.5A) and cell surface expression (Figure 5.5B), tested by qPCR and flow cytometry respectively, were reduced on unstimulated HD monocytes. Similar to the decrease in migration, CCR2 levels were significantly decreased throughout all HD disease stage, even in premanifest HD gene carriers. Interestingly, RNA levels for CCR1 and CCR5 were not changed in HD monocytes (Figure 5.5C/D). These findings suggest that the migration defect in primary human HD monocytes demonstrated in this study might at least partially be caused by reduced chemokine receptor expression.

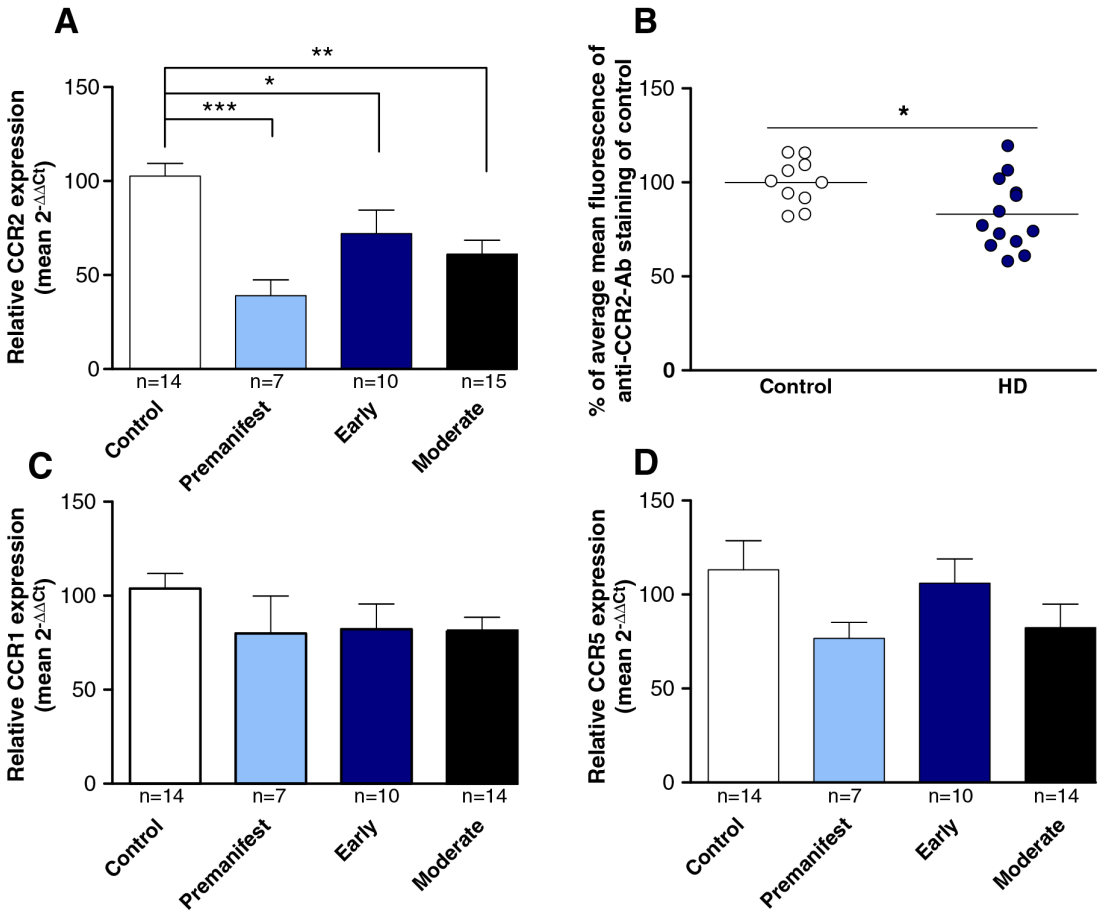

Figure 5.5: Chemokine receptor expression levels in HD patient monocytes. (A) qPCR analysis and **(B)** flow cytometry showed decreased CCR2 transcript and cell surface expression levels in HD monocytes compared with control. **(C)** CCR1 and **(D)** CCR5 transcript levels were unchanged in HD patient compared with control monocytes. Data shown as mean $\pm$SEM, unpaired two-tailed student t test for **(B)** and one-way ANOVA with Dunnett's multiple comparison test for **(A,C,D)**. * $p<0.05$; ** $p<0.01$, *** $p<0.001$. n= individual biological repeats.

5.4.3 HD macrophages produce increased levels of MCP-1

CCR2 expression can be regulated by different cytokines as well as directly by its own ligand, MCP-1 (Tangirala et al., 1997). As it has previously been shown that MCP-1 levels are elevated in HD plasma (Wild et al., 2011), MCP-1 production was analysed by ELISA in IFNγ-primed and LPS stimulated HD macrophages. Measuring MCP-1 levels in the culture supernatants 24 h post stimulation revealed the HD macrophages produce significantly more MCP-1 compared with control cells (Figure 5.6). This result suggests desensitisation of immune cells by high MCP-1 plasma levels as a possible cause for decreased CCR2 levels on HD monocytes.

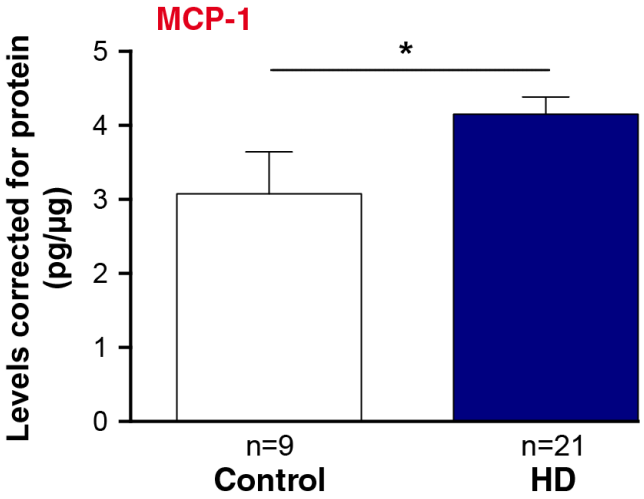

Figure 5.6: Human HD macrophages produce significantly more MCP-1. Monocyte-derived macrophages were stimulated with 10 ng/ml IFNγ and 2 μg/ml LPS for 24 h before MCP-1 levels in the culture media were assayed by ELISA quantification, showing elevated production of the chemokine by HD (all disease stages) compared with control cells. Data shown as mean $\pm$SEM, n= individual biological repeats, unpaired two-tailed student t test. * $p<0.05$.

5.4.4 Chemokine receptor levels on HD macrophages

Unlike the finding of lowered CCR2 levels in HD patient monocytes, CCR2 transcript levels (Figure 5.7A) and cell surface expression (Figure 5.7B) seems unchanged in HD patient macrophages compared with control cells. Supported by the fact that mRNA levels of P2Y12, the purinergic receptor that mediates migration in response to ATP (Haynes et al., 2006), and of the C5a receptor do not significantly differ between primary microglia from HD mice and WT littermates (Kwan et al., 2012b), these findings points towards a broader defect in macrophage migration independent of chemokine receptor levels.

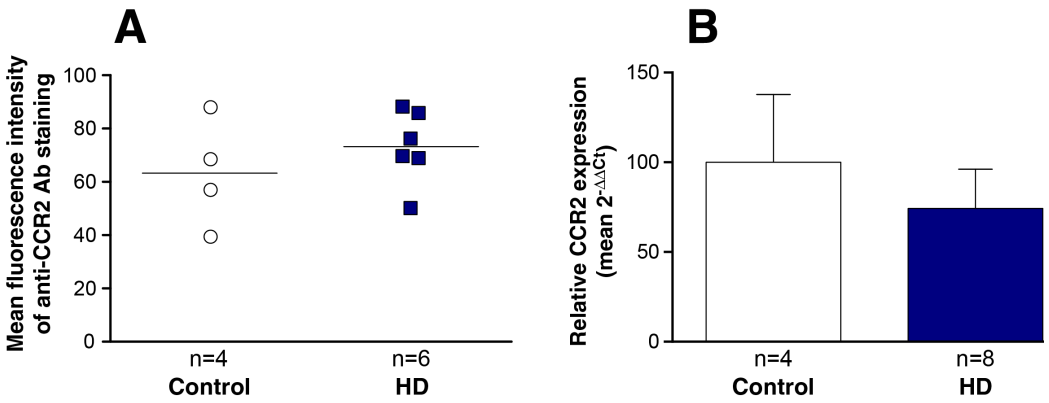

Figure 5.7: Chemokine receptor expression levels in HD patient macrophages. (A) qPCR analysis and **(B)** flow cytometry showed no difference in CCR2 transcript and cell surface expression in HD monocyte-derived macrophages (isolated from all disease stages) compared with control. Data shown as mean ±SEM, n= individual biological repeats, unpaired two-tailed student t test showed no significances.

5.4.5 Impaired actin remodelling in HD myeloid cells

Given that migration of immune cells requires rapid remodelling of the actin cytoskeleton (Jones, 2000) and a report of defective actin turnover via cofilin in HD during cellular stress response (Munsie et al., 2011), the actin cytoskeleton was analysed in primary human monocytes and macrophages. During the cellular response to a chemotactic stimuli, cells undergo a process called membrane ruffling by which they form lamellipodia as well as microspikes extending beyond the leading edge of the lamellipodia called filopodia (Mattila and Lappalainen, 2008). To test the hypothesis that actin remodelling is changed in HD macrophages, F-actin fibres were stained with phalloidin and the percentage of cells forming filopodia was quantified (Figure 5.8A). Upon stimulation with 50 ng/ml MCP-1 or 100 μM ATP for 10 min, a significantly reduced number of HD macrophages formed filopodia compared with control cells (Figure 5.8B). Five minute treatment with ATP, also, showed a trend to decreased filopodia formation in HD compared with control cells, while no difference was detected at baseline. These results are consistent with findings in HD microglia showing decreased membrane ruffling in BACHD compared with WT mice (Figure 5.2 from (Kwan et al., 2012b)).

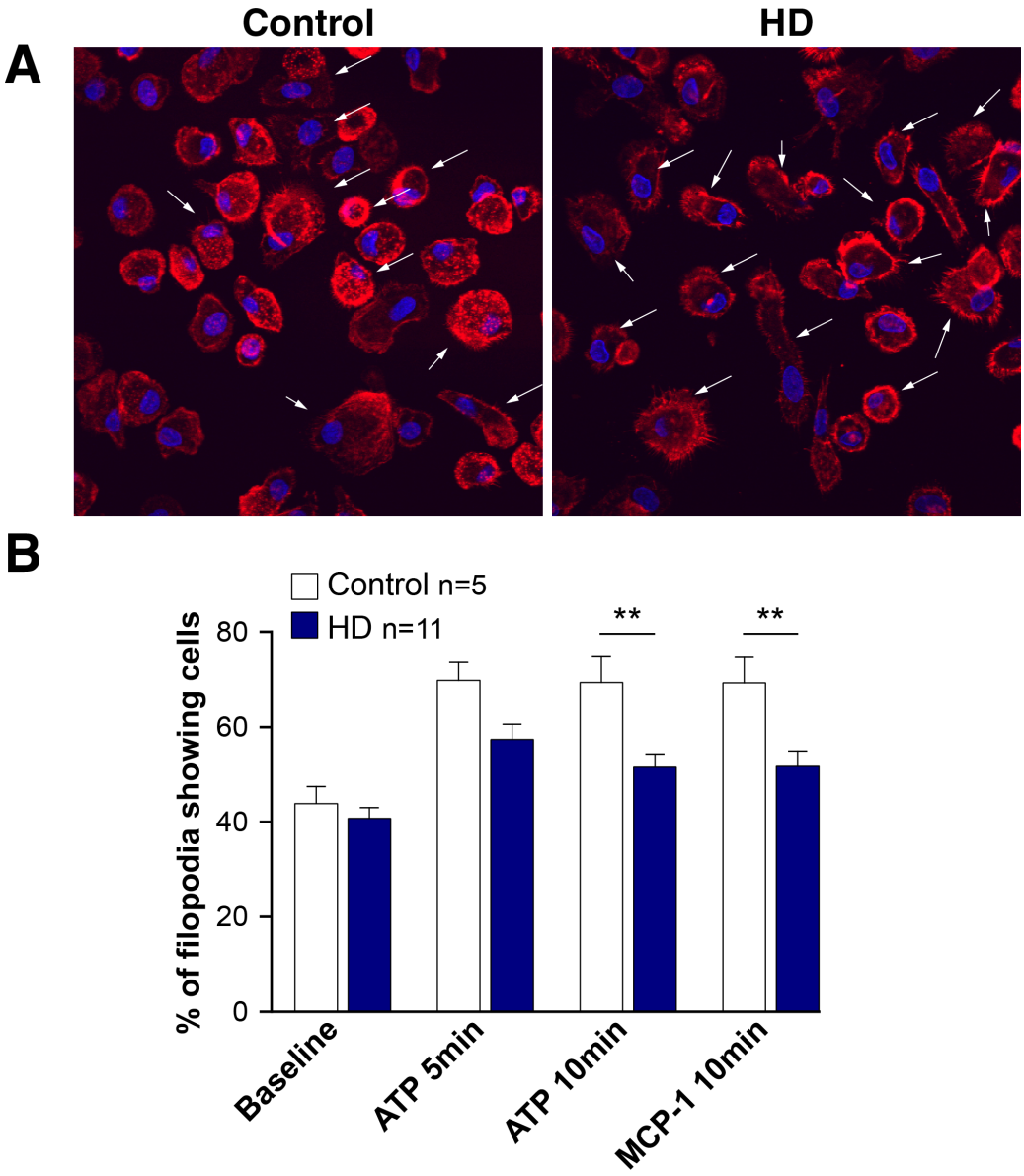

Figure 5.8: HD macrophages form less filopodia. Monocyte-derived macrophages, differentiated on 13 mm coverslips, were stimulated with either 50 ng/ml MCP-1 or 100 μM ATP for 5 or 10 min before F-actin was stained with Alexa Fluor 568 phalloidin. **(A)** Example pictures showing typical field of view used to quantify percentage of cells forming filopodia for both control and HD patients. Arrows indicated cells with filopodia. **(B)** Quantification of macrophages, showing filopodia as percentage of total macrophages in field of view, demonstrated a decreased number of cells with filopodia in response to 10 min ATP and MCP-1 in HD (both premanifest and manifest) samples compared with controls. Data shown as mean $\pm$SEM, one-way ANOVA with Dunnett's multiple comparison test * $p<0.05$; ** $p<0.01$, *** $p<0.001$. n= individual biological repeats.

The actin-binding protein cofilin is essential for the regulation of actin depolymerisation, and is required for effective cell migration. Cofilin is regulated by reversible phosphorylation, whereby phosphorylation inhibits cofilin's function. Cofilin inactivation leads to decreased actin severing, needed for fresh branching of actin fibres in lamellipodia and in general for the dynamic remodelling of the actin network (Dawe et al., 2003). Stimuli, such as ATP, can trigger changes in the actin cytoskeleton by activation of cofilin-phosphatase's and dephosphorylation of cofilin (Huang et al., 2006). Work in HD mouse models has shown decreased cofilin and p-cofilin levels in microglia (Figure 5.2B) as well as peripheral macrophages (Kwan et al., 2012b). Analysing p-cofilin levels using western blot showed significantly decreased levels of the actin-binding protein in primary human HD monocytes compared with controls (Figure 5.9). This finding supports the hypothesis that (m)HTT influences cofilin levels and thereby affected the actin filament dynamics necessary for cellular movement.

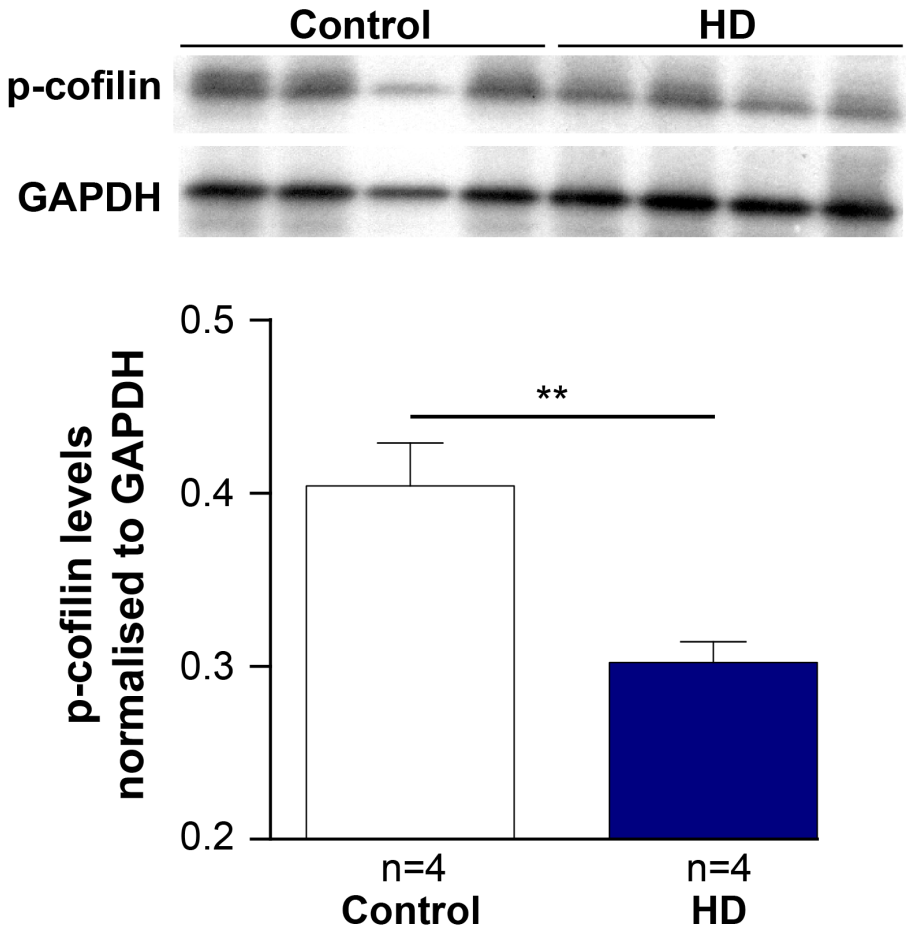

Figure 5.9: Decreased levels of p-cofilin in primary human HD monocytes. Western blot analysis on baseline monocytes lysates using a p-cofilin antibody demonstrated decreased p-cofilin levels in HD cells isolated from all disease stages compared with controls. An anti-GAPDH antibody was used as loading control and densitometry was performed to quantify band density. Data shown as mean $\pm$SEM, unpaired two-tailed student t test. * $p<0.05$. n= individual biological repeats.

5.5 Discussion

Abnormal immune cell function has been shown in primary human HD monocytes and macrophages (Chapter 4). Impaired migration of both peripheral (macrophages) and central (microglia) immune cells has been described in the BACHD and YAC128 HD mouse models (Kwan et al., 2012b). Here, the migration ability of HD patient cells was assessed *ex vivo*, demonstrating a striking defect in migration of both human HD monocytes and macrophages toward several chemokines. In keeping with the previous finding that cytokines are elevated in HD patient plasma years before symptom onset (Björkqvist et al., 2008), migration defects are already apparent in cells isolated from premanifest HD gene carriers. Furthermore, murine HD microglia, which also demonstrate migration defects, are isolated from early post-natal mice, long before significant neuronal loss occurs. The cells, therefore, resemble premanifest HD while showing striking defects consistent with early microglial dysfunction detected in HD patients using PET (Politis et al., 2011; Tai et al., 2007). Thus, these findings confirm that peripheral immune dysfunction is not a secondary phenomenon caused by degeneration of the basal ganglia, but is independently occurring beforehand.

The molecular mechanism behind the migration defect in HD immune cells is likely to be complex and remains to be fully explained. Decreased levels of the MCP-1 receptor CCR2 on primary human HD monocytes might be one contributing factor. Increased MCP-1 levels found in HD plasma (Wild et al., 2011) and the fact that HD macrophages produce more MCP-1 upon LPS stimulation suggest autocrine desensitisation as an explanation for the decreased CCR2 expression on HD monocytes. High concentrations of MCP-1 in the blood stream could, thereby, cause monocytes to down-regulate the MCP-1 receptor in a feed back loop (Tangirala et al., 1997). This would in turn result in HD monocytes migrating

less towards MCP-1 compared with control cells in *ex vivo* assays as performed in this study. HD patient macrophages derived from monocytes are in culture for six days before the assay, which in monocytes takes place immediately after isolation. This prolonged time under culture conditions away from plasma cytokines, decreases the possible effect of elevated plasma MCP-1 and may explain why normal CCR2 levels were found on HD macrophages while levels were decreased on HD monocytes.

Nonetheless, macrophages display a migration defect towards MCP-1 despite normal CCR2 levels suggesting a different, MCP-1/CCR2 independent mechanism causing the migration defect in macrophages and maybe also, at least partially, in monocytes. Moreover, migration defects were found towards several chemokines, which operate by different receptors and downstream signalling pathways (Deshmane et al., 2009; Miller and Stella, 2009), suggesting that the migration defect in HD immune cells is not likely due to a lack of chemokine receptor expression, but an impairment to engage downstream signalling mechanisms or machinery required for migration.

Increased filopodia formation and changed levels of the actin-binding protein cofilin in the impaired immune cells indicated that mHTT affects proper regulation of actin remodelling. These findings are supported by similar findings in HD mice showing decreased lammellipodia formation and decreased cofilin and p-cofilin levels in microglia upon stimulation (Kwan et al., 2012b). Interestingly, a recent study has shown that full-length wild-type huntingtin colocalises with actin-cofilin rods in the nucleus during stress response, while expression of mHTT leads to initial fewer, but more persistent nuclear rods (Munsie et al., 2011). Consistent with this, the investigators also found cross-linked actin-cofilin rods in HD patient lymphoblasts correlating with disease stages. Strikingly, the mHTT phenotype was also observed when lowering wild-type HTT levels. Further to this, *Dictyostelium*

discoideum cells lacking endogenous huntingtin demonstrate disorganised actin staining and defective chemotaxis while forming aggregates, suggesting an important role for wild-type HTT in actin remodelling and that migration defects may at least partially be due to a loss of wild-type HTT (Myre et al., 2011).

Studies using transgenic mice lacking the CX3CR1 chemokine receptor gene have shown that the impaired migration is accompanied by an increase in IL-1β production upon LPS stimulation (Cardona et al., 2006). Indeed, elevated plasma cytokine (Björkqvist et al., 2008) and chemokine (Wild et al., 2011) levels have been shown in HD patients, suggesting that elevated levels of pro-inflammatory marker might be a compensatory mechanism to induce immune cell migration. Additionally, actin remodelling defects could affect cytokine production as cytokine secretion relies on a functional cytoskeleton (Lacy and Stow, 2011). Transgenic mice lacking chemokine receptor genes have impaired wound healing (Ishida et al., 2008), are unable to clear infections and mount an ineffective immune response (Boring et al., 1997; Kurihara et al., 1997). While the incidence of infections or defects in wound healing have not been systematically studied in HD patients, a study identifying conditions associated with reduced survival in HD patients showed increased likelihood for chronic skin ulcers (Lanska et al., 1988), which may be related to the migration defect described here. Animal studies analysing healing of scratch wounds are ongoing in HD animal models.

Cell motility is not just impaired in peripheral immune cells, microglia isolated from HD mice also demonstrate defective migration in *in vitro* assays (Kwan et al., 2012b). Furthermore, *in vivo* murine HD microglia show less process extensions under basal conditions and respond delayed to brain injury modelled using laser ablation. This suggests a weaker immune response to injury and infection within the HD brain as well as impaired microglial function in the healthy brain, where resting microglia constantly survey their environment to check the integrity and

function of the brain (Nimmerjahn et al., 2005). Microglia provide trophic support for neurons and physically interact with synapses (Wake et al., 2009). Interestingly, a loss of synapses has been described in R6/2 and BACHD mice (Kwan et al., 2012a) suggesting that mHTT expressing microglia may not be efficient in synapse surveillance, possibly contributing to synapse and network dysfunction in HD.

Actin remodelling is not only crucial for immune cell migration towards injury but also for neuronal cell development, where filopodia guide the neuronal growth cone (Mattila and Lappalainen, 2008), and synapse function (Dillon and Goda, 2005). Interestingly actin polymerisation in dendritic spines of striatal neurons is greatly reduced in HD mice (Lynch et al., 2007), maybe explaining abnormal spine morphology found in striatal and cortical neurons of HD mice (Spires et al., 2004) and patients (Graveland et al., 1985)

In summary, these findings provide evidence that primary human HD immune cells do not migrate normally, which may be linked or contribute to early immune dysfunction and chronic cytokine elevation in HD. Migration defects are know to cause recurrent infections and immune dysregulation (Blundell et al., 2010). Further studies will be needed to determine the consequence of this defect on HD patients. In light of several recent publications supporting a role of the peripheral immune system as modifier of HD progression (Bouchard et al., 2012; Kwan et al., 2012a; Zwilling et al., 2011), this study underlines the critical link between blood cells and neurodegeneration in HD.

6 Immune dysfunction in different HD mouse models

6.1 Background

Animal models are a vital tool in the research of genetic diseases, as they allow the characterisation of the biology of the disease, genetic modifications of the system, and testing of possible treatments. Before using any model, however, the model needs to be evaluated as to whether it resembles the part of human disease pathology you want to study.

In the HD field, a large variety of animal models have been established: from invertebrate models such as *Drosophila melanogaster* (Kazemi-Esfarjani and Benzer, 2000) and *Caenorhabditis elegans* (Parker et al., 2001) to mammalian models, including rodent models such as mice (Sathasivam et al., 1999) and larger primate models (Yang et al., 2008). While invertebrate models have great potential for discovery studies, such as therapeutic screens (Voisine et al., 2007) due to their cost efficiency and short life-span, their lack of homology to the human genome (*C. elegans* genome is only 40 % homologous to the human one) often requires findings to be validated in more similar mammalian models. Furthermore, looking at immune dysfunction in HD, invertebrate's immune responses are very different to those in humans with the adaptive immune system not present

and innate immune cells showing distinct differences (Beck and Habicht, 1996).

Comparing mammalian models of HD, mouse models are the most commonly used due to their quick reproduction and the availability of hundreds of transgenic mouse strains allowing genetic manipulation within the HD models simply by breeding. The most widely used and best characterised mouse model of HD is the R6/2 mouse. This model ubiquitiously express the 5' end of the human *HTT* gene carrying only exon 1 with 150 CAG repeats (Mangiarini et al., 1996). R6/2 mice demonstrate a fast and progressive phenotype with a very early symptomatic onset at 6-8 weeks. They demonstrate motor symptoms such as chorea-like movements, brain volume loss and peripheral changes such as weight loss and diabetes (Björkqvist et al., 2005; Li et al., 2005; Mangiarini et al., 1996). The major disadvantage of this model is the fact that it only expresses a N-terminal fragment of the *HTT* gene, not the full-length gene. Therefore, R6/2 mice may not model the full impact the expression of endogenous *mHTT* has. However, several full-length HTT models have been developed. For example, bacterial and yeast artificial chromosomes were used to create the BACHD (Gray et al., 2008) and YAC128 mouse models (Slow et al., 2003), respectively. YAC128 mice, which express the full-length human *HTT* gene carrying 128 CAG repeats, develop a progressive motor deficits from the age of six months. At nine months, the mice show cortical and striatal atrophy with corresponding behavioural changes (Van Raamsdonk et al., 2005b). Other groups have taken a knock-in approach to expand the CAG repeat in the endogenous murine *Htt* gene rather than inducing overexpression of a human *HTT* sequence. In this study, *Hdh*$^{150Q/150Q}$ mice, expressing 150 CAG repeats (Lin et al., 2001) were used. With disease onset from 15 months, *Hdh*$^{150Q/150Q}$ mice demonstrate a phenotype similar to 12 week old R6/2 mice at 22 months of age, including features such as widespread mHTT aggregates throughout the brain, transcriptional dysregulation in the striatum and cerebellum, 20 % weight loss and motor deficits include gait abnormali-

ties and reduced performance at motor tasks (Woodman et al., 2007). All these mouse models have advantages and disadvantages; for examples, YAC128 mice are heavier than WT mice at all ages (Slow et al., 2003), while weight loss is a major feature of HD (Aziz et al., 2008) and is observed in both the R6/2 and *Hdh*$^{150Q/150Q}$ mouse models (Woodman et al., 2007). On the other hand, the YAC128 mice are the only model in which motor deficits and neuronal loss highly correlate (Slow et al., 2003). The TRACK-HD study showed a similar correlation in HD patients demonstrating significant difference in brain volume between premanifest HD gene carrier and early stage patients (Tabrizi et al., 2009, 2012, 2011). It is therefore important to validate the different HD mouse models in order to find out which best represents different aspects of HD pathology.

Here, different HD mouse models were evaluated in regard to the immunological changes found in peripheral immune cells from HD patients. HD patient plasma contains more pro-inflammatory cytokines compared with controls (Björkqvist et al., 2008; Wild et al., 2011). Furthermore, as shown in Chapter 4, primary human monocytes and macrophages are hyper-reactive upon LPS stimulation *in vitro*, demonstrating increased cytokine production and phagocytosis. Previous investigations have already shown elevated levels of pro-inflammatory cytokines such as IL-6 and IL-1β in the plasma of the fragment R6/2, the full-length *Hdh*$^{150Q/150Q}$ and YAC128 HD mouse models (Björkqvist et al., 2008). Moreover, peripheral immune cells were found to migrate abnormally in both the R6/2 and BACHD mice (Kwan et al., 2012b), clearly demonstrating abnormal immune function in HD mouse models.

During this PhD, cytokine production and other key immune cell functions were analysed using *ex vivo* murine cells. Assessing several commonly used sources for murine monocytes and macrophages, such as blood, spleen and bone marrow, allowed not only the comparison of different mouse models, but also of dif-

ferent isolation protocols and immune cell subsets, while trying to replicate and further investigate the HD immune dysfunction in mice.

6.2 Contributions

Cytokine production (from spleen and bone marrow cells) and functional analysis (adhesion and migration assays) of R6/2 was done in collaboration with Dr Ralph Andre, UCL London and Anna Magnusson-Lind, Lund University, Sweden. Experiments were carried our both in London (mice provided by Prof Gillian Bates at King's College London) and Lund (mice provided by Dr Maria Björkqvist at Brain Disease Biomarker Unit, Lund University). Cytokine profiling of *Hdh*$^{150Q/150Q}$ mice was done in collaboration with Dr Ralph Andre, UCL London in London (mice provided by Prof Gillian Bates at King's College London). Analysis of YAC128 mice was done by C. Connolly in Dr Blair Leavitt's lab in Vancouver. All FR-FRET assays were done by Dr Andreas Weiss at Novartis, Basel.

6.3 Methods

The cytokine production by murine CD11b^{+} cells, isolated from blood, peritoneum, spleen and bone marrow (Section 2.5.6) and stimulated with IFNγ and LPS for 24 h were analysed using multiplex ELISA (Section 2.7.2). HTT levels were measured by TR-FRET (Section 2.8.6) and the percentage of immune cell subsets in R6/2 spleens were analysed by flow cytometry (Section 2.9.1). For further functional analysis cells underwent phagocytosis (Section 2.6.3), adhesion (Section 2.6.4) and migration assays (Section 2.6.2).

6.4 Results

6.4.1 Cytokine profiling of myeloid cells in the R6/2 mouse model

In order to determine whether murine blood monocytes are similarly hyper-reactive as HD patient cells, IFNγ-primed murine monocytes isolated using anti-CD11b magnetic beads, were stimulated with LPS. After 24 h, supernatants were analysed using the MSD multiplex ELISA platform. To ensure sufficient cell numbers for the experiment (100 000 cells per well in 96-well plates), blood monocytes from WT and R6/2 mice were pooled from multiple individual animals according to genotype. Analysing multiple wells of each genotype showed an increase in IL-6 and TNFα but not in IL-1β production in R6/2 compared with WT cells (Figure 6.1A).

To further analyse innate immune function in R6/2 mice, the cytokine profiles of other R6/2 monocyte populations were characterised. Splenic and bone marrow monocytes were isolated using anti-CD11b magnetic beads, and cultures (established from individual mice seeding 500 000 cells per well in 24-well plates) were primed with IFNγ and stimulated with LPS for 24 h. Analysing cytokine production by splenic monocytes isolated from R6/2 mice demonstrated an increase in IL-1β, whilst IL-6 and TNFα levels were unchanged compared with WT mice (Figure 6.1B). Interestingly, R6/2 bone marrow monocytes showed no difference in cytokine production when compared with WT cells (Figure 6.1C).

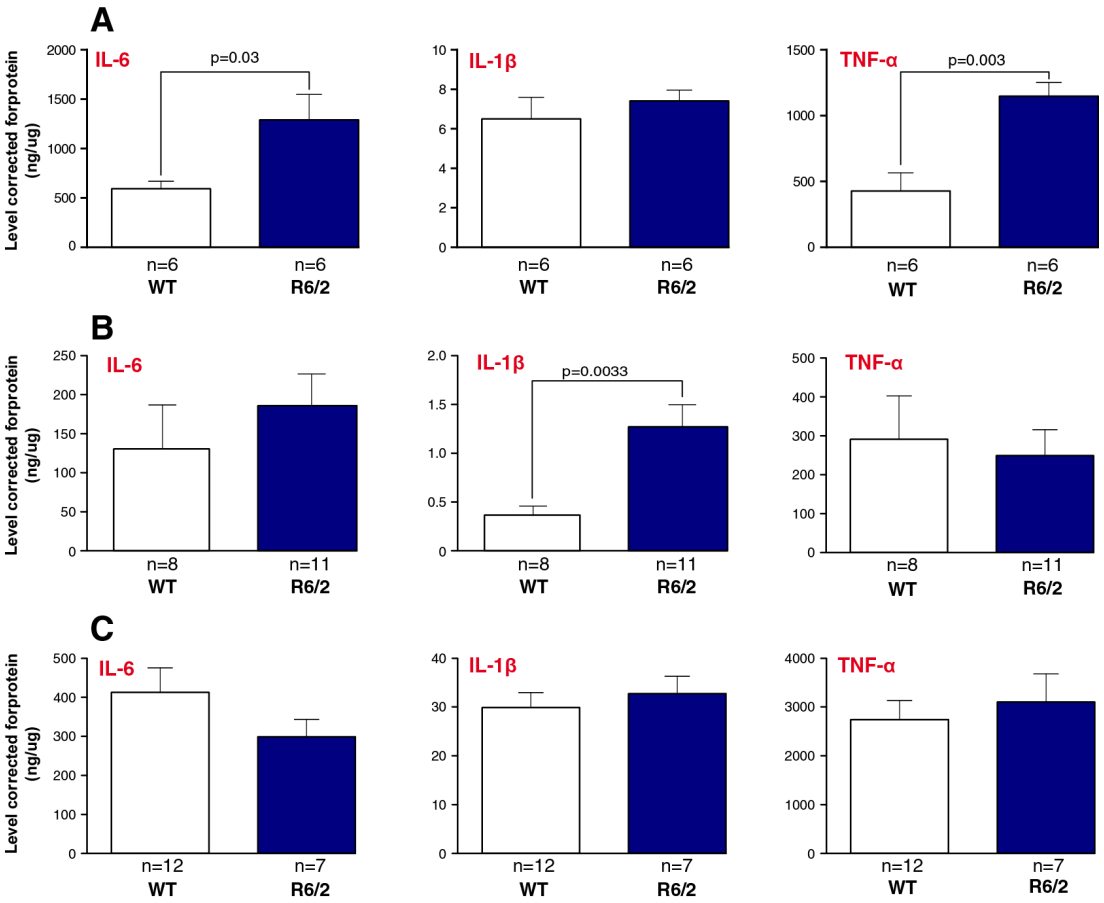

Figure 6.1: Altered cytokine production by monocytes from R6/2 mice. (A) $CD11b^{+}$ monocytes were isolated from pooled blood samples obtained from R6/2 and WT mice. Cell cultures primed with 10 ng/ml IFNγ and stimulated with 2 μg/ml LPS for 24 h showed significant differences in IL-6 and TNFα production. **(B)** R6/2 splenic monocytes and **(C)** R6/2 bone marrow monocytes were isolated using anti-CD11b magnetic beads, and individual cultures from each mouse were stimulated with 10 ng/ml IFNγ and 2 μg/ml LPS for 24 h. Measuring cytokine production in supernatants using the MSD multiplex ELISA platform, R6/2 spleen monocytes demonstrated changes in IL-1β levels, whilst bone marrow monocytes from R6/2 mice showed the same cytokine levels as WT cells. Graphs show mean concentrations corrected to protein content $\pm$ SEM. Unpaired two-tailed student t tests. **(A)** n=technical repeats of pooled samples from different mice, **(B+C)** n=biological repeats representing individual mice. Spleen and bone marrow cell profiling was done in collaboration with Dr Ralph Andre and Anna Magnusson-Lind.

In addition to monocyte subsets, IL-6 production from different tissue specific macrophages primed with IFNγ and stimulated with LPS was measured via ELISA. Surprisingly, IL-6 production by bone marrow-derived (Figure 6.2A) and peritoneal (Figure 6.2B) macrophages did not show any differences when comparing R6/2 and WT mice. In conclusion, increased cytokine production, as seen in HD patients monocytes and macrophages, could only partially be repeated in R6/2 monocytes and macrophage subsets.

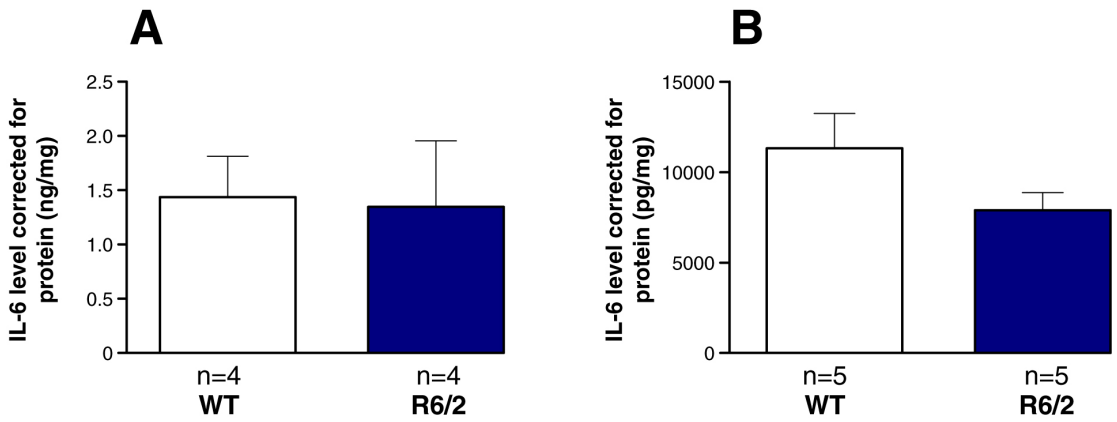

Figure 6.2: Cytokine production by macrophages from R6/2 mice. (A) Bone marrow monocytes were isolated using anti-CD11b magnetic beads and differentiated into macrophages using 20 ng/ml M-CSF for 6 days. Measuring cytokine production using IL-6 ELISAs after priming the cells with 10 ng/ml IFNγ and stimulation with 2 μg/ml LPS for 24 h showed no difference in IL-6 production comparing R6/2 and WT bone marrow-derived macrophages. **(B)** Similarly, peritoneal macrophages from R6/2 mice stimulated in the same way showed no difference in IL-6 production compared with WT cells. Graphs show mean concentrations corrected to protein content $\pm$ SEM. n=biological repeats representing individual mice. Unpaired two-tailed student t tests. Experiment was done in collaboration with Dr Ralph Andre and Anna Magnusson-Lind.

6.4.2 Cytokine profiling of myeloid cells in full-length HD mouse models

In addition to the R6/2 fragment model, which expresses only exon 1 of the human *HTT* gene, the *Hdh*$^{150Q/150Q}$ knock-in mouse model, expressing 150 CAG repeats in the endogenous mouse *Htt* gene (Lin et al., 2001), was analysed in regard to cytokine production. IFNγ-primed *Hdh*$^{150Q/150Q}$ blood monocytes stimulated with LPS demonstrated a significant increase in IL-1β and TNFα production when compared with WT mice. IL-6 levels were also elevated in *Hdh*$^{150Q/150Q}$ cells compared with WT cells (Figure 6.3A). Analysing splenic monocytes, *Hdh*$^{150Q/150Q}$ cell demonstrated significantly elevated IL-6 and TNFα production, and a slight increase in IL-1β levels compared with WT cells (Figure 6.3B). Interestingly, CD11b^{+} bone marrow monocytes isolated from *Hdh*$^{150Q/150Q}$ mice did not show any changes in cytokine production compared with WT mice (Figure 6.3C). This result, together with the lack of elevated cytokine production by R6/2 bone marrow monocytes and macrophages, indicates that bone marrow cells behave differently to mature peripheral myeloid cells.

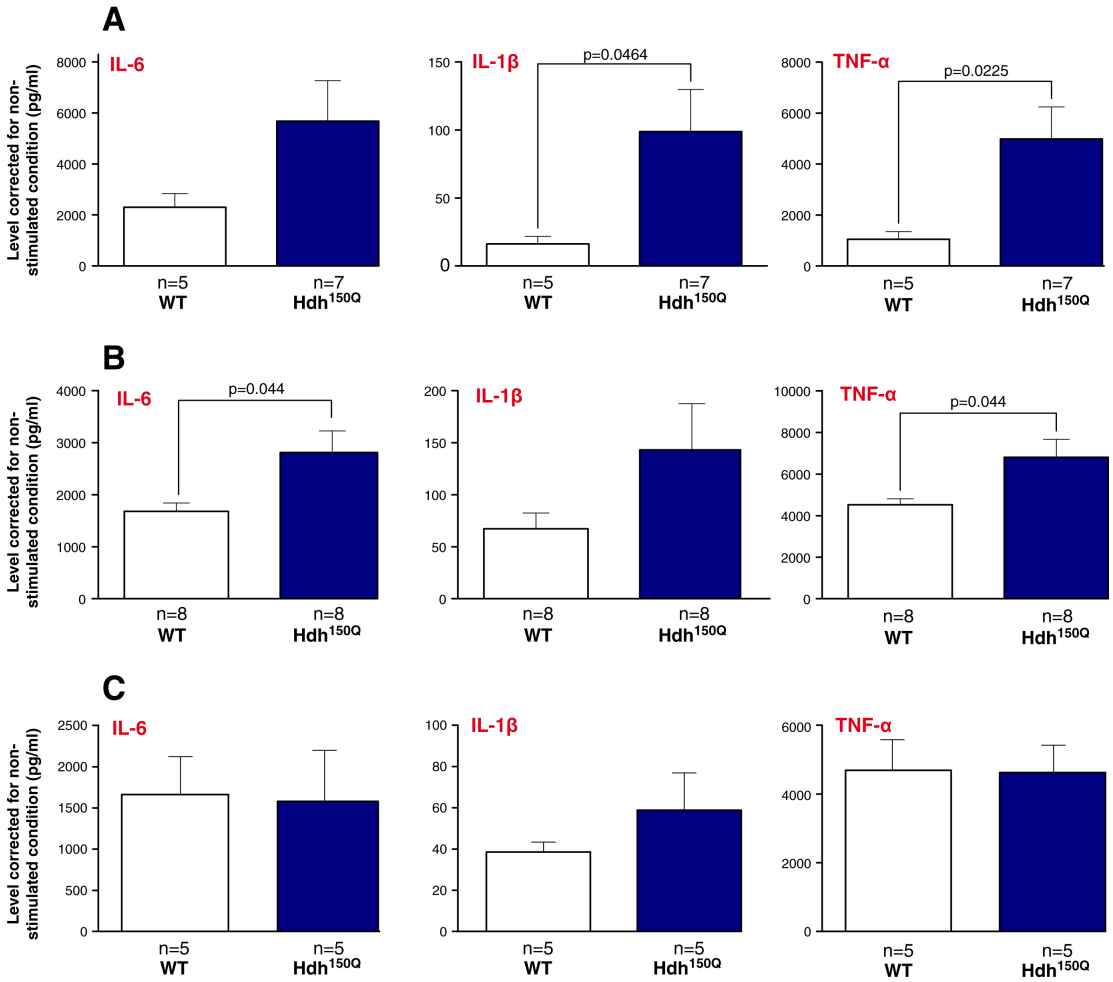

Figure 6.3: Altered cytokine production by monocytes from *Hdh*$^{150Q/150Q}$ mice. (A) Blood monocytes, **(B)** splenic monocytes and **(C)** bone marrow monocytes were isolated using anti-CD11b magnetic beads and individual mouse cultures were stimulated with 10 ng/ml IFNγ and 2 μg/ml LPS for 24 h. Cytokine production was analysed using the MSD multiplex ELISA platform. Whilst bone marrow cells produced similar levels of cytokine compared with WT, both blood and splenic monocytes produced significantly higher levels of pro-inflammatory cytokines. Graphs show mean concentrations corrected to protein content $\pm$ SEM. Unpaired two-tailed student t tests. n=biological repeats representing individual mice. Experiment was done in collaboration with Dr Ralph Andre and Anna Magnusson-Lind.

A third HD mouse model shown to have increased levels of plasma cytokine is the YAC128 model (Björkqvist et al., 2008), which expresses the entire human HD gene (Slow et al., 2003). When stimulating IFNγ-primed bone marrow-derived macrophages with control standard endotoxin (CSE), no difference in IL-6 production was detected comparing YAC128 and WT cells (Figure 6.4A), strengthening the hypothesis that bone marrow cells are not a good model for peripheral immune changes in HD. Stimulating peritoneal macrophages with CSE showed that IL-6 production by YAC128 cells was significantly increased compared with WT mice (Figure 6.4B), replicating the hyper-reactive macrophage phenotype seen in HD patients.

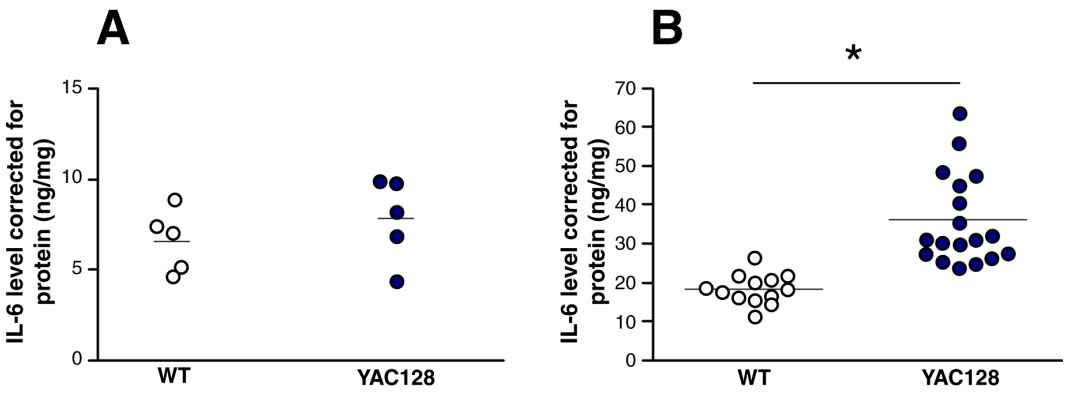

Figure 6.4: Altered cytokine production by macrophages from YAC128 mice. **(A)** Macrophages were differentiated from bone marrow monocytes and cultured with 20 ng/ml M-CSF for 6 days. Cultures were then stimulated for 24 h with 100 μg/l CSE. Measuring IL-6 levels using ELISA showed no difference in cytokine production from YAC128 bone marrow-derived cells compared with WT controls. **(B)** Peritoneal macrophages obtained via peritoneal lavage were stimulated with 100 μg/l CSE for 24 h before IL-6 levels were measured using ELISA. A significant increase in cytokine production by YAC128 peritoneal macrophages was seen when compared with WT. Graphs show mean concentrations corrected to protein content $\pm$ SEM. Unpaired two-tailed student t-tests. *$p<0.05$. Experiment done by C. Connolly.

6.4.3 HTT levels in bone marrow and spleen of R6/2 mice

Work presented in Chapter 3 linked mHTT levels measured in primary human immune cells with markers of disease progression such as disease stage, disease burden score and caudate atrophy. The fact that myeloid cells isolated from R6/2 bone marrow appear normal in comparison to myeloid cells found in peripheral organs isolated from the same mouse may therefore be explained by differences in mHTT expression levels. Assessing mHTT levels in whole bone marrow lysates, CD11b$^+$ sorted bone marrow cells and spleen lysates, using the TR-FRET immunoassay, showed that in two out of three R6/2 mice mHTT levels are nearly ten times lower in bone marrow cells compared with spleen (Figure 6.5). No mHTT signal was detectable in any organ isolated from control mice (data not shown). These results may explain the observation that bone marrow cells produce cytokine levels similar to WT cells.

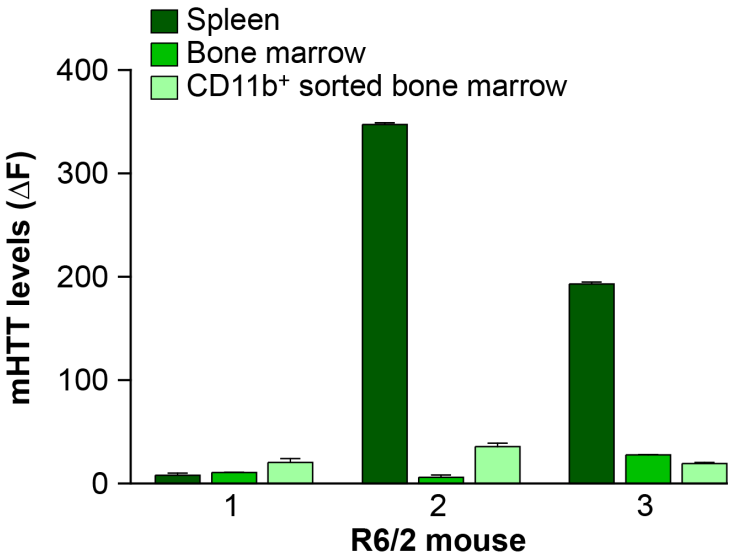

Figure 6.5: HTT levels in R6/2 spleen and bone marrow. R6/2 bone marrow cells, CD11b$^+$ cells isolated from bone marrow using magnetic cell sorting and spleen cells were lysed and used to assess mHTT levels. TR-FRET measures demonstrated that in two out of three mice spleen had ten times more mHTT than bone marrow cells. Data shown as percentage of the signal intensities over lysis buffer background signal after normalisation to total protein levels. was done in collaboration with Dr Andreas Weiss.

6.4.4 R6/2 mouse spleens demonstrate normal proportions of immune cells

In order to dissect immune dysfunction further, the proportions of immune cell subsets within the spleen of R6/2 mice were analysed. The main function of the spleen is the production and recycling of red blood cells. However, large populations of immune cells can be found in the white pulp of the spleen (Mebius and Kraal, 2005). Single cell suspensions prepared from digested spleens were stained with anti-CD3, anti-CD19 and anti-CD11b antibodies as markers for T cells, B cells and myeloid cells, respectively. Figure 6.6A shows the gating used in flow cytometry analysis to determine the percentage of the different cell types in the R6/2 spleen. No changes in the B cell, T cell and myeloid cell populations were found comparing R6/2 and WT mice (Figure 6.6B).

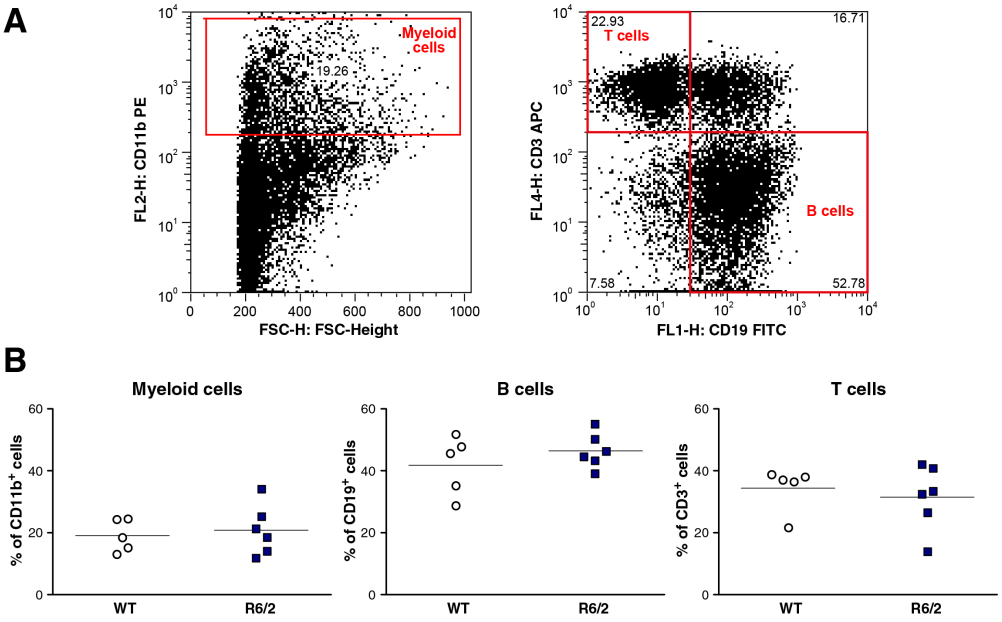

Figure 6.6: Splenic B cell, T cell and myeloid cell populations are unchanged in R6/2 mice. Spleens were digested, homogenised and, after red blood cell lysis, stained with 2 μg/ml anti-CD3 APC, 5 μg/ml anti-CD19 FITC and 2 μg/ml anti-CD11b PE antibodies. **(A)** Percentage of each cell population was determined via flow cytometry analysis using the gating as shown. **(B)** No differences in the percentage of B cells, T cells and myeloid cells were detected comparing R6/2 and WT mice spleens using unpaired two-tailed student t tests.

Next, spleen cells were stained with anti-CD3, anti-CD4 and anti-CD8 antibodies to investigated the abundance of $CD4^+$ T_h cells and $CD8^+$ cytotoxic T cells in the spleens of R6/2 compared with WT mice. No difference in T cell subsets was detected in R6/2 mice (Figure 6.7).

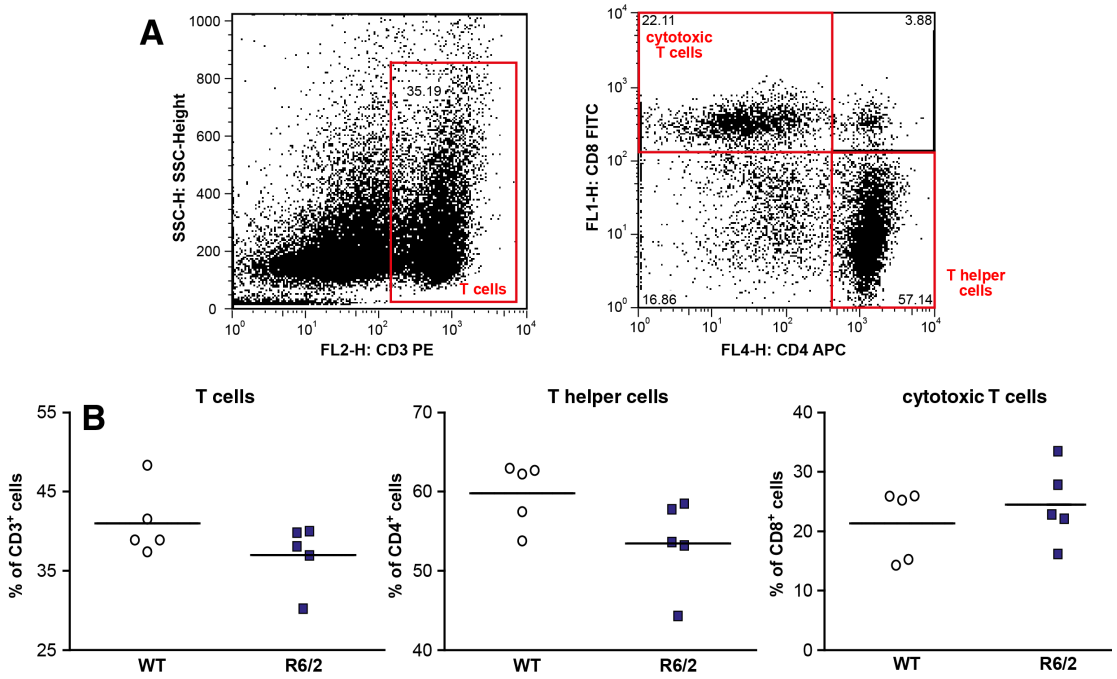

Figure 6.7: T cell subtypes are unchanged in R6/2 spleen of mice. Spleens were digested, homogenised and, after red blood cell lysis, stained with 2 μg/ml anti-CD3 PE, 5 μg/ml anti-CD8 FITC and 2 μg/ml anti-CD4 APC antibodies. **(A)** Percentage of each cell population was determined via flow cytometry analysis using the gating shown here. **(B)** No changes in the percentage of total, helper and cytotoxic T cells in spleen were detected comparing R6/2 and WT mice using unpaired two-tailed student t tests.

Looking at myeloid cell subsets in detail, spleen cell suspensions were stained with anti-F4/80 antibody as a macrophage marker and a combination of anti-CD11c, anti-B220 and anti-CD11b antibodies to distinguish between $CD11c^+$, $B220^+$ plasmacytoid DCs; $CD11c^+$, $B220^-$, $CD11b^-$ lymphoid-derived DCs; and $CD11c^+$, $B220^-$, $CD11b^+$ myeloid-derived DCs. Comparing R6/2 and WT mice, no difference in the percentage of macrophage and DC subsets was detectable (Figure 6.8).

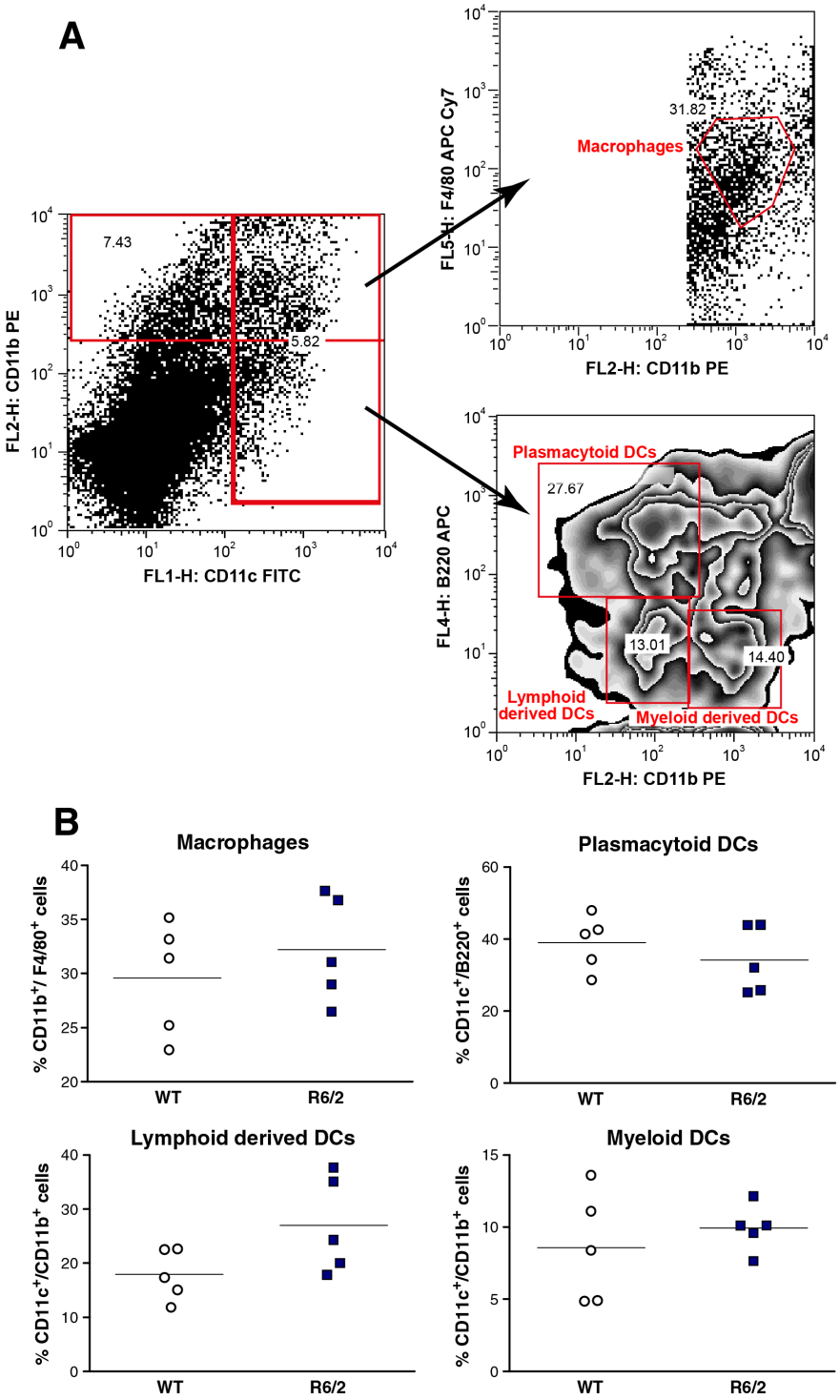

Figure 6.8: Myeloid cell subsets are unchanged in spleens of R6/2 mice. Spleens were digested, homogenised and, after red blood cell lysis, stained with 2 μg/ml anti-CD11b PE, 2 μg/ml anti-CD11c FITC, 2 μg/ml anti-F4/80 APC Cy7 and 2 μg/ml anti-B220 APC antibodies. **(A)** Percentages of each cell population were determined via flow cytometry analysis using the gating as shown. **(B)** No changes in the percentage of macrophages, plasmacytoid, myeloid-derived and lymphoid-derived DCs were found in the spleens of R6/2 and WT mice using unpaired two-tailed student t tests.

Looking specifically at CD11b^{+} spleen cells, MHC class II expression was used to categorise myeloid cells in a resting or activated state. Comparing the percentage of resting (CD11b^{+}, MHCII^{low}) and activated (CD11b^{+}, MHCII^{high}) myeloid cells in spleens from 8 week old animals did not show a difference between R6/2 and WT mice (Figure 6.9A). However, 12 week old R6/2 mice demonstrated a significant decrease of activated myeloid cells in their spleens whilst the percentage of resting monocytes was significantly increased (Figure 6.9B). This change in myeloid cell activation is likely to be a side-effect of the progressing disease in end-stage 12 week old R6/2 mice, as the effect was not seen in mice at 8 weeks old.

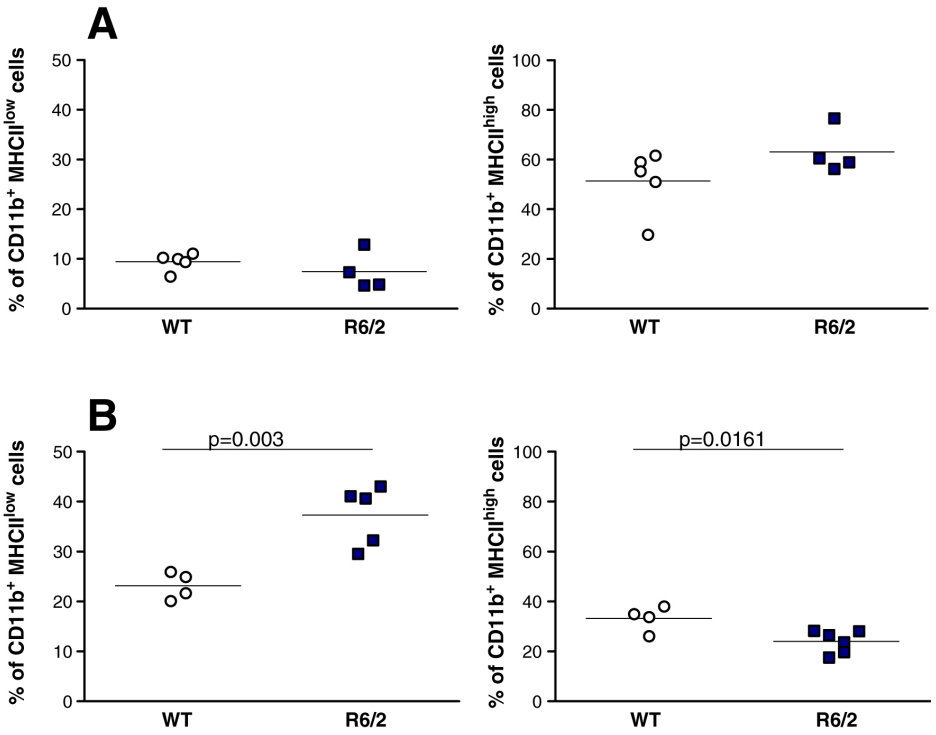

Figure 6.9: Ratio of resting versus activated myeloid cells is altered in end-stage R6/2 mice. Spleens were digested, homogenised and, after red blood cell lysis, stained with 2 μg/ml anti-CD11b PE, 2 μg/ml anti-CD11c FITC, 2 μg/ml anti-MHCII APC antibodies. **(A)** At 8 weeks of age, no differences in resting (CD11b^{+}, MHCII^{low}) and activated (CD11b^{+}, MHCII^{high}) myeloid cells were detected between R6/2 and WT mice. **(B)** At 12 weeks, R6/2 mice demonstrated a significant increase in CD11b^{+}/ MHCII^{low} resting cells while CD11b^{+}/ MHCII^{high} activated myeloid cells are significantly decreased. Unpaired two-tailed student t test.

6.4.5 Peritoneal macrophages from R6/2 mice show increased phagocytosis

Phagocytosis is a key function of macrophages and in Section 4.4.4 a significant elevation in phagocytosis was observed in LPS-stimulated blood-derived HD patient macrophages compared with control cells. To see whether R6/2 mice demonstrate a similar phenotype, bone marrow-derived and peritoneal macrophages were incubated with green fluorescent latex beads and the percentage of cells phagocytosing beads was analysed via flow cytometry. LPS-stimulated bone marrow-derived macrophages from R6/2 mice did not demonstrate a difference in phagocytosis levels compared with WT mice (Figure 6.10A). Peritoneal macrophages isolated from R6/2 mice, however, showed a small elevation in the percentage of phagocytosing cells upon LPS stimulation, similar to the results in HD patients (Figure 6.10B).

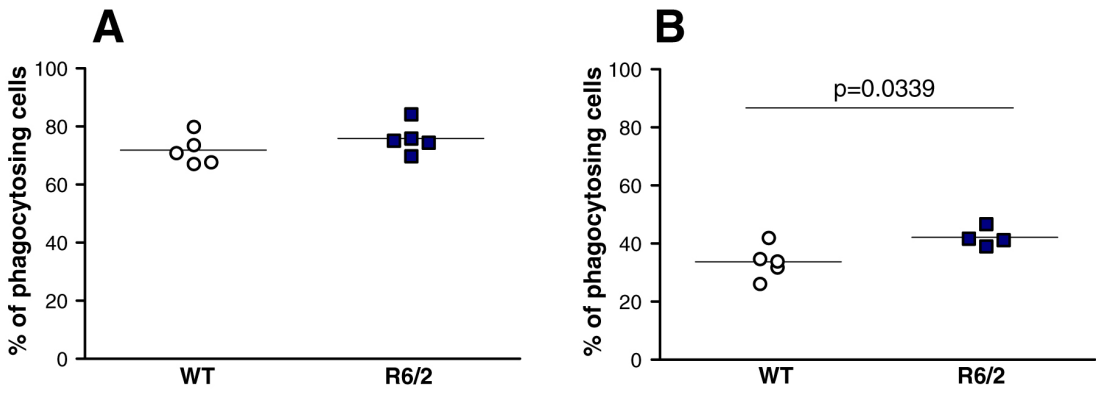

Figure 6.10: Phagocytosis levels in macrophages isolated from R6/2 mice. Macrophages were incubated with green fluorescent latex beads for 1 h before the number of cells taking up beads was analysed using flow cytometry. **(A)** Levels of phagocytosis in LPS (2 μg/ml) stimulated bone marrow-derived macrophages were similar in WT and R6/2 mice, whilst **(B)** peritoneal macrophages from R6/2 mice stimulated with 2 μg/ml LPS for 24 h showed a significant increase in phagocytosis levels. Data are representative of two independent experiments. n= biological repeats representing individual mice. Unpaired two-tailed student t test.

6.4.6 Other myeloid cell functions are unchanged in R6/2 mice

Analysing the differentiation of macrophages from blood monocytes showed no difference in cell morphology or differentiation rate in HD patients (Section 4.4.1). Counting the number of differentiated, adhered bone marrow-derived macrophages four days after seeding also showed no difference in R6/2 compared with WT cells (Figure 6.11A). In addition, adhesion of peritoneal macrophages appeared to be normal in R6/2 mice, as the same number of R6/2 and WT macrophages adhered to the tissue culture plastic 2 h after seeding (Figure 6.11B).

HD patients demonstrate a striking defect in monocyte and macrophage migration towards the chemoattractant MCP-1 (Section 5.4.1). To test this phenotype in R6/2 mice peritoneal macrophages were seeded on to transwells and the number of cells migrating towards MCP-1 located in the lower chamber of the transwell system was counted. Interestingly, peritoneal macrophages from R6/2 and WT mice showed similar levels of migration, both under basal conditions and towards MCP-1 (Figure 6.11C).

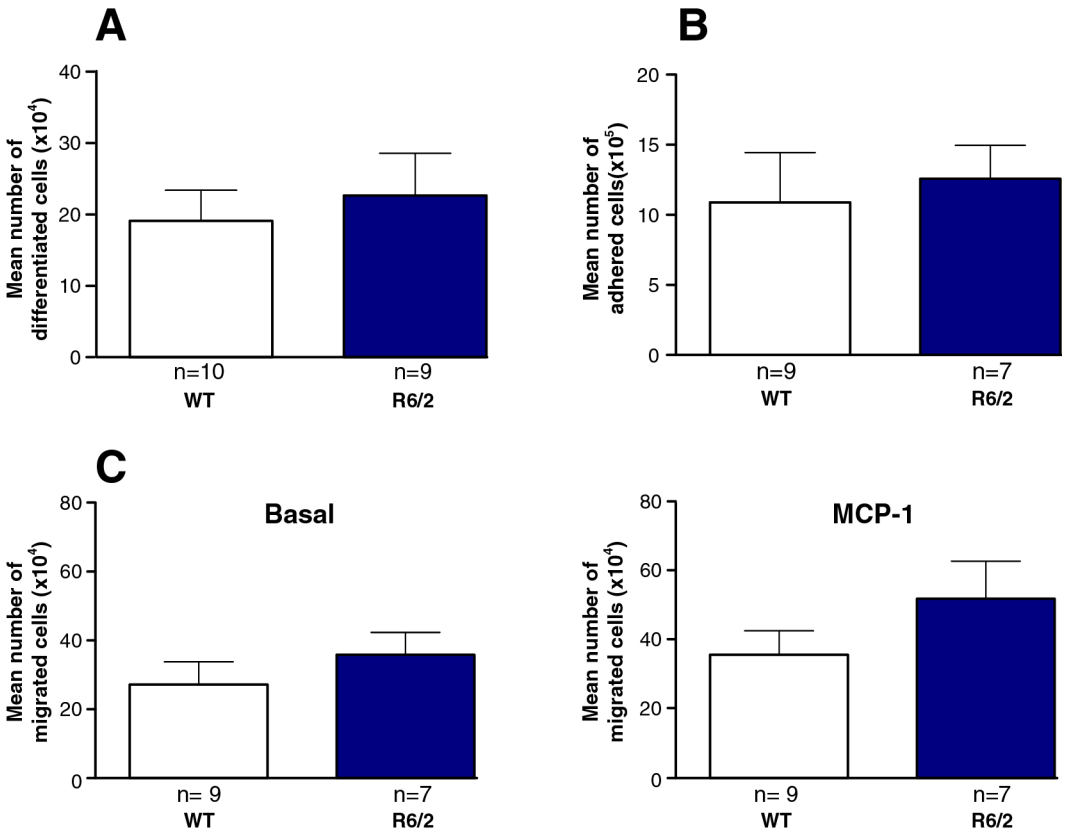

Figure 6.11: Monocytes from R6/2 mice demonstrate no functional changes in cell adhesion, migration and differentiation. (A) Bone marrow monocytes were isolated using anti-CD11b magnetic beads and were differentiated using 20 ng/ml M-CSF. Four days post seeding, adhered differentiated macrophages were detached and counted. **(B)** Peritoneal macrophages obtained via peritoneal lavage were seeded on to tissue culture plates. After 2 h the number of adhered cells was counted and no difference in adherence was observed when comparing WT and R6/2 cells. **(C)** Using an 8μm transwell system peritoneal macrophages from R6/2 mice did not show a difference in basal or MCP-1 (50 ng/ml) induced migration. Data shown as mean $\pm$ SEM. n= biological repeats representing individual mice. Unpaired two-tailed student t tests. Experiments were done in collaboration with Dr Ralph Andre and Anna Magnusson-Lind.

6.5 Discussion

It has been shown previously that different HD mouse models recapitulate the human HD phenotype in regard to increased plasma cytokine levels. Cytokine levels have been found to be increased the plasma from R6/2, *Hdh*$^{150Q/150Q}$ and YAC128 mice (Björkqvist et al., 2008). In this study blood monocytes isolated from R6/2 and *Hdh*$^{150Q/150Q}$ were shown to be hyper-reactive upon LPS stimulation *in vitro*, producing high levels of IL-6 and TNFα and replicating the human phenotype described in Chapter 4.

Bone marrow-derived cells, both CD11b^{+} monocytes and monocyte-derived macrophages, do not exhibit increased pro-inflammatory cytokine production in any of the HD mouse models analysed. Interestingly, mHTT expression in bone marrow cells was found to be ten times less compared with spleen tissue in two out of three R6/2 mice analysed. As bone marrow consists of different types of stem cells and we are especially interested in myeloid cells, CD11b^{+} cells were isolated and their mHTT expression levels were compared with whole bone marrow mHTT levels, showing no difference. So whilst this result needs to be replicated, it indicates that low mHTT levels in bone marrow cells may be the cause for the different phenotype seem in bone marrow compared with peripheral cells. These results are particularly interesting in light of a recent paper describing how bone marrow transplants, when given from HD donor to HD recipient mice, can improve certain aspects of HD pathology such as behavioural changes (Kwan et al., 2012a). Bone marrow transplantation from both WT and BACHD mice into irradiated BACHD mice decreased the time the animal took to cross a beam in the balance beam task at 6 months of age. Furthermore, while BACHD mice that did not receive a bone marrow transplant develop deficits in total open-field activity at 12 months of age, WT and BACHD mice receiving WT or BACHD bone mar-

row transplants show no difference. Bone marrow transplants, both from WT and BACHD donors do not improve all behavioural deficits and it is apparent that WT bone marrow transplant have greater benefit for the recipient. While it remains to be shown how the transplants confer their benefits, the lower mHTT load in bone marrow cells may play a role, especially when replacing microglia, which are thought to be self-renewing (Ransohoff and Perry, 2009) and therefore may accumulate mHTT over their life time.

Looking at cytokine production by CD11b$^+$ myeloid cells isolated from the spleen, *Hdh*$^{150Q/150Q}$ mice demonstrated elevated IL-6, IL-1β and TNFα levels similar to the changes seen from *Hdh*$^{150Q/150Q}$ blood monocytes. The same cells from R6/2 mice, however, only showed an increase in IL-1β, whilst IL-6 and TNFα levels were unchanged. In contrast to blood, CD11b$^+$ cells from spleen comprise a cell suspension that includes macrophages and DCs as well as the desired monocytes. Testing whether a shift in the percentage of these different cell type within the spleen accounts for the rise in IL-1β levels in R6/2 compared with control cells, no difference in the macrophage, DC and monocyte populations was detected. However, when looking at activation levels in splenic monocytes using MHCII expression levels as a marker, significantly more resting and fewer activated monocytes were found in R6/2 mice at 12 weeks of age. It might be, therefore, that this difference in the isolated population from spleen, and not a cell-intrinsic hyperreactivity of the cells accounts for the difference in IL-1β levels detected in R6/2 spleen. This means splenic cells from R6/2 mice may not be a good model for the peripheral myeloid cell function in HD.

While R6/2 monocytes isolated from blood recapitulate the human immune phenotype, cytokine production by peritoneal macrophages isolated from R6/2 mice was unchanged compared with WT cells. Interestingly, peritoneal macrophages isolated from YAC128 mice produced increased levels of IL-6 upon CSE stim-

ulation compared with WT. It is unclear why macrophages from R6/2 mice do not exhibit the same hyper-reactive phenotype as YAC128 mice. The difference could be due to the fact that R6/2 mice only express a N-terminal fragment of the mutant protein (Mangiarini et al., 1996), while YAC128 mice express the full-length protein (Slow et al., 2003). Alternatively, the R6/2 colony used in this study was on a CBA$\times$C57Bl/6 background whilst the YAC128 mice were on a FVB background and this difference in background genetics could explain the differences in the phenotype. The influence of different genetic backgrounds has been shown in YAC128 mice when comparing the mice on three different backgrounds (C57BL/6, FVB/N and 129 strains) (Van Raamsdonk et al., 2007). Strain influenced motor dysfunction, cognitive deficits, brain pathology and peripheral changes such as weight by modulating the nuclear localisation of mHTT as opposed to altered mHTT expression levels. Interestingly, mice on the FVB background showed a stronger HD phenotype compared with C57BL. For obvious reasons it is not possible to compare strain effects between different mouse models. It is important however, to keep this difference in mind as it might influence some of the differences seen in this study.

Looking at other cellular functions, phagocytosis in peritoneal macrophages from R6/2 mice was increased upon LPS stimulation, resembling the human phenotype. However, R6/2 peritoneal macrophages did not demonstrate any migration defect in our hands. In a different study, R6/2 mice demonstrate decreased numbers of infiltrating peritoneal macrophages after inducing a peritonitis with thioglycolate, when compared with WT mice (Kwan et al., 2012b). Although our *ex vivo* experiments did not show the same trend, it is important to note that the two experiments are not looking at the same aspect of migration. In our *in vitro* migration assay, the ability of peritoneal macrophages to migrate through a membrane towards one chemokine was tested, while an induced peritonitis is not only looking at macrophage migration but also monocyte infiltration from the blood stream into

the peritoneum. This process requires migration though epithelium and cell-cell interactions (Imhof and Aurrand-Lions, 2004), which might be affected in HD and are not modelled in the *in vitro* assay used here. Furthermore, the *in vivo* peritonitis experiment showed that R6/2 mice have decreased infiltration of monocytes and macrophages into the peritoneum, but infiltration did still occur (Kwan et al., 2012b). It might be that as an unintentional consequence of isolating peritoneal macrophages, more functional cells were selected, which despite a possible defect managed to migrate into the peritoneum in the first place.

Both the fragment R6/2 and full-length HD models, YAC128 and *Hdh*$^{150Q/150Q}$ recapitulate aspects of the human disease and all three models should be considered for future studies investigating the immune dysfunction in HD and/or targeting it for therapeutics. The use of mouse models is especially interesting as it allows us to not only study the peripheral immune system, but also the immune cells within the CNS, and this will yield answers as to whether peripheral myeloid cells can provide insights into the function of, in humans inaccessible, microglia.

Deciding which tissue is the best for isolation of HD myeloid cells, is difficult. Both R6/2 and *Hdh*$^{150Q/150Q}$ blood monocytes mimic the human phenotype well and are a good model for the human disease, as these are the exact same cells the human disease has been studied in. Unfortunately, especially when isolated from 12 week old end-stage R6/2 mice, only around 100,000 to 300,000 monocytes can be recovered from one mouse. Large animal number are therefore required for any experiments. The use of alternative sources for monocytes and macrophages such as bone marrow and spleen also demonstrated caveats. Bone marrow monocytes and bone marrow monocyte-derived macrophages did not show differences in cytokine production and phagocytosis, leading to the conclusion that immature bone marrow cells are not a good model to assess monocyte cell function in HD. Splenic monocytes from the R6/2 and *Hdh*$^{150Q/150Q}$

mouse models, on the other hand, respond in a hyper-reactive manner to LPS, but due to their diverse composition ($CD11b^+$ cells isolated from spleen can be monocytes, macrophages or DCs), this does not resemble studies on human blood cells that are 100 % monocytes. As flow cytometry showed that the abundance of the different cell types does not differ between WT and R6/2, splenic cells may still be used to compare the genotypes, although conclusions as to which cell type is responsable for changes in phenotype would be difficult to draw.

Even if *ex vivo* immune cell studies are not easy to perform due to cell numbers, after proving dysfunction of the immune system in HD mouse models in form of increased plasma cytokine level (Björkqvist et al., 2008) and cytokine production by murine blood monocytes *in vitro*, the mouse models can now be used to target different molecules in the pathway identified in human cells (Chapter 4) and thereby help to understand the role the peripheral immune system plays in HD progression.

7 Conclusions and future work

In neurodegenerative diseases such as HD, disability is primarily caused by death and dysfunction of neurons. However, non-neuronal cells have been shown to contribute to the progressive neuronal loss. Transgenic expression of N-terminal mHTT solely in astrocytes causes an age-dependent neurological phenotype similar to HD (Bradford et al., 2009), providing evidence that non-neuronal cells might be crucial for disease progression. Understanding dysfunction in non-neuronal cells may therefore provide insights into HD pathology, biomarkers and therapeutic targets.

7.1 Innate immune cell function in HD

The work presented in this thesis demonstrates dysfunction in several key functions of innate immune cells. The hyper-reactive phenotype of HD monocytes and macrophages, characterised by increased cytokine production and phagocytosis upon LPS stimulation was shown to be caused by dysregulation of the NFκB pathway. Functioning as a scaffolding protein for IKKγ, mHTT binds the protein, allowing quicker activation of the kinase and the downstream pathway upon stimulation via LPS. Contrasting this hyper-reactive phenotype, data presented in Chapter 5 showed decreased migration of human HD myeloid cells. Decreased levels of MCP-1's receptor CCR2, found on HD monocytes, may pro-

vide a link between the hyper-reactive phenotype and the migration defect in the HD cells, as increased production of MCP-1 may lead to decreased levels of its receptor via autocrine desensitisation. However, normal levels of CCR-2 found on HD macrophages indicated a different mechanism and indeed, mHTT-dependent changes in actin remodeling were found in this thesis and several other studies (Munsie et al., 2011; Myre et al., 2011). It is therefore likely that the migration defect and the hyper-reactive phenotype in HD myeloid cells are not directly linked, but caused by effects of mHTT expression on different cellular pathways.

This thesis further demonstrated that by lowering total HTT levels in primary human HD monocytes and macrophages HD-specific phenotypes such as increased cytokine production and transcriptional dysregulation can be, at least partially, reversed. This is the first report showing that lowering HTT levels in *ex vivo* human cells can reverse cellular dysfunction in HD. This finding validate the potential of HTT lowering therapy and opens the possibility of using *ex vivo* cells to test siRNA efficiency and safety in addition to mouse models.

Tracking total and mHTT levels in immune cells revealed that mean mHTT levels in monocytes, T cells and B cells differ significantly between HD patients and controls, as well as between premanifest and manifest patients. mHTT levels associated significantly with measures of disease progression in monocyte and T cells from HD patients. Interestingly, looking at epithelial cells no such correlation was observed, emphasising the potential pathogenic role of immune cells in HD. The fact that mHTT levels measured in T cells tracked with disease burden and caudate atrophy indicates a pathogenic accumulation of mHTT in adaptive immune cells similar to that demonstrated in the innate immune system. Future work should therefore address whether the increase in mHTT levels in B and T cells leads to functional changes in the adaptive immune system. Different T and B cell subsets found in the blood could be compared between control and HD

samples, analysing their overall abundance. Furthermore, T cell functions such as cytokine production, cell proliferation, cytotoxicity and T helper function should be investigated.

7.2 Modeling human immune dysfunction in mice

Analysing immune cell function in different HD mouse models, this thesis showed similar hyper-activation of blood monocytes in the *Hdh*$^{150Q/150Q}$ and R6/2 mouse models of HD, while bone marrow cells showed no differences compared with controls. The use of transgenic animals as models of HD has caveats. Most models carry a CAG repeat length significantly greater than adult-onset HD patients, who normally range between 40-50 CAGs. Additionally, R6/2 mice overexpress a N-terminal HTT fragment, which cannot recapitulate all functions of the full-length HTT protein and causes a fast progression more similar to juvenile HD (Mangiarini et al., 1996). However, while these limitations should be kept in mind, rodent models are crucial in understanding disease pathology and testing potential therapies.

Several recent studies in HD mice have demonstrated that, using bone marrow transplants (Kwan et al., 2012a) and by modulating the immune response via CB2 signalling (Bouchard et al., 2012), the immune system is a modifier of HD progression. To objectively test the effect a bacterial or viral challenge, in a controlled environment, will have on HD progression, mice should be injected with viral components or LPS peripherally. A questionnaire based study in AD has linked systemic inflammatory incidents in AD patients with increased serum levels of pro-inflammatory cytokines and an increased rate of cognitive decline over a 6-month period (Holmes et al., 2009). While the reports on the inflammatory incidents are subjective, a similar study in HD may be of use. In addition to this,

a conditional gene knock-out of *HTT* in myeloid cells, using the myeloid cell specific LysM promoter (Clausen et al., 1999), will provide the answer to the question which role myeloid cells play in HD pathology.

7.3 Need for biomarkers in HD

Biomarkers are indicators of a certain biological state. In case of disease, biomarkers should be significantly elevated or decreased in comparisons to controls and ideally also change with disease progression. While this thesis described significant changes in cytokine production by HD myeloid cells, no differences were seen between the different disease stages. The lack of correlation with disease progression, overlap in measures between control and HD patient cells, and the lengthy protocol make LPS-induced cytokine production an unlikely biomarker. In addition, caution needs to be taken when using immune markers as biomarkers. Cytokines are known to vary diurnally and that this pattern changes with disease progression, which makes standardised sample collection challenging. Furthermore, cytokine levels can be altered by infections, immunomodulatory substances such as cortisol, body mass index, smoking, diet and exercise adding to the challenge of reliably using cytokine levels as specific disease markers. In addition, neurodegenerative diseases are slowly progressive and changes in immune markers are subtle (Björkqvist et al., 2009). More likely perhaps, immune molecule levels should be used in a large panel, or in conjunction with other biomarkers such as CSF immune markers and neuroimaging. The use of large panels has already been suggested for AD, where eighteen plasma proteins, including TNFα, IL-11, IL1-β and CCL5, have been used to classify blinded samples from AD and control subjects with 90 % accuracy, and identify patients that will progress from mild cognitive impairments to AD in the following 2-6 years (Ray et al., 2007).

In the case of HD, which can be diagnosed before symptom onset due to its monogenetic nature, biomarkers will be crucial for clinical trials and potential treatments for the premanifest gene carriers as classical end points such as functional score do not exist for this group. The significant differences in mHTT levels between controls, premanifest and manifest subjects, described in this thesis, may therefore provide a valuable biomarker able to track disease progression for clinical trials. However given overlap in the measurements between groups, more data will be needed to assess how robust mHTT level track disease progression. Additionally, multiple-end point data will always provide a better picture of disease progression and effectiveness of treatment than relying on a single measure.

7.4 Therapy targeting immune dysfunction

Given the results in this thesis, the involvement of NFκB pathway dysregulation in HD should be further investigated, especially as NFκB signalling is not only crucial in innate immune activation but also in neuronal survival (Teng and Tang, 2010). Targeting the NFκB pathway to lower its activation using drugs, first in cellular HD models then *in vivo* in HD mice will inform us whether the NFκB pathway is a possible target for therapy. A study in rat PC12 cells has already shown, that blocking NFκB function leads to reduced mHTT toxicity (Khoshnan et al., 2004). Drugs targeting the pathway for HD should, therefore, be designed to target immune cells as well as neurons and for *in vivo* studies should be able to cross the BBB. Additionally, crossing HD mice onto conditional NFκB knock-out mice will further our understanding of the role immune activation plays in HD. Targeting the pathway further downstream is also a possibility and indeed, an peripherally administered neutralising anti-IL-6 antibody treatment has been shown to improve both weight loss and disease progression in R6/2 mice (Bouchard et al., 2012). However, while limiting unwanted immune responses during neurodegenerative

diseases may be neuroprotective, it is important to understand which immune activation is helpful, by for example clearing dead cells or protein aggregates and which immune response is toxic to the surrounding tissue. In the case of AD, targeted stimulation of macrophages to increase the phagocytosis of Aβ has beneficial effects on disease outcome (Frenkel et al., 2005), the same could be true for early microglial activation in HD.

Lowering HTT levels is one major strategy for HD therapy. The novel method of siRNA delivery used in this thesis has potential therapeutic relevance to HD and other diseases where immune dysregulation is a feature. Glucan particles are a versatile phagocytic cell targeted delivery system and have been administered by oral, subcutaneous, intraperitoneal and intravenous routes in mice and rats (Aouadi et al., 2009). In future studies, administration of GeRPs loaded with anti-*HTT* siRNA to reverse the inflammatory phenotype will test the therapeutic potential of lowering HTT levels in immune cells. GeRPs could be administered either intrathecally to directly target phagocytic microglial cells and infiltrating monocyte/macrophages, or intravenously to target circulating monocytes, a precursor pool for inflammatory cells trafficking into inflamed brain sites.

Overall, work presented in this thesis has helped understanding the cellular mechanisms causing of immune cell dysfunction in HD, has implications for the role of the innate immune system in neurodegeneration and has provided new possible targets for therapeutics both in form of the NFκB pathway and in targeting immune cells via HTT lowering using GeRPs.

A Appendices

A.1 Appendix I - RPMI1640 media formulation

Table A.1: Components of RPMI 1640 media. Formulation of RPMI1640 media bought from Invitrogen #31870074.

Components	Molecular Weight	Concentration (mg/L)	mM
Glycine	75	10	0.133
L-Arginine	174	200	1.15
L-Asparagine	132	50	0.379
L-Aspartic acid	133	20	0.15
L-Cystine	240	50	0.208
L-Glutamic Acid	147	20	0.136
L-Histidine	155	15	0.0968
L-Hydroxyproline	131	20	0.153
L-Isoleucine	131	50	0.382
L-Leucine	131	50	0.382
L-Lysine hydrochloride	146	40	0.274
L-Methionine	149	15	0.101
L-Phenylalanine	165	15	0.0909
L-Proline	115	20	0.174

L-Serine	105	30	0.286
L-Threonine	119	20	0.168
L-Tryptophan	204	5	0.0245
L-Tyrosine	181	20	0.11
L-Valine	117	20	0.171
Biotin	244	0.2	0.00082
Choline chloride	140	3	0.0214
D-Calcium pantothenate	477	0.25	0.000524
Folic Acid	441	1	0.00227
Niacinamide	122	1	0.0082
Para-Aminobenzoic Acid	137	1	0.0073
Pyridoxine hydrochloride	206	1	0.00485
Riboflavin	376	0.2	0.000532
Thiamine hydrochloride	337	1	0.00297
Vitamin B12	1355	0.005	3.7E-06
i-Inositol	180	35	0.194
Calcium nitrate (Ca(NO3)2 4H2O)	236	100	0.424
Magnesium Sulfate (MgSO4-7H2O)	246	100	0.407
Potassium Chloride (KCl)	75	400	5.33
Sodium Bicarbonate (NaHCO3)	84	2000	23.81
Sodium Chloride (NaCl)	58	6000	103.45
Sodium Phosphate dibasic (Na2HPO4)	142	800	5.63
D-Glucose (Dextrose)	180	2000	11.11
Glutathione (reduced)	307	1	0.00326
Phenol Red	376.4	5	0.0133

A.2 Appendix II - Vector maps

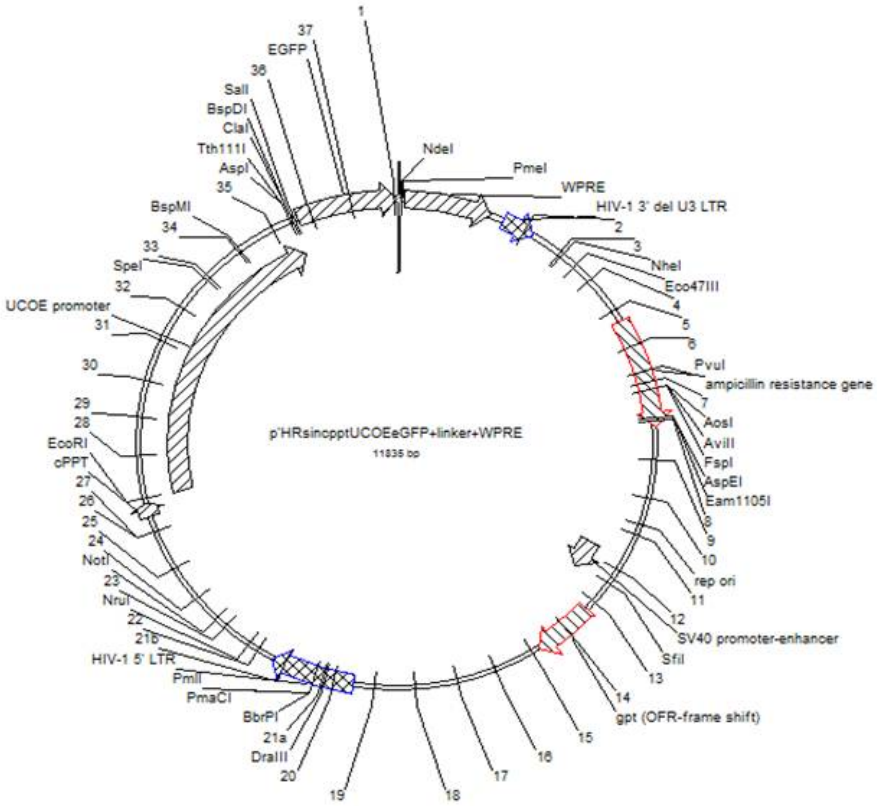

Figure A.1: Vector map for A2UCOE without *HTT* exon 1. Vector map of p'HRsincpptUCOEeGFP+linker+WPRE showing sites of the GFP insert and the ampicillin resistance.

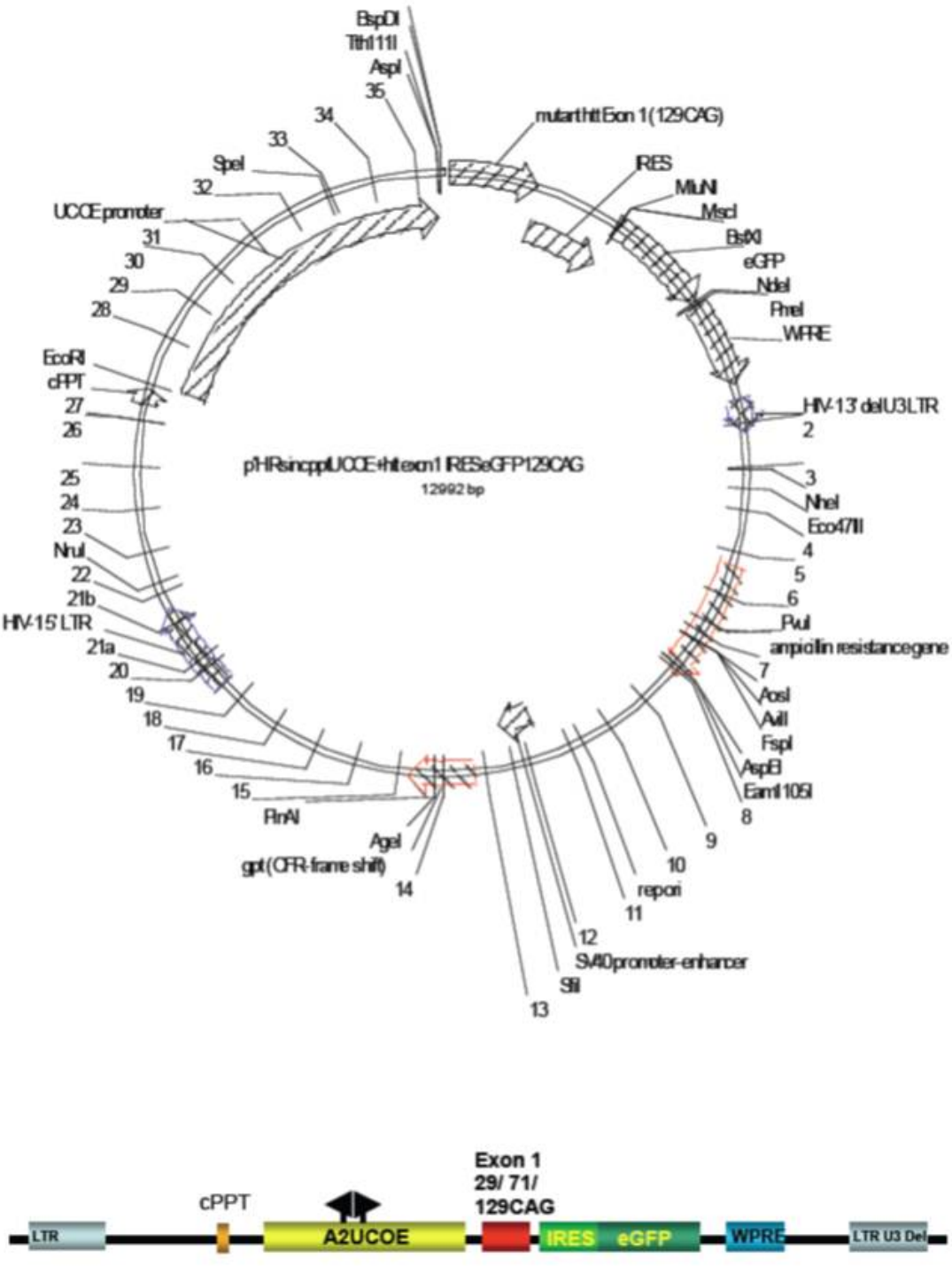

Figure A.2: Vector map for A2UCOE with *HTT* exon 1. Vector map of p'HRsincpptUCOE+htt exon1 IRES eGFP 129CAG as example for all three HTT exon 1 carrying vectors, showing sites of the exon 1 insertion, GFP site and the ampicillin resistance gene.

A.3 Appendix III - Sequencing

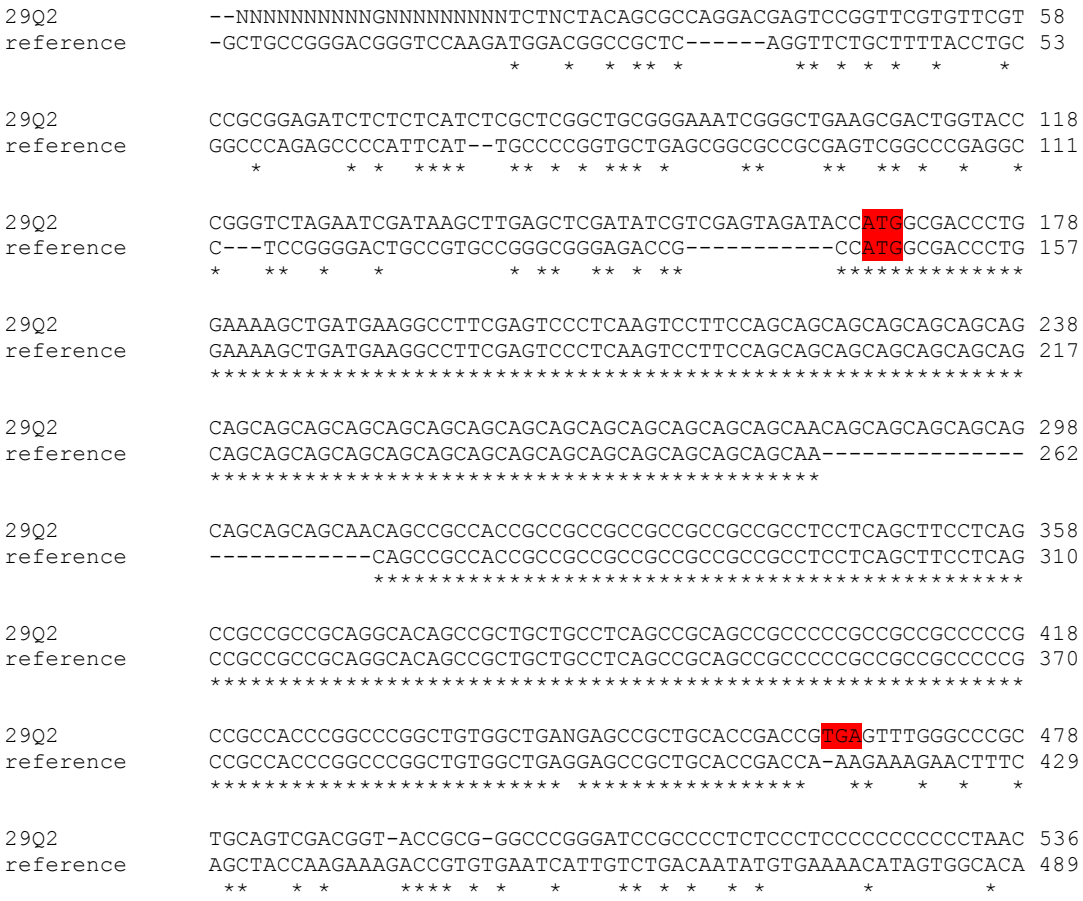

Figure A.3: Alignment of the A2UCOE 29Q vector with the reference *HTT* sequence. Plasmid DNA was sequenced and aligned to a reference *HTT* sequence using CLUSTAL 2.0.12. Sequencing matched between the starting codon and the first nucleotides of the vector backbone (in red). A2UCOE demonstrated small expansion of the CAG repeat from 29 to 31 repeats.

```
71Q             --NNNNNNNNNNNNNNNNNNNNNAGTTCTNCTACAGCGCCAGGACGAGTCCGGTTCGTGTT 58
reference       ----------GCTGCCGGGACGGGTCCAAGATGGACGGCCGCTCAGGTTCTGCTTTTACC 50
                                                ** * *  *  ** * * *  *

71Q             CGTCCGCGGAGATCTCTCTCATCTCGCTCGGCTGCGGGAAATCGGGCTGAAGCGACTGGT 118
reference       TGCGGCCCAGAGCCCCATTCAT--TGCCCCGGTGCTGAGCGGCGCCGCGAGTCGGCCCGA 108
                 *    *      * *  * **   ** * * *** *     **    **  ** *  *

71Q             ACCCGGGTCTAGAATCGATAAGCTTGAGCTCGATATCGTCGAGTAGATACCATGGCGACC 178
reference       GGCC---TCCGGGGACTGCCGTGCCGGGCGGGAGACCG-----------CCATGGCGACC 154
                  **   **  *   *          * **  ** * **           ***********

71Q             CTGGAAAAGCTGATGAAGGCCTTCGAGTCCCTCAAGTCCTTCCAGCAGCAGCAGCAGCAG 238
reference       CTGGAAAAGCTGATGAAGGCCTTCGAGTCCCTCAAGTCCTTCCAGCAGCAGCAGCAGCAG 214
                ************************************************************

71Q             CAGCAGCAGCAGCAGCAGCAGCAGCAGCAGCAGCAGCAGCAGCAGCAGCAGCAGCAGCAG 298
reference       CAGCAGCAGCAGCAGCAGCAGCAGCAGCAGCAGCAGCAGCAGCAACAG--------- 265
                ************************************************

71Q             CAGCAGCAGCAGCAGCAGCAGCAGCAGCAGCAGCAGCAGCAGCAGCAGCAGCAGCAGCAG 358
reference       ------------------------------------------------------------


71Q             CAGCAGCAGCAGCAGCAGCAGCAGCAGCAGCAGCAGCAGCAGCAGCAGCAGCAGCAGCAG 418
reference       ------------------------------------------------------------


71Q             CAGCAGCAGCAGCAACAGCCGCCACCGCCGCCGCCGCCGCCGCCTCCTNANCTT 478
reference       ---------------CAACAGCCGCCACCGCCGCCGCCGCCGCCGCCTCCTCAGCTT 306
                               ************************************ * ***

71Q             CCTCAGCCGCCGCCGCAGGCACAGCCGCTGCTGCCTCAGCCGCAGCCGCCCCCGCCGCCG 366
reference       CCTCAGCCGCCGCCGCAGGCACAGCCGCTGCTGCCTCAGCCGCAGCCGCCCCCGCCGCCG 538
                ************************************************************

71Q             CCCCCGCCGCCACCCGGCCNGGCTGTGGCTGAGGAGCCGNTGCACCGNNCGTGAGGNTNG 426
reference       CCCCCGCCGCCACCCGGCCCGGCTGTGGCTGAGGAGCCGCTGCACCGACCA-AAGAAAGA 598
                ****************** ****************** *******  *    *
```

Figure A.4: Alignment of the A2UCOE 71Q vector with the reference *HTT* sequence. Plasmid DNA was sequenced and aligned to a reference *HTT* sequence using CLUSTAL 2.0.12. Sequencing matched between the starting codon and the first nucleotides of the vector backbone (in red) and verified 71 CAG repeats in this construct.

```
129Q            -----NNNNNNNNNNNAGTTCTNCTACAGCGCCAGGACGAGTCCGGTTCGTGTTCGTCCG 55
reference       ----GCTGCCGGGACGGGTCCAAGATGGACGGCCGCTCAGGTTCTGCTTTTACCTGCGGC 56
                          ** *        ** * *  *   ** * * *  *    *

129Q            CGGAGATCTCTCTCATCTCGCTCGGCTGCGGGAAATCGGGCTGAAGCGACTGGTACCCGG 115
reference       CCAGAGCCCCATTCAT--TGCCCCGGTGCTGAGCGGCGCCGCGAGTCGGCCCGAGGCC-- 112
                *      * *  ****   ** * * *** *     **    **  ** *  *   **

129Q            GTCTAGAATCGATAAGCTTGAGCTCGATATCGTCGAGTAGATACCATGGCGACCCTGGAA 175
reference       -TCCGGGGACTGCCGTGCCGGGCGGGAGACCG-----------CCATGGCGACCCTGGAA 160
                 **  *   *          * **  ** * **           *****************


129Q            AAGCTGATGAAGGCCTTCGAGTCCCTCAAGTCCTTCCAGCAGCAGCAGCAGCAGCAGCAG 235
reference       AAGCTGATGAAGGCCTTCGAGTCCCTCAAGTCCTTCCAGCAGCAGCAGCAGCAGCAGCAG 220
                ************************************************************

129Q            CAGCAGCAGCAGCAGCAGCAGCAGCAGCAGCAGCAGCAGCAGCAGCAGCAGCAGCAGCAG 295
reference       CAGCAGCAGCAGCAGCAGCAGCAGCAGCAGCAGCAGCAACAG--------------- 265
                ************************************* **** **  * ** ** * *

129Q            CAGCAGCAGCAGCAGCAGCAGCAGCAGCAGCAGCAGCAGCAGCAGCAGCAGCAGCAG 255
reference       ------------------------------------------------------------ 265


129Q            CAGCAGCAGCAGCAGCAGCAGCAGCAGCAGCAGCAGCAGCAGCAGCAGCAGCAGCAG 215
reference       ------------------------------------------------------------ 265


129Q            CAGCAGCAGCAGCAGCAGCAGCAGCAGCAGCAGCAGCAGCAGCAGCAGCAGCAGCAG 275
reference       ------------------------------------------------------------ 265

129Q            CAGCAGCAGCAGCAGCAGCAGCAGCAGCAGCAGCAGCAGCAGCAGCAGCAGCAGCAG 335
reference       ------------------------------------------------------------ 265

129Q            CAGCAGCAGCAGCAGCAGCAGCAGCAGCAGCAGCAGCAGCAGCCGCCACCGCCGCCG 395
reference       ---------------------------------------------CCGCCGCCGCCGCCT 265
                                                             ***** ********
```

Figure A.5: Alignment of the A2UCOE 129Q vector with the reference *HTT* sequence. Plasmid DNA was sequenced and aligned to a reference *HTT* sequence using CLUSTAL 2.0.12. Sequencing failed to go past the CAG repeat due to the large number of repeats, but the number of repeats could be validated as 129.

A.4 Appendix IV - Patient details

Table A.2: *HTT* CAG repeat length for HD patients participating in the study reported in Chapter 3. The CAG repeat length for patients in the cohort was 40-47 CAG repeats, with the exception of one early stage patient with a larger repeat size of 59.

Experiment	Disease stage	n number	CAG (mean±SD)
Monocytes	Premanifest	8	43.00 ± 1.92
	Early	10	45.20 ± 5.45
	Moderate	7	43.29 ± 2.75
T cells	Premanifest	7	42.57 ± 1.62
	Early	10	45.20 ± 5.45
	Moderate	7	43.29 ± 2.75
B cells	Premanifest	7	42.57 ± 1.62
	Early	10	45.20 ± 5.45
	Moderate	7	43.29 ± 2.75
Monocytes	Premanifest	15	43.53 ± 1.77
	Early	31	43.45 ± 3.52
	Moderate	5	44.60 ± 1.95

Table A.3: *HTT* CAG repeat length and age for all subjects participating in the study presented in Chapter 4. Cohorts listed separately for each experiment.

Experiment	Subject group	n number	Age (mean±SD)	CAG (mean±SD)
Monocyte cytokine profiling I	Control	27	45.4 ± 11.7	-
	Premanifest HD	17	42.2 ± 9.9	42.8 ± 2.1
	Early HD	22	49.1 ± 11.7	43.5 ± 2.8
	Moderate HD	14	59.4 ± 7.3	43 ± 1.3
Monocyte cytokine profiling II	Control	6	25.0 ±1.1	-
	Young onset HD	4	27.2 ±4.0	56.8 ± 5.4
Macrophage cytokine profiling	Control	9	45.2 ± 11.9	-
	Premanifest HD	6	47.9 ± 6.6	42.7 ± 1.0
	Early HD	10	46.7 ± 7.3	44.2 ± 2.8
	Moderate HD	5	59.4 ± 7.3	44.8 ± 3.8
Phagocytosis	Control	5	48.7 ± 15.5	-
	HD	5	49.0 ± 10.8	42.6 ± 2.1
TLR4 qPCR	Control	7	45.0 ± 12.2	-
	Premanifest HD	6	43.5 ± 9.0	42.5 ± 2.0
	Early HD	6	48.3 ± 10.1	44.2 ± 3.1
	Moderate HD	7	54.5 ± 16.0	43.2 ± 2.8
Imaging flow cytometry	Control	7	47.4 ± 17.9	-
	HD	7	50.2 ± 13.4	44.6 ± 4.3
STAT flow analysis	Control	18	45.1 ± 14.5	-
	Premanifest HD	11	49.7 ± 8.3	41.1 ± 2.5
	Early HD	11	46.0 ± 13.0	45.8 ± 5.7
	Moderate HD	8	57.1 ± 10.1	44.7 ± 3.4
PCR arrays	Control	10	45.8 ± 9.3	-
	Early HD	10	48.7 ± 8.5	43.9 ± 2.8
Validation+ knock-down cell PCR	Control	10	48.2 ± 13.7	-
	HD	10	52.3 ± 11.1	43.1 ± 2.2
HTT knock-down test	Control	10	42.5± 13.1	-
	HD	10	51.5±7.4	42.8 ± 0.8
Cytokine profile of knock-down cells	Control	9	48.0 ± 9.9	-
	HD	8	51.3 ± 10.6	43.4 ± 1.6

Table A.4: *HTT* CAG repeat length and age for all subjects participating in the study presented in Chapter 5. Cohorts listed separately for each experiment.

Experiment	Subject group	n number	Age (mean±SD)	CAG (mean±SD)
Monocyte migration towards ATP/C5a	Control	10	47.2 ± 16.3	-
	Premanifest HD	4	38.6 ± 6.9	43.0 ± 9.4
	Early HD	5	43.3 ± 16.4	48.4 ± 6.7
	Moderate HD	8	54.4 ± 16.6	45.6 ± 5.3
Monocyte migration towards MCP-1	Control	8	45.1 ± 13.9	-
	Premanifest HD	9	43.0 ± 9.4	42.3 ± 2.8
	Early HD	9	45.3 ± 15.0	46.4 ± 7.7
	Moderate HD	11	61.1 ± 9.7	42.7 ± 2.1
Monocyte migration towards RANTES	Control	6	38.6 ± 13.1	-
	Premanifest HD	4	49.0 ± 11.3	41.57 ± 1.3
	Early HD	5	52.7 ± 11.1	43.2 ± 1.5
	Moderate HD	5	56.3 ± 9.3	42.0 ± 1.6
Macrophage migration towards ATP/C5a	Control	8	47.6 ± 15.3	-
	HD	8	50.1 ± 14.5	44.6 ± 55.5
Macrophage migration towards MCP-1	Control	10	50.5± 15.9	-
	HD	15	59.9± 11.8	42.9 ± 2.3
Macrophage migration towards RANTES	Control	8	50.2 ± 17.8	-
	HD	13	48.9 ± 11.3	42.77 ± 2.1

A.5 Appendix V - PCR signaling array results

Table A.5: Expression changes within the NFκB pathway observed in HD monocytes. Data presented as fold change calculated from $\Delta\Delta$CT values, unpaired two-tailed student t tests used as for statistical analysis.

Gene name	Fold change	p-value
AGT	2.20	0.31
AKT1	1.54	0.03
ATF1	1.16	0.07
BCL10	0.90	0.43
BIRC2	0.95	0.53
CASP1	1.12	0.19
CASP8	0.79	0.23
CCL2	1.57	0.16
CD27	2.02	0.22
CD40	1.51	0.02
CFB	1.01	0.92
CFLAR	0.91	0.48
CHUK	0.77	0.02
CSF2	1.06	0.90
CSF3	0.86	0.69
EDARRADD	1.69	0.32
ELK1	1.17	0.14
ERG1	1.65	0.32
F2R	2.23	0.04
FADD	1.08	0.61
FASLG	1.08	0.61

FOS	1.87	0.06
GJA1	0.61	0.08
HMOX1	1.20	0.82
HTR2B	0.80	0.30
ICAM1	1.41	0.011
IFNB1	1.09	0.75
IFNG	2.60	0.25
IKBKB	1.03	0.78
IKBKE	1.04	0.67
IKBKG	1.21	0.20
IL10	1.85	0.04
IL1A	1.26	0.27
IL1B	1.95	0.19
IL1R1	0.88	0.60
IL6	2.49	0.08
IL8	1.52	0.19
IRAK1	2.00	0.05
IRAK2	1.31	0.12
c-JUN	2.22	0.05
LPAR1	0.95	0.79
LTA	1.14	0.66
LTBR	1.35	0.01
MALT1	1.35	0.56
MAP3K1	1.04	0.77
MYD88	1.26	0.05
NFKB1	1.10	0.37
NFKB2	0.99	0.96

NFKBIA	1.16	0.56
NLRP12	1.26	0.11
NOD1	1.11	0.30
PPM1A	0.96	0.76
RAF1	1.12	0.07
REL	0.97	0.81
RELA	1.15	0.22
RELB	1.21	0.39
RHOA	1.02	0.75
RIPK1	1.10	0.46
SCL3	1.25	0.21
SLC20A1	1.05	0.21
SLC44A2	1.29	0.07
STAT1	1.27	0.30
TBK1	1.03	0.68
TICAM1	1.06	0.64
TICAM2	1.32	0.05
TLR1	0.86	0.46
TLR2	1.48	0.01
TLR3	1.37	0.22
TLR4	1.07	0.59
TLR6	1.09	0.45
TLR7	0.98	0.95
TLR8	0.98	0.92
TLR9	0.79	0.26
TMED4	1.23	0.02
TNF	1.11	0.72

TNFAIP3	1.15	0.41
TNFSRF10A	1.20	0.21
TNFSRF10B	1.04	0.74
TNFRAF14	1.19	0.17
TNFSF10	1.14	0.41
TNFSF14	1.04	0.83
TRADD	1.25	0.06
TRIM12	1.10	0.44

Bibliography

Adams, R. A., Bauer, J., Flick, M. J., Sikorski, S. L., Nuriel, T., Lassmann, H., Degen, J. L. and Akassoglou, K. (2007), 'The fibrin-derived gamma377-395 peptide inhibits microglia activation and suppresses relapsing paralysis in central nervous system autoimmune disease', *J Exp Med* **204**(3), 571–82.

Ajami, B., Bennett, J. L., Krieger, C., Tetzlaff, W. and Rossi, F. M. (2007), 'Local self-renewal can sustain CNS microglia maintenance and function throughout adult life.', *Nat Neurosci* **10**(12), 1538–43.

Alciato, F., Sainaghi, P. P., Sola, D., Castello, L. and Avanzi, G. C. (2010), 'TNF-alpha, IL-6, and IL-1 expression is inhibited by GAS6 in monocytes/macrophages.', *J Leukoc Biol* **87**(5), 869–75.

Alderson, M. R., Armitage, R. J., Tough, T. W., Strockbine, L., Fanslow, W. C. and Spriggs, M. K. (1993), 'CD40 expression by human monocytes: regulation by cytokines and activation of monocytes by the ligand for CD40', *J Exp Med* **178**(2), 669–74.

Altar, C. A., Cai, N., Bliven, T., Juhasz, M., Conner, J. M., Acheson, A. L., Lindsay, R. M. and Wiegand, S. J. (1997), 'Anterograde transport of brain-derived neurotrophic factor and its role in the brain', *Nature* **389**(6653), 856–60.

An, M. C., Zhang, N., Scott, G., Montoro, D., Wittkop, T., Mooney, S., Melov, S.

and Ellerby, L. M. (2012), 'Genetic correction of Huntington's disease phenotypes in induced pluripotent stem cells', *Cell Stem Cell* **11**(2), 253–63.

Anderson, A. J., Cummings, B. J. and Cotman, C. W. (1994), 'Increased immunoreactivity for Jun- and Fos-related proteins in Alzheimer's disease: association with pathology', *Exp Neurol* **125**(2), 286–95.

Andrew, S. E., Goldberg, Y. P., Kremer, B., Telenius, H., Theilmann, J., Adam, S., Starr, E., Squitieri, F., Lin, B. and Kalchman, M. A. (1993), 'The relationship between trinucleotide (CAG) repeat length and clinical features of Huntington's disease', *Nat Genet* **4**(4), 398–403.

Angel, P., Hattori, K., Smeal, T. and Karin, M. (1988), 'The jun proto-oncogene is positively autoregulated by its product, Jun/AP-1', *Cell* **55**(5), 875–85.

Aouadi, M., Tesz, G. J., Nicoloro, S. M., Wang, M., Chouinard, M., Soto, E., Ostroff, G. R. and Czech, M. P. (2009), 'Orally delivered siRNA targeting macrophage Map4k4 suppresses systemic inflammation.', *Nature* **458**(7242), 1180–4.

Arrasate, M., Mitra, S., Schweitzer, E. S., Segal, M. R. and Finkbeiner, S. (2004), 'Inclusion body formation reduces levels of mutant huntingtin and the risk of neuronal death', *Nature* **431**(7010), 805–10.

Aubry, L., Bugi, A., Lefort, N., Rousseau, F., Peschanski, M. and Perrier, A. L. (2008), 'Striatal progenitors derived from human ES cells mature into DARPP32 neurons in vitro and in quinolinic acid-lesioned rats', *Proc Natl Acad Sci USA* **105**(43), 16707–12.

Auffray, C., Sieweke, M. H. and Geissmann, F. (2009), 'Blood monocytes: development, heterogeneity, and relationship with dendritic cells.', *Annu Rev Immunol* **27**, 669–92.

Aziz, N. A., Pijl, H., Frölich, M., van der Graaf, A. W., Roelfsema, F. and Roos,

R. A. (2009), 'Increased hypothalamic-pituitary-adrenal axis activity in Huntington's disease.', *J Clin Endocrinol Metab* **94**(4), 1223–8.

Aziz, N. A., van der Burg, J. M., Landwehrmeyer, G. B., Brundin, P., Stijnen, T., Roos, R. A. and Group, E. S. (2008), 'Weight loss in Huntington disease increases with higher CAG repeat number', *Neurology* **71**(19), 1506–13.

Bachoud-Lévi, A. C., Rémy, P., Nguyen, J. P., Brugières, P., Lefaucheur, J. P., Bourdet, C., Baudic, S., Gaura, V., Maison, P., Haddad, B., Boissè, M. F., Grandmougin, T., Jény, R., Bartolomeo, P., Dalla Barba, G., Degos, J. D., Lisovoski, F., Ergis, A. M., Pailhous, E., Cesaro, P., Hantraye, P. and Peschanski, M. (2000), 'Motor and cognitive improvements in patients with Huntington's disease after neural transplantation', *Lancet* **356**(9246), 1975–9.

Baldo, B., Paganetti, P., Grueninger, S., Marcellin, D., Kaltenbach, L. S., Lo, D. C., Semmelroth, M., Zivanovic, A., Abramowski, D., Smith, D., Lotz, G. P., Bates, G. P. and Weiss, A. (2012), 'TR-FRET-based duplex immunoassay reveals an inverse correlation of soluble and aggregated mutant huntingtin in Huntington's disease', *Chem Biol* **19**(2), 264–75.

Barton, G. M. and Medzhitov, R. (2003), 'Toll-like receptor signaling pathways', *Science* **300**(5625), 1524–5.

Bates, G., Harper, P., Jones, L. and editors (2002), *Huntington's Disease*, Oxford University Press, Oxford.

Beal, M. F., Ferrante, R. J., Swartz, K. J. and Kowall, N. W. (1991), 'Chronic quinolinic acid lesions in rats closely resemble Huntington's disease', *J Neurosci* **11**(6), 1649–59.

Beck, G. and Habicht, G. S. (1996), 'Immunity and the invertebrates', *Sci Am* **275**(5), 60–3, 66.

Beinke, S. and Ley, S. C. (2004), 'Functions of NF-kappaB1 and NF-kappaB2 in immune cell biology.', *Biochem J* **382**(Pt 2), 393–409.

Benn, C. L., Fox, H. and Bates, G. P. (2008), 'Optimisation of region-specific reference gene selection and relative gene expression analysis methods for pre-clinical trials of Huntington's disease', *Mol Neurodegener* **3**, 17.

Bennett, C. F. and Swayze, E. E. (2010), 'RNA targeting therapeutics: molecular mechanisms of antisense oligonucleotides as a therapeutic platform', *Annu Rev Pharmacol Toxicol* **50**, 259–93.

Bennett, E. J., Shaler, T. A., Woodman, B., Ryu, K. Y., Zaitseva, T. S., Becker, C. H., Bates, G. P., Schulman, H. and Kopito, R. R. (2007), 'Global changes to the ubiquitin system in Huntington's disease.', *Nature* **448**(7154), 704–8.

Benraiss, A. and Goldman, S. A. (2011), 'Cellular therapy and induced neuronal replacement for Huntington's disease', *Neurotherapeutics* **8**(4), 577–90.

Bhide, P. G., Day, M., Sapp, E., Schwarz, C., Sheth, A., Kim, J., Young, A. B., Penney, J., Golden, J., Aronin, N. and DiFiglia, M. (1996), 'Expression of normal and mutant huntingtin in the developing brain', *J Neurosci* **16**(17), 5523–35.

Björkqvist, M., Fex, M., Renström, E., Wierup, N., Petersén, A., Gil, J., Bacos, K., Popovic, N., Li, J. Y., Sundler, F., Brundin, P. and Mulder, H. (2005), 'The R6/2 transgenic mouse model of Huntington's disease develops diabetes due to deficient beta-cell mass and exocytosis.', *Hum Mol Genet* **14**(5), 565–74.

Björkqvist, M., Petersén, A., Bacos, K., Isaacs, J., Norléchon, P., Gil, J., Popovic, N., Sundler, F., Bates, G. P., Tabrizi, S. J., Brundin, P. and Mulder, H. (2006), 'Progressive alterations in the hypothalamic-pituitary-adrenal axis in the R6/2 transgenic mouse model of Huntington's disease', *Hum Mol Genet* **15**(10), 1713–21.

Björkqvist, M., Wild, E. J. and Tabrizi, S. J. (2009), 'Harnessing immune alterations in neurodegenerative diseases', *Neuron* **64**(1), 21–4.

Björkqvist, M., Wild, E. J., Thiele, J., Silvestroni, A., Andre, R., Lahiri, N., Raibon, E., Lee, R. V., Benn, C. L., Soulet, D., Magnusson, A., Woodman, B., Landles, C., Pouladi, M. A., Hayden, M. R., Khalili-Shirazi, A., Lowdell, M. W., Brundin, P., Bates, G. P., Leavitt, B. R., Möller, T. and Tabrizi, S. J. (2008), 'A novel pathogenic pathway of immune activation detectable before clinical onset in Huntington's disease', *J Exp Med* **205**(8), 1869–77.

Blundell, M. P., Worth, A., Bouma, G. and Thrasher, A. J. (2010), 'The Wiskott-Aldrich syndrome: The actin cytoskeleton and immune cell function', *Dis Markers* **29**(3-4), 157–75.

Boring, L., Gosling, J., Chensue, S. W., Kunkel, S. L., Farese, R. V., Broxmeyer, H. E. and Charo, I. F. (1997), 'Impaired monocyte migration and reduced type 1 (Th1) cytokine responses in C-C chemokine receptor 2 knockout mice', *J Clin Invest* **100**(10), 2552–61.

Bouchard, J., Truong, J., Bouchard, K., Dunkelberger, D., Desrayaud, S., Moussaoui, S., Tabrizi, S. J., Stella, N. and Muchowski, P. J. (2012), 'Cannabinoid receptor 2 signaling in peripheral immune cells modulates disease onset and severity in mouse models of Huntington's disease', *J Neurosci* **32**(50), 18259–18268.

Boudreau, R. L., McBride, J. L., Martins, I., Shen, S., Xing, Y., Carter, B. J. and Davidson, B. L. (2009), 'Nonallele-specific silencing of mutant and wild-type huntingtin demonstrates therapeutic efficacy in Huntington's disease mice', *Mol Ther* **17**(6), 1053–63.

Bradford, J., Shin, J. Y., Roberts, M., Wang, C. E., Li, X. J. and Li, S. (2009), 'Ex-

pression of mutant huntingtin in mouse brain astrocytes causes age-dependent neurological symptoms.', *Proc Natl Acad Sci USA* **106**(52), 22480–5.

Brinkman, R. R., Mezei, M. M., Theilmann, J., Almqvist, E. and Hayden, M. R. (1997), 'The likelihood of being affected with Huntington disease by a particular age, for a specific CAG size', *Am J Hum Genet* **60**(5), 1202–10.

Brooks, S., Higgs, G., Jones, L. and Dunnett, S. B. (2012), 'Longitudinal analysis of the behavioural phenotype in Hdh(CAG)150 Huntington's disease knock-in mice', *Brain Res Bull* **88**(2-3), 182–8.

Browne, S. E. (2008), 'Mitochondria and Huntington's disease pathogenesis: insight from genetic and chemical models.', *Ann N Y Acad Sci* **1147**, 358–82.

Campesan, S., Green, E. W., Breda, C., Sathyasaikumar, K. V., Muchowski, P. J., Schwarcz, R., Kyriacou, C. P. and Giorgini, F. (2011), 'The kynurenine pathway modulates neurodegeneration in a Drosophila model of Huntington's disease.', *Curr Biol* **21**(11), 961–6.

Cardona, A. E., Pioro, E. P., Sasse, M. E., Kostenko, V., Cardona, S. M., Dijkstra, I. M., Huang, D., Kidd, G., Dombrowski, S., Dutta, R., Lee, J. C., Cook, D. N., Jung, S., Lira, S. A., Littman, D. R. and Ransohoff, R. M. (2006), 'Control of microglial neurotoxicity by the fractalkine receptor', *Nat Neurosci* **9**(7), 917–24.

Carroll, J. B., Warby, S. C., Southwell, A. L., Doty, C. N., Greenlee, S., Skotte, N., Hung, G., Bennett, C. F., Freier, S. M. and Hayden, M. R. (2011), 'Potent and selective antisense oligonucleotides targeting single-nucleotide polymorphisms in the Huntington disease gene / allele-specific silencing of mutant huntingtin', *Mol Ther* **19**(12), 2178–85.

Carter, R. J., Lione, L. A., Humby, T., Mangiarini, L., Mahal, A., Bates, G. P., Dunnett, S. B. and Morton, A. J. (1999), 'Characterization of progressive mo-

tor deficits in mice transgenic for the human Huntington's disease mutation', *J Neurosci* **19**(8), 3248–57.

Chan, W. Y., Kohsaka, S. and Rezaie, P. (2007), 'The origin and cell lineage of microglia: new concepts.', *Brain Res Rev* **53**(2), 344–54.

Chang, D. T., Rintoul, G. L., Pandipati, S. and Reynolds, I. J. (2006), 'Mutant huntingtin aggregates impair mitochondrial movement and trafficking in cortical neurons', *Neurobiol Dis* **22**(2), 388–400.

Chaturvedi, R. K., Adhihetty, P., Shukla, S., Hennessy, T., Calingasan, N., Yang, L., Starkov, A., Kiaei, M., Cannella, M., Sassone, J., Ciammola, A., Squitieri, F. and Beal, M. F. (2009), 'Impaired PGC-1alpha function in muscle in Huntington's disease', *Hum Mol Genet* **18**(16), 3048–65.

Chen-Plotkin, A. S., Sadri-Vakili, G., Yohrling, G. J., Braveman, M. W., Benn, C. L., Glajch, K. E., DiRocco, D. P., Farrell, L. A., Krainc, D., Gines, S., MacDonald, M. E. and Cha, J. H. (2006), 'Decreased association of the transcription factor Sp1 with genes downregulated in Huntington's disease', *Neurobiol Dis* **22**(2), 233–41.

Chesarone, M. A., DuPage, A. G. and Goode, B. L. (2010), 'Unleashing formins to remodel the actin and microtubule cytoskeletons', *Nat Rev Mol Cell Biol* **11**(1), 62–74.

Cho, S. R., Benraiss, A., Chmielnicki, E., Samdani, A., Economides, A. and Goldman, S. A. (2007), 'Induction of neostriatal neurogenesis slows disease progression in a transgenic murine model of Huntington disease', *J Clin Invest* **117**(10), 2889–902.

Choo, Y. S., Johnson, G. V., MacDonald, M., Detloff, P. J. and Lesort, M. (2004), 'Mutant huntingtin directly increases susceptibility of mitochondria to

the calcium-induced permeability transition and cytochrome c release', *Hum Mol Genet* **13**(14), 1407–20.

Ciammola, A., Sassone, J., Alberti, L., Meola, G., Mancinelli, E., Russo, M. A., Squitieri, F. and Silani, V. (2006), 'Increased apoptosis, Huntingtin inclusions and altered differentiation in muscle cell cultures from Huntington's disease subjects', *Cell Death Differ* **13**(12), 2068–78.

Clausen, B. E., Burkhardt, C., Reith, W., Renkawitz, R. and Förster, I. (1999), 'Conditional gene targeting in macrophages and granulocytes using LysMcre mice.', *Transgenic Res* **8**(4), 265–77.

Colin, E., Régulier, E., Perrin, V., Dürr, A., Brice, A., Aebischer, P., Déglon, N., Humbert, S. and Saudou, F. (2005), 'Akt is altered in an animal model of Huntington's disease and in patients', *Eur J Neurosci* **21**(6), 1478–88.

Cong, X., Held, J. M., DeGiacomo, F., Bonner, A., Chen, J. M., Schilling, B., Czerwieniec, G. A., Gibson, B. W. and Ellerby, L. M. (2011), 'Mass spectrometric identification of novel lysine acetylation sites in huntingtin', *Mol Cell Proteomics* **10**(10), M111.009829.

Cui, L., Jeong, H., Borovecki, F., Parkhurst, C. N., Tanese, N. and Krainc, D. (2006), 'Transcriptional repression of PGC-1alpha by mutant huntingtin leads to mitochondrial dysfunction and neurodegeneration', *Cell* **127**(1), 59–69.

Dalrymple, A., Wild, E. J., Joubert, R., Sathasivam, K., Björkqvist, M., Petersén, A., Jackson, G. S., Isaacs, J. D., Kristiansen, M., Bates, G. P., Leavitt, B. R., Keir, G., Ward, M. and Tabrizi, S. J. (2007), 'Proteomic profiling of plasma in Huntington's disease reveals neuroinflammatory activation and biomarker candidates.', *J Proteome Res* **6**(7), 2833–40.

Dan, H. C., Cooper, M. J., Cogswell, P. C., Duncan, J. A., Ting, J. P. and Baldwin,

A. S. (2008), 'Akt-dependent regulation of NFkappaB is controlled by mTOR and Raptor in association with IKK', *Genes Dev* **22**(11), 1490–500.

Davies, S. W., Turmaine, M., Cozens, B. A., DiFiglia, M., Sharp, A. H., Ross, C. A., Scherzinger, E., Wanker, E. E., Mangiarini, L. and Bates, G. P. (1997), 'Formation of neuronal intranuclear inclusions underlies the neurological dysfunction in mice transgenic for the HD mutation', *Cell* **90**(3), 537–48.

Dawe, H. R., Minamide, L. S., Bamburg, J. R. and Cramer, L. P. (2003), 'ADF/cofilin controls cell polarity during fibroblast migration', *Curr Biol* **13**(3), 252–7.

de Almeida, L. P., Ross, C. A., Zala, D., Aebischer, P. and Dóglon, N. (2002), 'Lentiviral-mediated delivery of mutant huntingtin in the striatum of rats induces a selective neuropathology modulated by polyglutamine repeat size, huntingtin expression levels, and protein length.', *J Neurosci* **22**(9), 3473–83.

Deshmane, S. L., Kremlev, S., Amini, S. and Sawaya, B. E. (2009), 'Monocyte chemoattractant protein-1 (MCP-1): an overview.', *J Interferon Cytokine Res* **29**(6), 313–26.

DiFiglia, M., Sapp, E., Chase, K. O., Davies, S. W., Bates, G. P., Vonsattel, J. P. and Aronin, N. (1997), 'Aggregation of huntingtin in neuronal intranuclear inclusions and dystrophic neurites in brain.', *Science* **277**(5334), 1990–3.

DiFiglia, M., Sena-Esteves, M., Chase, K., Sapp, E., Pfister, E., Sass, M., Yoder, J., Reeves, P., Pandey, R. K., Rajeev, K. G., Manoharan, M., Sah, D. W., Zamore, P. D. and Aronin, N. (2007), 'Therapeutic silencing of mutant huntingtin with siRNA attenuates striatal and cortical neuropathology and behavioral deficits.', *Proc Natl Acad Sci USA* **104**(43), 17204–9.

Dillon, C. and Goda, Y. (2005), 'The actin cytoskeleton: integrating form and function at the synapse', *Annu Rev Neurosci* **28**, 25–55.

Diserbo, M., Agin, A., Lamproglou, I., Mauris, J., Staali, F., Multon, E. and Amourette, C. (2002), 'Blood-brain barrier permeability after gamma whole-body irradiation: an in vivo microdialysis study', *Can J Physiol Pharmacol* **80**(7), 670–8.

Djoussé, L., Knowlton, B., Cupples, L. A., Marder, K., Shoulson, I. and Myers, R. H. (2002), 'Weight loss in early stage of Huntington's disease', *Neurology* **59**(9), 1325–30.

Dlugosz, M. and Trylska, J. (2011), 'Secondary structures of native and pathogenic huntingtin N-terminal fragments', *J Phys Chem B* **115**(40), 11597–608.

Dragatsis, I., Levine, M. S. and Zeitlin, S. (2000), 'Inactivation of Hdh in the brain and testis results in progressive neurodegeneration and sterility in mice', *Nat Genet* **26**(3), 300–6.

Dunah, A. W., Jeong, H., Griffin, A., Kim, Y. M., Standaert, D. G., Hersch, S. M., Mouradian, M. M., Young, A. B., Tanese, N. and Krainc, D. (2002), 'Sp1 and TAFII130 transcriptional activity disrupted in early Huntington's disease', *Science* **296**(5576), 2238–43.

Eder, C. (2009), 'Mechanisms of interleukin-1beta release', *Immunobiology* **214**(7), 543–53.

Faber, P. W., Barnes, G. T., Srinidhi, J., Chen, J., Gusella, J. F. and MacDonald, M. E. (1998), 'Huntingtin interacts with a family of WW domain proteins', *Hum Mol Genet* **7**(9), 1463–74.

Fan, J., Gladding, C. M., Wang, L., Zhang, L. Y., Kaufman, A. M., Milnerwood, A. J. and Raymond, L. A. (2012), 'P38 MAPK is involved in enhanced NMDA receptor-dependent excitotoxicity in YAC transgenic mouse model of Huntington disease', *Neurobiol Dis* **45**(3), 999–1009.

Farrer, L. A. (1986), 'Suicide and attempted suicide in Huntington disease: implications for preclinical testing of persons at risk.', *Am J Med Genet* **24**(2), 305–11.

Ferrante, R. J., Kubilus, J. K., Lee, J., Ryu, H., Beesen, A., Zucker, B., Smith, K., Kowall, N. W., Ratan, R. R., Luthi-Carter, R. and Hersch, S. M. (2003), 'Histone deacetylase inhibition by sodium butyrate chemotherapy ameliorates the neurodegenerative phenotype in Huntington's disease mice', *J Neurosci* **23**(28), 9418–27.

Feyeux, M., Bourgois-Rocha, F., Redfern, A., Giles, P., Lefort, N., Aubert, S., Bonnefond, C., Bugi, A., Ruiz, M., Déglon, N., Jones, L., Peschanski, M., Allen, N. D. and Perrier, A. L. (2012), 'Early transcriptional changes linked to naturally occurring Huntington's disease mutations in neural derivatives of human embryonic stem cells', *Hum Mol Genet* **21**(17), 3883–95.

Franke, T. F., Kaplan, D. R., Cantley, L. C. and Toker, A. (1997), 'Direct regulation of the Akt proto-oncogene product by phosphatidylinositol-3,4-bisphosphate', *Science* **275**(5300), 665–8.

Frenkel, D., Maron, R., Burt, D. S. and Weiner, H. L. (2005), 'Nasal vaccination with a proteosome-based adjuvant and glatiramer acetate clears beta-amyloid in a mouse model of alzheimer disease', *J Clin Invest* **115**(9), 2423–33.

Furtado, S., Sossi, V., Hauser, R. A., Samii, A., Schulzer, M., Murphy, C. B., Freeman, T. B. and Stoessl, A. J. (2005), 'Positron emission tomography after fetal transplantation in Huntington's disease', *Ann Neurol* **58**(2), 331–7.

Gauthier, L. R., Charrin, B. C., Borrell-Pagès, M., Dompierre, J. P., Rangone, H., Cordelières, F. P., De Mey, J., MacDonald, M. E., Lessmann, V., Humbert, S. and Saudou, F. (2004), 'Huntingtin controls neurotrophic support and survival

of neurons by enhancing BDNF vesicular transport along microtubules', *Cell* **118**(1), 127–38.

Geissmann, F., Manz, M. G., Jung, S., Sieweke, M. H., Merad, M. and Ley, K. (2010), 'Development of monocytes, macrophages, and dendritic cells', *Science* **327**(5966), 656–61.

Gereige, L. M. and Mikkola, H. K. (2009), 'DNA methylation is a guardian of stem cell self-renewal and multipotency', *Nat Genet* **41**(11), 1164–6.

Ginhoux, F., Greter, M., Leboeuf, M., Nandi, S., See, P., Gokhan, S., Mehler, M. F., Conway, S. J., Ng, L. G., Stanley, E. R., Samokhvalov, I. M. and Merad, M. (2010), 'Fate mapping analysis reveals that adult microglia derive from primitive macrophages', *Science* **330**(6005), 841–5.

Giorgini, F., Guidetti, P., Nguyen, Q., Bennett, S. C. and Muchowski, P. J. (2005), 'A genomic screen in yeast implicates kynurenine 3-monooxygenase as a therapeutic target for Huntington disease.', *Nat Genet* **37**(5), 526–31.

Gómez-Tortosa, E., MacDonald, M. E., Friend, J. C., Taylor, S. A., Weiler, L. J., Cupples, L. A., Srinidhi, J., Gusella, J. F., Bird, E. D., Vonsattel, J. P. and Myers, R. H. (2001), 'Quantitative neuropathological changes in presymptomatic Huntington's disease.', *Ann Neurol* **49**(1), 29–34.

Goodman, A. O. and Barker, R. A. (2011), 'Body composition in premanifest Huntington's disease reveals lower bone density compared to controls', *PLoS Curr* **3**, RRN1214.

Goodman, A. O., Murgatroyd, P. R., Medina-Gomez, G., Wood, N. I., Finer, N., Vidal-Puig, A. J., Morton, A. J. and Barker, R. A. (2008), 'The metabolic profile of early Huntington's disease-a combined human and transgenic mouse study', *Exp Neurol* **210**(2), 691–8.

Gordon, S. and Taylor, P. R. (2005), 'Monocyte and macrophage heterogeneity.', *Nat Rev Immunol* **5**(12), 953–64.

Graham, R. K., Deng, Y., Slow, E. J., Haigh, B., Bissada, N., Lu, G., Pearson, J., Shehadeh, J., Bertram, L., Murphy, Z., Warby, S. C., Doty, C. N., Roy, S., Wellington, C. L., Leavitt, B. R., Raymond, L. A., Nicholson, D. W. and Hayden, M. R. (2006), 'Cleavage at the caspase-6 site is required for neuronal dysfunction and degeneration due to mutant huntingtin.', *Cell* **125**(6), 1179–91.

Graveland, G. A., Williams, R. S. and DiFiglia, M. (1985), 'Evidence for degenerative and regenerative changes in neostriatal spiny neurons in Huntington's disease', *Science* **227**(4688), 770–3.

Gray, M., Shirasaki, D. I., Cepeda, C., André, V. M., Wilburn, B., Lu, X. H., Tao, J., Yamazaki, I., Li, S. H., Sun, Y. E., Li, X. J., Levine, M. S. and Yang, X. W. (2008), 'Full-length human mutant huntingtin with a stable polyglutamine repeat can elicit progressive and selective neuropathogenesis in BACHD mice', *J Neurosci* **28**(24), 6182–95.

Grewal, I. S. and Flavell, R. A. (1998), 'CD40 and CD154 in cell-mediated immunity', *Annu Rev Immunol* **16**, 111–35.

Gross, S. and Piwnica-Worms, D. (2005), 'Real-time imaging of ligand-induced IKK activation in intact cells and in living mice', *Nat Methods* **2**(8), 607–14.

Gu, X., André, V. M., Cepeda, C., Li, S. H., Li, X. J., Levine, M. S. and Yang, X. W. (2007), 'Pathological cell-cell interactions are necessary for striatal pathogenesis in a conditional mouse model of Huntington's disease', *Mol Neurodegener* **2**, 8.

Gu, X., Greiner, E. R., Mishra, R., Kodali, R., Osmand, A., Finkbeiner, S., Steffan, J. S., Thompson, L. M., Wetzel, R. and Yang, X. W. (2009), 'Serines 13

and 16 are critical determinants of full-length human mutant huntingtin induced disease pathogenesis in HD mice.', *Neuron* **64**(6), 828–40.

Gu, X., Li, C., Wei, W., Lo, V., Gong, S., Li, S. H., Iwasato, T., Itohara, S., Li, X. J., Mody, I., Heintz, N. and Yang, X. W. (2005), 'Pathological cell-cell interactions elicited by a neuropathogenic form of mutant Huntingtin contribute to cortical pathogenesis in HD mice', *Neuron* **46**(3), 433–44.

Guidetti, P., Bates, G. P., Graham, R. K., Hayden, M. R., Leavitt, B. R., MacDonald, M. E., Slow, E. J., Wheeler, V. C., Woodman, B. and Schwarcz, R. (2006), 'Elevated brain 3-hydroxykynurenine and quinolinate levels in Huntington disease mice', *Neurobiol Dis* **23**(1), 190–7.

Gusella, J. F., Wexler, N. S., Conneally, P. M., Naylor, S. L., Anderson, M. A., Tanzi, R. E., Watkins, P. C., Ottina, K., Wallace, M. R. and Sakaguchi, A. Y. (1983), 'A polymorphic DNA marker genetically linked to Huntington's disease.', *Nature* **306**(5940), 234–8.

Halliday, G. M., McRitchie, D. A., Macdonald, V., Double, K. L., Trent, R. J. and McCusker, E. (1998), 'Regional specificity of brain atrophy in Huntington's disease.', *Exp Neurol* **154**(2), 663–72.

Hamer, M. and Chida, Y. (2009), 'Physical activity and risk of neurodegenerative disease: a systematic review of prospective evidence', *Psychol Med* **39**(1), 3–11.

Harold, D., Abraham, R., Hollingworth, P., Sims, R., Gerrish, A., Hamshere, M. L., Pahwa, J. S., Moskvina, V., Dowzell, K., Williams, A., Jones, N., Thomas, C., Stretton, A., Morgan, A. R., Lovestone, S., Powell, J., Proitsi, P., Lupton, M. K., Brayne, C., Rubinsztein, D. C., Gill, M., Lawlor, B., Lynch, A., Morgan, K., Brown, K. S., Passmore, P. A., Craig, D., McGuinness, B., Todd, S., Holmes, C., Mann, D., Smith, A. D., Love, S., Kehoe, P. G., Hardy, J., Mead, S., Fox,

N., Rossor, M., Collinge, J., Maier, W., Jessen, F., Schürmann, B., van den Bussche, H., Heuser, I., Kornhuber, J., Wiltfang, J., Dichgans, M., Frölich, L., Hampel, H., Höll, M., Rujescu, D., Goate, A. M., Kauwe, J. S., Cruchaga, C., Nowotny, P., Morris, J. C., Mayo, K., Sleegers, K., Bettens, K., Engelborghs, S., De Deyn, P. P., Van Broeckhoven, C., Livingston, G., Bass, N. J., Gurling, H., McQuillin, A., Gwilliam, R., Deloukas, P., Al-Chalabi, A., Shaw, C. E., Tsolaki, M., Singleton, A. B., Guerreiro, R., Mühleisen, T. W., Nöthen, M. M., Moebus, S., Jöckel, K. H., Klopp, N., Wichmann, H. E., Carrasquillo, M. M., Pankratz, V. S., Younkin, S. G., Holmans, P. A., O'Donovan, M., Owen, M. J. and Williams, J. (2009), 'Genome-wide association study identifies variants at CLU and PICALM associated with Alzheimer's disease', *Nat Genet* **41**(10), 1088–93.

Harper, S. Q., Staber, P. D., He, X., Eliason, S. L., Martins, I. H., Mao, Q., Yang, L., Kotin, R. M., Paulson, H. L. and Davidson, B. L. (2005), 'RNA interference improves motor and neuropathological abnormalities in a Huntington's disease mouse model', *Proc Natl Acad Sci USA* **102**(16), 5820–5.

Hay, D. G., Sathasivam, K., Tobaben, S., Stahl, B., Marber, M., Mestril, R., Mahal, A., Smith, D. L., Woodman, B. and Bates, G. P. (2004), 'Progressive decrease in chaperone protein levels in a mouse model of Huntington's disease and induction of stress proteins as a therapeutic approach', *Hum Mol Genet* **13**(13), 1389–405.

Hayden, M. S. and Ghosh, S. (2012), 'NFκB, the first quarter-century: remarkable progress and outstanding questions', *Genes Dev* **26**(3), 203–34.

Haynes, S. E., Hollopeter, G., Yang, G., Kurpius, D., Dailey, M. E., Gan, W. B. and Julius, D. (2006), 'The P2Y12 receptor regulates microglial activation by extracellular nucleotides', *Nat Neurosci* **9**(12), 1512–9.

Hilditch-Maguire, P., Trettel, F., Passani, L. A., Auerbach, A., Persichetti, F. and

MacDonald, M. E. (2000), 'Huntingtin: an iron-regulated protein essential for normal nuclear and perinuclear organelles', *Hum Mol Genet* **9**(19), 2789–97.

Hockly, E., Richon, V. M., Woodman, B., Smith, D. L., Zhou, X., Rosa, E., Sathasivam, K., Ghazi-Noori, S., Mahal, A., Lowden, P. A., Steffan, J. S., Marsh, J. L., Thompson, L. M., Lewis, C. M., Marks, P. A. and Bates, G. P. (2003), 'Suberoylanilide hydroxamic acid, a histone deacetylase inhibitor, ameliorates motor deficits in a mouse model of Huntington's disease.', *Proc Natl Acad Sci USA* **100**(4), 2041–6.

Hodges, A., Strand, A. D., Aragaki, A. K., Kuhn, A., Sengstag, T., Hughes, G., Elliston, L. A., Hartog, C., Goldstein, D. R., Thu, D., Hollingsworth, Z. R., Collin, F., Synek, B., Holmans, P. A., Young, A. B., Wexler, N. S., Delorenzi, M., Kooperberg, C., Augood, S. J., Faull, R. L., Olson, J. M., Jones, L. and Luthi-Carter, R. (2006), 'Regional and cellular gene expression changes in human Huntington's disease brain.', *Hum Mol Genet* **15**(6), 965–77.

Hodgson, J. G., Agopyan, N., Gutekunst, C. A., Leavitt, B. R., LePiane, F., Singaraja, R., Smith, D. J., Bissada, N., McCutcheon, K., Nasir, J., Jamot, L., Li, X. J., Stevens, M. E., Rosemond, E., Roder, J. C., Phillips, A. G., Rubin, E. M., Hersch, S. M. and Hayden, M. R. (1999), 'A YAC mouse model for Huntington's disease with full-length mutant huntingtin, cytoplasmic toxicity, and selective striatal neurodegeneration', *Neuron* **23**(1), 181–92.

Hoek, R. M., Ruuls, S. R., Murphy, C. A., Wright, G. J., Goddard, R., Zurawski, S. M., Blom, B., Homola, M. E., Streit, W. J., Brown, M. H., Barclay, A. N. and Sedgwick, J. D. (2000), 'Down-regulation of the macrophage lineage through interaction with OX2 (CD200)', *Science* **290**(5497), 1768–71.

Holmberg, C. I., Staniszewski, K. E., Mensah, K. N., Matouschek, A. and Morimoto, R. I. (2004), 'Inefficient degradation of truncated polyglutamine proteins

by the proteasome', *EMBO J* **23**(21), 4307–18.

Holmes, C., Cunningham, C., Zotova, E., Woolford, J., Dean, C., Kerr, S., Culliford, D. and Perry, V. H. (2009), 'Systemic inflammation and disease progression in Alzheimer disease', *Neurology* **73**(10), 768–74.

Hoogeveen, A. T., Willemsen, R., Meyer, N., de Rooij, K. E., Roos, R. A., van Ommen, G. J. and Galjaard, H. (1993), 'Characterization and localization of the Huntington disease gene product', *Hum Mol Genet* **2**(12), 2069–73.

Huang, T. Y., DerMardirossian, C. and Bokoch, G. M. (2006), 'Cofilin phosphatases and regulation of actin dynamics', *Curr Opin Cell Biol* **18**(1), 26–31.

Hunot, S., Brugg, B., Ricard, D., Michel, P. P., Muriel, M. P., Ruberg, M., Faucheux, B. A., Agid, Y. and Hirsch, E. C. (1997), 'Nuclear translocation of NF-kappaB is increased in dopaminergic neurons of patients with Parkinson's disease', *Proc Natl Acad Sci USA* **94**(14), 7531–6.

Huntington, G. (1872), 'On Chorea', *In Medical and Surgical Reporter* **26**, 320–321.

Huntington Study Group (1996), 'Unified Huntington's Disease Rating Scale: reliability and consistency.', *Mov Disord* **11**(2), 136–42.

Hurelbrink, C. B., Armstrong, R. J., Dunnett, S. B., Rosser, A. E. and Barker, R. A. (2002), 'Neural cells from primary human striatal xenografts migrate extensively in the adult rat CNS', *Eur J Neurosci* **15**(7), 1255–66.

Imarisio, S., Carmichael, J., Korolchuk, V., Chen, C. W., Saiki, S., Rose, C., Krishna, G., Davies, J. E., Ttofi, E., Underwood, B. R. and Rubinsztein, D. C. (2008), 'Huntington's disease: from pathology and genetics to potential therapies.', *Biochem J* **412**(2), 191–209.

Imhof, B. A. and Aurrand-Lions, M. (2004), 'Adhesion mechanisms regulating the migration of monocytes.', *Nat Rev Immunol* **4**(6), 432–44.

Inoue, K. (2002), 'Microglial activation by purines and pyrimidines', *Glia* **40**(2), 156–63.

Ishida, Y., Gao, J. L. and Murphy, P. M. (2008), 'Chemokine receptor CX3CR1 mediates skin wound healing by promoting macrophage and fibroblast accumulation and function', *J Immunol* **180**(1), 569–79.

Israël, A. (2000), 'The IKK complex: an integrator of all signals that activate NF-kappaB?', *Trends Cell Biol* **10**(4), 129–33.

Jacobsen, J. C., Bawden, C. S., Rudiger, S. R., McLaughlan, C. J., Reid, S. J., Waldvogel, H. J., MacDonald, M. E., Gusella, J. F., Walker, S. K., Kelly, J. M., Webb, G. C., Faull, R. L., Rees, M. I. and Snell, R. G. (2010), 'An ovine transgenic Huntington's disease model', *Hum Mol Genet* **19**(10), 1873–82.

Jensen, L. J., Kuhn, M., Stark, M., Chaffron, S., Creevey, C., Muller, J., Doerks, T., Julien, P., Roth, A., Simonovic, M., Bork, P. and von Mering, C. (2009), 'STRING 8–a global view on proteins and their functional interactions in 630 organisms', *Nucleic Acids Res* **37**(Database issue), D412–6.

Jones, G. E. (2000), 'Cellular signaling in macrophage migration and chemotaxis', *J Leukoc Biol* **68**(5), 593–602.

Kaltschmidt, B., Uherek, M., Volk, B., Baeuerle, P. A. and Kaltschmidt, C. (1997), 'Transcription factor NF-kappaB is activated in primary neurons by amyloid beta peptides and in neurons surrounding early plaques from patients with Alzheimer disease', *Proc Natl Acad Sci USA* **94**(6), 2642–7.

Kang, F., Purich, D. L. and Southwick, F. S. (1999), 'Profilin promotes barbed-end actin filament assembly without lowering the critical concentration', *J Biol Chem* **274**(52), 36963–72.

Kazantsev, A., Preisinger, E., Dranovsky, A., Goldgaber, D. and Housman, D. (1999), 'Insoluble detergent-resistant aggregates form between pathological and nonpathological lengths of polyglutamine in mammalian cells', *Proc Natl Acad Sci USA* **96**(20), 11404–9.

Kazemi-Esfarjani, P. and Benzer, S. (2000), 'Genetic suppression of polyglutamine toxicity in Drosophila', *Science* **287**(5459), 1837–40.

Kegel, K. B., Kim, M., Sapp, E., McIntyre, C., Castaño, J. G., Aronin, N. and DiFiglia, M. (2000), 'Huntingtin expression stimulates endosomal-lysosomal activity, endosome tubulation, and autophagy', *J Neurosci* **20**(19), 7268–78.

Khoshnan, A., Ko, J., Watkin, E. E., Paige, L. A., Reinhart, P. H. and Patterson, P. H. (2004), 'Activation of the IkappaB kinase complex and nuclear factor-kappaB contributes to mutant huntingtin neurotoxicity.', *J Neurosci* **24**(37), 7999–8008.

Khoshnan, A. and Patterson, P. H. (2011), 'The role of IκB kinase complex in the neurobiology of Huntington's disease', *Neurobiol Dis* **43**(2), 305–11.

Kierdorf, K., Erny, D., Goldmann, T., Sander, V., Schulz, C., Perdiguero, E. G., Wieghofer, P., Heinrich, A., Riemke, P., Hlscher, C., Mller, D. N., Luckow, B., Brocker, T., Debowski, K., Fritz, G., Opdenakker, G., Diefenbach, A., Biber, K., Heikenwalder, M., Geissmann, F., Rosenbauer, F. and Prinz, M. (2013), 'Microglia emerge from erythromyeloid precursors via pu.1- and irf8-dependent pathways', *Nat Neurosci* **16**(3), 273–80.

Kim, M. W., Chelliah, Y., Kim, S. W., Otwinowski, Z. and Bezprozvanny, I. (2009), 'Secondary structure of Huntingtin amino-terminal region', *Structure* **17**(9), 1205–12.

Ko, J., Ou, S. and Patterson, P. H. (2001), 'New anti-huntingtin monoclonal anti-

bodies: implications for huntingtin conformation and its binding proteins.', *Brain Res Bull* **56**(3-4), 319–29.

Koizumi, S., Shigemoto-Mogami, Y., Nasu-Tada, K., Shinozaki, Y., Ohsawa, K., Tsuda, M., Joshi, B. V., Jacobson, K. A., Kohsaka, S. and Inoue, K. (2007), 'UDP acting at P2Y6 receptors is a mediator of microglial phagocytosis', *Nature* **446**(7139), 1091–5.

Kopyov, O. V., Jacques, S., Lieberman, A., Duma, C. M. and Eagle, K. S. (1998), 'Safety of intrastriatal neurotransplantation for Huntington's disease patients', *Exp Neurol* **149**(1), 97–108.

Kuhn, A., Goldstein, D. R., Hodges, A., Strand, A. D., Sengstag, T., Kooperberg, C., Becanovic, K., Pouladi, M. A., Sathasivam, K., Cha, J. H., Hannan, A. J., Hayden, M. R., Leavitt, B. R., Dunnett, S. B., Ferrante, R. J., Albin, R., Shelbourne, P., Delorenzi, M., Augood, S. J., Faull, R. L., Olson, J. M., Bates, G. P., Jones, L. and Luthi-Carter, R. (2007), 'Mutant huntingtin's effects on striatal gene expression in mice recapitulate changes observed in human Huntington's disease brain and do not differ with mutant huntingtin length or wild-type huntingtin dosage', *Hum Mol Genet* **16**(15), 1845–61.

Kumar, H., Kawai, T. and Akira, S. (2009), 'Toll-like receptors and innate immunity.', *Biochem Biophys Res Commun* **388**(4), 621–5.

Kurihara, T., Warr, G., Loy, J. and Bravo, R. (1997), 'Defects in macrophage recruitment and host defense in mice lacking the CCR2 chemokine receptor', *J Exp Med* **186**(10), 1757–62.

Kwan, W., Magnusson, A., Chou, A., Adame, A., Carson, M. J., Kohsaka, S., Masliah, E., Möller, T., Ransohoff, R., Tabrizi, S. J., Björkqvist, M. and Muchowski, P. J. (2012a), 'Bone marrow transplantation confers modest benefits in mouse models of Huntington's disease', *J Neurosci* **32**(1), 133–42.

Kwan, W., Träger, U., Davalos, D., Chou, A., Bouchard, J., Andre, R., Miller, A., Weiss, A., Giorgini, F., Cheah, C., Möller, T., Stella, N., Akassoglou, K., Tabrizi, S. J. and Muchowski, P. J. (2012b), 'Mutant huntingtin impairs immune cell migration in Huntington disease', *J Clin Invest* **122**(12), 4737–47.

Labbadia, J., Cunliffe, H., Weiss, A., Katsyuba, E., Sathasivam, K., Seredenina, T., Woodman, B., Moussaoui, S., Frentzel, S., Luthi-Carter, R., Paganetti, P. and Bates, G. P. (2011), 'Altered chromatin architecture underlies progressive impairment of the heat shock response in mouse models of Huntington disease', *J Clin Invest* **121**(8), 3306–19.

Lacy, P. and Stow, J. L. (2011), 'Cytokine release from innate immune cells: association with diverse membrane trafficking pathways', *Blood* **118**(1), 9–18.

Laird, M. H., Rhee, S. H., Perkins, D. J., Medvedev, A. E., Piao, W., Fenton, M. J. and Vogel, S. N. (2009), 'TLR4/MyD88/PI3K interactions regulate TLR4 signaling', *J Leukoc Biol* **85**(6), 966–77.

Lambert, J. C., Heath, S., Even, G., Campion, D., Sleegers, K., Hiltunen, M., Combarros, O., Zelenika, D., Bullido, M. J., Tavernier, B., Letenneur, L., Bettens, K., Berr, C., Pasquier, F., Fiévet, N., Barberger-Gateau, P., Engelborghs, S., De Deyn, P., Mateo, I., Franck, A., Helisalmi, S., Porcellini, E., Hanon, O., de Pancorbo, M. M., Lendon, C., Dufouil, C., Jaillard, C., Leveillard, T., Alvarez, V., Bosco, P., Mancuso, M., Panza, F., Nacmias, B., Bossù, P., Piccardi, P., Annoni, G., Seripa, D., Galimberti, D., Hannequin, D., Licastro, F., Soininen, H., Ritchie, K., Blanché, H., Dartigues, J. F., Tzourio, C., Gut, I., Van Broeckhoven, C., Alpérovitch, A., Lathrop, M., Amouyel, P. and European Alzheimer's Disease Initiative Investigators (2009), 'Genome-wide association study identifies variants at CLU and CR1 associated with Alzheimer's disease', *Nat Genet* **41**(10), 1094–9.

Landles, C., Sathasivam, K., Weiss, A., Woodman, B., Moffitt, H., Finkbeiner, S., Sun, B., Gafni, J., Ellerby, L. M., Trottier, Y., Richards, W. G., Osmand, A., Paganetti, P. and Bates, G. P. (2010), 'Proteolysis of mutant huntingtin produces an exon 1 fragment that accumulates as an aggregated protein in neuronal nuclei in Huntington disease.', *J Biol Chem* **285**(12), 8808–23.

Lang, A. E., Gill, S., Patel, N. K., Lozano, A., Nutt, J. G., Penn, R., Brooks, D. J., Hotton, G., Moro, E., Heywood, P., Brodsky, M. A., Burchiel, K., Kelly, P., Dalvi, A., Scott, B., Stacy, M., Turner, D., Wooten, V. G., Elias, W. J., Laws, E. R., Dhawan, V., Stoessl, A. J., Matcham, J., Coffey, R. J. and Traub, M. (2006), 'Randomized controlled trial of intraputamenal glial cell line-derived neurotrophic factor infusion in Parkinson disease', *Ann Neurol* **59**(3), 459–66.

Lanska, D. J., Lanska, M. J., Lavine, L. and Schoenberg, B. S. (1988), 'Conditions associated with Huntington's disease at death. A case-control study', *Arch Neurol* **45**(8), 878–80.

Leavitt, B. R., van Raamsdonk, J. M., Shehadeh, J., Fernandes, H., Murphy, Z., Graham, R. K., Wellington, C. L., Raymond, L. A. and Hayden, M. R. (2006), 'Wild-type huntingtin protects neurons from excitotoxicity', *J Neurochem* **96**(4), 1121–9.

Lee, J. H., Lee, J. M., Ramos, E. M., Gillis, T., Mysore, J. S., Kishikawa, S., Hadzi, T., Hendricks, A. E., Hayden, M. R., Morrison, P. J., Nance, M., Ross, C. A., Margolis, R. L., Squitieri, F., Gellera, C., Gomez-Tortosa, E., Ayuso, C., Suchowersky, O., Trent, R. J., McCusker, E., Novelletto, A., Frontali, M., Jones, R., Ashizawa, T., Frank, S., Saint-Hilaire, M. H., Hersch, S. M., Rosas, H. D., Lucente, D., Harrison, M. B., Zanko, A., Abramson, R. K., Marder, K., Sequeiros, J., Landwehrmeyer, G. B., Shoulson, I., Myers, R. H., MacDonald, M. E., Gusella, J. F. and Registry Study of the European Huntington's Disease Network and Huntington Study Group COHORT project (2012), 'TAA repeat

variation in the GRIK2 gene does not influence age at onset in Huntington's disease', *Biochem Biophys Res Commun* **424**(3), 404–8.

Leung, K. K., Clarkson, M. J., Bartlett, J. W., Clegg, S., Jack, C. R., Weiner, M. W., Fox, N. C., Ourselin, S. and Alzheimer's Disease Neuroimaging Initiative (2010), 'Robust atrophy rate measurement in Alzheimer's disease using multi-site serial MRI: tissue-specific intensity normalization and parameter selection.', *Neuroimage* **50**(2), 516–23.

Levy, D. E. and Darnell, J. E. (2002), 'Stats: transcriptional control and biological impact.', *Nat Rev Mol Cell Biol* **3**(9), 651–62.

Li, J. Y., Popovic, N. and Brundin, P. (2005), 'The use of the R6 transgenic mouse models of Huntington's disease in attempts to develop novel therapeutic strategies.', *NeuroRx* **2**(3), 447–64.

Li, S. H., Cheng, A. L., Zhou, H., Lam, S., Rao, M., Li, H. and Li, X. J. (2002), 'Interaction of Huntington disease protein with transcriptional activator Sp1', *Mol Cell Biol* **22**(5), 1277–87.

Li, S. H., Schilling, G., Young, W. S., Li, X. J., Margolis, R. L., Stine, O. C., Wagster, M. V., Abbott, M. H., Franz, M. L. and Ranen, N. G. (1993), 'Huntington's disease gene (IT15) is widely expressed in human and rat tissues.', *Neuron* **11**(5), 985–93.

Li, W., Serpell, L. C., Carter, W. J., Rubinsztein, D. C. and Huntington, J. A. (2006), 'Expression and characterization of full-length human huntingtin, an elongated HEAT repeat protein.', *J Biol Chem* **281**(23), 15916–22.

Liévens, J. C., Woodman, B., Mahal, A., Spasic-Boscovic, O., Samuel, D., Kerkerian-Le Goff, L. and Bates, G. P. (2001), 'Impaired glutamate uptake in the R6 Huntington's disease transgenic mice', *Neurobiol Dis* **8**(5), 807–21.

Lin, C. H., Tallaksen-Greene, S., Chien, W. M., Cearley, J. A., Jackson, W. S.,

Crouse, A. B., Ren, S., Li, X. J., Albin, R. L. and Detloff, P. J. (2001), 'Neurological abnormalities in a knock-in mouse model of Huntington's disease.', *Hum Mol Genet* **10**(2), 137–44.

Lione, L. A., Carter, R. J., Hunt, M. J., Bates, G. P., Morton, A. J. and Dunnett, S. B. (1999), 'Selective discrimination learning impairments in mice expressing the human Huntington's disease mutation', *J Neurosci* **19**(23), 10428–37.

Lombardi, M. S., Jaspers, L., Spronkmans, C., Gellera, C., Taroni, F., Di Maria, E., Donato, S. D. and Kaemmerer, W. F. (2009), 'A majority of Huntington's disease patients may be treatable by individualized allele-specific RNA interference', *Exp Neurol* **217**(2), 312–9.

Lunkes, A., Lindenberg, K. S., Ben-Haïem, L., Weber, C., Devys, D., Landwehrmeyer, G. B., Mandel, J. L. and Trottier, Y. (2002), 'Proteases acting on mutant huntingtin generate cleaved products that differentially build up cytoplasmic and nuclear inclusions', *Mol Cell* **10**(2), 259–69.

Luthi-Carter, R., Strand, A. D., Hanson, S. A., Kooperberg, C., Schilling, G., La Spada, A. R., Merry, D. E., Young, A. B., Ross, C. A., Borchelt, D. R. and Olson, J. M. (2002), 'Polyglutamine and transcription: gene expression changes shared by DRPLA and Huntington's disease mouse models reveal context-independent effects', *Hum Mol Genet* **11**(17), 1927–37.

Luthi-Carter, R., Strand, A., Peters, N. L., Solano, S. M., Hollingsworth, Z. R., Menon, A. S., Frey, A. S., Spektor, B. S., Penney, E. B., Schilling, G., Ross, C. A., Borchelt, D. R., Tapscott, S. J., Young, A. B., Cha, J. H. and Olson, J. M. (2000), 'Decreased expression of striatal signaling genes in a mouse model of Huntington's disease', *Hum Mol Genet* **9**(9), 1259–71.

Lynch, G., Kramar, E. A., Rex, C. S., Jia, Y., Chappas, D., Gall, C. M. and Simmons, D. A. (2007), 'Brain-derived neurotrophic factor restores synap-

tic plasticity in a knock-in mouse model of Huntington's disease', *J Neurosci* **27**(16), 4424–34.

MacDonald, M. E., Barnes, G., Srinidhi, J., Duyao, M. P., Ambrose, C. M., Myers, R. H., Gray, J., Conneally, P. M., Young, A. and Penney, J. (1993), 'Gametic but not somatic instability of CAG repeat length in Huntington's disease.', *J Med Genet* **30**(12), 982–6.

MacDonald, M. E., Vonsattel, J. P., Shrinidhi, J., Couropmitree, N. N., Cupples, L. A., Bird, E. D., Gusella, J. F. and Myers, R. H. (1999), 'Evidence for the GluR6 gene associated with younger onset age of Huntington's disease.', *Neurology* **53**(6), 1330–2.

Manderson, A. P., Kay, J. G., Hammond, L. A., Brown, D. L. and Stow, J. L. (2007), 'Subcompartments of the macrophage recycling endosome direct the differential secretion of IL-6 and TNFalpha', *J Cell Biol* **178**(1), 57–69.

Mangiarini, L., Sathasivam, K., Seller, M., Cozens, B., Harper, A., Hetherington, C., Lawton, M., Trottier, Y., Lehrach, H., Davies, S. W. and Bates, G. P. (1996), 'Exon 1 of the HD gene with an expanded CAG repeat is sufficient to cause a progressive neurological phenotype in transgenic mice.', *Cell* **87**(3), 493–506.

Markianos, M., Panas, M., Kalfakis, N. and Vassilopoulos, D. (2005), 'Plasma testosterone in male patients with Huntington's disease: relations to severity of illness and dementia.', *Ann Neurol* **57**(4), 520–5.

Martinez, F. O., Gordon, S., Locati, M. and Mantovani, A. (2006), 'Transcriptional profiling of the human monocyte-to-macrophage differentiation and polarization: new molecules and patterns of gene expression.', *J Immunol* **177**(10), 7303–11.

Martinez-Vicente, M., Talloczy, Z., Wong, E., Tang, G., Koga, H., Kaushik, S., de Vries, R., Arias, E., Harris, S., Sulzer, D. and Cuervo, A. M. (2010), 'Cargo

recognition failure is responsible for inefficient autophagy in Huntington's disease.', *Nat Neurosci* **13**(5), 567–76.

Mattila, P. K. and Lappalainen, P. (2008), 'Filopodia: molecular architecture and cellular functions', *Nat Rev Mol Cell Biol* **9**(6), 446–54.

Mattson, M. P. and Meffert, M. K. (2006), 'Roles for NF-kappaB in nerve cell survival, plasticity, and disease', *Cell Death Differ* **13**(5), 852–60.

McBride, J. L., Boudreau, R. L., Harper, S. Q., Staber, P. D., Monteys, A. M., Martins, I., Gilmore, B. L., Burstein, H., Peluso, R. W., Polisky, B., Carter, B. J. and Davidson, B. L. (2008), 'Artificial miRNAs mitigate shRNA-mediated toxicity in the brain: implications for the therapeutic development of RNAi', *Proc Natl Acad Sci USA* **105**(15), 5868–73.

McBride, J. L., Pitzer, M. R., Boudreau, R. L., Dufour, B., Hobbs, T., Ojeda, S. R. and Davidson, B. L. (2011), 'Preclinical safety of RNAi-mediated HTT suppression in the rhesus macaque as a potential therapy for Huntington's disease', *Mol Ther* **19**(12), 2152–62.

Meade, C. A., Deng, Y. P., Fusco, F. R., Del Mar, N., Hersch, S., Goldowitz, D. and Reiner, A. (2002), 'Cellular localization and development of neuronal intranuclear inclusions in striatal and cortical neurons in R6/2 transgenic mice.', *J Comp Neurol* **449**(3), 241–69.

Mebius, R. E. and Kraal, G. (2005), 'Structure and function of the spleen', *Nat Rev Immunol* **5**(8), 606–16.

Menalled, L. B., Sison, J. D., Dragatsis, I., Zeitlin, S. and Chesselet, M. F. (2003), 'Time course of early motor and neuropathological anomalies in a knock-in mouse model of Huntington's disease with 140 CAG repeats', *J Comp Neurol* **465**(1), 11–26.

Merad, M., Manz, M. G., Karsunky, H., Wagers, A., Peters, W., Charo, I., Weiss-

man, I. L., Cyster, J. G. and Engleman, E. G. (2002), 'Langerhans cells renew in the skin throughout life under steady-state conditions.', *Nat Immunol* **3**(12), 1135–41.

Mestre, T., Ferreira, J., Coelho, M. M., Rosa, M. and Sampaio, C. (2009), 'Therapeutic interventions for symptomatic treatment in Huntington's disease', *Cochrane Database Syst Rev* (3), CD006456.

Mielcarek, M., Benn, C. L., Franklin, S. A., Smith, D. L., Woodman, B., Marks, P. A. and Bates, G. P. (2011), 'SAHA decreases HDAC 2 and 4 levels in vivo and improves molecular phenotypes in the R6/2 mouse model of Huntington's disease', *PLoS One* **6**(11), e27746.

Mihm, M. J., Amann, D. M., Schanbacher, B. L., Altschuld, R. A., Bauer, J. A. and Hoyt, K. R. (2007), 'Cardiac dysfunction in the R6/2 mouse model of Huntington's disease', *Neurobiol Dis* **25**(2), 297–308.

Milakovic, T., Quintanilla, R. A. and Johnson, G. V. (2006), 'Mutant huntingtin expression induces mitochondrial calcium handling defects in clonal striatal cells: functional consequences', *J Biol Chem* **281**(46), 34785–95.

Miller, A. M. and Stella, N. (2009), 'Microglial cell migration stimulated by ATP and C5a involve distinct molecular mechanisms: quantification of migration by a novel near-infrared method', *Glia* **57**(8), 875–83.

Miller, J., Arrasate, M., Brooks, E., Libeu, C. P., Legleiter, J., Hatters, D., Curtis, J., Cheung, K., Krishnan, P., Mitra, S., Widjaja, K., Shaby, B. A., Lotz, G. P., Newhouse, Y., Mitchell, E. J., Osmand, A., Gray, M., Thulasiramin, V., Saudou, F., Segal, M., Yang, X. W., Masliah, E., Thompson, L. M., Muchowski, P. J., Weisgraber, K. H. and Finkbeiner, S. (2011), 'Identifying polyglutamine protein species in situ that best predict neurodegeneration', *Nat Chem Biol* **7**(12), 925–34.

Milnerwood, A. J., Gladding, C. M., Pouladi, M. A., Kaufman, A. M., Hines, R. M., Boyd, J. D., Ko, R. W., Vasuta, O. C., Graham, R. K., Hayden, M. R., Murphy, T. H. and Raymond, L. A. (2010), 'Early increase in extrasynaptic NMDA receptor signaling and expression contributes to phenotype onset in Huntington's disease mice', *Neuron* **65**(2), 178–90.

Miyamoto, S. (2011), 'Nuclear initiated NF-κB signaling: NEMO and ATM take center stage', *Cell Res* **21**(1), 116–30.

Mochel, F., Charles, P., Seguin, F., Barritault, J., Coussieu, C., Perin, L., Le Bouc, Y., Gervais, C., Carcelain, G., Vassault, A., Feingold, J., Rabier, D. and Durr, A. (2007), 'Early energy deficit in Huntington disease: identification of a plasma biomarker traceable during disease progression', *PLoS One* **2**(7), e647.

Moffitt, H., McPhail, G. D., Woodman, B., Hobbs, C. and Bates, G. P. (2009), 'Formation of polyglutamine inclusions in a wide range of non-CNS tissues in the HdhQ150 knock-in mouse model of Huntington's disease', *PLoS One* **4**(11), e8025.

Moser, B., Wolf, M., Walz, A. and Loetscher, P. (2004), 'Chemokines: multiple levels of leukocyte migration control.', *Trends Immunol* **25**(2), 75–84.

Mosser, D. M. and Edwards, J. P. (2008), 'Exploring the full spectrum of macrophage activation.', *Nat Rev Immunol* **8**(12), 958–69.

Munsie, L., Caron, N., Atwal, R. S., Marsden, I., Wild, E. J., Bamburg, J. R., Tabrizi, S. J. and Truant, R. (2011), 'Mutant huntingtin causes defective actin remodeling during stress: defining a new role for transglutaminase 2 in neurodegenerative disease', *Hum Mol Genet* **20**(10), 1937–51.

Myers, R. H. (2004), 'Huntington's disease genetics.', *NeuroRx* **1**(2), 255–62.

Myre, M. A., Lumsden, A. L., Thompson, M. N., Wasco, W., MacDonald, M. E.

and Gusella, J. F. (2011), 'Deficiency of huntingtin has pleiotropic effects in the social amoeba Dictyostelium discoideum', *PLoS Genet* **7**(4), e1002052.

Nance, M. A. and Myers, R. H. (2001), 'Juvenile onset Huntington's disease-clinical and research perspectives', *Ment Retard Dev Disabil Res Rev* **7**(3), 153–7.

Nasir, J., Floresco, S. B., O'Kusky, J. R., Diewert, V. M., Richman, J. M., Zeisler, J., Borowski, A., Marth, J. D., Phillips, A. G. and Hayden, M. R. (1995), 'Targeted disruption of the Huntington's disease gene results in embryonic lethality and behavioral and morphological changes in heterozygotes', *Cell* **81**(5), 811–23.

Nicholls, D. G. (2009), 'Spare respiratory capacity, oxidative stress and excitotoxicity', *Biochem Soc Trans* **37**(Pt 6), 1385–8.

Nimmerjahn, A., Kirchhoff, F. and Helmchen, F. (2005), 'Resting microglial cells are highly dynamic surveillants of brain parenchyma in vivo.', *Science* **308**(5726), 1314–8.

Nobes, C. D. and Hall, A. (1995), 'Rho, rac, and cdc42 GTPases regulate the assembly of multimolecular focal complexes associated with actin stress fibers, lamellipodia, and filopodia', *Cell* **81**(1), 53–62.

Novak, M. J. and Tabrizi, S. J. (2010), 'Huntington's disease', *BMJ* **340**, c3109.

Nucifora, F. C., Sasaki, M., Peters, M. F., Huang, H., Cooper, J. K., Yamada, M., Takahashi, H., Tsuji, S., Troncoso, J., Dawson, V. L., Dawson, T. M. and Ross, C. A. (2001), 'Interference by huntingtin and atrophin-1 with CBP-mediated transcription leading to cellular toxicity', *Science* **291**(5512), 2423–8.

Okun, E., Griffioen, K. J., Lathia, J. D., Tang, S. C., Mattson, M. P. and Arumugam, T. V. (2009), 'Toll-like receptors in neurodegeneration.', *Brain Res Rev* **59**(2), 278–92.

Okun, M. S., DeLong, M. R., Hanfelt, J., Gearing, M. and Levey, A. (2004), 'Plasma testosterone levels in Alzheimer and Parkinson diseases', *Neurology* **62**(3), 411–3.

O'Neill, L. A. and Kaltschmidt, C. (1997), 'NF-kappa B: a crucial transcription factor for glial and neuronal cell function', *Trends Neurosci* **20**(6), 252–8.

Pahl, H. L. (1999), 'Activators and target genes of Rel/NF-kappaB transcription factors.', *Oncogene* **18**(49), 6853–66.

Palazuelos, J., Aguado, T., Pazos, M. R., Julien, B., Carrasco, C., Resel, E., Sagredo, O., Benito, C., Romero, J., Azcoitia, I., Fernández-Ruiz, J., Guzmán, M. and Galve-Roperh, I. (2009), 'Microglial CB2 cannabinoid receptors are neuroprotective in Huntington's disease excitotoxicity', *Brain* **132**(Pt 11), 3152–64.

Palfi, S., Condé, F., Riche, D., Brouillet, E., Dautry, C., Mittoux, V., Chibois, A., Peschanski, M. and Hantraye, P. (1998), 'Fetal striatal allografts reverse cognitive deficits in a primate model of Huntington disease', *Nat Med* **4**(8), 963–6.

Panov, A. V., Gutekunst, C. A., Leavitt, B. R., Hayden, M. R., Burke, J. R., Strittmatter, W. J. and Greenamyre, J. T. (2002), 'Early mitochondrial calcium defects in Huntington's disease are a direct effect of polyglutamines', *Nat Neurosci* **5**(8), 731–6.

Park, I. H., Arora, N., Huo, H., Maherali, N., Ahfeldt, T., Shimamura, A., Lensch, M. W., Cowan, C., Hochedlinger, K. and Daley, G. Q. (2008), 'Disease-specific induced pluripotent stem cells', *Cell* **134**(5), 877–86.

Parker, J. A., Connolly, J. B., Wellington, C., Hayden, M., Dausset, J. and Neri, C. (2001), 'Expanded polyglutamines in Caenorhabditis elegans cause axonal abnormalities and severe dysfunction of PLM mechanosensory neurons without cell death', *Proc Natl Acad Sci USA* **98**(23), 13318–23.

Passlick, B., Flieger, D. and Ziegler-Heitbrock, H. W. (1989), 'Identification

and characterization of a novel monocyte subpopulation in human peripheral blood.', *Blood* **74**(7), 2527–34.

Patel, N. K., Bunnage, M., Plaha, P., Svendsen, C. N., Heywood, P. and Gill, S. S. (2005), 'Intraputamenal infusion of glial cell line-derived neurotrophic factor in PD: a two-year outcome study', *Ann Neurol* **57**(2), 298–302.

Paulsen, J. S., Nehl, C., Hoth, K. F., Kanz, J. E., Benjamin, M., Conybeare, R., McDowell, B. and Turner, B. (2005), 'Depression and stages of Huntington's disease', *J Neuropsychiatry Clin Neurosci* **17**(4), 496–502.

Pavese, N., Gerhard, A., Tai, Y. F., Ho, A. K., Turkheimer, F., Barker, R. A., Brooks, D. J. and Piccini, P. (2006), 'Microglial activation correlates with severity in Huntington disease: a clinical and PET study.', *Neurology* **66**(11), 1638–43.

Penney, J. B., Vonsattel, J. P., MacDonald, M. E., Gusella, J. F. and Myers, R. H. (1997), 'CAG repeat number governs the development rate of pathology in Huntington's disease.', *Ann Neurol* **41**(5), 689–92.

Perrin, V., Dufour, N., Raoul, C., Hassig, R., Brouillet, E., Aebischer, P., Luthi-Carter, R. and Déglon, N. (2009), 'Implication of the JNK pathway in a rat model of Huntington's disease', *Exp Neurol* **215**(1), 191–200.

Perutz, M. F., Johnson, T., Suzuki, M. and Finch, J. T. (1994), 'Glutamine repeats as polar zippers: their possible role in inherited neurodegenerative diseases', *Proc Natl Acad Sci USA* **91**(12), 5355–8.

Pfister, E. L., Kennington, L., Straubhaar, J., Wagh, S., Liu, W., DiFiglia, M., Landwehrmeyer, B., Vonsattel, J. P., Zamore, P. D. and Aronin, N. (2009), 'Five siRNAs targeting three SNPs may provide therapy for three-quarters of Huntington's disease patients.', *Curr Biol* **19**(9), 774–8.

Politis, M., Pavese, N., Tai, Y. F., Kiferle, L., Mason, S. L., Brooks, D. J., Tabrizi, S. J., Barker, R. A. and Piccini, P. (2011), 'Microglial activation in regions re-

lated to cognitive function predicts disease onset in Huntington's disease: a multimodal imaging study', *Hum Brain Mapp* **32**(2), 258–70.

Politis, M., Pavese, N., Tai, Y. F., Tabrizi, S. J., Barker, R. A. and Piccini, P. (2008), 'Hypothalamic involvement in Huntington's disease: an in vivo PET study', *Brain* **131**(Pt 11), 2860–9.

Pollard, J. W. (2009), 'Trophic macrophages in development and disease.', *Nat Rev Immunol* **9**(4), 259–70.

Prehoda, K. E., Scott, J. A., Mullins, R. D. and Lim, W. A. (2000), 'Integration of multiple signals through cooperative regulation of the N-WASP-Arp2/3 complex', *Science* **290**(5492), 801–6.

Pridmore, S. A. and Adams, G. C. (1991), 'The fertility of HD-affected individuals in Tasmania', *Aust N Z J Psychiatry* **25**(2), 262–4.

Pundt, L. L., Kondoh, T., Conrad, J. A. and Low, W. C. (1996), 'Transplantation of human fetal striatum into a rodent model of Huntington's disease ameliorates locomotor deficits', *Neurosci Res* **24**(4), 415–20.

Rajesh, M., Mukhopadhyay, P., Bátkai, S., Haskó, G., Liaudet, L., Huffman, J. W., Csiszar, A., Ungvari, Z., Mackie, K., Chatterjee, S. and Pacher, P. (2007), 'CB2-receptor stimulation attenuates TNF-alpha-induced human endothelial cell activation, transendothelial migration of monocytes, and monocyte-endothelial adhesion', *Am J Physiol Heart Circ Physiol* **293**(4), H2210–8.

Rand, T. A., Petersen, S., Du, F. and Wang, X. (2005), 'Argonaute2 cleaves the anti-guide strand of siRNA during RISC activation', *Cell* **123**(4), 621–9.

Ransohoff, R. M. and Perry, V. H. (2009), 'Microglial physiology: unique stimuli, specialized responses.', *Annu Rev Immunol* **27**, 119–45.

Ravikumar, B., Vacher, C., Berger, Z., Davies, J. E., Luo, S., Oroz, L. G., Scar-

avilli, F., Easton, D. F., Duden, R., O'Kane, C. J. and Rubinsztein, D. C. (2004), 'Inhibition of mTOR induces autophagy and reduces toxicity of polyglutamine expansions in fly and mouse models of Huntington disease', *Nat Genet* **36**(6), 585–95.

Rawlins, M. (2010), 'Huntington's disease out of the closet?', *Lancet* **376**(9750), 1372–3.

Ray, S., Britschgi, M., Herbert, C., Takeda-Uchimura, Y., Boxer, A., Blennow, K., Friedman, L. F., Galasko, D. R., Jutel, M., Karydas, A., Kaye, J. A., Leszek, J., Miller, B. L., Minthon, L., Quinn, J. F., Rabinovici, G. D., Robinson, W. H., Sabbagh, M. N., So, Y. T., Sparks, D. L., Tabaton, M., Tinklenberg, J., Yesavage, J. A., Tibshirani, R. and Wyss-Coray, T. (2007), 'Classification and prediction of clinical Alzheimer's diagnosis based on plasma signaling proteins', *Nat Med* **13**(11), 1359–62.

Renna, M., Jimenez-Sanchez, M., Sarkar, S. and Rubinsztein, D. C. (2010), 'Chemical inducers of autophagy that enhance the clearance of mutant proteins in neurodegenerative diseases.', *J Biol Chem* **285**(15), 11061–7.

Ridley, A. J. (2011), 'Life at the leading edge', *Cell* **145**(7), 1012–22.

Rodriguez-Lebron, E., Denovan-Wright, E. M., Nash, K., Lewin, A. S. and Mandel, R. J. (2005), 'Intrastriatal rAAV-mediated delivery of anti-huntingtin shRNAs induces partial reversal of disease progression in R6/1 Huntington's disease transgenic mice', *Mol Ther* **12**(4), 618–33.

Rosas, H. D., Goodman, J., Chen, Y. I., Jenkins, B. G., Kennedy, D. N., Makris, N., Patti, M., Seidman, L. J., Beal, M. F. and Koroshetz, W. J. (2001), 'Striatal volume loss in HD as measured by MRI and the influence of CAG repeat.', *Neurology* **57**(6), 1025–8.

Rosas, H. D., Hevelone, N. D., Zaleta, A. K., Greve, D. N., Salat, D. H. and Fischl,

B. (2005), 'Regional cortical thinning in preclinical Huntington's disease and its relationship to cognition', *Neurology* **65**(5), 745–7.

Rosas, H. D., Koroshetz, W. J., Chen, Y. I., Skeuse, C., Vangel, M., Cudkowicz, M. E., Caplan, K., Marek, K., Seidman, L. J., Makris, N., Jenkins, B. G. and Goldstein, J. M. (2003), 'Evidence for more widespread cerebral pathology in early HD: an MRI-based morphometric analysis.', *Neurology* **60**(10), 1615–20.

Rosenblatt, A., Brinkman, R. R., Liang, K. Y., Almqvist, E. W., Margolis, R. L., Huang, C. Y., Sherr, M., Franz, M. L., Abbott, M. H., Hayden, M. R. and Ross, C. A. (2001), 'Familial influence on age of onset among siblings with Huntington disease.', *Am J Med Genet* **105**(5), 399–403.

Ross, C. A. and Poirier, M. A. (2004), 'Protein aggregation and neurodegenerative disease.', *Nat Med* **10 Suppl**, S10–7.

Ross, C. A. and Tabrizi, S. J. (2011), 'Huntington's disease: from molecular pathogenesis to clinical treatment.', *Lancet Neurol* **10**(1), 83–98.

Roy, N. S., Cleren, C., Singh, S. K., Yang, L., Beal, M. F. and Goldman, S. A. (2006), 'Functional engraftment of human ES cell-derived dopaminergic neurons enriched by coculture with telomerase-immortalized midbrain astrocytes', *Nat Med* **12**(11), 1259–68.

Rubinsztein, D. C., Leggo, J., Chiano, M., Dodge, A., Norbury, G., Rosser, E. and Craufurd, D. (1997), 'Genotypes at the Glur6 kainate receptor locus are associated with variation in the age of onset of Huntington disease', *Proc Natl Acad Sci USA* **94**(8), 3872–6.

Runne, H., Régulier, E., Kuhn, A., Zala, D., Gokce, O., Perrin, V., Sick, B., Aebischer, P., Déglon, N. and Luthi-Carter, R. (2008), 'Dysregulation of gene expression in primary neuron models of Huntington's disease shows that

polyglutamine-related effects on the striatal transcriptome may not be dependent on brain circuitry', *J Neurosci* **28**(39), 9723–31.

Ryu, H., Lee, J., Hagerty, S. W., Soh, B. Y., McAlpin, S. E., Cormier, K. A., Smith, K. M. and Ferrante, R. J. (2006), 'ESET/SETDB1 gene expression and histone H3 (K9) trimethylation in Huntington's disease', *Proc Natl Acad Sci USA* **103**(50), 19176–81.

Sackley, C., Hoppitt, T. J., Calvert, M., Gill, P., Eaton, B., Yao, G. and Pall, H. (2011), 'Huntington's disease: current epidemiology and pharmacological management in UK primary care', *Neuroepidemiology* **37**(3-4), 216–21.

Sadri-Vakili, G., Bouzou, B., Benn, C. L., Kim, M. O., Chawla, P., Overland, R. P., Glajch, K. E., Xia, E., Qiu, Z., Hersch, S. M., Clark, T. W., Yohrling, G. J. and Cha, J. H. (2007), 'Histones associated with downregulated genes are hypo-acetylated in Huntington's disease models', *Hum Mol Genet* **16**(11), 1293–306.

Sah, D. W. and Aronin, N. (2011), 'Oligonucleotide therapeutic approaches for Huntington disease', *J Clin Invest* **121**(2), 500–7.

Saleh, N., Moutereau, S., Durr, A., Krystkowiak, P., Azulay, J. P., Tranchant, C., Broussolle, E., Morin, F., Bachoud-Lévi, A. C. and Maison, P. (2009), 'Neuroendocrine disturbances in Huntington's disease.', *PLoS One* **4**(3), e4962.

Sanberg, P. R., Fibiger, H. C. and Mark, R. F. (1981), 'Body weight and dietary factors in Huntington's disease patients compared with matched controls.', *Med J Aust* **1**(8), 407–9.

Sapp, E., Kegel, K. B., Aronin, N., Hashikawa, T., Uchiyama, Y., Tohyama, K., Bhide, P. G., Vonsattel, J. P. and DiFiglia, M. (2001), 'Early and progressive accumulation of reactive microglia in the Huntington disease brain.', *J Neuropathol Exp Neurol* **60**(2), 161–72.

Sapp, E., Schwarz, C., Chase, K., Bhide, P. G., Young, A. B., Penney, J., Vonsat-

tel, J. P., Aronin, N. and DiFiglia, M. (1997), 'Huntingtin localization in brains of normal and Huntington's disease patients', *Ann Neurol* **42**(4), 604–12.

Sathasivam, K., Hobbs, C., Mangiarini, L., Mahal, A., Turmaine, M., Doherty, P., Davies, S. W. and Bates, G. P. (1999), 'Transgenic models of Huntington's disease.', *Philos Trans R Soc Lond B Biol Sci* **354**(1386), 963–9.

Sathasivam, K., Neueder, A., Gipson, T. A., Landles, C., Benjamin, A. C., Bondulich, M. K., Smith, D. L., Faull, R. L., Roos, R. A., Howland, D., Detloff, P. J., Housman, D. E. and Bates, G. P. (2013), 'Aberrant splicing of htt generates the pathogenic exon 1 protein in huntington disease', *Proc Natl Acad Sci U S A* **110**(6), 2366–70.

Schaffar, G., Breuer, P., Boteva, R., Behrends, C., Tzvetkov, N., Strippel, N., Sakahira, H., Siegers, K., Hayer-Hartl, M. and Hartl, F. U. (2004), 'Cellular toxicity of polyglutamine expansion proteins: mechanism of transcription factor deactivation', *Mol Cell* **15**(1), 95–105.

Scherzinger, E., Sittler, A., Schweiger, K., Heiser, V., Lurz, R., Hasenbank, R., Bates, G. P., Lehrach, H. and Wanker, E. E. (1999), 'Self-assembly of polyglutamine-containing huntingtin fragments into amyloid-like fibrils: implications for Huntington's disease pathology', *Proc Natl Acad Sci USA* **96**(8), 4604–9.

Schilling, G., Becher, M. W., Sharp, A. H., Jinnah, H. A., Duan, K., Kotzuk, J. A., Slunt, H. H., Ratovitski, T., Cooper, J. K., Jenkins, N. A., Copeland, N. G., Price, D. L., Ross, C. A. and Borchelt, D. R. (1999), 'Intranuclear inclusions and neuritic aggregates in transgenic mice expressing a mutant N-terminal fragment of huntingtin.', *Hum Mol Genet* **8**(3), 397–407.

Schwarcz, R., Whetsell, W. O. and Mangano, R. M. (1983), 'Quinolinic acid: an

endogenous metabolite that produces axon-sparing lesions in rat brain', *Science* **219**(4582), 316–8.

Seo, H., Sonntag, K. C. and Isacson, O. (2004), 'Generalized brain and skin proteasome inhibition in Huntington's disease', *Ann Neurol* **56**(3), 319–28.

Shannon, P., Markiel, A., Ozier, O., Baliga, N. S., Wang, J. T., Ramage, D., Amin, N., Schwikowski, B. and Ideker, T. (2003), 'Cytoscape: a software environment for integrated models of biomolecular interaction networks', *Genome Res* **13**(11), 2498–504.

Shoulson, I. (1981), 'Huntington disease: functional capacities in patients treated with neuroleptic and antidepressant drugs', *Neurology* **31**(10), 1333–5.

Shuai, K. and Liu, B. (2003), 'Regulation of jak-stat signalling in the immune system', *Nat Rev Immunol* **3**(11), 900–11.

Shurety, W., Merino-Trigo, A., Brown, D., Hume, D. A. and Stow, J. L. (2000), 'Localization and post-golgi trafficking of tumor necrosis factor-alpha in macrophages', *J Interferon Cytokine Res* **20**(4), 427–38.

Simard, A. R. and Rivest, S. (2004), 'Bone marrow stem cells have the ability to populate the entire central nervous system into fully differentiated parenchymal microglia.', *FASEB J* **18**(9), 998–1000.

Singhrao, S. K., Neal, J. W., Morgan, B. P. and Gasque, P. (1999), 'Increased complement biosynthesis by microglia and complement activation on neurons in Huntington's disease.', *Exp Neurol* **159**(2), 362–76.

Slow, E. J., van Raamsdonk, J., Rogers, D., Coleman, S. H., Graham, R. K., Deng, Y., Oh, R., Bissada, N., Hossain, S. M., Yang, Y. Z., Li, X. J., Simpson, E. M., Gutekunst, C. A., Leavitt, B. R. and Hayden, M. R. (2003), 'Selective striatal neuronal loss in a YAC128 mouse model of Huntington disease', *Hum Mol Genet* **12**(13), 1555–67.

Smith, R., Bacos, K., Fedele, V., Soulet, D., Walz, H. A., Obermüller, S., Lindqvist, A., Björkqvist, M., Klein, P., Onnerfjord, P., Brundin, P., Mulder, H. and Li, J. Y. (2009), 'Mutant huntingtin interacts with beta-tubulin and disrupts vesicular transport and insulin secretion', *Hum Mol Genet* **18**(20), 3942–54.

Soto, E. R., Caras, A. C., Kut, L. C., Castle, M. K. and Ostroff, G. R. (2012), 'Glucan particles for macrophage targeted delivery of nanoparticles', *J Drug Deliv* **2012**, 143524.

Soulet, D. and Cicchetti, F. (2011), 'The role of immunity in Huntington's disease.', *Mol Psychiatry* **16**(9), 889–902.

Southwell, A. L., Khoshnan, A., Dunn, D. E., Bugg, C. W., Lo, D. C. and Patterson, P. H. (2008), 'Intrabodies binding the proline-rich domains of mutant huntingtin increase its turnover and reduce neurotoxicity', *J Neurosci* **28**(36), 9013–20.

Spires, T. L., Grote, H. E., Garry, S., Cordery, P. M., Van Dellen, A., Blakemore, C. and Hannan, A. J. (2004), 'Dendritic spine pathology and deficits in experience-dependent dendritic plasticity in R6/1 Huntington's disease transgenic mice', *Eur J Neurosci* **19**(10), 2799–807.

Squitieri, F., Berardelli, A., Nargi, E., Castellotti, B., Mariotti, C., Cannella, M., Lavitrano, M. L., de Grazia, U., Gellera, C. and Ruggieri, S. (2000), 'Atypical movement disorders in the early stages of Huntington's disease: clinical and genetic analysis', *Clin Genet* **58**(1), 50–6.

Squitieri, F., Frati, L., Ciarmiello, A., Lastoria, S. and Quarrell, O. (2006), 'Juvenile Huntington's disease: does a dosage-effect pathogenic mechanism differ from the classical adult disease?', *Mech Ageing Dev* **127**(2), 208–12.

Steffan, J. S. (2010), 'Does Huntingtin play a role in selective macroautophagy?', *Cell Cycle* **9**(17), 3401–13.

Steffan, J. S., Agrawal, N., Pallos, J., Rockabrand, E., Trotman, L. C., Slepko, N.,

Illes, K., Lukacsovich, T., Zhu, Y. Z., Cattaneo, E., Pandolfi, P. P., Thompson, L. M. and Marsh, J. L. (2004), 'SUMO modification of Huntingtin and Huntington's disease pathology.', *Science* **304**(5667), 100–4.

Steffan, J. S., Kazantsev, A., Spasic-Boskovic, O., Greenwald, M., Zhu, Y. Z., Gohler, H., Wanker, E. E., Bates, G. P., Housman, D. E. and Thompson, L. M. (2000), 'The Huntington's disease protein interacts with p53 and CREB-binding protein and represses transcription', *Proc Natl Acad Sci USA* **97**(12), 6763–8.

Stossel, T. P., Fenteany, G. and Hartwig, J. H. (2006), 'Cell surface actin remodeling', *J Cell Sci* **119**(Pt 16), 3261–4.

Stout, J. C., Paulsen, J. S., Queller, S., Solomon, A. C., Whitlock, K. B., Campbell, J. C., Carlozzi, N., Duff, K., Beglinger, L. J., Langbehn, D. R., Johnson, S. A., Biglan, K. M. and Aylward, E. H. (2011), 'Neurocognitive signs in prodromal Huntington disease', *Neuropsychology* **25**(1), 1–14.

Sundström, C. and Nilsson, K. (1976), 'Establishment and characterization of a human histiocytic lymphoma cell line (U-937).', *Int J Cancer* **17**(5), 565–77.

Tabrizi, S. J., Langbehn, D. R., Leavitt, B. R., Roos, R. A., Durr, A., Craufurd, D., Kennard, C., Hicks, S. L., Fox, N. C., Scahill, R. I., Borowsky, B., Tobin, A. J., Rosas, H. D., Johnson, H., Reilmann, R., Landwehrmeyer, B., Stout, J. C. and TRACK-HD investigators (2009), 'Biological and clinical manifestations of Huntington's disease in the longitudinal TRACK-HD study: cross-sectional analysis of baseline data', *Lancet Neurol* **8**(9), 791–801.

Tabrizi, S. J., Reilmann, R., Roos, R. A., Durr, A., Leavitt, B., Owen, G., Jones, R., Johnson, H., Craufurd, D., Hicks, S. L., Kennard, C., Landwehrmeyer, B., Stout, J. C., Borowsky, B., Scahill, R. I., Frost, C., Langbehn, D. R. and TRACK-HD investigators (2012), 'Potential endpoints for clinical trials in premanifest

and early Huntington's disease in the TRACK-HD study: analysis of 24 month observational data.', *Lancet Neurol* **11**(1), 42–53.

Tabrizi, S. J., Scahill, R. I., Durr, A., Roos, R. A., Leavitt, B. R., Jones, R., Landwehrmeyer, G. B., Fox, N. C., Johnson, H., Hicks, S. L., Kennard, C., Craufurd, D., Frost, C., Langbehn, D. R., Reilmann, R., Stout, J. C. and TRACK-HD investigators (2011), 'Biological and clinical changes in premanifest and early stage Huntington's disease in the TRACK-HD study: the 12-month longitudinal analysis', *Lancet Neurol* **10**(1), 31–42.

Taherzadeh-Fard, E., Saft, C., Andrich, J., Wieczorek, S. and Arning, L. (2009), 'PGC-1alpha as modifier of onset age in Huntington disease', *Mol Neurodegener* **4**, 10.

Tai, Y. F., Pavese, N., Gerhard, A., Tabrizi, S. J., Barker, R. A., Brooks, D. J. and Piccini, P. (2007), 'Microglial activation in presymptomatic Huntington's disease gene carriers.', *Brain* **130**(Pt 7), 1759–66.

Takahashi, K., Tanabe, K., Ohnuki, M., Narita, M., Ichisaka, T., Tomoda, K. and Yamanaka, S. (2007), 'Induction of pluripotent stem cells from adult human fibroblasts by defined factors', *Cell* **131**(5), 861–72.

Takeda, K., Kaisho, T. and Akira, S. (2003), 'Toll-like receptors', *Annu Rev Immunol* **21**, 335–76.

Tangirala, R. K., Murao, K. and Quehenberger, O. (1997), 'Regulation of expression of the human monocyte chemotactic protein-1 receptor (hCCR2) by cytokines', *J Biol Chem* **272**(12), 8050–6.

Taylor, D. L., Diemel, L. T. and Pocock, J. M. (2003), 'Activation of microglial group III metabotropic glutamate receptors protects neurons against microglial neurotoxicity', *J Neurosci* **23**(6), 2150–60.

Teng, F. Y. and Tang, B. L. (2010), 'NF-kappaB signaling in neurite growth and neuronal survival', *Rev Neurosci* **21**(4), 299–313.

Tesz, G. J., Aouadi, M., Prot, M., Nicoloro, S. M., Boutet, E., Amano, S. U., Goller, A., Wang, M., Guo, C. A., Salomon, W. E., Virbasius, J. V., Baum, R. A., O'Connor, M. J., Soto, E., Ostroff, G. R. and Czech, M. P. (2011), 'Glucan particles for selective delivery of siRNA to phagocytic cells in mice', *Biochem J* **436**(2), 351–62.

The HD IPSC Consortium (2012), 'Induced pluripotent stem cells from patients with Huntington's disease show CAG-repeat-expansion-associated phenotypes', *Cell Stem Cell* **11**(2), 264–78.

The Huntington's Disease Collaborative Research Group (1993), 'A novel gene containing a trinucleotide repeat that is expanded and unstable on Huntington's disease chromosomes. The Huntington's Disease Collaborative Research Group.', *Cell* **72**(6), 971–83.

Thompson, L. M., Aiken, C. T., Kaltenbach, L. S., Agrawal, N., Illes, K., Khoshnan, A., Martinez-Vincente, M., Arrasate, M., O'Rourke, J. G., Khashwji, H., Lukacsovich, T., Zhu, Y. Z., Lau, A. L., Massey, A., Hayden, M. R., Zeitlin, S. O., Finkbeiner, S., Green, K. N., LaFerla, F. M., Bates, G., Huang, L., Patterson, P. H., Lo, D. C., Cuervo, A. M., Marsh, J. L. and Steffan, J. S. (2009), 'IKK phosphorylates Huntingtin and targets it for degradation by the proteasome and lysosome.', *J Cell Biol* **187**(7), 1083–99.

Toneff, T., Mende-Mueller, L., Wu, Y., Hwang, S. R., Bundey, R., Thompson, L. M., Chesselet, M. F. and Hook, V. (2002), 'Comparison of huntingtin proteolytic fragments in human lymphoblast cell lines and human brain.', *J Neurochem* **82**(1), 84–92.

Trejo, A., Tarrats, R. M., Alonso, M. E., Boll, M. C., Ochoa, A. and Velsquez, L.

(2004), 'Assessment of the nutrition status of patients with Huntington's disease', *Nutrition* **20**(2), 192–6.

Trembath, M. K., Horton, Z. A., Tippett, L., Hogg, V., Collins, V. R., Churchyard, A., Velakoulis, D., Roxburgh, R. and Delatycki, M. B. (2010), 'A retrospective study of the impact of lifestyle on age at onset of Huntington disease', *Mov Disord* **25**(10), 1444–50.

Trottier, Y., Biancalana, V. and Mandel, J. L. (1994), 'Instability of CAG repeats in Huntington's disease: relation to parental transmission and age of onset.', *J Med Genet* **31**(5), 377–82.

van Dellen, A., Blakemore, C., Deacon, R., York, D. and Hannan, A. J. (2000), 'Delaying the onset of Huntington's in mice', *Nature* **404**(6779), 721–2.

van der Burg, J. M., Bacos, K., Wood, N. I., Lindqvist, A., Wierup, N., Woodman, B., Wamsteeker, J. I., Smith, R., Deierborg, T., Kuhar, M. J., Bates, G. P., Mulder, H., Erlanson-Albertsson, C., Morton, A. J., Brundin, P., Petersén, A. and Björkqvist, M. (2008), 'Increased metabolism in the R6/2 mouse model of Huntington's disease.', *Neurobiol Dis* **29**(1), 41–51.

van der Burg, J. M., Björkqvist, M. and Brundin, P. (2009), 'Beyond the brain: widespread pathology in Huntington's disease.', *Lancet Neurol* **8**(8), 765–74.

van der Burg, J. M., Winqvist, A., Aziz, N. A., Maat-Schieman, M. L., Roos, R. A., Bates, G. P., Brundin, P., Björkqvist, M. and Wierup, N. (2011), 'Gastrointestinal dysfunction contributes to weight loss in Huntington's disease mice', *Neurobiol Dis* **44**(1), 1–8.

Van Ginderachter, J. A., Movahedi, K., Hassanzadeh Ghassabeh, G., Meerschaut, S., Beschin, A., Raes, G. and De Baetselier, P. (2006), 'Classical and alternative activation of mononuclear phagocytes: picking the best of both worlds for tumor promotion.', *Immunobiology* **211**(6-8), 487–501.

Van Raamsdonk, J. M., Metzler, M., Slow, E., Pearson, J., Schwab, C., Carroll, J., Graham, R. K., Leavitt, B. R. and Hayden, M. R. (2007), 'Phenotypic abnormalities in the YAC128 mouse model of Huntington disease are penetrant on multiple genetic backgrounds and modulated by strain.', *Neurobiol Dis* **26**(1), 189–200.

Van Raamsdonk, J. M., Murphy, Z., Slow, E. J., Leavitt, B. R. and Hayden, M. R. (2005b), 'Selective degeneration and nuclear localization of mutant huntingtin in the YAC128 mouse model of Huntington disease', *Hum Mol Genet* **14**(24), 3823–35.

Van Raamsdonk, J. M., Pearson, J., Slow, E. J., Hossain, S. M., Leavitt, B. R. and Hayden, M. R. (2005a), 'Cognitive dysfunction precedes neuropathology and motor abnormalities in the YAC128 mouse model of Huntington's disease', *J Neurosci* **25**(16), 4169–80.

Velier, J., Kim, M., Schwarz, C., Kim, T. W., Sapp, E., Chase, K., Aronin, N. and DiFiglia, M. (1998), 'Wild-type and mutant huntingtins function in vesicle trafficking in the secretory and endocytic pathways', *Exp Neurol* **152**(1), 34–40.

Voisine, C., Varma, H., Walker, N., Bates, E. A., Stockwell, B. R. and Hart, A. C. (2007), 'Identification of potential therapeutic drugs for Huntington's disease using Caenorhabditis elegans', *PLoS One* **2**(6), e504.

von Hörsten, S., Schmitt, I., Nguyen, H. P., Holzmann, C., Schmidt, T., Walther, T., Bader, M., Pabst, R., Kobbe, P., Krotova, J., Stiller, D., Kask, A., Vaarmann, A., Rathke-Hartlieb, S., Schulz, J. B., Grasshoff, U., Bauer, I., Vieira-Saecker, A. M., Paul, M., Jones, L., Lindenberg, K. S., Landwehrmeyer, B., Bauer, A., Li, X. J. and Riess, O. (2003), 'Transgenic rat model of Huntington's disease', *Hum Mol Genet* **12**(6), 617–24.

Vonsattel, J. P. (2008), 'Huntington disease models and human neuropathology:

similarities and differences.', *Acta Neuropathol* **115**(1), 55–69.

Vonsattel, J. P. and DiFiglia, M. (1998), 'Huntington disease', *J Neuropathol Exp Neurol* **57**(5), 369–84.

Vonsattel, J. P., Keller, C. and Cortes Ramirez, E. P. (2011), 'Huntington's disease - neuropathology.', *Handb Clin Neurol* **100**, 83–100.

Vonsattel, J. P., Myers, R. H., Stevens, T. J., Ferrante, R. J., Bird, E. D. and Richardson, E. P. (1985), 'Neuropathological classification of Huntington's disease', *J Neuropathol Exp Neurol* **44**(6), 559–77.

Wake, H., Moorhouse, A. J., Jinno, S., Kohsaka, S. and Nabekura, J. (2009), 'Resting microglia directly monitor the functional state of synapses in vivo and determine the fate of ischemic terminals', *J Neurosci* **29**(13), 3974–80.

Walport, M., Murphy, K. and Travers, P. (2008), *Janeway's immune biology*, seventh edn, Garland Science.

Warby, S. C., Visscher, H., Collins, J. A., Doty, C. N., Carter, C., Butland, S. L., Hayden, A. R., Kanazawa, I., Ross, C. J. and Hayden, M. R. (2011), 'HTT haplotypes contribute to differences in Huntington disease prevalence between Europe and East Asia', *Eur J Hum Genet* **19**(5), 561–6.

Weir, D. W., Sturrock, A. and Leavitt, B. R. (2011), 'Development of biomarkers for Huntington's disease', *Lancet Neurol* **10**(6), 573–90.

Weiss, A., Grueninger, S., Abramowski, D., Giorgio, F. P., Lopatin, M. M., Rosas, H. D., Hersch, S. and Paganetti, P. (2011), 'Microtiter plate quantification of mutant and wild-type huntingtin normalized to cell count.', *Anal Biochem* **410**(2), 304–6.

Weiss, A., Träger, U., Wild, E. J., Grueninger, S., Farmer, R., Landles, C., Scahill, R. I., Lahiri, N., Haider, S., Macdonald, D., Frost, C., Bates, G. P., Bilbe,

G., Kuhn, R., Andre, R. and Tabrizi, S. J. (2012), 'Mutant huntingtin fragmentation in immune cells tracks Huntington's disease progression', *J Clin Invest* **122**(10), 3731–6.

Wexler, N. S., Lorimer, J., Porter, J., Gomez, F., Moskowitz, C., Shackell, E., Marder, K., Penchaszadeh, G., Roberts, S. A., Gayán, J., Brocklebank, D., Cherny, S. S., Cardon, L. R., Gray, J., Dlouhy, S. R., Wiktorski, S., Hodes, M. E., Conneally, P. M., Penney, J. B., Gusella, J., Cha, J. H., Irizarry, M., Rosas, D., Hersch, S., Hollingsworth, Z., MacDonald, M., Young, A. B., Andresen, J. M., Housman, D. E., De Young, M. M., Bonilla, E., Stillings, T., Negrette, A., Snodgrass, S. R., Martinez-Jaurrieta, M. D., Ramos-Arroyo, M. A., Bickham, J., Ramos, J. S., Marshall, F., Shoulson, I., Rey, G. J., Feigin, A., Arnheim, N., Acevedo-Cruz, A., Acosta, L., Alvir, J., Fischbeck, K., Thompson, L. M., Young, A., Dure, L., O'Brien, C. J., Paulsen, J., Brickman, A., Krch, D., Peery, S., Hogarth, P., Higgins, D. S., Landwehrmeyer, B. and U.S.-Venezuela Collaborative Research Project (2004), 'Venezuelan kindreds reveal that genetic and environmental factors modulate Huntington's disease age of onset.', *Proc Natl Acad Sci USA* **101**(10), 3498–503.

Wexler, N. S., Young, A. B., Tanzi, R. E., Travers, H., Starosta-Rubinstein, S., Penney, J. B., Snodgrass, S. R., Shoulson, I., Gomez, F. and Ramos Arroyo, M. A. (1987), 'Homozygotes for Huntington's disease', *Nature* **326**(6109), 194–7.

Weydt, P., Soyal, S. M., Gellera, C., Didonato, S., Weidinger, C., Oberkofler, H., Landwehrmeyer, G. B. and Patsch, W. (2009), 'The gene coding for PGC-1alpha modifies age at onset in Huntington's disease', *Mol Neurodegener* **4**, 3.

Wheeler, V. C., Auerbach, W., White, J. K., Srinidhi, J., Auerbach, A., Ryan, A., Duyao, M. P., Vrbanac, V., Weaver, M., Gusella, J. F., Joyner, A. L. and MacDonald, M. E. (1999), 'Length-dependent gametic CAG repeat instability in the

Huntington's disease knock-in mouse', *Hum Mol Genet* **8**(1), 115–22.

Whitelaw, D. M. (1966), 'The intravascular lifespan of monocytes.', *Blood* **28**(3), 455–64.

Wild, E. J. and Tabrizi, S. J. (2007), 'The differential diagnosis of chorea.', *Pract Neurol* **7**(6), 360–73.

Wild, E., Magnusson, A., Lahiri, N., Krus, U., Orth, M., Tabrizi, S. J. and Björkqvist, M. (2011), 'Abnormal peripheral chemokine profile in Huntington's disease.', *PLoS Curr* **3**, RRN1231.

Woodman, B., Butler, R., Landles, C., Lupton, M. K., Tse, J., Hockly, E., Moffitt, H., Sathasivam, K. and Bates, G. P. (2007), 'The knock-in mouse model of HD and the R6/2 exon 1 model develop comparable and widespread molecular phenotypes.', *Brain Res Bull* **72**(2-3), 83–97.

Xia, J., Lee, D. H., Taylor, J., Vandelft, M. and Truant, R. (2003), 'Huntingtin contains a highly conserved nuclear export signal.', *Hum Mol Genet* **12**(12), 1393–403.

Xie, Y., Hayden, M. R. and Xu, B. (2010), 'BDNF overexpression in the forebrain rescues Huntington's disease phenotypes in YAC128 mice', *J Neurosci* **30**(44), 14708–18.

Yamamoto, A., Lucas, J. J. and Hen, R. (2000), 'Reversal of neuropathology and motor dysfunction in a conditional model of Huntington's disease', *Cell* **101**(1), 57–66.

Yamamoto, M., Sato, S., Hemmi, H., Hoshino, K., Kaisho, T., Sanjo, H., Takeuchi, O., Sugiyama, M., Okabe, M., Takeda, K. and Akira, S. (2003), 'Role of adaptor TRIF in the MyD88-independent toll-like receptor signaling pathway.', *Science* **301**(5633), 640–3.

Yanai, A., Huang, K., Kang, R., Singaraja, R. R., Arstikaitis, P., Gan, L., Orban, P. C., Mullard, A., Cowan, C. M., Raymond, L. A., Drisdel, R. C., Green, W. N., Ravikumar, B., Rubinsztein, D. C., El-Husseini, A. and Hayden, M. R. (2006), 'Palmitoylation of huntingtin by HIP14 is essential for its trafficking and function', *Nat Neurosci* **9**(6), 824–31.

Yang, D., Wang, C. E., Zhao, B., Li, W., Ouyang, Z., Liu, Z., Yang, H., Fan, P., O'Neill, A., Gu, W., Yi, H., Li, S., Lai, L. and Li, X. J. (2010), 'Expression of Huntington's disease protein results in apoptotic neurons in the brains of cloned transgenic pigs', *Hum Mol Genet* **19**(20), 3983–94.

Yang, S. H., Cheng, P. H., Banta, H., Piotrowska-Nitsche, K., Yang, J. J., Cheng, E. C., Snyder, B., Larkin, K., Liu, J., Orkin, J., Fang, Z. H., Smith, Y., Bachevalier, J., Zola, S. M., Li, S. H., Li, X. J. and Chan, A. W. (2008), 'Towards a transgenic model of Huntington's disease in a non-human primate', *Nature* **453**(7197), 921–4.

Zala, D., Colin, E., Rangone, H., Liot, G., Humbert, S. and Saudou, F. (2008), 'Phosphorylation of mutant huntingtin at S421 restores anterograde and retrograde transport in neurons', *Hum Mol Genet* **17**(24), 3837–46.

Zeitlin, S., Liu, J. P., Chapman, D. L., Papaioannou, V. E. and Efstratiadis, A. (1995), 'Increased apoptosis and early embryonic lethality in mice nullizygous for the Huntington's disease gene homologue.', *Nat Genet* **11**(2), 155–63.

Zeng, W., Gillis, T., Hakky, M., Djouss, L., Myers, R. H., MacDonald, M. E. and Gusella, J. F. (2006), 'Genetic analysis of the GRIK2 modifier effect in Huntington's disease', *BMC Neurosci* **7**, 62.

Zhai, W., Jeong, H., Cui, L., Krainc, D. and Tjian, R. (2005), 'In vitro analysis of huntingtin-mediated transcriptional repression reveals multiple transcription factor targets', *Cell* **123**(7), 1241–53.

Zhang, F., Thornhill, S. I., Howe, S. J., Ulaganathan, M., Schambach, A., Sinclair, J., Kinnon, C., Gaspar, H. B., Antoniou, M. and Thrasher, A. J. (2007), 'Lentiviral vectors containing an enhancer-less ubiquitously acting chromatin opening element (UCOE) provide highly reproducible and stable transgene expression in hematopoietic cells', *Blood* **110**(5), 1448–57.

Ziegler-Heitbrock, L. (2007), 'The CD14+ CD16+ blood monocytes: their role in infection and inflammation', *J Leukoc Biol* **81**(3), 584–92.

Zuccato, C., Ciammola, A., Rigamonti, D., Leavitt, B. R., Goffredo, D., Conti, L., MacDonald, M. E., Friedlander, R. M., Silani, V., Hayden, M. R., Timmusk, T., Sipione, S. and Cattaneo, E. (2001), 'Loss of huntingtin-mediated BDNF gene transcription in Huntington's disease', *Science* **293**(5529), 493–8.

Zuccato, C., Tartari, M., Crotti, A., Goffredo, D., Valenza, M., Conti, L., Cataudella, T., Leavitt, B. R., Hayden, M. R., Timmusk, T., Rigamonti, D. and Cattaneo, E. (2003), 'Huntingtin interacts with REST/NRSF to modulate the transcription of NRSE-controlled neuronal genes', *Nat Genet* **35**(1), 76–83.

Zwilling, D., Huang, S. Y., Sathyasaikumar, K. V., Notarangelo, F. M., Guidetti, P., Wu, H. Q., Lee, J., Truong, J., Andrews-Zwilling, Y., Hsieh, E. W., Louie, J. Y., Wu, T., Scearce-Levie, K., Patrick, C., Adame, A., Giorgini, F., Moussaoui, S., Laue, G., Rassoulpour, A., Flik, G., Huang, Y., Muchowski, J. M., Masliah, E., Schwarcz, R. and Muchowski, P. J. (2011), 'Kynurenine 3-monooxygenase inhibition in blood ameliorates neurodegeneration.', *Cell* **145**(6), 863–74.

Publications relating to this thesis

Weiss A, Träger U, Wild EJ, Grueninger S, Farmer R, Landles C, Scahill RI, Lahiri N, Haider S, Macdonald D, Frost C, Bates GP, Bilbe G, Kuhn R, Andre R, Tabrizi SJ (2012) Mutant huntingtin fragmentation in immune cells tracks Huntington's disease progression. *J Clin Invest* 122: 3731-3736

Kwan, W., Träger, U., Davalos, D., Chou, A., Bouchard, J., Andre, R., Miller, A., Weiss, A., Giorgini, F., Cheah, C., Möller, T., Stella, N., Akassoglou, K., Tabrizi, S. J. and Muchowski, P. J. (2012b), Mutant huntingtin impairs immune cell migration in Huntington disease, J Clin Invest 122(12), 473747.